UNIVERSITY OF MINNESOTA

CENTER FOR TRANSPORTATION STUDIES

RESEARCH REPORT

STATIC AND DYNAMIC BOUNDARY ELEMENT METHODS FOR LAYERED PAVEMENT SYSTEMS

B. Birgisson * S.L. Crouch * D.E. Newcomb
Department of Civil Engineering

CTS 97-06

Technical Report Documentation Page

1. Report No.
CTS 97-06

2.

3. Recipient's Accession No.

4. Title and Subtitle
Static and Dynamic Boundary Element Methods for Layered Pavement Systems

5. Report Date
December, 1997

6.

7. Author(s)
B. Birgisson, S. L. Crouch, and D. E. Newcomb

8. Performing Organization Report No.

9. Performing Organization Name and Address
Department of Civil Engineering
500 Pillsbury Drive S.E.
Minneapolis, MN 55455-0220

10. Project/Task/Work Unit No.

11. Contract (C) or Grant (G) No.
(C)
(G)

12. Sponsoring Organization Name and Address
Center for Transportation Studies
200 Transportation and Safety Building
511 Washington Ave. S.E.
Minneapolis, MN 55455

13. Type of Report and Period Covered
Final Report 1992

14. Sponsoring Agency Code

15. Supplementary Notes

16. Abstract (Limit: 200 words)

The main objective of this report is to present two numerical computer models that compute the static and the transient displacements and stresses in pavement systems consisting of one or more distinct layers of material. Both models are based on the boundary element method, which is described in detail in the attachment. The static model is capable of predicting the static solution, which is sometimes also the steady-state distribution of stresses and displacements anywhere within a layered pavement system. The dynamic model is capable of representing the propagation of displacement and stress waves across the interfaces separating the layers and includes the wave scattering effects of reflection and refraction from these interfaces. The transient displacements and stresses tend towards the static or steady-state solution as time tends to infinity, thus complimenting the solution obtained with the static boundary element method. Both of these methods are validated through a comparison with existing analytical and numerical solutions in the literature. Finally, both the static and dynamic computer models are applied to typical three layered rigid pavement configurations and loads to provide examples of the potential usefulness of these methods in developing appropriate guidelines for transient loading conditions.

17. Document Analysis/Descriptors
static and the transient displacements
stresses in pavement systems
boundary element method

18. Availability Statement
No restrictions. Document available from.
National Technical Information Services,
Springfield, Virginia 22161

19. Security Class (this report)
Unclassified

20. Security Class (this page)
Unclassified

21. No. of Pages

22. Price

Static and Dynamic Boundary Element Methods for Layered Pavement Systems

B. Birgisson, S.L. Crouch, and D.E. Newcomb

November 25, 1996

The financial support of oil overcharge funds distributed through the Minnesota Department of Administration is acknowledged, but the authors assume complete responsibility for the contents herein.

University of Minnesota
Department of Civil Engineering

A Repot Prepared for the Center for Transportation Studies

1. Introduction

1.1. Background

A rigid pavement system consists of a relatively thin slab of concrete overlying a subgrade or a base course. The loads on a pavement system during its life span consist of both static and dynamic loads. The distribution of displacements and stresses throughout the pavement system resulting from these loads dictates the life-time performance of the system. In current practice, the effects of static loads on a pavement system are obtained by simple analytical methods that model the concrete slab as a beam resting on an elastic foundation. The dynamic loading response is obtained by multiplying the elastostatic response with a dynamic load factor. This simplification does not model the wave phenomenon associated with elastodynamic problems. Another drawback with this approach is that it also does not adequately account for the interaction between the concrete slab and the layered subgrade under loading. Any effort to develop more cost-effective design procedures for pavement systems has to account for the distribution of displacements and stresses throughout the concrete slab and the layered subgrade.

Currently, there are no simple analytical methods available that adequately account for the elastostatic load response of layered pavement systems, let alone the complicated wave phenomenon initiated by the dynamic nature of most pavement loads. However, several numerical techniques allow for the modeling of the load response of layered materials. This study presents one such numerical technique, called the boundary element method. This method is well suited to model the semi-infinite boundaries associated with layered pavement systems and has the added benefit that only the boundaries of the region of interest need to be divided into elements, which effectively reduces a three-dimensional problem to a two-dimensional one (or a two-dimensional problem to a one-dimensional one), with a corresponding saving of computational effort. The method presented in this report is also capable of accounting for the displacements and stresses anywhere in a pavement system due to static and dynamic loads. The approach therefore provides an alternative to the more "conventional" analysis of rigid pavement systems using methods that discretize the whole region of interest, such as the finite element and finite difference methods.

1.2. Objectives

The main objective of this report is to present two numerical computer models that compute the static and the transient displacements and stresses in pavement systems consisting of one or more distinct layers of material. Both models are based on the boundary element method, which is described in detail in the attachment. The static model is capable of predicting the static solution, which is sometimes also the steady-state distribution of stresses and displacements anywhere within a layered pavement system. The dynamic model is capable of representing the propagation of displacement and stress waves across the interfaces separating the layers and includes the wave scattering effects of reflection and refraction from these interfaces. The transient displacements and stresses tend towards the static or steady-state solution as time tends to infinity, thus complimenting the solution obtained with the static boundary element method. Both of these methods are validated through a comparison with existing analytical and numerical solutions in the literature. Finally, both the static and dynamic computer models are applied to typical three layered rigid pavement configurations and loads to provide examples of the potential usefulness of these methods in developing appropriate guidelines for transient loading conditions.

1.3. Scope

The attachment to this report (Birgisson, B. 1996. "A Two-Dimensional Dynamic Direct Boundary Element Method for Piecewise Homogeneous Elastic Media." Ph.D. Thesis. University of Minnesota) describes in detail the mathematical and numerical implementations, and the verification of both static and dynamic boundary element methods for layered pavement systems. Both methods are general in nature and are not limited to layers only. Examples of other possible problems are inclusions of one material embedded in another, and the added complication of existing underground openings (for example tunnels and culverts) in these inclusions or layers. It is shown that both the static and the dynamic computer models presented are ideally suited for studying both the elastostatic and the elastodynamic load response of layered pavement systems. Finally, Section 2 of this report contains examples in which the static and dynamic computer models are used to obtain the loading response of of three typical layered rigid pavement configurations.

2. Three-Layered Pavement Systems

2.1. Elastostatic Case

Most problems of practical interest in rigid pavement engineering involve a top layer that is made of concrete, overlying a pavement base that is underlain by a layer of material called the subgrade. The base consists of class 5 granular fill, but the subgrade frequently consists of the native or *in situ* material, sometimes compacted to some specified consistency. The validity of the elastostatic boundary element computer model presented in this report for modeling layer problems has already been established (see Chapter 6 in the attachment). It is however of interest to establish the usefulness of the computer model for modeling pavement problems with realistic loads, dimensions and material properties.

The geometry shown in Figure 2.1 is adopted for this example. The layered half-plane is approximated by a closed domain that is extended suffiently far away from the loaded to minimize the influence of the far-field enclosing elements. Three distinct cases are evaluated: (1) the same elastic constants for the concrete layer and the base are used, namely, $E_1 = E_2 = 4.0 \times 10^6$ psi, with $\nu_1 = \nu_2 = 0.2$, whereas for the subgrade, $E_3 = 8.0 \times 10^4$ psi and $\nu_3 = 0.4$, (2) the elastic constants for the base and the subgrade are the same, $E_2 = E_3 = 8.0 \times 10^4$ psi, with $\nu_2 = \nu_3 = 0.4$, but the concrete pavement properties are $E_1 = 4.0 \times 10^6$ psi and with $\nu_1 = 0.2$, and finally (3) the values for the elastic constants for the concrete, base, and subgrade are taken to be representative of typical rigid pavement systems, with $E_1 = 4.0 \times 10^6$ psi, $E_2 =$, and $E_3 = 8.0 \times 10^4$ psi, with $\nu_1 = 0.2$, and $\nu_2 = \nu_3 = 0.4$. The geometry of the pavement system is modeled with a top row of 30 elements, with 30 elements on each layer interface, with 9 elements on each side, and 6 elements on the bottom. The boundary conditions at the bottom of the grid are displacement boundary conditions, with zero normal and tangential displacements. The nodal boundary conditions on the left and right hand sides of the grid are mixed, with zero normal displacement and tangential traction components. The applied surface strip load was taken to be $p_o = 100$ psi.

To evaluate the differences in load response due to the three loading cases discussed previously, a number of comparison studies were performed. Figure 2.2 shows the variation in normalized displacements along the surface of the layered half-plane. Figure 2.3 shows the variation in vertical stress along the interface between regions 1 and 2, and Figure 2.4 shows a comparison of the vertical

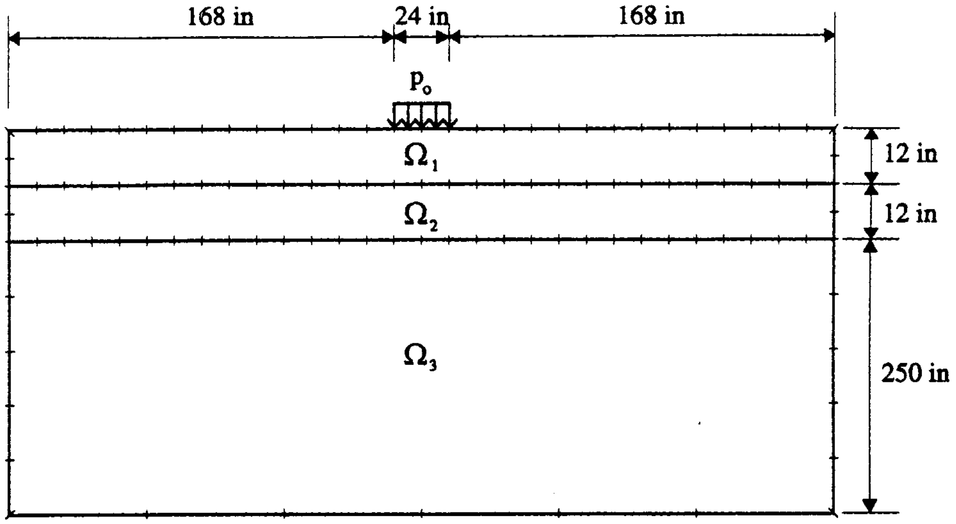

Figure 2.1: Strip-loaded pavement system.

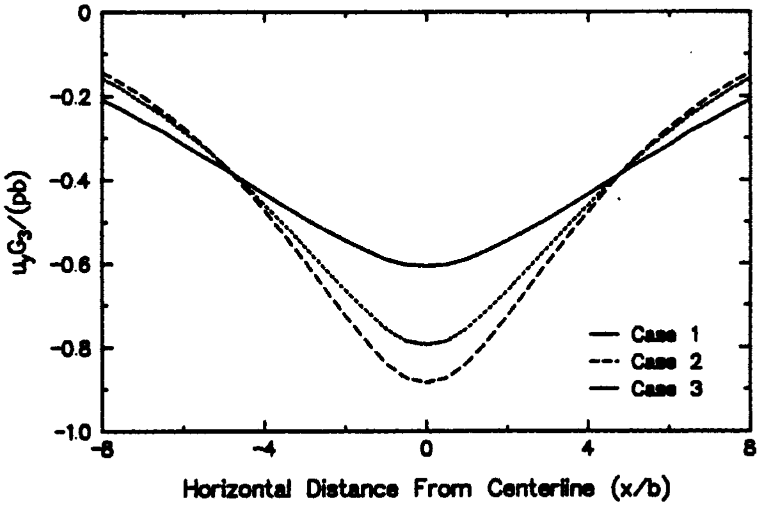

Figure 2.2: Vertical displacements along surface of loaded layered half-plane.

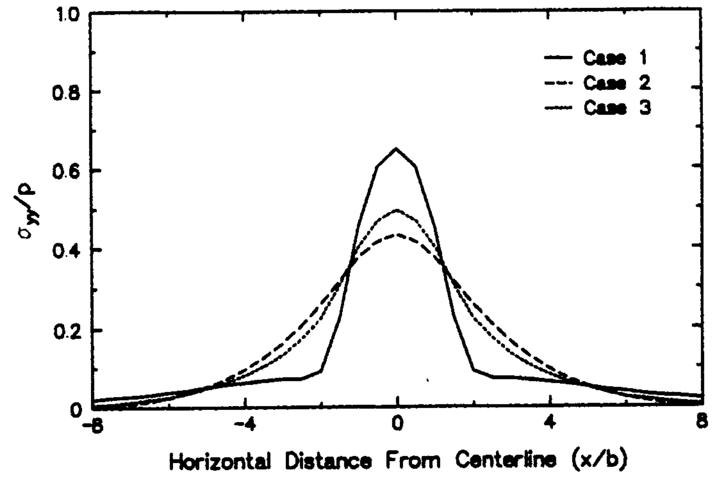

Figure 2.3: Vertical stress along top interface.

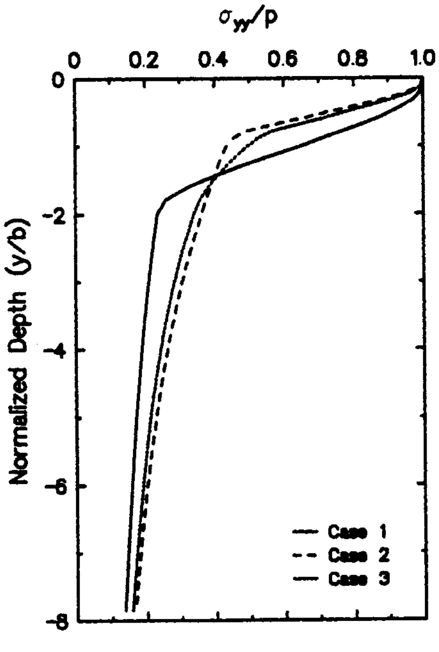

Figure 2.4: Vertical stress below centerline of strip loaded area.

stresses along the centerline ($x = 0$) with normalized depth. As expected, due to the stiff nature of the concrete pavement, the vertical displacements for Case 1 are smaller around the loaded area than those for the other two cases, but they also dissipate more slowly than those for Cases 2 and 3. This behavior is supported by the variation of vertical stresses at the top interface, shown in Figure 2.3, in which the vertical stresses around the centerline of the loaded area are higher for Case 1, but dissipate rapidly away from the centerline. Figure 2.4 shows how the vertical stresses for Case 1 remain higher in most of the concrete section ($y/b \leq 2$), but lower and almost constant in the soft soil below the concrete. Another interesting observation from Figures 2.2, 2.3, and 2.4 is that the loading responses for Cases 2 and 3 are very similar. Both the vertical stresses and displacements follow the same pattern, with only small variations in values. This indicates that the essence of the loading response of a three-layered pavement system (Case 3) can be captured by a simpler system, in which the concrete pavement is assumed to overlay a semi-infinite subgrade. The base layer does not significantly influence the loading response of the system.

2.2. Elastodynamic Case

By recognizing that the influence of loads far away from their points of action is often negligible, it is possible to approximate the dynamic loading response of the layered half-plane by cutting the discretized boundaries at a distance remote from the loaded area. It has been found that distances of $15 \leq x/b \leq 20$ away from the centerline of the loaded area are typically quite sufficient, in which b is the lateral extent of loading away from the centerline. Figure 2.5 shows the discretization used to evaluate the dynamic loading response for multi-layered halfplanes. In this case, the discretized boundaries are cut off at a distance of $x/b = 15$ away from the centerline of the loaded area. The surface of the half-plane is modeled with 30 elements, and each side of the interface between layers is modeled with 30 elements, for a total of 150 elements. The length of each element is $\Delta x = 12$ inches, and the number of time steps is $n_t = 400$. In this example, b was also conveniently selected as being equal to one element length, Δx. The size of the time step was selected so that the longitudinal wave would travel exactly 85 percent of an element length at each time step. This can be expressed by a dimensionless parameter

$$Q_1 = 1.7 = \frac{c_1 \Delta t}{a_l} \tag{2.1}$$

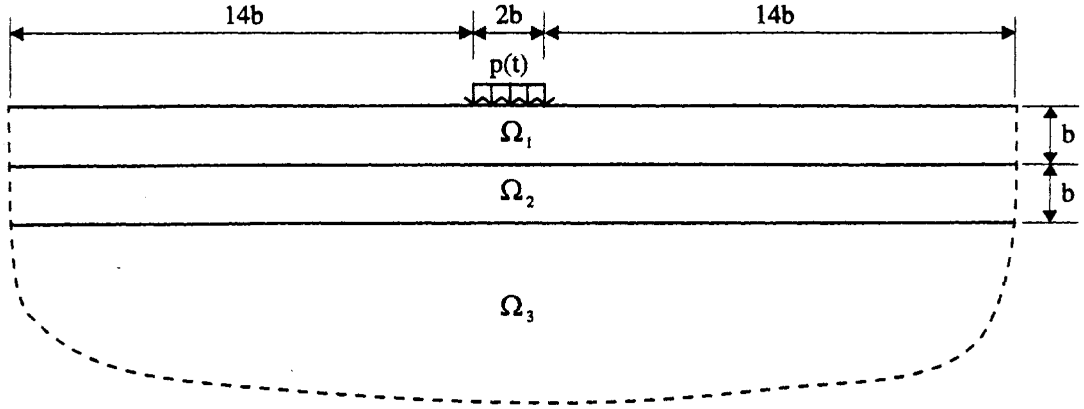

Figure 2.5: A suddenly loaded three-layered half-plane.

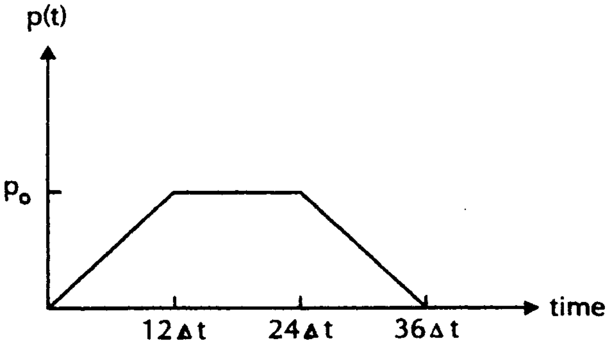

Figure 2.6: Time history of applied loading.

where $a_l = \Delta x/2 =$ element half-length. Finally, a part of the surface at time $t = 0$ is loaded by the vertical traction $p(t)$, whose time history of loading is given by Figure 2.6.

The three cases studied previously for elastostatic loading conditions are evaluated again, namely (1) the elastic constants for the concrete layer and the base are the same, (2) the elastic constants for the base and the subgrade are the same, and (3) the elastic constants for the concrete, base, and subgrade are representative of those values typically found in rigid pavement systems. The elastic properties of Cases 1 and 2 are contained within Case 3. Therefore, only the compressional and shear wave velocities, c_1, c_2, along with the mass densities of each layer for Case 3 are given below as:

Layer	c_1 (in/s)	c_2 (in/s)	ρ (lbf-s^2/in^4)
1	140546.0	86066.0	2.25×10^{-4}
2	57416.9	23440.4	1.95×10^{-4}
3	29650.0	12104.6	1.95×10^{-4}

To evaluate the differences in loading response among the three cases, the horizontal and vertical displacements are monitored at Stations $P\,(x/b = 3)$ and $Q\,(x/b = 8)$. Figures 2.7 and 2.8 show the normalized horizontal and vertical displacements versus normalized time for Station P, whereas Figures 2.9 and 2.10 show the results for Station Q. Both the shear wave velocity c_2 and the shear modulus G_3 used in the normalized time and displacements were always taken to correspond to Layer 3, namely $G_3 = 28571.4$ psi, and $c_2 = 12104.6$ in/s. Similarly, then $b = 12$ inches, and $p_o = 100$ psi. Just as in the elastostatic case, Figures 2.7, 2.8, 2.9, and 2.10 show that the loading responses of Cases 2 and 3 are very similar. Both the horizontal and vertical displacements follow the same pattern, with only small variations in values. This indicates that the dynamic loading response of a three-layered pavement system (Case 3) can be captured by a simple two-layered system, in which the concrete pavement is assumed to overlay a semi-infinite subgrade.

A comparison of Figures 2.8 and 2.10 shows that the maximum vertical displacements increase in amplitude between Stations $P\,(x/b = 3)$ and $Q\,(x/b = 8)$ for Case 1, but decrease slightly for Cases 2 and 3. This behavior is due to multiple reflections within the very stiff concrete layer which act to increase the amplitude of displacements away from the loaded area as the concrete becomes thicker. This means that it may not always be justified to increase the thickness of concrete pavement systems. Rather, these results

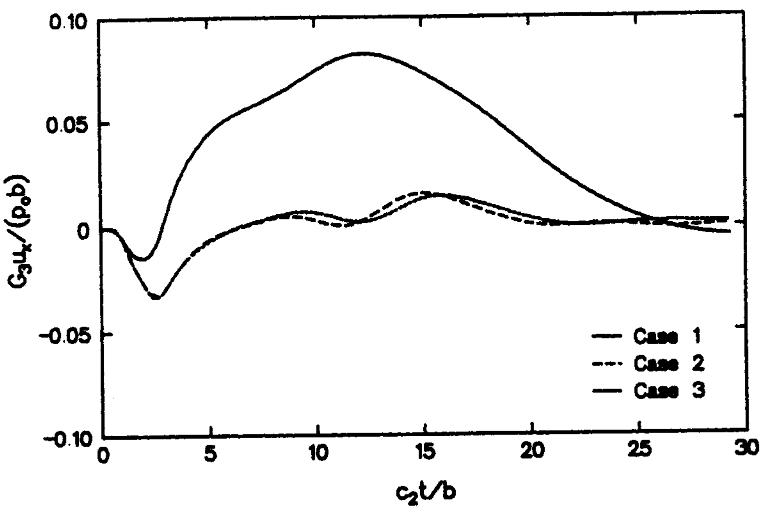

Figure 2.7: Horizontal displacements at Station P (x/b =3).

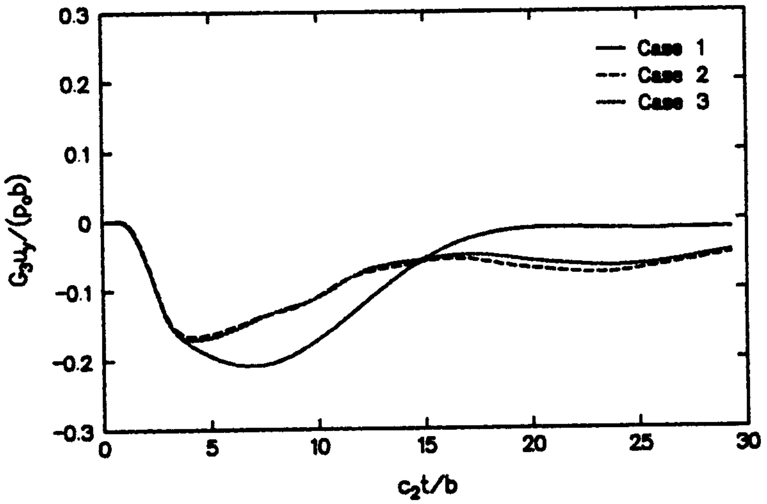

Figure 2.8: Vertical displacements at Station P (x/b = 3).

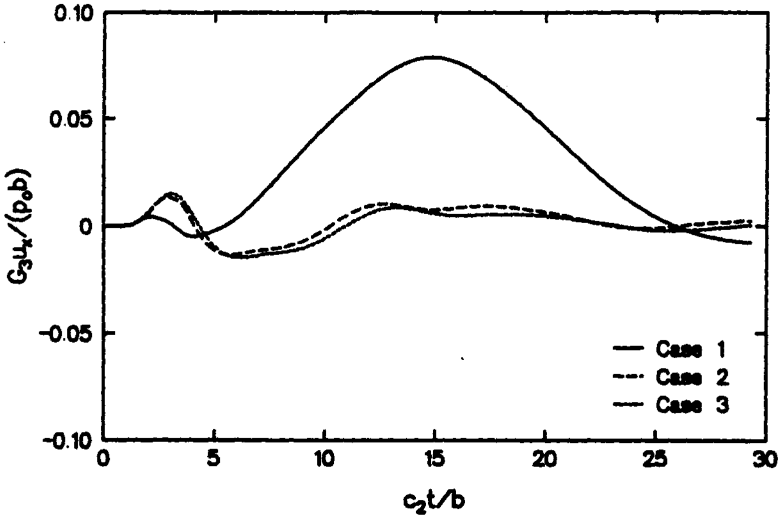

Figure 2.9: Horizontal displacements at Station Q (x/b = 8).

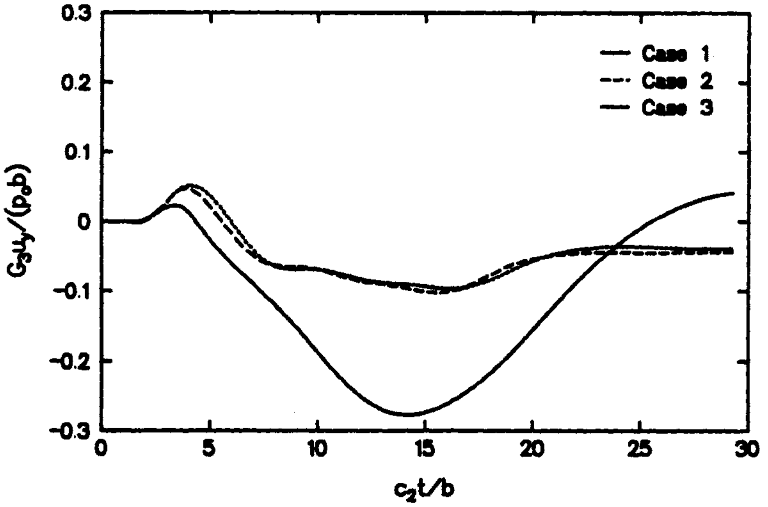

Figure 2.10: Vertical displacements at Station Q (x/b = 8).

indicate that it may be better to simply provide an adequately thick concrete based on bearing capacity considerations for the given base material.

Figures 2.8 and 2.10 show another interesting feature of the results at Stations $P\,(x/b = 3)$ and $Q\,(x/b = 8)$, namely how the maximum vertical displacements are larger for Case 1 than for Cases 2 and 3, which is opposite to the trends observed for the elastostatic results, shown in Figure 2.2. Again, this shows that any evaluation of the loading response of pavement systems should consider both the static and the dynamic results together.

2.3. Conclusions

Two boundary element methods for the analysis of elastostatic and elastodynamic layered pavement problems have been presented. Both methods assume that the pavement system is two-dimensional in nature. These methods have been verified through multiple comparison studies with both existing analytical solutions as well as published numerical results, and have been shown to capture the essence of the elastostatic and elastodynamic loading response of pavement problems. Additionally, the methods have been used to solve multiple layered pavement problems with realistic material properties and geometries to gain insight into the behavior of pavements under static and dynamic loading conditions.

ATTACHMENT

A Two-dimensional Dynamic Direct Boundary Element Method for Piecewise Homogeneous Elastic Media

A THESIS
SUBMITTED TO THE FACULTY OF THE GRADUATE SCHOOL
OF THE UNIVERSITY OF MINNESOTA
BY

Björn Birgisson

IN PARTIAL FULFILLMENT OF THE REQUIREMENTS
FOR THE DEGREE OF
DOCTOR OF PHILOSOPHY

February 1996

To my parents and Grace

Abstract

Two boundary element methods are presented that compute the static and the transient displacements and stresses in piecewise homogeneous bodies. These numerical models are based on the direct boundary element method in which the boundary displacements and tractions for a given body are solved directly in terms of each other. The dynamic boundary element method is based on an implicit time-domain algorithm using a time-stepping scheme. The integrations over each element are carried out analytically, which increases the numerical accuracy and stability of solutions and reduces the computer time and memory requirements.

The methods are well suited for the studying of wave scattering phenomena associated with complicated layer and inclusion problems, such as those encountered in pavement engineering and mining. These methods are verified for a wide variety of problems, ranging in scope from well-defined homogeneous half-plane and layered problems to cases in which more complicated geometries are common, such as in the blasting of underground openings in multi-layered rock. Both methods assume that the boundary is composed of a number of straight-line elements, and both are currently limited to linearly elastic problems where the material is piecewise homogeneous within a given subregion. Two or more subregions can be connected together at an interface to form a body with an arbitrary number of connected subregions.

Acknowledgements

First and foremost, I would like to thank my advisor Professor Steven L. Crouch for first encouraging me to enter the Geomechanics program at the University of Minnesota and then providing me with the financial support, guidance, constant encouragement and excellent computing and graphics facilities needed to complete this thesis. I also thank the Center for Transportation Studies at the University of Minnesota for providing financial support during a critical stage of this work, as well as Barr Engineering Company for providing me with the use of their computing facilities and time off when needed to pursue my studies. In particular, I would like to thank Douglas Barr and Philip Solseng for their support and encouragement, and Richard Gustner for his assistance in preparing some of the figures in this thesis.

I am also indepted to Professor Andrew Drescher for his belief in my abilities, his encouragement, and our many interesting discussions about the behavior of soil and rock, as well as Professors Joe Labuz, Emmanuel Detournay, and Henryk Stolarski for our many discussions and their review of this work. I also thank Professor Theodor Galambos for his encouragement and for sharing his refreshingly down to earth views on life.

I also thank Dr. Eddie Siebrits and Dr. Anthony Peirce for sharing their work on the stability of dynamic boundary element methods, as well as my former colleagues Dr. You Tian and Dr. Marc Loken for their guidance during my first steps into the realm of boundary elements.

Finally, I would like to thank both my parents and Grace for not giving up on me during my long stay in school.

Contents

Abstract i

Acknowledgements ii

1 Introduction 1

1.1 Background 1

1.2 Objective 4

1.3 Scope 5

2 Literature Review 7

2.1 Static Boundary Element Methods 7

2.2 Dynamic Boundary Element Methods 9

2.3 Layers and Inclusions with Boundary Element Methods 14

3 Theory of Linear Elasticity 17

3.1 Governing Equations of Linear Elasticity 18

3.2 Fundamental Solutions in Elastostatics 20

3.3 Fundamental Solutions in Elastodynamics 22

3.4 Influence of Layers and Inclusions on Wave Patterns 26

3.4.1 The Infinite Medium 27

3.4.2 Surface Waves 28

3.4.3 A Finite Thickness Layer on a Half-Plane 29

4 Boundary Integral Equation Formulation 31

4.1 The Elastostatic Integral Representation . . . 32

4.2 The Elastodynamic Integral Representation . . . 33

4.3 The Direct Boundary Element Formulation . . . 35

5 Numerical Implementation 38

5.1 Elastostatic Boundary Element Formulation . . . 39

5.1.1 Spatial Interpolations of Boundary Parameters . . . 42

5.1.2 Piecewise Homogeneous Media in Elastostatics . . . 48

5.2 Elastodynamic Boundary Element Formulation . . . 51

5.2.1 Temporal Interpolations of Boundary Parameters . . . 56

5.2.2 Spatial Interpolations of Boundary Parameters . . . 60

5.2.3 Piecewise Homogeneous Media in Elastodynamics . . . 66

5.3 State of Stress at the Boundary . . . 68

5.4 Interior Displacements, Stresses and Velocities . . . 70

6 Verification and Examples 75

6.1 Elastostatic Problems . . . 76

6.1.1 Annulus Inside a Circular Hole in a Plate . . . 76

6.1.2 A Strip-Loaded Half-plane . . . 77

6.1.3 A Strip-Loaded Layered Half-Plane . . . 81

6.1.4 A Three-Layered Soil System . . . 84

6.2 Elastodynamic Problems . . . 87

6.2.1 Suddenly Loaded Half-plane . . . 89

6.2.2 Triangular Open Trench in a Half-plane . . . 94

6.2.3 Lamb's Problem . . . 98

6.2.4 Selberg's Problem . . . 103

6.2.5 Suddenly Loaded Annulus . . . 105

6.2.6 Wave Propagation Through Layered Material . . . 114

6.2.7 Underground Explosion in a Two-Layered Rock . . . 125

6.3 Numerical Stability and the Size of Time-Step . . . 130

7 Conclusions and Recommendations for Future Work 134

References 136

A Elastostatic Integrations 149

B Elastodynamic Integrations 153

C Derivatives for the Calculation of Interior Dynamic Stresses 161

D Additional Results for Dynamic Problems 164

Chapter 1

Introduction

1.1 Background

Many engineering problems are concerned with the way in which a material deforms in response to suddenly applied loads. Examples of cases in which dynamic loading effects are important include deformations in pavements due to moving wheel loads and stress concentrations around underground excavations caused by blasting, rockbursts and earthquakes. The response of a material to dynamic loading is generally very complicated, because the displacement and stress fields change continuously in both space and time. Accurate modeling of these dynamic changes in displacements and stresses is fundamental to developing safer and more cost effective design procedures for underground structures and pavements.

To model the interaction between the stresses applied on a body and its subsequent deformation, a set of constants that depend on material type are needed. A body whose material constants change from point to point is said to be inhomogeneous. Sometimes it is possible to divide an inhomogeneous body into a finite number of homogeneous portions. Examples of such piecewise homogeneous bodies include soil and rock layers, pavement layers and rock inclusions in an otherwise homogeneous rock mass. In current practice, an exact dynamic analysis of the dynamic load response of such problems is not feasible, even for idealized elastic materials and simplified geometries, because of the wave phenomenon associated with dynamic problems. The reflection and refraction of waves from the interfaces between two or more different media will interfere with the original wave patterns to create new superimposed waves that will again reflect and refract. To model this dynamic behavior, a numerical technique is needed that accounts for the continuous changes in stresses and displacements both in space and time. This numerical technique should be able to model both the transient, short term response due to a dynamic load and the long term steady-state load response of the body. The transient load response tends towards the steady-state or static load response as time increases. In some cases, however, it is only the long term steady-state or static response that is of interest, rather than the short term transient load response. Any numerical model that is to be used in practice should have the option of obtaining just the transient load response, just the static load response, or both the transient and the static load responses.

Numerical methods of analysis for elasticity problems are based on an approximate solution of a differential equation or a set of equations describing a physical problem. Currently, there are three main categories of numerical techniques available. The first widely used method to be developed was the finite difference method which replaces the differential equations describing a physical problem with local linearized expansions for the variables, such as truncated Taylor series. The finite difference method requires both the domain and the boundary of a body to be discretized. A second, more popular method is the finite element method, which is based on variational principles or, sometimes more generally, on weighted residual expressions. The differential equation or its weak formulation is satisfied in an average sense over a finite subdomain, called a finite element. As with the finite difference method, the finite element method requires both the boundary and the domain to be discretized. For complex problems, the necessary number of degrees of freedom can become very large, leading to high computation costs.

The third method is the boundary element method, which, for linear problems, is based on the discretization of the exterior boundary only. The basic idea is to transform the partial differential equations into a corresponding integral description of the boundary effects, in the form of boundary integral equations. Most boundary element formulations for elasticity problems use a reciprocal work theorem that considers the work done by stresses in one solution state on the strains of another distinct solution state. Typically, one of the solution states is a known analytical solution to the governing differential equation. The other solution state consists of the unknown boundary displacements and stresses of the domain of interest. The boundary element method reduces the dimension of the problem by one, with a corresponding saving of computational effort, because only boundaries are discretized.

The boundary element method is well suited to model the semi-infinite boundaries found in pavement systems, as well as the infinite boundaries common to deep tunneling and mining applications (Crouch and Starfield, 1983). This method models the material directly as a semi-infinite or infinite region, consequently satisfying the equilibrium conditions at infinity. Other available numerical techniques such as the finite element method (Zienkiewicz, 1977) and the finite difference method (Cundall, 1971) require the introduction of artificial boundaries to simulate conditions at infinity. These artificial boundaries cause troublesome stress-wave reflections which distort the actual stress wave behavior in the medium. It is possible to evaluate all integrals in a boundary element formulation either numerically or analytically. The use of analytical integration is particularly important in elastodynamic boundary element formulations, because it leads to computational schemes that are more accurate and stable. The use of numerical integration schemes is made very tedious by the singular nature of the kernels and the fact that the kernels have moving jumps at the wavefront. Any numerical integration scheme is very sensitive to the passing of the wave front through an element, despite computationally costly attempts to divide the element into a small number of subsegments as proposed by Israil and Banerjee (1990a). A numerical integration scheme that can satisfactorily deal with these moving jumps currently has not been reported in the literature. Another reason for using analytical integration is in evaluating the "self-effect" coefficients, when the source point lies within the same element as the field point. The integrals involved in evaluating self-effect coefficients are singular. Therefore, the integrals can only be evaluated in the Cauchy Principal Value sense. Again, numerical integration techniques tend not to capture this singular behavior very well.

1.2 Objective

The objective of this study is to develop two numerical computer models that compute the static and the transient displacements and stresses in media consisting of more than one material type. Both of these numerical models are based on the boundary element method in which the boundary displacements and tractions are expressed directly in terms of each other through a system of influence coefficients. The static model is capable of predicting the static or the long term steady-state distribution of stresses and displacements anywhere within a multi-material body. The dynamic model is capable of representing the propagation of stress waves across the interfaces separating two or more different materials, and includes the wave scattering effects of reflection and refraction from these interfaces. The transient displacements and tractions tend towards the steady-state or static solution as time tends to infinity. Both computer models are general in formulation so that they can model both layers of piecewise homogeneous materials and arbitrarily shaped inclusions in an otherwise homogeneous body.

To achieve the stated objective, simplifying assumptions are made about the material behavior and the boundary element formulation. The following assumptions about the material behavior are made: (a) the region of interest is two-dimensional, (b) small displacement theory is used to model the material behavior as linearly elastic, (c) within each layer or inclusion the material is assumed to be isotropic and homogeneous, and (d) continuity of displacements and tractions is assumed across the interface between two different materials. The assumption that the displacements and tractions are continuous across an interface between piecewise homogeneous media in a linear elastic body is needed to solve for the tractions and displacements at the interface. This assumes that no slip or movement takes place across the interface between the two discrete homogeneous regions. The following assumptions about the boundary element formulation are also made: (a) the boundaries of interest are modeled by straight-line boundary elements, (b) boundary displacements and tractions are assumed to vary quadratically over each element, (c) boundary displacements are continuous at boundary element connections, (d) displacements and tractions vary linearly across each time step in the time domain for the dynamic model, and (e) body forces and initial conditions are assumed to be zero.

Both models solve the specified boundary value problem directly. The transient numerical model solves the specified boundary value problem in the time domain using a time-stepping technique. Direct solution in the time domain with the use of straight-line boundary elements allows the fundamental solution to be evaluated analytically.

1.3 Scope

This study focuses on the development of both static and dynamic multi-domain boundary element computer models. In what follows, a description is given of the general mathematical formulation and numerical implementation needed to develop these computer models. Subsequently, the models are applied to a number of new and previously published verification and example problems.

Chapter 2 presents a brief literature review of both static and dynamic boundary element methods, applied to layers and inclusion problems. Section 3 presents the governing equations for linear elastostatics and elastodynamics in the time domain. The fundamental solutions of elastostatics and elastodynamics are discussed and some useful properties of the elastodynamic fundamental solutions are reviewed. The theory of elastodynamic wave propagation in semi-infinite and infinite space is reviewed, and the influence of layers and inclusions on wave patterns is discussed briefly. Chapter 4 presents the boundary integral equation formulation for elastostatics and elastodynamics. Chapter 5 discusses the numerical implementation of the boundary integral equations, given in Chapter 4. Chapter 6 is devoted to a discussion of several example and verification problems that demonstrate the applicability of this work. Finally, Chapter 7 presents conclusions from this study, and recommendations for future work using the elastodynamic boundary element method.

Chapter 2

Literature Review

In this Chapter, the recent history of boundary element development in three main areas is summarized. First, the historical development of static boundary element methods is reviewed. Then, recent developments of elastodynamic boundary element methods are discussed, with a special emphasis on methods in the time domain. Finally, a brief review is given of formulations that deal with the modeling of layers and inclusion problems.

2.1 Static Boundary Element Methods

Boundary element methods are based on transforming the partial differential equations that describe a physical problem into a corresponding integral description of the boundary effects, in the form of boundary integral equations. The English mathematician G. Green was the first one to show how to pass from a differential domain formulation to a boundary integral description. His work is the basis for Betti's (1876) reciprocal theorem, which allows for the solution of an unknown boundary value problem in terms of a known analytical equilibrium solution. This known analytical equilibrium solution is generally referred to as the fundamental solution for the governing differential equation. Somigliana (1885) was the first to use Betti's reciprocal theorem to derive a fundamental solution to Laplace's equation for potential theory applications. Somewhat later, Fredholm (1903) used Somigliana's integral identities to develop existence and uniqueness proofs for the solutions to Laplace's equation.

It is due to the work of the Russian mathematicians Muskhelishivili (1953; 1963), Mikhlin (1957), Smirnov (1964) and Kupradze (1965) that the theory of singular integral equations and the development of integral equation methods made a decisive step forward. These methods were gradually introduced into fluid mechanics and potential theory under names such as "source method" or "indirect method." The term "indirect" implies that the actual boundary conditions were replaced by non-physical surface density functions. The resulting integral equations had singularities in the density functions at any corner or edge of the problem geometry. This formulation requires two steps to solve a boundary value problem. First, solutions that satisfy the specified boundary conditions are obtained in terms of the density function singularities. Second, the rest of the boundary parameters are computed in terms of these singular solutions.

Muskhelishivili and Kupradze were the first to apply these integral equations to elasticity problems. Muskhelishivili formulated the problem with the aid of complex variable theory, which limits the formulation of elasticity problems to two dimensions. To overcome this restriction, Kupradze used Fredholm type of equations that allow for both two- and three-dimensional formulations. Very extensive investigations of the "indirect methods" were performed by, for example, Kellogg (1954), Jaswon (1963), Symm (1963) and Massonet (1966).

In the 1960s various workers started to use computers to solve numerically Fredholm type of nonsingular integral equations. Examples of this include Friedman and Shaw (1962), Banaugh and Goldsmith (1963), and Massonet (1966). Subsequently, Rizzo (1967) developed a computer solution for the singular elasticity formulation in which the unknown boundary displacements and tractions were solved directly. Rizzo's approach is based on writing Somigiliana's identities directly in terms of the physical boundary conditions of an elasticity problem and was therefore termed the direct boundary integral equation method, as opposed to the indirect method, described previously. Today, the literature on boundary element methods in elasticity is more or less divided between the indirect and the direct methods, even though the direct method remains somewhat more favored. Further examples of indirect methods may be found by Benjumea and Sikarskie (1972), Crouch (1976a), Banerjee (1976) and Brady and Bray (1978), while further examples of direct methods are found by Rizzo and Shippy (1968; 1970) and Cruse (1969).

The earliest formulations of the boundary integral equation method used piecewise constant variation of the boundary data, until Cruse (1974) implemented a piecewise-linear interpolation of both the surface geometry and boundary conditions, resulting in a great improvement in accuracy. Lachat and Watson (1976) were the first to implement an isoparametric representation for boundary elements similar to that used in finite element formulations. The method requires numerical integration of the boundary integral equation terms, and a complicated set of algorithms to deal with the singular integral equations. The modeling accuracy may have increased somewhat for curved geometries, but as shown in Chapter 6 in this study, it is possible to model curved boundaries well with a sufficient number of straight-line elements.

2.2 Dynamic Boundary Element Methods

A number of texts summarize the theoretical treatment of linear elastodynamics using integral techniques. The most noteworthy are the texts by Love (1906), Wheeler and Sternberg (1968), Pao and Mow (1973), Achenbach (1973), Graff (1975), Eringen and Suhubi (1975), Miklowitz (1977) and Aki and Richards (1980). General texts that deal with the elastodynamic formulations using the boundary element method are those of Banerjee and Butterfield (1981), Beskos (1987), Manolis and Beskos (1988) and Dominguez (1994). The first application of the boundary element method to elastodynamics was by Banaugh and Goldsmith (1963), who applied the indirect formulation to a steady-state plane elastodynamics problem. Since then, a number of applications have been presented by many authors, demonstrating the versatility and usefulness of elastodynamic boundary element methods.

Today, a survey of the literature reveals that two general approaches have been used for modeling elastodynamic problems by boundary element methods. The first is a transform domain approach, in which the problem is formulated and solved in a Laplace or Fourier integral transform domain. Once the solution has been obtained in the transform domain, the results have to be transformed back to the time domain. The principal advantage of this method is that the problem is easy to formulate in the transform domain, where the problem becomes essentially static. Also, it is relatively easy to incorporate material damping into this formulation, if desired. The second method is based on a time domain formulation that allows the problem to be solved directly using a time-stepping technique. The principal advantages of this method are that rapidly changing loading conditions can be modeled easily, and the fundamental solution can be integrated analytically, resulting in more accurate numerical solutions and faster execution times. It should be noted that transform domain techniques are not capable of incorporating nonlinear behavior, because the transform domain solution is essentially a superposition of steady-state solutions. Nonlinear elastodynamic problems must therefore be solved using the time domain approach.

In general, it can be concluded that transform domain techniques are well suited for linear problems with long and slowly varying time histories, whereas the time domain method is well suited for linear and nonlinear problems with rapidly changing time histories of short duration. As the time history becomes longer, the time domain method becomes more inefficient, because the solution for the current time step is formulated in terms of all the previous time steps.

The first work on a transform domain elastodynamic integral formulation was that of Cruse and Rizzo (1968) and Cruse (1968), who presented a boundary element formulation to solve a wave propagation problem in a half-plane. In their approach, the boundary integral equations were formulated and subsequently solved in the Laplace domain. Then, the results were transformed back into the time domain through a numerical inversion algorithm developed by Papoulis (1957). This transform domain technique was found to give good results only for early times. Later, Manolis (1980) and Manolis and Beskos (1981) used a Fourier transform approach with a more accurate inversion algorithm by Durbin (1974). Niwa et al. (1975; 1976) and Kobayashi and Nishimura (1982) also used Fourier transform methods to solve general two-dimensional elastodynamic problems.

A big computational problem in wave propagation analysis by transform domain methods is the existence, in certain cases, of fictitious eigenfrequencies, which create solution errors. This is particularly prevalent in both half-space and half-plane problems if use is made of the half-space fundamental solution (see, for example, Rizzo et al., 1985; Dominguez and Meise, 1991), as well as in the modeling of underground structures with the full space fundamental solution. This problem can be controlled by using the full-space fundamental function in conjunction with a free surface discretization, or by the introduction of viscoelastic damping.

Currently, most of the reported work in the literature on elastodynamic boundary elements uses transform domain formulations, rather than time-domain formulations. This may be explained partly by the fact that the time-domain formulation is considerably more complicated than the transform domain formulation, and that the nature of the governing partial differential equations in the time-domain is hyperbolic, rather than elliptic as in the transform domain case. Elliptic equations are more amenable to numerical approximations than hyperbolic equations (Cruse, 1987). More importantly, numerical noise can be more easily damped out by the introduction of viscoelastic damping in the transform domain formulation than in the time domain formulation. However, the introduction of artificial damping tends to reduce significantly the amplitudes of predicted displacements and stresses, which cannot be justified on theoretical grounds.

Karabalis and Beskos (1984) were the first to develop general three-dimensional elastodynamic methods in the time domain using the direct boundary integral equation formulation. Later, Ahmad and Banerjee (1988) and Banerjee et al. (1989) presented a three-dimensional time-domain algorithm using higher order variations of the functions in both time and space. However, Karabalis and Beskos (1990) have shown, using a number of boundary element and finite element discretizations, that the results claimed by Banerjee and his co-workers are not consistent with the formulation upon which the results were allegedly based.

In the two-dimensional area, the earlier work in time-domain transient elastodynamics is credited to Cole et al. (1978), even though it was restricted to the anti-plane case. Unfortunately, their method was found to be unstable due to an incorrect numerical treatment of the convolutions involved (Banerjee et al. 1987). Later, Niwa et al. (1980) developed a supposedly two-dimensional transient elastodynamic formulation, by using three-dimensional transient kernels with the third spatial coordinate playing the role of a time-related variable. This formulation was found to contain an error in the time domain kernels (see Siebrits, 1992), which may explain the relatively inaccurate results that they obtained. Mansur (1983) was the first to formulate a time-stepping algorithm using two-dimensional transient kernels. Linear and constant time interpolation functions were used to approximate displacements and tractions, respectively, but constant interpolation functions were used to approximate tractions and displacements over the boundary elements. The time integrations were performed analytically, but the spatial integrations were performed numerically. The traction kernel was derived from the two-dimensional displacement kernel, through a complex manipulation of the Heaviside function present in the displacement kernel. This kernel was obtained by assuming a linear variation of displacements and therefore it can not be used for any other temporal variation, such as a constant variation. Antes (1985) extended this formulation to include non-zero initial conditions. The same formulation was again used by Antes and von Estorff (1986) to study the transient response of strip foundations. Dominguez (1994) extended the formulation used by Mansur to include isoparametric quadratic elements with a constant temporal variation of tractions and a linear variation of displacements with time. In order to evaluate the diagonal self-effect terms of the singular boundary influence coefficients, Dominguez used the method of rigid body motions (see e.g. Brebbia and Dominguez, 1992) which requires that the domain be closed. Israil and Banerjee (1990a; 1990b) presented a two-dimensional transient elastodynamic boundary element formulation, using isoparametric quadratic elements and constant and linear temporal variation of tractions and displacements, respectively. Their formulation is only strictly valid for closed domains, because they use "enclosing elements" in their formulation. Unfortunately, the authors do not explain the concept of "enclosing elements" in sufficient detail in their papers.

An essential difficulty with the isoparametric element formulation is that it requires the use of numerical quadrature to evaluate the boundary integrals. The time-domain formulation does not lend itself easily to the use of numerical integration schemes in the evaluation of the diagonal self-effect terms of the singular boundary influence coefficients, unless the domain is closed (see, for example, Ahmad and Banerjee, 1988; Beskos, 1993). The use of analytical integration schemes is a novel idea in elastodynamic boundary element applications (Tian, 1990; Mack, 1991; Siebrits, 1992; Loken, 1992) and has been shown to lead to highly accurate results, with an associated reduction in computer time.

Tian (1990) was the first to develop two-dimensional direct and indirect time domain boundary element methods, using analytical integrations in both space and time. The direct approach used a linear temporal and a quadratic spatial variation, and the indirect approach used a constant spatial and linear temporal variation. Tian's work was followed by that of Mack (1991), Siebrits (1992) and Loken (1992), who also used time domain formulations with analytical integrations in both space and time. Mack used the fundamental singular solution for a three-dimensional displacement discontinuity in an infinite medium to solve elastodynamics problems having crack-like geometries. He used constant in space and linear in time elements. Siebrits formulated the two-dimensional complement of Mack's work, with linear elements in both space and time. Finally, Loken presented a general three-dimensional indirect elastodynamics formulation. He used linear in time and constant in space elements.

Another contribution by Tian (1990) and Siebrits (1992) dealt with the question of causality. A spatial domain is termed "causal" if (a) the response anywhere within the domain is caused by a source located in the interior or on its boundaries, and (b) the straight-line distance between the source and field points in the domain does not cross the boundary of the domain anywhere. Therefore, a causal domain is just a convex spatial domain in the mathematical sense. Previously, Triantafylliadas and Dasgupta (1987) had concluded that problems involving non-causal domains must be solved using convex subdomains, and they attributed inaccurate results and numerical instabilities in their formulations to non-convex domains. Tian (1990) and Siebrits (1992) demonstrated that this presumed relationship between causal domains and numerical instability was incorrect. They illustrated that the pre-existence of the fundamental solution and the satisfaction of boundary conditions guarantees that the boundary element method is applicable directly to non-causal domains. Recently, however, the causality problem was again brought up by Triantafyllidis (1993) in a study in which the problem of diffraction of SH-waves by a cylindrical cavity in an infinite space was formulated and analytically solved with integral equations that were based on both direct and indirect boundary element formulations. The results of the indirect boundary element method were identical to the exact analytical solution, but the results obtained with the direct boundary element method were not. This issue will be investigated further in the current study (Section 6.2.2).

2.3 Layers and Inclusions with Boundary Element Methods

The methodology of modeling piecewise homogeneous materials with elastostatic boundary element methods has been reasonably well developed. Rizzo and Shippy (1968) were the first to develop a solution procedure based on the direct boundary element formulation to solve a general non-homogeneous elastic inclusion problem. Somewhat later, Butterfield and Tomlin (1972) and Banerjee (1976) employed an indirect method for piecewise homogeneous elastic solids.

In the field of elastodynamic boundary element methods, numerous transform domain formulations exist for modeling layers and inclusion problems. Most of these formulations use full-space fundamental solutions, rather than half-space fundamental solutions, and just extend the surface discretization only a short distance from the region of interest. This approach has been used in the frequency domain (Fourier integral transform domain) for wave propagation in a layered medium by Beskos et al. (1986), Dravinski and Mossessian (1987) and Hadley et al. (1991) under plane strain loading conditions, and for three-dimensional conditions by Abascal and Dominguez

(1986), von Estorff and Schmid (1984), Ahmad and Banerjee (1988), Gaul et al. (1991), Habault (1990) and Chouw et al. (1991). Beskos (1993) has observed that. for most loading conditions, the elements far from the region of interest have very little effect due to the existence of radiation damping both in the fundamental and actual solutions. However, the existence in the actual problem of surface waves which do not damp out produces large inaccuracies for certain frequency ranges in the transform domain. In particular, Emperador et al. (1989) and Gonsalves et al. (1990) have observed that in three-dimensional problems the discretization can be truncated at a distance far enough from the region of interest. In two dimensions, Abascal et al. (1986) and Dominguez and Meise (1991) have observed that some damping has to be introduced, because waves propagate towards infinity at frequencies higher than the first cut-off frequency of the system.

The only time domain formulation of elastodynamic multi-material problems published to date is that by Israil and Banerjee (1990a; 1990b). Their formulation is limited in scope, because it requires that the domain be closed. They also use numerical integration of the spatial integrals, which may in certain cases not be as accurate as analytical integration schemes.

All of the above formulations use some kind of a "substructuring technique" that can be described roughly by the following two steps. First, the boundary integral equations for each material subregion are formulated separately. Second, the appropriate compatibility and equilibrium conditions are enforced at the interface boundaries to formulate the boundary integral equations for each interface. The advantages of the substructuring approach are the following. First, complicated problem geometries can be handled in a straight-forward manner. Second, with proper nodal numbering, the resultant set of algebraic equations can be made banded, which may lead to a reduction in the time required to solve these equations. Third, to obtain results for interior points, only those boundary elements corresponding to the sub-region containing the interior point need be included in the computation. Therefore, the time required to compute results for interior points also is reduced.

The substructuring approach also has disadvantages. First, extra degrees of freedom are introduced at the inter-region boundaries. These extra degrees of freedom offset some of the potential savings in solution time. Second, the numerical form of the boundary integral equation formulation is an equilibrium solution that tries to satisfy the sometimes contradictory states of piecewise variations of surface tractions and surface displacements. This equilibrium state includes various degrees of stress singularities at the connections between boundary elements. The strength of these singularities depends on the types of elements and boundary data approximations being used. Therefore, some errors are always introduced as a result of the boundary data approximations (Cruse, 1988).

Chapter 3

Theory of Linear Elasticity

Although the ultimate goal of this thesis is to describe an elastodynamic boundary element method, it is recognized that an equivalent elastostatic boundary element method should be an integral component of that development. Not only are the solutions to problems of linear elastostatics of great interest in many engineering applications, but the elastostatic solution provides a good check of the elastodynamic results, because the elastodynamic results for infinite domains should always tend towards the elastostatic solution as time goes to infinity. Also, Tian et al. (1990) have shown that engineering problems such as the modeling of blasting of an underground opening require a static initial condition to determine the boundary conditions for the dynamic problem.

In this Chapter, the governing equations for boundary value problems in elastostatics and elastodynamics are reviewed. Then, the fundamental solutions to these governing equations are presented. Finally, highlights of the propagation of elastic waves in infinite and semi-infinite media are discussed, and the scattering and diffraction behavior of elastic waves due to layers and inclusions are reviewed.

Throughout the remainder of this thesis the Cartesian tensor notation is used and Einstein's summation convention is valid. The indices $i, j, k = 1, 2, 3$ represent the Cartesian coordinates x, y, z (or generally x_i). Subscripted indices refer to space, superscripts refer to time, commas indicate spatial differentiation and dots denote time differentiation.

3.1 Governing Equations of Linear Elasticity

Before stresses and displacements can be determined in a body subjected to static or dynamic loading, a boundary value problem must be formulated that allows for the calculation of both displacements and stresses. In elastodynamics this boundary value problem is formulated from the basic equations of linear elastodynamics, which are the equations of motion, the kinematical relationships and the constitutive law relating strains and stresses. In the elastostatic formulation, there are no inertial forces present, whereas in the general elastodynamic case inertial effects have to be included in the formulation. In the following, first the elastodynamic case is reviewed. Then, the elastostatic case is presented and shown to be a special case of the elastodynamic case.

The equations of motion can be written as

$$\sigma_{ji,j} + \rho b_i = \rho \ddot{u}_i \tag{3-1}$$

in which ρ is the material density, u_i is the displacement vector, b_i is the body force vector per unit mass, and σ_{ij} is the stress tensor. The kinematical equations relate the strain tensor ϵ_{ij} to the displacements as

$$\epsilon_{ij} = \frac{1}{2}\left(u_{i,j} + u_{j,i}\right) \tag{3-2}$$

The constitutive law that relates strains to stresses for a homogeneous, isotropic, linear elastic material is

$$\sigma_{ij} = \lambda \epsilon_{kk} \delta_{ij} + 2G\epsilon_{ij} \tag{3-3}$$

in which λ is a material constant called a Lamé constant, G is the shear modulus, and δ_{ij} is the Kronecker delta ($\delta_{ij} = 1$ if $i = j$; $\delta_{ij} = 0$ if $i \neq j$). Substitution of equations (3.2) and (3.3) into (3.1) results in the desired displacement form of the equations of motion

$$\left(c_1^2 - c_2^2\right) u_{j,ji} + c_2^2 u_{i,jj} + f_i = \ddot{u}_i \tag{3-4}$$

in which $f_i = \rho b_i$ is the body force vector and c_1 and c_2 are the compressional and shear wave velocities of the material. These velocities are material dependent and can be defined in terms of the elastic constants and material density as $c_1^2 = (\lambda + 2G)/\rho$ and $c_2^2 = G/\rho$.

This form (3-4) of the equations of motion, which is often referred to as the Navier-Cauchy equations, must be accompanied by initial and boundary conditions to represent a well-posed elastodynamic problem. At every point $\underline{x} \in V$, where V denotes the internal volume of the loaded body, the displacements and velocities must satisfy the initial conditions

$$\begin{aligned} u_i(\underline{x}, 0) &= \overset{\circ}{\bar{u}}_i(\underline{x}) \\ \dot{u}_i(\underline{x}, 0) &= \overset{\circ}{\bar{v}}_i(\underline{x}) \end{aligned} \tag{3-5}$$

and at every point $\underline{x}$, for time $t > 0$, the tractions $t_j(\underline{x}, t)$ and displacements $u_j(\underline{x}, t)$ are prescribed as

$$\begin{aligned} t_i &= \sigma_{ji} n_j = \bar{t}_i(\underline{x}, t) && \text{on } \underline{x} \in S_t \\ u_i &= \bar{u}_i(\underline{x}, t) && \text{on } \underline{x} \in S_u \end{aligned} \tag{3-6}$$

in which n_j is the i-th component of the outward unit normal of boundary S at a given point $\underline{x} \in S$, and where S_u and S_t denote the portions of the boundary $S = S_u + S_t$ on which the displacements and tractions are specified. For a properly posed boundary value problem, u_i is unknown on S_t and t_i is unknown on S_u.

In the elastostatic case, there are no inertial forces and (3-1) can be written as

$$\sigma_{ji,j} + \rho b_i = 0 \tag{3-7}$$

The displacement form of the equilibrium equations is obtained by substituting the kinematic equations (3-2) and the constitutive equations (3-3) into (3-7), resulting in

$$\left(\alpha^2 - \beta^2\right) u_{j,ji} + \beta^2 u_{i,jj} + f_i = 0 \tag{3-8}$$

which is equivalent to (3-4) without the inertial effects. In the absence of body forces, (3-8) can be written as

$$\frac{1}{1-2\nu} u_{j,ji} + u_{i,jj} = 0 \tag{3-9}$$

in which ν denotes the Poisson's ratio, which is related to λ and G as $\nu = 0.5\lambda / (\lambda + G)$. A well-posed boundary value problem in elastostatics requires that at every point $\underline{x} \in S$ the tractions $t_j(\underline{x})$ and displacements $u_j(\underline{x})$ are prescribed as

$$\begin{aligned} t_i = \sigma_{ji} n_j = \bar{t}_i(\underline{x}) \quad & \text{on } \underline{x} \in S_t \\ u_i = \bar{u}_i(\underline{x}) \quad & \text{on } \underline{x} \in S_u \end{aligned} \tag{3-10}$$

which is the equivalent to (3-6), without the time component.

3.2 Fundamental Solutions in Elastostatics

The direct boundary element method for linear elastostatics in two dimensions relies on Kelvin's solution (Sokolnikoff, 1956) of (3-8) due to a concentrated unit line load acting in the j-direction at a point in an infinite elastic solid. If $\underline{\xi}$ denotes the source point at which the load is applied, and $\underline{x}$ denotes the field point at which the effects of the load are evaluated, then the displacements caused by the unit line load applied at $\underline{\xi}$ can be written in the form

$$u_i = U_{ij}\left(\underline{x}, \underline{\xi}\right) e_j \tag{3-11}$$

where $U_{ij}\left(\underline{x}, \underline{\xi}\right)$ represents the displacements in the i-direction at point $\underline{x}$ corresponding to the unit line load e_j at the source point $\underline{\xi}$. This solution is called the fundamental solution of two-dimensional elastostatics, and the tensor expression $U_{ij}\left(\underline{x}, \underline{\xi}\right)$ is given by (see, for example, Kuhn, 1988)

$$U_{ij}\left(\underline{x}, \underline{\xi}\right) = -\frac{1}{8\pi(1-\nu)G}\left\{(3-4\nu)\ln(r)\,\delta_{ij} - r_{,i}\, r_{,j}\right\} \tag{3-12}$$

for the two-dimensional plane strain problem. In these expressions, r denotes the distance between the field point $\underline{x}$ and the source point $\underline{\xi}$ and can be written as

$$r\left(\underline{x}, \underline{\xi}\right) = \sqrt{(x_i - \xi_i)(x_i - \xi_i)} \tag{3-13}$$

The derivatives of $r\left(\underline{x},\underline{\xi}\right)$ with the respect to the coordinates of $\underline{x}$ are

$$r_{,i} = \frac{\partial r}{\partial x_i} = \frac{r_i}{r} \tag{3-14}$$

in which $r_i = x_i - \xi_i$.

Sometimes it is preferred to write the tensor $U_{ij}\left(\underline{x},\underline{\xi}\right)$ in terms of a function $g\left(\underline{x},\underline{\xi}\right)$, which is given by

$$g\left(\underline{x},\underline{\xi}\right) = -\frac{1}{4\pi\left(1-\nu\right)}\ln r \tag{3-15}$$

This results in a new form for the tensor $U_{ij}\left(\underline{x},\underline{\xi}\right)$, which can be written as

$$U_{ij}\left(\underline{x},\underline{\xi}\right) = \frac{1}{2G}\left\{\left(3-4\nu\right)g\delta_{ij} - r_j g_{,i}\right\} \tag{3-16}$$

The stress tensor can be derived by applying Hooke's law (3-3) to the displacement tensor $U_{ij}\left(\underline{x},\underline{\xi}\right)$, resulting in

$$S_{ijk} = \lambda U_{mk,m}\delta_{ij} + G\left(U_{ik,j} + U_{jk,i}\right) \tag{3-17}$$

in which S_{ijk} denotes the stress tensor, σ_{ij}, due to a line load in the k-direction. Using (3-17) results in

$$S_{ijk} = \left\{\left(1-2\nu\right)\left[\delta_{ij}g_{,k} + \delta_{jk}g_{,i}\right] - r_j g_{,ik} + 2\nu\delta_{ik}g_{,j}\right\} \tag{3-18}$$

In the boundary element formulation, the stresses are expressed in terms of tractions t_i on the boundary. These tractions can be written as

$$t_i = T_{ij}e_j \tag{3-19}$$

in which the tensor T_{ij} represents the boundary traction in the i-th direction at point $\underline{x}$, due to the concentrated line load at location $\underline{\xi}$ in the j-direction. For a given unit outward normal n_k, the tensor function T_{ij} can be computed from the stress tensor

(3-18) as

$$T_{ij} = S_{kij} n_k \tag{3-20}$$

The fundamental displacements (3-11) and tractions (3-19) form the basic building blocks of the direct boundary element formulation in elastostatics.

3.3 Fundamental Solutions in Elastodynamics

The boundary element method for linear elastodynamics is based on Stokes's (1883) fundamental solution to the Navier-Cauchy equations of motion (3-4), due to a time-varying concentrated unit load in an infinite domain. The form of the applied time-varying load determines the nature of the fundamental singular solution. In three dimensions, the singular solution describes the displacements generated in time and space by a time-varying unit load in space, whereas in two dimensions the singular solution describes displacements caused by a time-varying line load extending infinitely in a direction perpendicular to the two-dimensional plane, because the two-dimensional solution is obtained by integrating the three-dimensional solution from negative to positive infinity along the x_3 axis. These loading differences between the two- and three-dimensional cases produce a basic difference in the way localized external disturbances generate displacement fields in two and three dimensions.

The three-dimensional solution is due to a load that is applied at a single instant in space and time, and once the waves have passed the point of interest, $\underset{\sim}{x}$, the fundamental solution returns to zero. Any external disturbance of finite duration that is applied at a source point $\underset{\sim}{\xi}$ is observed later with an unchanged time history at any different field point $\underset{\sim}{x}$. This preservation of the time history, called Huygen's principle (see e.g. Achenbach, 1973), is not valid in two dimensions, because the two-dimensional fundamental solution never returns to its original value after the first arrival of the waves. Signals emitted from different points on the line source continue to arrive at the point $\underset{\sim}{x}$ at all later times, creating the appearance of a distinctive "tail" in the two-dimensional fundamental solution (Eringen and Suhubi, 1975).

The displacements u_i at point $\underset{\sim}{x}$ caused by the unit line load at $\underset{\sim}{\xi}$ are given by

(Eringen and Suhubi, 1975)

$$u_i = U_{ij}\left(\underline{x}, t; \underline{\xi}, \tau = 0 \mid f(t)\right) e_j \tag{3-21}$$

in which the fundamental solution tensor U_{ij} represents the displacements in the i-direction at point $\underline{x}$ and time t, due to a line load acting in the j-direction at location $\underline{\xi}$, applied at time $\tau = 0$ and with a time variation described by a specified function $f(t)$. The tensor U_{ij} is given as (Eringen and Suhubi, 1975)

$$\begin{aligned} U_{ij}\left(\underline{x}, t; \underline{\xi}, \tau = 0 \mid f(t)\right) = {} & \frac{1}{2\pi\rho}\left\{\frac{\partial^2}{\partial\xi_i\partial\xi_j}\left[H\left(t - \frac{r}{c_1}\right)\int_r^{c_1 t}\frac{d\eta}{\sqrt{\eta^2 - r^2}}\right.\right. \\ & \left. \times \int_0^{t-\eta/c_1} \nu f\left(t - \frac{\eta}{c_1} - \nu\right) d\nu\right] \\ & - H\left(t - \frac{r}{c_2}\right)\int_r^{c_2 t}\frac{d\eta}{\sqrt{\eta^2 - r^2}} \times \\ & \int_0^{t-\eta/c_2} \nu f\left(t - \frac{\eta}{c_2} - \nu\right) d\nu \\ & \left. + \frac{\delta_{ij}}{c_2} H\left(t - \frac{r}{c_2}\right)\int_r^{c_2 t} f(t - \eta)\frac{d\eta}{\sqrt{\eta^2 - r^2}}\right\} \end{aligned} \tag{3-22}$$

in which $i, j = 1, 2$ and $H(t)$ denotes the Heaviside function. Also, $r = \sqrt{r_i r_i}$ is the distance between $\underline{x}$ and $\underline{\xi}$, $r_i = x_i - \xi_i$, δ_{ij} is the Kronecker delta and c_1 and c_2 are the compressional and shear wave velocities, respectively (see Section 3.4.1).

For simplicity of presentation, the load function $f(t)$ was assumed to start at time τ equal to zero. For any other desired starting time τ, the variable t in the fundamental solution should be replaced by a new variable, $t - \tau$. Assuming a linear temporal variation $f(t) = t$ allows (3-22) to be integrated analytically,

$$\int_0^{t-\eta/c_\alpha} \nu f\left(t - \frac{\eta}{c_\alpha} - \nu\right) d\nu = \int_0^{t-\eta/c_\alpha} \nu\left(t - \frac{\eta}{c_\alpha} - \nu\right) d\nu = \frac{1}{6}\left(t - \frac{\eta}{c_\alpha}\right)^3 \tag{3-23}$$

This result leads to

$$\begin{aligned}
&\int_{r}^{c_\alpha t} \frac{1}{\sqrt{\eta^2 - r^2}} \left(t - \frac{\eta}{c_\alpha}\right)^3 d\eta = \frac{t}{2}\left(\frac{t^2}{3} + \frac{r^2}{2c_\alpha^2}\right)\cosh^{-1}\left(\frac{c_\alpha t}{r}\right) \\
&-\frac{}{18c_\alpha}\left(\frac{11}{2}t^2 + 2\frac{r^2}{c_\alpha^2}\right)\sqrt{c_\alpha^2 t^2 - r^2}
\end{aligned} \tag{3-24}$$

in which $c_\alpha = c_1$ or c_2. Substitution of (3-23) and (3-24) into (3-22) gives

$$\begin{aligned}
U_{ij} \;=\; & \frac{1}{2\pi\rho}\Bigg\{ H\left(t - \frac{r}{c_1}\right)\frac{1}{c_1^3}\Bigg[\frac{r_i r_j}{3r^4}\left(c_1^2 t^2 - r^2\right)^{\frac{3}{2}} - \delta_{ij}\Bigg(\frac{1}{3}\sqrt{c_1^2 t^2 - r^2} \\
& + \frac{c_1^2 t^2}{6r^2}\sqrt{c_1^2 t^2 - r^2} - \frac{c_1 t}{2}\cosh^{-1}\left(\frac{c_1 t}{r}\right)\Bigg)\Bigg] \\
& - H\left(t - \frac{r}{c_2}\right)\frac{1}{c_2^3}\Bigg[\frac{r_i r_j}{3r^4}\left(c_2^2 t^2 - r^2\right)^{\frac{3}{2}} - \delta_{ij}\Bigg(\frac{1}{3}\sqrt{c_2^2 t^2 - r^2} \\
& + \frac{c_2^2 t^2}{6r^2}\sqrt{c_2^2 t^2 - r^2} - \frac{c_1 t}{2}\cosh^{-1}\left(\frac{c_1 t}{r}\right)\Bigg)\Bigg] \\
& + H\left(t - \frac{r}{c_2}\right)\frac{\delta_{ij}}{c_2^3}\left(c_2 t\cosh^{-1}\left(\frac{c_2 t}{r}\right) - \sqrt{c_2^2 t - r^2}\right)\Bigg\}
\end{aligned} \tag{3-25}$$

Just as in the elastostatic case, the stress tensor can be obtained by applying Hooke's law (3-3) to the displacement tensor (3-25) to get

$$S_{ijk} = \rho\left[\left(c_1^2 - 2c_2^2\right)U_{mk,m}\delta_{ij} + c_2^2\left(U_{ik,j} + U_{jk,i}\right)\right] \tag{3-26}$$

in which S_{ijk} denotes the stress tensor, σ_{ij}, due to a time-varying line load in the k-direction. Using (3-26) results in

$$\begin{aligned}
S_{ijk} \;=\; & \frac{1}{2\pi}\Bigg\{ H\left(t - \frac{r}{c_1}\right)\frac{c_{21}^2}{c_1}\Bigg[\frac{2}{3r^4}\left(\delta_{ij}r_k + \delta_{kj}r_i + \delta_{ik}r_j\right)\left(c_1^2 t^2 - r^2\right)^{\frac{3}{2}} \\
& - \frac{2r_i r_j r_k}{r^4}\left(\sqrt{c_1^2 t^2 - r^2} + \frac{4}{3r^2}\left(c_1^2 t^2 - r^2\right)^{\frac{3}{2}}\right) \\
& + \left(2 - c_{12}^2\right)\frac{r_k \delta_{ij}}{r^2}\sqrt{c_1^2 t^2 - r^2}\Bigg] \\
& - H\left(t - \frac{r}{c_2}\right)\frac{1}{c_2}\Bigg[\frac{2}{3r^4}\left(\delta_{ij}r_k + \delta_{kj}r_i + \delta_{ik}r_j\right)\left(c_2^2 t^2 - r^2\right)^{\frac{3}{2}} \\
& - \frac{2r_i r_j r_k}{r^4}\left(\sqrt{c_2^2 t^2 - r^2} + \frac{4}{3r^2}\left(c_2^2 t^2 - r^2\right)^{\frac{3}{2}}\right)
\end{aligned} \tag{3-27}$$

$$+\frac{\delta_{ik}r_j+\delta_{jk}r_i}{r^2}\sqrt{c_2^2t^2-r^2}\Bigg]\Bigg\}$$

Just as in the elastostatic boundary element formulation, the stresses inside the body are expressed in terms of tractions t_i on the boundary. These tractions can be written by (3-19), in which case the tensor T_{ij} in (3-20) now represents the boundary traction in the i-th direction at point $\underline{x}$, due to the concentrated time-varying line load $f(t)$ acting at location $\underline{\xi}$ in the j-direction. The resulting fundamental displacements and tractions are the foundations upon which the elastodynamic boundary element formulation in this study is built.

The fundamental solution tensor U_{ij} has three important properties: causality, symmetry and time translation. The causality property implies that a receiving point can only experience effects of a load that is applied at a source point after the fastest wave arrives from the source point. Therefore, the fundamental solution tensor $U_{ij}\left(\underline{x},t;\underline{\xi},\tau \mid f(t)\right)$ is identically zero if $t-\tau<0$. The causality property controls the analytical integration process in the direct boundary element formulation, because it implies that integration need only be done over elements and parts of elements that are dynamically active. The traction tensor $T_{ij}\left(\underline{x},t;\underline{\xi},\tau \mid f(t)\right)$ also obeys causality. The second property is the symmetry property, which can be written as

$$U_{ij}\left(\underline{x},t;\underline{\xi},\tau \mid f(t)\right)=U_{ij}\left(\underline{\xi},\tau;\underline{x},t \mid f(t)\right) \tag{3-28}$$

This property implies that the dynamic effects at point $\underline{x}$ due to a load applied at point $\underline{\xi}$ are the same as the effects at point $\underline{\xi}$ due to a load applied at point $\underline{x}$. The traction tensor $T_{ij}\left(\underline{x},t;\underline{\xi},\tau \mid f(t)\right)$ does not follow the symmetry property. The last important property is the time translation property, which states that time need only be measured relative to the time of application of the load. Mathematically, this can be written as

$$U_{ij}\left(\underline{x},t;\underline{\xi},0 \mid f(t)\right)=U_{ij}\left(\underline{x},t+\tau;\underline{\xi},\tau \mid f(t)\right) \tag{3-29}$$

in which τ denotes an arbitrary time increment. The time translation property implies that the dynamic history of the solution need only be expressed in terms of incremental time. It should be noted that the the traction tensor $T_{ij}\left(\underline{x}, t; \underline{\xi}, \tau \mid f(t)\right)$ also obeys the time translation property. In this study, the time-translation property is used repeatedly during the temporal discretization of the equations, resulting in a numerical formulation that uses incremental time, rather than absolute time, and thereby reducing substantially the amount of computation that is required to account for the dynamic history of a given problem.

3.4 Influence of Layers and Inclusions on Wave Patterns

It has been shown (e.g., Tian, 1990, Siebrits, 1992) that the boundary element method for elastodynamics can accurately predict the arrival times and magnitudes of waves in a elastic body. The characteristics of these waves govern the displacements and stresses in the body. The elastodynamic part of this study focuses on predicting displacements and stresses due to waves that are initiated by a loaded boundary in media consisting of multiple material types, such as layered media and materials with inclusions of finite spatial extent. The wave behavior associated with these problems is generally very complicated. When a wave propagating in a medium encounters an inclusion or an interface between adjacent layers, it undergoes reflection and refraction, which is a process that produces new waves that propagate inside and/or outside the inclusion or the adjacent layer. This phenomenon is known as diffraction (see, for example, Eringen and Suhubi, 1975) when the incoming wave impinges on an inclusion with sharp edges, and scattering when the incoming wave impinges on a smooth material interface. Any treatment of a diffraction/scattering problem with elastodynamic boundary element methods is based on the numerical solution to the Navier-Cauchy equations (3-4), with appropriate boundary conditions at the surface of the scatterer. These boundary conditions can be simple, such as in the case of a partially loaded half-plane or a traction-free underground opening, or complicated such as in the case of multiple material interfaces associated with a layered material.

To gain an appreciation for the different types of wave behavior that can arise in plane strain diffraction/scattering problems, it is necessary to review briefly the more common types of waves associated with linear elastic media. The nature of these waves depends on the material type and the geometry of the media, but three highly idealized cases can be identified to provide insight into more complicated wave scattering behavior: (1) an infinite medium, (2) a half-plane, which is either in contact with air or with another half-plane, and (3) a layer resting on a half-plane.

3.4.1 The Infinite Medium

Only two types of waves can propagate through a solid, isotropic, homogeneous medium of infinite extent. These waves are called compressional and shear waves. Sometimes the compressional wave is called a primary wave (P-wave) and the shear wave is called a secondary (S-wave). Each wave has a distinct velocity vector associated with it that depends on the properties of the elastic medium. Compressional waves travel through the medium with a particle velocity pointed in the direction of wave propagation, whereas shear waves travel through the medium with a particle velocity vector that is perpendicular to the direction of wave propagation. The displacement vector of a shear wave can be decomposed into two-components, one in the (x_1, x_2) plane and the other perpendicular to it. The former is called an SV-wave (vertically polarized shear wave), while the latter is known as an SH-wave (horizontally polarized shear wave). The P- and SV-waves constitute components of a plane motion, whereas the SH-waves represent anti-plane motion.

When a wave impinges on a discontinuity in the medium, other types of waves may be formed. The nature of these newly formed waves depends on the boundary conditions of the discontinuity. It has been found (e.g., Kolsky, 1953) that when a wave of either the compressional or shear type impinges on a boundary between two media, both reflection and refraction take place (See Figure 3-1). In the most general case, a shear or compressional wave will produce both shear and compressional reflected and refracted waves.

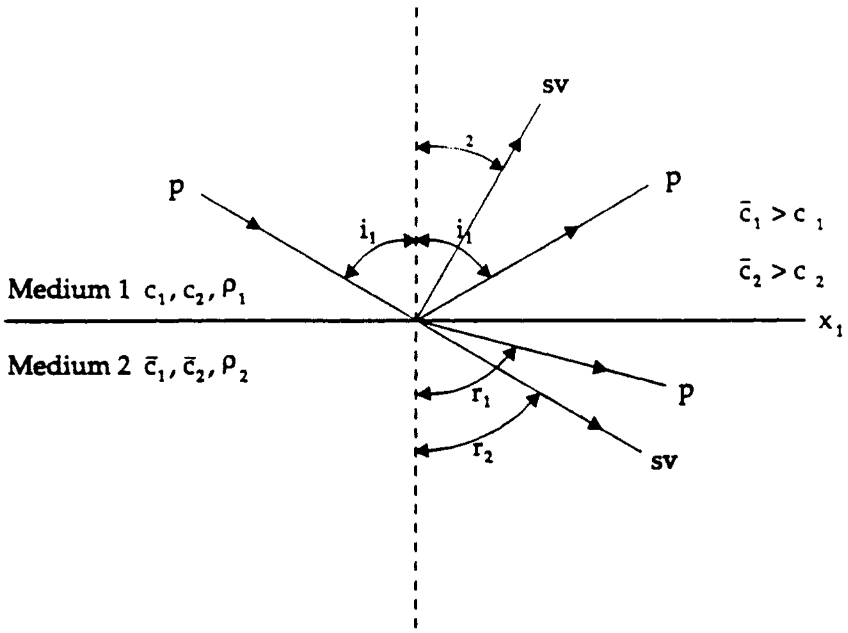

Figure 3-1: Reflection and refraction of a plane wave at an interface.

3.4.2 Surface Waves

There are some special boundary conditions that produce new types of waves. An important example is a half-plane in contact with either air or another half-plane, in which cases waves are formed at the interface between the two media. These waves propagate parallel to the material interface. The type of wave formed depends on the nature of the two media. If one medium is air, a surface wave called a Rayleigh wave is formed, and when both media are solids an interface wave called a Stoneley wave results.

Rayleigh waves are formed when compressional and shear waves are forced to meet the boundary conditions associated with a free boundary. In this case, wave refraction can be ignored, and only reflections need be considered (see, for example, Eringen and Suhubi, 1975). This results in a characteristic equation that determines the velocity of the wave. Rayleigh waves have two main characteristics. The first is that the displacements decay exponentially with distance from the free surface, such that the wave penetrates only a distance of about twice its wavelength into the interior of a body. The second is that the wave velocity is independent of frequency. Such waves are said to be non-dispersive. An important characteristic of non-dispersive waves is that they do not change their shape as they travel.

Stoneley waves are formed when compressional and shear waves are forced to meet the boundary conditions associated with an interface between two different elastic solids in welded contact. They exist only under complicated requirements about the ratio of material densities and shear wave velocities associated with the two solids. These conditions have been the focus of many studies (e.g. Cagniard (1939; 1962), Sezawa and Kanai (1939) and Scholte (1947), Koppe (1948)) and are beyond the scope of this study. A useful discussion about some of the findings from these studies is provided by Brekhovskikh (1980). An important finding by Scholte was that for seismic waves it can be reasonably assumed that the ratio of mass densities of the two adjacent media is close to unity, so Stoneley waves can occur only if two adjacent media have nearly equal shear moduli. It should also be noted that Stoneley waves are non-dispersive just like Rayleigh waves.

3.4.3 A Finite Thickness Layer on a Half-Plane

The introduction of a finite length scale (such as a finite layer thickness) into a problem, results in dispersive surface waves that are sometimes referred to as generalized Rayleigh waves (Eringen and Suhubi, 1975). A simple and illustrative example of this phenomenon is the case of a finite layer resting on a half-plane. In this case, the surface waves traveling along the layer are dispersive, resulting in a dependence of the velocity of propagation on the frequency of the waves. For example, in the simplified case of harmonic waves, each simple harmonic constituent of the initial disturbance travels with a different velocity, and, therefore, the shape of the initial disturbance will be altered as it travels. The disturbance will spread out into trains of waves, resulting in an oscillatory motion in the x_2-direction propagating in the x_1-direction. The disturbances in the layer decay exponentially with depth in the substratum, resulting in most of the wave activity being focused within the finite thickness layer. These oscillatory surface waves can only happen when the body wave velocities of the layer are less than those of the underlying half-plane, namely when $c_2 < c_1 < c < \bar{c}_2 < \bar{c}_1$, in which c_1 and c_2 are the compressional and shear wave velocities of the upper layer, $\bar{c}_1$ and $\bar{c}_2$ are the compressional and shear wave velocities of the underlying half-plane, and c is the propagational wave velocity of the generalized Rayleigh wave. A detailed discussion on generalized Rayleigh waves can be found in Achenbach (1973), Eringen and Suhubi (1975) and Aki and Richards (1980).

An extension of the case of a finite layer on a half-plane to the case of a number of layers of finite thickness may lead to the formation of interface waves that are similar to Stoneley waves, except that they are dispersive in nature. The occurrence of these waves is dictated by the same conditions that govern the existence of Stoneley waves, with the additional requirement that at least one of the adjacent layers be of finite thickness.

Chapter 4

Boundary Integral Equation Formulation

The basis for the boundary element method in elasticity is that the displacements and stresses inside an elastic domain are determined uniquely by the boundary displacements and tractions of that domain (Love, 1906). The basic idea behind the method is to transform the governing partial differential equations of linear elasticity presented in Chapter 3 into a corresponding integral representation of the boundary effects in the form of boundary integral equations. These transformations are presented in this chapter for both elastostatics and elastodynamics. Betti's reciprocal work theorem is used to obtain the elastostatic integral representation, whereas Graffi's (1947) reciprocal theorem is used in the elastodynamic case. Graffi's reciprocal theorem is the dynamic equivalent of Betti's theorem.

The integral representations for both elastostatics and elastodynamics involve two different elasticity solutions, of which one has to be a known analytical solution. The unknown solution states consist of the boundary displacements and tractions at the boundary of the domain of interest. The known solution state is chosen so that it accommodates arbitrary distributions of these unknown boundary displacements and tractions. The fundamental solutions presented in Chapter 3 have the necessary properties needed for a known solution state.

4.1 The Elastostatic Integral Representation

To obtain an integral description of a boundary value problem, it is necessary to first transform an equivalent problem described by the partial differential equations to one described by integral equations. The resulting integral equations require discretization only over the boundary of the domain, thus reducing the dimension of the problem by one. The boundary integral formulation can be deduced in different ways. Within linear elastostatics the derivation can be performed by (a) Green's third identity, (b) Somigliana's identity, (c) weighted residual methods or (d) Betti's reciprocal work theorem. The classical way of derivation is based on Betti's theorem, and this is the method that will be described below. Other methods are discussed in great detail by Brebbia et al. (1984), Cruse (1988) and Kuhn (1988).

Betti's theorem relates the actual unknown distribution of displacements and tractions on the boundary of a domain and body forces (u_i, t_i, b_i) to a reference solution state $(\bar{u}_i, \bar{t}_i, \bar{b}_i)$:

$$\int_S t_i \bar{u}_i dS + \int_V b_i u_i dV = \int_S \bar{t}_i u_i dS + \int_V \bar{b}_i u_i dV \tag{4-1}$$

in which S is the boundary of the elastic domain V. In the classical boundary element formulation the fundamental Kelvin solution (3-9) of a unit line load applied to an arbitrary source point $P\left(\underline{\xi}\right)$, with $\underline{\xi} \in V$ is considered for the reference solution state. The unit line load acts in either of the two orthogonal directions, indicated by the unit vector e_i. This can be represented with a body force description

$$\bar{b}_i = \delta\left(\underline{x}, \underline{\xi}\right) e_i \tag{4-2}$$

where $\delta\left(\underline{x}, \underline{\xi}\right)$ represents the Kronecker delta function, $\underline{\xi}$ indicates the source point and $\underline{x}$ the current field point. Each component of the unit line load causes corresponding displacements and tractions, which can be written in the form

$$\bar{u}_i(\underline{x}) \quad = \quad U_{ij}(\underline{x}, \underline{\xi}) e_j \tag{4-3}$$

$$\bar{t}_i(\underline{x}) \quad = \quad T_{ij}(\underline{x},\underline{\xi})e_j$$

where U_{ij} and T_{ij} are given by (3-16) and (3-20), respectively. In the absence of body forces in the unknown solution state, substitution of (4-3) into (4-1) leads to (Love, 1906):

$$\epsilon\left(\underline{\xi}\right) u_i\left(\underline{\xi}\right) = \int_S t_j\left(\underline{x}\right) U_{ij}\left(\underline{x},\underline{\xi}\right) ds\left(\underline{x}\right) - \int_S u_j\left(\underline{x}\right) T_{ij}\left(\underline{x},\underline{\xi}\right) ds\left(\underline{x}\right) \tag{4-4}$$

in which $\underline{\xi} \notin S$ and ϵ is defined as

$$\epsilon\left(\underline{\xi}\right) = \begin{cases} 0 & \underline{\xi} \notin V \\ 1 & \underline{\xi} \in V \end{cases} \tag{4-5}$$

The identities (4-4) and (4-5) form an integral representation that relates an unknown elastostatics solution state (u_i, t_i) to a known fundamental solution state $(\bar{u}_i, \bar{t}_i)$. This integral representation can be used to determine displacements u_i within the domain V. The case $\epsilon\left(\underline{\xi}\right) = 1$ for $\underline{\xi} \in V$ is the well-known Somigliana's identity.

4.2 The Elastodynamic Integral Representation

The reciprocal work theorem between two elastodynamic states extends Betti's static reciprocal theorem (4-1) to include inertial forces and time history of loading. This theorem was first stated by Graffi (1947) for bounded domains, and later extended by Wheeler and Sternberg (1968) to include unbounded domains. The similarity of the equations in this section to those in the previous section will be apparent, illustrating that the elastodynamic boundary element formulation in the time domain is a direct extension of the elastostatic formulation.

The dynamic reciprocal theorem relates two distinct elastodynamic solution states of displacements, tractions and body forces that satisfy the Navier-Cauchy equations (3-4) on a regular domain V; the first is the unknown solution state (u_i, t_i, b_i) with initial and boundary conditions defined by equations (3-5) and (3-6), and the second is a known reference solution state $(\bar{u}_i, \bar{t}_i, \bar{b}_i)$. Assuming that the solution states have a quiescent past and that the initial conditions are zero, Graffi's (1947) dynamic reciprocal theorem can be written as:

$$\int_0^t\int_S \bar{t}_i u_i dS d\tau + \int_0^t\int_V \bar{b}_i u_i dV d\tau = \int_0^t\int_S t_i \bar{u}_i dS d\tau + \int_0^t\int_V b_i \bar{u}_i dV d\tau \tag{4-6}$$

In the elastodynamic boundary element formulation the fundamental displacement solution (3-21) of a line load $\delta(\underline{x}-\underline{\xi})\delta(\underline{t}-\underline{\tau})e_j$ applied to an arbitrary source point $\underline{\xi}$, with $\underline{\xi} \in V$, is considered for the reference solution state. The equivalent fundamental solution tractions $\bar{t}_i$ can be obtained by first substituting (3-27) into (3-20) and then using (3-19) to obtain $\bar{t}_i$. If it is assumed that the body forces in the unknown solution state are absent, then the displacement u_j in V can be expressed in terms of integrals of the tractions and displacements on S as follows:

$$\epsilon\left(\underline{\xi}\right) u_i\left(\underline{\xi},t\right) = \int_S U_{ij}\left(\underline{x},t;\underline{\xi},0 \mid t_j\left(\underline{x},t\right)\right) ds\left(\underline{x}\right) - \int_S T_{ij}\left(\underline{x},t,\underline{\xi},0 \mid u_j\left(\underline{x},t\right)\right) ds\left(\underline{x}\right) \tag{4-7}$$

in which ϵ is defined by equation (4-5), U_{ij} is the fundamental solution tensor given by (3-25) and T_{ij} is obtained by substituting (3-27) into (3-20). The time t is the receiving time of the fundamental solution U_{ij} and T_{ij} and the boundary displacements u_j and t_j represent loading functions that have been acting at point $\underline{x}$ from time zero to time t. The time integrations from zero to t in (4-6) are already included in the formulation of the fundamental solution tensors U_{ij} and T_{ij}, because

$$\begin{aligned}
U_{ij}\left(\underline{x},t;\underline{\xi},0 \mid t_j\left(\underline{x},t\right)\right) &= \int_0^t V_{ij}\left(\underline{x},t;\underline{\xi},\tau\right) t_j\left(\underline{x},\tau\right) d\tau && \text{(no sum)} \\
T_{ij}\left(\underline{x},t;\underline{\xi},0 \mid u_j\left(\underline{x},t\right)\right) &= \int_0^t S_{ij}\left(\underline{x},t;\underline{\xi},\tau\right) u_j\left(\underline{x},\tau\right) d\tau && \text{(no sum)}
\end{aligned} \tag{4-8}$$

where V_{ij} and S_{ij} are the fundamental solution tensors for displacements and tractions in the i-th direction due the line load $\delta(\underline{x}-\underline{\xi})\delta(\underline{t}-\underline{\tau})e_j$. Equation (4-7) illustrates that the time-varying displacements at any point $\underline{\xi}$ within an elastic body are determined uniquely by the values of the time-varying boundary displacements and tractions, in the absence of body forces and with zero initial conditions.

4.3 The Direct Boundary Element Formulation

The direct boundary element method is designed to compute the unknown boundary displacements and tractions in a well-posed boundary value problem directly from the specified tractions and displacements on the boundary, without discretizing the interior domain V. Inspection of equations (4-4) and (4-7), which form the basis for the direct boundary element formulation in elastostatics and elastodynamics, respectively, reveals that these equations are only valid inside or outside the domain V. In their current form, these equations solve for displacements at any point $\underline{\xi}$, inside or outside the domain V, due to displacements u_j and tractions t_j applied at a boundary point $\underline{x}$. In order to include the case when $\underline{\xi}$ lies on the boundary, the point $\underline{\xi}$ has to be allowed to approach a point on the boundary S in the limit.

There are two equivalent ways of allowing point $\underline{\xi}$ to approach the receiver point $\underline{x}$ on boundary S. The first method allows the point $\underline{\xi}$ to approach the boundary S from the inside of domain V, followed by the integration of the boundary integrals. The second method which assumes that the point $\underline{\xi}$ lies outside domain V, evaluates the integrals first, and then allows the point $\underline{\xi}$ to approach the boundary S. These methods are formally equivalent and will be described briefly below.

The first method (allowing the point $\underline{\xi}$ to approach a boundary from the interior of the domain V) results in the elastostatic equation (4-4) becoming

$$c_{ij}\left(\underline{\xi}\right) u_j\left(\underline{\xi}\right) = \mathfrak{P} \int\limits_S t_j\left(\underline{x}\right) U_{ij}\left(\underline{x},\underline{\xi}\right) ds\left(\underline{x}\right) - \mathfrak{P} \int\limits_S u_j\left(\underline{x}\right) T_{ij}\left(\underline{x},\underline{\xi}\right) ds\left(\underline{x}\right) \tag{4-9}$$

and the elastodynamic equation (4-7) becoming

$$c_{ij}\left(\underline{\xi}\right) u_j\left(\underline{\xi},t\right) = \mathfrak{P} \int\limits_S U_{ij}\left(\underline{x},t;\underline{\xi},0 \mid t_j\left(\underline{x},t\right)\right) ds\left(\underline{x}\right) - \mathfrak{P} \int\limits_S T_{ij}\left(\underline{x},t,\underline{\xi},0 \mid u_j\left(\underline{x},t\right)\right) ds\left(\underline{x}\right) \tag{4-10}$$

in which the symbol $\mathfrak{P}$ denotes that the integrals must be evaluated in the Cauchy principal value sense. The coefficient $c_{ij}\left(\underline{\xi}\right)$ is a jump term that results when point $\underline{\xi}$ passes to the boundary S from inside the domain V. For a smooth boundary, $c_{ij}\left(\underline{\xi}\right) = 0.5$ at the boundary, but when the point $\underline{\xi}$ approaches a corner on the boundary, the jump term takes on different values, depending on the sharpness of the corner (see, for example Brebbia et al., 1984). Most of the published work in the literature takes these singular integral equations as a starting point for the numerical direct boundary element solution technique (e.g. Brebbia et al., 1984; Banerjee et al., 1986; Kobayashi, 1987). In this formulation, the boundary integral equations are discretized by using either straight-line or curved boundary elements. The Cauchy principal value integrals can be evaluated numerically over curved elements and analytically over straight-line elements. The use of numerical integration schemes for evaluating the Cauchy integrals requires extreme care so that the quadrature points do not coincide with the point $\underline{\xi}$, in which case the boundary integrals become singular.

The second method, which is due to Crouch and Starfield (1983) assumes that the point $\underline{\xi}$ lies outside the domain V. This results in the elastostatic equation (4-4) becoming

$$\int_S t_j\left(\underline{x}\right) U_{ij}\left(\underline{x},\underline{\xi}\right) ds\left(\underline{x}\right) = \int_S u_j\left(\underline{x}\right) T_{ij}\left(\underline{x},\underline{\xi}\right) ds\left(\underline{x}\right) \qquad (4\text{-}11)$$

and the elastodynamic equation (4-7) becoming

$$\int_S U_{ij}\left(\underline{x},t;\underline{\xi},0 \mid t_j\left(\underline{x},t\right)\right) ds\left(\underline{x}\right) = \int_S T_{ij}\left(\underline{x},t,\underline{\xi},0 \mid u_j\left(\underline{x},t\right)\right) ds\left(\underline{x}\right) \qquad (4\text{-}12)$$

in which every integral is regular and not a Cauchy principal value integral. This formulation allows the boundary integrals in (4-11) and (4-12) to be evaluated analytically, with point $\underline{\xi}$ outside the domain V. Then, to obtain the case when $\underline{\xi}$ approaches point $\underline{x}$, the limits are taken from the outside of the domain V. This approach avoids the difficulties involved with evaluating numerically any Cauchy principal value integrals. However, it is assumed that the integrations can be evaluated analytically so that the limits can be obtained. In this work, (4-11) and (4-12) are used as the starting points for the elastostatic and elastodynamic direct boundary element method.

Once the boundary displacements and tractions are obtained, equations (4-4) and (4-7) can be used to obtain displacements at any interior point $\underline{\xi}$ in the domain V. Comparable formulations for the interior stresses can be obtained by applying the kinematic equations (3-2) and Hooke's law (3-3) to equations (4-4) and (4-7) resulting in

$$\begin{aligned}
\sigma_{ij}\left(\underline{\xi}\right) = & \int_S \Big[\lambda\, U_{mk,m}\left(\underline{x},\underline{\xi}\right) t_k\left(\underline{x}\right)\delta_{ij} \\
& + G\left(U_{ik,j}\left(\underline{x},\underline{\xi}\right) + U_{jk,i}\left(\underline{x},\underline{\xi}\right)\right) t_k\left(\underline{x}\right)\Big]\, ds\left(\underline{x}\right) \\
& - \int_S \Big[\lambda\, T_{mk,m}\left(\underline{x},\underline{\xi}\right) u_k\left(\underline{x}\right)\delta_{ij} \\
& + G\left(T_{ik,j}\left(\underline{x},\underline{\xi}\right) + T_{jk,i}\left(\underline{x},\underline{\xi}\right)\right) u_k\left(\underline{x}\right)\Big]\, ds\left(\underline{x}\right)
\end{aligned} \tag{4-13}$$

for the elastostatic case and

$$\begin{aligned}
\sigma_{ij}\left(\underline{\xi}\right) = & \int_S \Big[\lambda\, U_{mk,m}\left(\underline{x},t,\underline{\xi},0 \mid t_k\left(\underline{x},t\right)\right)\delta_{ij} \\
& + G U_{ik,j}\left(\underline{x},t,\underline{\xi},0 \mid t_k\left(\underline{x},t\right)\right) \\
& + G U_{jk,i}\left(\underline{x},t,\underline{\xi},0 \mid t_k\left(\underline{x},t\right)\right)\Big]\, ds\left(\underline{x}\right) \\
& - \int_S \Big[\lambda\, T_{mk,m}\left(\underline{x},t,\underline{\xi},0 \mid u_k\left(\underline{x},t\right)\right)\delta_{ij} \\
& + G T_{ik,j}\left(\underline{x},t,\underline{\xi},0 \mid u_k\left(\underline{x},t\right)\right) \\
& + G T_{jk,i}\left(\underline{x},t,\underline{\xi},0 \mid u_k\left(\underline{x},t\right)\right)\Big]\, ds\left(\underline{x}\right)
\end{aligned} \tag{4-14}$$

for the elastodynamic case. The elastodynamic formulation (4-14) is often written in terms of mass density ρ and compressional and shear wave velocities c_1 and c_2. This can be accomplished by substituting $\rho\left(c_1^2 - 2c_2^2\right)$ for λ and ρc_2^2 for G in (4-14).

Chapter 5

Numerical Implementation

The boundary integral equations (4-11) and (4-12) provide the mathematical formulation of the elastostatic and elastodynamic direct boundary element method. It is obvious that closed form solutions to these equations are attainable only for very simple geometries and boundary conditions. For realistic engineering applications, the boundary element technique employs a numerical model to implement equations (4-11) and (4-12) in a computer program. In this chapter, the basic steps of this numerical solution technique are described.

The basic idea behind this numerical technique is to transform the fundamental integral equations (4-11) and (4-12) into a system of linear algebraic equations by means of discretization of the boundary geometry and the boundary displacements and tractions. The unknown boundary tractions and displacements can then be obtained by solving the system of equations for given boundary conditions. Once the boundary displacement and tractions are known, equations (4-4) and (4-13) can be used to obtain static displacements and stresses at any interior point in the domain of interest. Similarly, equations (4-7) and (4-14) can be used to obtain the dynamic displacements and stresses at any point within the domain.

This chapter is be divided into four main sections. The first deals with a numerical implementation of the elastostatic equations (4-11). First, the case for a homogeneous medium will be discussed, followed by the case for a general piecewise homogeneous medium. The second section describes the equivalent numerical implementation of the elastodynamic equations (4-12). The elastodynamic numerical formulation employs a numerical time-stepping algorithm that accounts for the temporal variation in boundary displacements and tractions. A time-stepping algorithm developed by Tian (1990) for homogenous media is generalized to accommodate piecewise homogeneous bodies. This algorithm determines the boundary displacements and tractions at each increment in time, by assuming a functional variation in the boundary parameters in both time and space. The boundary displacements and tractions are assumed to change linearly over each time step, and quadratically over the boundary of the body. The shape of the boundary is approximated by straight-line elements.

The third section in this chapter deals with the evaluation of stresses at the boundary for both the elastostatic and elastodynamic formulations. Finally, the fourth section deals with the calculation of displacements and stresses at internal points within any domain. Both the elastostatic and the elastodynamic cases are discussed.

For simplicity, the following presentation is restricted to traction boundary value problems. However, the algorithms developed can easily be applied to displacement or mixed boundary value problems.

5.1 Elastostatic Boundary Element Formulation

The integral equations described by equation (4-11) serve as the starting point for the numerical implementation of the elastostatic boundary element formulation. The procedure for the numerical implementation of this equation is to first discretize the boundary into a series of elements over which displacements and tractions are written in terms of their values at a series of nodal points. Writing the discretized form of (4-11) for every nodal point, a system of linear algebraic equations is obtained. Once the boundary conditions are applied, the system can be solved to obtain a numerical solution to the boundary value problem. This numerical solution allows all boundary displacements and tractions to be known, so that (4-4) and (4-13) can be used to obtain the displacements and stresses at any internal point within the domain of interest. All integrals are evaluated analytically at the element level and the boundary is approached from the outside of the domain, as described in Chapter 4.

The discretized version of (4-11) involves integrals of the products of the kernel functions $U_{ij}\left(\underline{x},\underline{\xi}\right)$ and $T_{ij}\left(\underline{x},\underline{\xi}\right)$ and the boundary parameters $t_j\left(\underline{x}\right)$ and $u_j\left(\underline{x}\right)$. The boundary contour S of the elastic body is divided into N straight-line elements, denoted by S_b, $b = 1, 2, \ldots N$, resulting in

$$\sum_{b=1}^{N} \int_{S_b} T_{ij}\left(\underline{x},\underline{\xi}\right) u_j\left(\underline{x}\right) ds\left(\underline{x}\right) = \sum_{b=1}^{N} \int_{S_b} U_{ij}\left(\underline{x},\underline{\xi}\right) t_j\left(\underline{x}\right) ds\left(\underline{x}\right) \tag{5-1}$$

in which all the kernel functions and boundary parameters are written in terms of global coordinates. The displacements and tractions along each element on S are assumed to vary quadratically.

The analytical evaluation of the integrals in (5-1) can be simplified greatly by evaluating them in terms of local element coordinates, instead of global coordinates. Unfortunately, a formulation that only uses local coordinates is not efficient either. The assumption of a quadratic variation in displacements and tractions across each element requires three nodal points per element to ensure the continuity of boundary values between neighboring elements. The use of a local coordinate system in the formulation of the problem would require different local expressions at any end node connecting two elements with different inclination angles. To simplify the formulation at such end nodes, the boundary displacements and tractions are denoted in the global coordinate system. Because U_{ij} and T_{ij} are already written in terms of the global coordinates (x, y), it is necessary to express these global coordinates in terms of local coordinates $(\bar{x}, \bar{y})$.

To establish a relationship between local and global coordinates, the local coordinates $(\bar{x}, \bar{y})$ are aligned such that the $\bar{x}$ axis coincides with the local straight-line element that approximates the boundary and the $\bar{y}$ axis aims in the direction of a normal pointing away from the element, as shown in Figure 5-1. Without loss of generality it can be assumed that the origin of the global coordinate system is at the center of the receiving element. Then, the coordinates of the loading point $\underline{\xi}$ are $x = \xi$ and $y = \eta$ in the global coordinate system and $\bar{x} = \bar{\xi}$ and $\bar{y} = \bar{\eta}$ in the local coordinate system. The global (x, y) coordinate system in Figure 5-1 is then defined by the transformation formulas

$$\begin{aligned} x - \xi &= (\bar{x} - \bar{\xi})\cos\beta - (\bar{y} - \bar{\eta})\sin\beta \\ y - \eta &= (\bar{x} - \bar{\eta})\sin\beta + (\bar{y} - \bar{\eta})\cos\beta \end{aligned} \tag{5-2}$$

in which β is the angle of inclination of the local element.

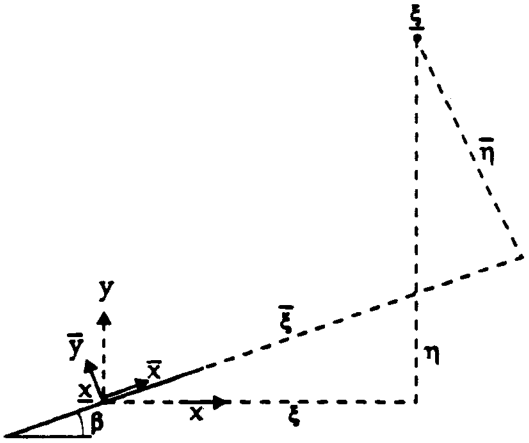

Figure 5-1: Local and global coordinate systems.

Now, relationship (5-2) can be used to write the fundamental displacement and traction tensors U_{ij} and T_{ij} in the global coordinate system, with its space variables expressed in terms of the local coordinate system, resulting in

$$\sum_{b=1}^{N} \int_{S_b} T_{ij} u_j d\bar{x} = \sum_{b=1}^{N} \int_{S_b} U_{ij} t_j d\bar{x} \tag{5-3}$$

where U_{ij} and T_{ij} are in the global co-ordinate system (x, y). The integral variable $\bar{x}$ is in the local coordinate system, as well as the omitted $\underline{x}$ and $\underline{\xi}$. The quantities U_{ij} and T_{ij} in (5-3) are obtained from definitions (3-16), (3-18) and (3-20) by using coordinate transformation formulas (5-2), and can be written as (Crouch and Starfield, 1983)

$$U_{xx} = \frac{1}{2G}\left[(3 - 4\nu)\, g - \bar{\eta}\left(\sin 2\beta \frac{\partial g}{\partial \bar{x}} + \cos 2\beta \frac{\partial g}{\partial \bar{y}}\right)\right]$$

$$\begin{aligned}
U_{yx} &= \frac{1}{2G}\left[\bar{\eta}\left(\cos 2\beta\frac{\partial g}{\partial \bar{x}} - \sin 2\beta\frac{\partial g}{\partial \bar{y}}\right)\right] \\
U_{xy} &= U_{yx} \\
U_{yy} &= \frac{1}{2G}\left[(3-4\nu)\,g + \bar{\eta}\left(\sin 2\beta\frac{\partial g}{\partial \bar{x}} - \cos 2\beta\frac{\partial g}{\partial \bar{y}}\right)\right]
\end{aligned} \tag{5-4}$$

and

$$\begin{aligned}
T_{xx} &= 2(1-\nu)\frac{\partial g}{\partial \bar{y}} - \bar{\eta}\left(\sin 2\beta\frac{\partial^2 g}{\partial \bar{x}\partial \bar{y}} + \cos 2\beta\frac{\partial^2 g}{\partial \bar{y}^2}\right) \\
T_{yx} &= (1-2\nu)\frac{\partial g}{\partial \bar{x}} + \bar{\eta}\left(\cos 2\beta\frac{\partial^2 g}{\partial \bar{x}\partial \bar{y}} - \sin 2\beta\frac{\partial^2 g}{\partial \bar{y}^2}\right) \\
T_{xy} &= -(1-2\nu)\frac{\partial g}{\partial \bar{x}} + \bar{\eta}\left(\cos 2\beta\frac{\partial^2 g}{\partial \bar{x}\partial \bar{y}} - \sin 2\beta\frac{\partial^2 g}{\partial \bar{y}^2}\right) \\
T_{yy} &= 2(1-\nu)\frac{\partial g}{\partial \bar{y}} + \bar{\eta}\left(\sin 2\beta\frac{\partial^2 g}{\partial \bar{x}\partial \bar{y}} + \cos 2\beta\frac{\partial^2 g}{\partial \bar{y}^2}\right)
\end{aligned} \tag{5-5}$$

where the function $g(\bar{x},\bar{y})$ is defined as

$$g(\bar{x},\bar{y}) = -\frac{1}{4\pi(1-\nu)}\ln\left[(\bar{x}-\xi)^2 + (\bar{y}-\bar{\eta})^2\right]^{1/2} \tag{5-6}$$

This function and all of its derivatives are to be evaluated for $\bar{y}=0$ in (5-4) and (5-5).

5.1.1 Spatial Interpolations of Boundary Parameters

As stated previously, the boundary displacements and tractions are assumed to vary quadratically over each boundary element. This quadratic variation of boundary parameters across each element is taken with respect to the left ($\bar{x}=-a$), right ($\bar{x}=+a$) and center ($\bar{x}=0$) boundary element nodal points, in which a denotes the element half-length. The boundary displacements and tractions across an arbitrary element S_b can then be written as

$$\begin{aligned}
u_j(\bar{x}) &= (u_j)_{bL}\,\phi_L(\bar{x}) + (u_j)_{bC}\,\phi_C(\bar{x}) + (u_j)_{bR}\,\phi_R(\bar{x}) \\
t_j(\bar{x}) &= (t_j)_{bL}\,\phi_L(\bar{x}) + (t_j)_{bC}\,\phi_C(\bar{x}) + (t_j)_{bR}\,\phi_R(\bar{x})
\end{aligned} \tag{5-7}$$

in which $(\ )_{bL}$, $(\ )_{bC}$ and $(\ )_{bR}$ denote the nodal displacements or tractions at the left, center and right nodes of element S_b. The functions $\phi_L(\bar{x})$, $\phi_C(\bar{x})$ and $\phi_R(\bar{x})$ are the corresponding quadratic interpolation functions given by

$$\begin{aligned}
\phi_L(\bar{x}) &= \frac{1}{2}\frac{\bar{x}}{a}\left(\frac{\bar{x}}{a} - 1.0\right) \\
\phi_C(\bar{x}) &= 1.0 - \frac{\bar{x}^2}{a^2} \\
\phi_R(\bar{x}) &= \frac{1}{2}\frac{\bar{x}}{a}\left(\frac{\bar{x}}{a} + 1.0\right)
\end{aligned} \tag{5-8}$$

The substitution of (5-7) and (5-8) into (5-3) results in the left side of (5-3) being expressed as

$$\begin{aligned}
\sum_{b=1}^{N}\int_{S_b} T_{ij}u_j(\bar{x})\,d\bar{x} &= \sum_{b=1}^{N}(u_j)_{bL}\int_{S_b} T_{ij}\phi_L(\bar{x})\,d\bar{x} \\
&+\sum_{b=1}^{N}(u_j)_{bC}\int_{S_b} T_{ij}\phi_C(\bar{x})\,d\bar{x} \\
&+\sum_{b=1}^{N}(u_j)_{bR}\int_{S_b} T_{ij}\phi_R(\bar{x})\,d\bar{x}
\end{aligned} \tag{5-9}$$

and the right side as

$$\begin{aligned}
\sum_{b=1}^{N}\int_{S_b} U_{ij}t_j(\bar{x})\,d\bar{x} &= \sum_{b=1}^{N}(t_j)_{bL}\int_{S_b} U_{ij}\phi_L(\bar{x})\,d\bar{x} \\
&+\sum_{b=1}^{N}(t_j)_{bC}\int_{S_b} U_{ij}\phi_C(\bar{x})\,d\bar{x} \\
&+\sum_{b=1}^{N}(t_j)_{bR}\int_{S_b} U_{ij}\phi_R(\bar{x})\,d\bar{x}
\end{aligned} \tag{5-10}$$

in which U_{ij} and T_{ij} are given by (5-4) and (5-5), respectively. Now, substituting (5-4) and (5-5) into (5-9) and (5-10) results in the following algebraic expressions

$$\left(B_{xx}^{L}\right)_J = \int_{-a}^{+a}\frac{1}{2}\frac{\bar{x}}{a}\left(\frac{\bar{x}}{a} - 1.0\right)U_{xx}d\bar{x}$$

$$
\begin{aligned}
&= \frac{1}{4G}\int_{-a}^{+a}\left[(3-4\nu)\,g-\bar{\eta}\left(\sin 2\beta\frac{\partial g}{\partial \bar{x}}+\cos 2\beta\frac{\partial g}{\partial \bar{y}}\right)\right]\frac{\bar{x}^2}{a^2}d\bar{x}\\
&\quad -\frac{1}{4G}\int_{-a}^{+a}\left[(3-4\nu)\,g-\bar{\eta}\left(\sin 2\beta\frac{\partial g}{\partial \bar{x}}+\cos 2\beta\frac{\partial g}{\partial \bar{y}}\right)\right]\frac{\bar{x}}{a}d\bar{x}
\end{aligned}
$$

$$
\begin{aligned}
\left(B_{xx}^{C}\right)_J &= \int_{-a}^{+a}\left(1.0-\frac{\bar{x}^2}{a^2}\right)U_{xx}d\bar{x}\\
&= \frac{1}{4G}\int_{-a}^{+a}\left[(3-4\nu)\,g-\bar{\eta}\left(\sin 2\beta\frac{\partial g}{\partial \bar{x}}+\cos 2\beta\frac{\partial g}{\partial \bar{y}}\right)\right]d\bar{x}\\
&\quad -\frac{1}{2G}\int_{-a}^{+a}\left[(3-4\nu)\,g-\bar{\eta}\left(\sin 2\beta\frac{\partial g}{\partial \bar{x}}+\cos 2\beta\frac{\partial g}{\partial \bar{y}}\right)\right]\frac{\bar{x}^2}{a^2}d\bar{x}
\end{aligned}
\tag{5-11}
$$

$$
\begin{aligned}
\left(B_{xx}^{R}\right)_J &= \int_{-a}^{+a}\frac{1}{2}\frac{\bar{x}}{a}\left(\frac{\bar{x}}{a}+1.0\right)U_{xx}d\bar{x}\\
&= \frac{1}{4G}\int_{-a}^{+a}\left[(3-4\nu)\,g-\bar{\eta}\left(\sin 2\beta\frac{\partial g}{\partial \bar{x}}+\cos 2\beta\frac{\partial g}{\partial \bar{y}}\right)\right]\frac{\bar{x}^2}{a^2}d\bar{x}\\
&\quad +\frac{1}{4G}\int_{-a}^{+a}\left[(3-4\nu)\,g-\bar{\eta}\left(\sin 2\beta\frac{\partial g}{\partial \bar{x}}+\cos 2\beta\frac{\partial g}{\partial \bar{y}}\right)\right]\frac{\bar{x}}{a}d\bar{x}
\end{aligned}
$$

and so forth for the traction coefficients, and

$$
\begin{aligned}
\left(A_{xx}^{L}\right)_J &= \int_{-a}^{+a}\frac{1}{2}\frac{\bar{x}}{a}\left(\frac{\bar{x}}{a}-1.0\right)T_{xx}d\bar{x}\\
&= \frac{1}{2}\int_{-a}^{+a}\left[2\,(1-\nu)\,\frac{\partial g}{\partial \bar{y}}-\bar{\eta}\left(\sin 2\beta\frac{\partial^2 g}{\partial \bar{x}\partial \bar{y}}+\cos 2\beta\frac{\partial^2 g}{\partial \bar{y}^2}\right)\right]\frac{\bar{x}^2}{a^2}d\bar{x}\\
&\quad -\frac{1}{2}\int_{-a}^{+a}\left[2\,(1-\nu)\,\frac{\partial g}{\partial \bar{y}}-\bar{\eta}\left(\sin 2\beta\frac{\partial^2 g}{\partial \bar{x}\partial \bar{y}}+\cos 2\beta\frac{\partial^2 g}{\partial \bar{y}^2}\right)\right]\frac{\bar{x}}{a}d\bar{x}
\end{aligned}
$$

$$\begin{aligned}\left(A^{C}_{\bar{x}\bar{x}}\right)_J &= \int\limits_{-a}^{+a}\left(1.0-\frac{\bar{x}^2}{a^2}\right)T_{\bar{x}\bar{x}}d\bar{x}\\ &= \int\limits_{-a}^{+a}\left[2\left(1-\nu\right)\frac{\partial g}{\partial\bar{y}}-\bar{\eta}\left(\sin 2\beta\frac{\partial^2 g}{\partial\bar{x}\partial\bar{y}}+\cos 2\beta\frac{\partial^2 g}{\partial\bar{y}^2}\right)\right]d\bar{x}\\ &\quad-\int\limits_{-a}^{+a}\left[2\left(1-\nu\right)\frac{\partial g}{\partial\bar{y}}-\bar{\eta}\left(\sin 2\beta\frac{\partial^2 g}{\partial\bar{x}\partial\bar{y}}+\cos 2\beta\frac{\partial^2 g}{\partial\bar{y}^2}\right)\right]\frac{\bar{x}^2}{a^2}d\bar{x}\end{aligned}\tag{5-12}$$

$$\begin{aligned}\left(A^{R}_{\bar{x}\bar{x}}\right)_J &= \int\limits_{-a}^{+a}\frac{1}{2}\frac{\bar{x}}{a}\left(\frac{\bar{x}}{a}+1.0\right)T_{\bar{x}\bar{x}}d\bar{x}\\ &= \frac{1}{2}\int\limits_{-a}^{+a}\left[2\left(1-\nu\right)\frac{\partial g}{\partial\bar{y}}-\bar{\eta}\left(\sin 2\beta\frac{\partial^2 g}{\partial\bar{x}\partial\bar{y}}+\cos 2\beta\frac{\partial^2 g}{\partial\bar{y}^2}\right)\right]d\bar{x}\\ &\quad+\frac{1}{2}\int\limits_{-a}^{+a}\left[2\left(1-\nu\right)\frac{\partial g}{\partial\bar{y}}-\bar{\eta}\left(\sin 2\beta\frac{\partial^2 g}{\partial\bar{x}\partial\bar{y}}+\cos 2\beta\frac{\partial^2 g}{\partial\bar{y}^2}\right)\right]\frac{\bar{x}^2}{a^2}d\bar{x}\end{aligned}$$

and so forth for the displacement coefficients. The notation $(\quad)_J$ denotes that the coefficients are associated with element J. Substitution of the algebraic expressions (5-11) and (5-12) into (5-9) and (5-10) results in

$$\sum_{b=1}^{N}\int\limits_{S_b}T_{ij}u_j\left(\bar{x}\right)d\bar{x}=\sum_{J=1}^{N}\left\{(u_j)_{JL}\left(A^{L}_{ij}\right)_J+(u_j)_{JC}\left(A^{C}_{ij}\right)_J+(u_j)_{JR}\left(A^{R}_{ij}\right)_J\right\}\tag{5-13}$$

and

$$\sum_{b=1}^{N}\int\limits_{S_b}U_{ij}t_j\left(\bar{x}\right)d\bar{x}=\sum_{J=1}^{N}\left\{(t_j)_{JL}\left(B^{L}_{ij}\right)_J+(t_j)_{JC}\left(B^{C}_{ij}\right)_J+(t_j)_{JR}\left(B^{R}_{ij}\right)_J\right\}\tag{5-14}$$

Subsequently, substitution of (5-13) and (5-14) into (5-3) gives the following expressions

$$\sum_{J=1}^{N}\left\{(u_j)_{JL}\left(A^{L}_{ij}\right)_J+(u_j)_{JC}\left(A^{C}_{ij}\right)_J+(u_j)_{JR}\left(A^{R}_{ij}\right)_J\right\}$$

$$= \sum_{J=1}^{N} \left\{ (t_j)_{JL} \left(B^L_{ij}\right)_J + (t_j)_{JC} \left(B^C_{ij}\right)_J + (t_j)_{JR} \left(B^R_{ij}\right)_J \right\} \qquad (5\text{-}15)$$

in which $i = x, y$ and $j = x, y$. All the integrals needed in (5-15) can be evaluated analytically. The results of the necessary integrations are listed in Appendix A.

Finally, it should be noted that (5-15) can be rearranged so that the summations are performed over the nodal points rather than the elements. In this case, a closed boundary contour approximated by N elements will have $2N$ nodes. Then, for any given element J, the boundary displacements at the center nodes wc are denoted by $\overset{wc}{(u_j)}_J$ and the boundary displacements at the end nodes we are denoted by $\overset{we}{(u_j)}_J$, where wc and we denote odd and even nodal numbers ranging from 1 to $2N-1$ and from 2 to $2N$, respectively. This allows expression (5-15) to be rewritten as

$$\begin{aligned} &\sum_{wc=1,3,..}^{2N-1} \overset{wc}{(u_j)}_J \overset{wc}{\left(A^C_{ij}\right)}_J + \sum_{we=2,4,..}^{2N} \left[\overset{we}{(u_j)}_{J-1} \overset{we}{\left(A^R_{ij}\right)}_{J-1} + \overset{we}{(u_j)}_J \overset{we}{\left(A^L_{ij}\right)}_J \right] \\ = &\sum_{wc=1,3,..}^{2N-1} \overset{wc}{(t_j)}_J \overset{wc}{\left(B^C_{ij}\right)}_J + \sum_{we=2,4,..}^{2N} \left[\overset{we}{(t_j)}_{J-1} \overset{we}{\left(B^R_{ij}\right)}_{J-1} + \overset{we}{(t_j)}_J \overset{we}{\left(B^L_{ij}\right)}_J \right] \qquad (5\text{-}16) \end{aligned}$$

The analytical evaluation of the boundary integrals in (5-16) results in an algebraic equation with $4N$ unknown displacements, because there are two unknown displacements $(\overset{i}{u_x})$ and $(\overset{i}{u_y})$ at each node i. To obtain the same number of equations as unknowns, the loading point $\underline{\xi}$ is allowed to approach every node on the boundary, resulting in two algebraic equations for each node. The loading point $\underline{\xi}$ approaches each center node from the outside of the domain in a direction normal to the boundary element, as shown in Figure 5-2a. Similarly, it is convenient to let the loading point $\underline{\xi}$ approach each end node along a straight line bisecting the exterior angle between two neighboring elements, as shown in Figure 5-2b. The displacement and traction coefficients in (5-16) are called self-effect coefficients (Crouch and Starfield, 1983) when the loading point $\underline{\xi}$ and the receiving point $\underline{x}$ are located on the same boundary element. All of these self-effect coefficients are listed in Appendix A.

The final system of algebraic equations consists of $4N$ by $4N$ equations, and can be

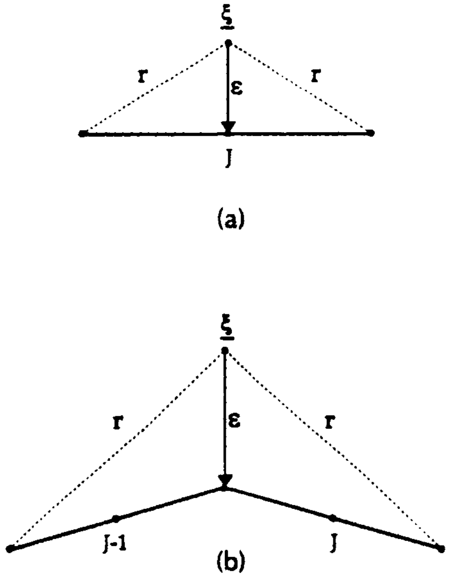

(a)

(b)

Figure 5-2: Self-coefficients for (a) center and (b) end nodes.

written as

$$\mathbf{Au} = \mathbf{Bt} \tag{5-17}$$

in which $\mathbf{u}$ and $\mathbf{t}$ denote the vectors of nodal displacements and tractions, and the coefficient matrices $\mathbf{A}$ and $\mathbf{B}$ are defined as $[A_{ij}]_{pq}$ and $[B_{ij}]_{pq}$, in which i and j denote either the x or y direction and p and q denote the boundary nodal source and receiving points, respectively. Both p and q take on values from 1 to $2N$. Therefore, $\mathbf{A}$ can be written as

$$\mathbf{A} = \begin{bmatrix} [A_{ij}]_{11} & \cdots & [A_{ij}]_{12N} \\ \vdots & & \vdots \\ [A_{ij}]_{2N1} & \cdots & [A_{ij}]_{2N2N} \end{bmatrix} \tag{5-18}$$

The sub-matrices in (5-18) can be written as

$$[A_{ij}]_{pq} = \begin{bmatrix} A_{xx} & A_{xy} \\ A_{yx} & A_{yy} \end{bmatrix} \tag{5-19}$$

The coefficient matrix $\mathbf{B}$ is to be written in an identical way to (5-18) and (5-19). This completes the description of the algebraic equations that are necessary for the numerical implementation of the elastostatic direct boundary element method for homogeneous media.

5.1.2 Piecewise Homogeneous Media in Elastostatics

In the following, the preceding numerical algorithm for homogenous domains is extended to include multiple materials. The method used in this thesis for modeling piecewise homogeneous regions consists of combining numerically two or more homogeneous regions along common straight-line or curved interfaces with a "substructuring" technique. Figure 5-3 illustrates this technique with a body consisting of two material sub-regions, represented by Ω_1 and Ω_2. For the numerical modeling of such piecewise homogeneous bodies, the boundary of each material sub-region is discretized into a number of straight-line elements, including interfaces between any two sub-regions. Each region is then discretized as if it were a separate body. This discretization process results in all interfaces between sub-regions being represented by two sets of boundary elements. Elements along one side of an interface must match the elements on the adjoining side of the interface exactly. Once each sub-region has been discretized it is formulated as a separate boundary element region. Applying the boundary element algorithm (5-17) to each sub-region results in

$$\begin{bmatrix} \mathbf{A}_{11} & \mathbf{A}_{1I} \\ \mathbf{A}_{I1} & \mathbf{A}_{II} \end{bmatrix} \begin{bmatrix} \mathbf{u}_1 \\ \mathbf{u}_{1I} \end{bmatrix} = \begin{bmatrix} \mathbf{B}_{11} & \mathbf{B}_{1I} \\ \mathbf{B}_{I1} & \mathbf{B}_{II} \end{bmatrix} \begin{bmatrix} \mathbf{t}_1 \\ \mathbf{t}_{1I} \end{bmatrix} \tag{5-20}$$

for sub-region Ω_1 and

$$\begin{bmatrix} \bar{\mathbf{A}}_{22} & \bar{\mathbf{A}}_{2I} \\ \bar{\mathbf{A}}_{I2} & \bar{\mathbf{A}}_{II} \end{bmatrix} \begin{bmatrix} \bar{\mathbf{u}}_2 \\ \bar{\mathbf{u}}_{2I} \end{bmatrix} = \begin{bmatrix} \bar{\mathbf{B}}_{22} & \bar{\mathbf{B}}_{2I} \\ \bar{\mathbf{B}}_{I2} & \bar{\mathbf{B}}_{II} \end{bmatrix} \begin{bmatrix} \bar{\mathbf{t}}_2 \\ \bar{\mathbf{t}}_{2I} \end{bmatrix} \tag{5-21}$$

for sub-region Ω_2. The bars in (5-21) denote sub-region Ω_2, the first subscript in the sub-matrices in (5-20) and (5-21) denotes the location of the source point and the

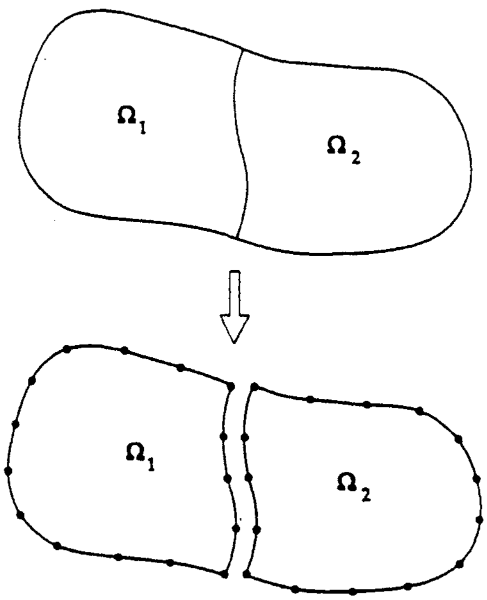

Figure 5-3: Substructuring of a body consisting of two materials.

second subscript denotes the location of the receiver point. For example, the sub-matrices $\mathbf{A}_{11}$, $\mathbf{A}_{1I}$ denote that the source point is located on the free boundary of sub-region Ω_1 and the receiver point is located on the free boundary of sub-region Ω_1 and on the interface I between sub-regions Ω_1 and Ω_2, respectively. The vector $\mathbf{u}_1$ denotes the displacements at the free boundary of the sub-region Ω_1 and $\mathbf{u}_{1I}$ denotes the displacements on the interface part of the discretized sub-region Ω_1.

The interface displacements and tractions can not be obtained from (5-20) and (5-21) as written, because at each interface node both quantities are unknown. If it is assumed that the two homogeneous sub-regions Ω_1 and Ω_2 are fully bonded at the interface, such that no slip or separation can occur, then the interface displacements are continuous across the interface and the tractions associated with each sub-region are equal in magnitude, but opposite in sign, namely

$$\begin{aligned} \mathbf{u}_{1I} &= \bar{\mathbf{u}}_{2I} \\ \mathbf{t}_{1I} &= -\bar{\mathbf{t}}_{2I} \end{aligned} \qquad (5\text{-}22)$$

This relationship must be satisfied at every nodal point on the interface between the two sub-regions. In the presence of interface corners this formulation assumes that nodal tractions and displacements are continuous across a node. It is shown in Chapter 6 that this assumption is reasonable for many cases, such as the case of a loaded annulus in an infinite plate.

Equations (5-20) and (5-21) can be combined using the fully bonded interface condition expressed by (5-22), resulting in

$$\begin{bmatrix} \mathbf{A}_{11} & \mathbf{A}_{1I} & \mathbf{B}_{1I} & 0 \\ \mathbf{A}_{I1} & \mathbf{A}_{II} & \mathbf{B}_{II} & 0 \\ 0 & \bar{\mathbf{A}}_{2I} & -\bar{\mathbf{B}}_{2I} & \bar{\mathbf{A}}_{22} \\ 0 & \bar{\mathbf{A}}_{II} & -\bar{\mathbf{B}}_{II} & \bar{\mathbf{A}}_{I2} \end{bmatrix} \begin{bmatrix} \mathbf{u}_1 \\ \mathbf{u}_{1I} \\ \bar{\mathbf{t}}_{2I} \\ \bar{\mathbf{u}}_2 \end{bmatrix} = \begin{bmatrix} \mathbf{B}_{11} & 0 \\ \mathbf{B}_{I1} & 0 \\ 0 & \bar{\mathbf{B}}_{22} \\ 0 & \bar{\mathbf{B}}_{I2} \end{bmatrix} \begin{bmatrix} \mathbf{t}_1 \\ \bar{\mathbf{t}}_2 \end{bmatrix} \tag{5-23}$$

in which the terms on the right-hand side are the known traction boundary conditions and the terms on the left-hand side denote the unknown boundary and interface displacements and tractions. Equation (5-23) can be rewritten as

$$\mathbf{Cx} = \mathbf{b} \tag{5-24}$$

in which

$$\mathbf{C} = \begin{bmatrix} \mathbf{A}_{11} & \mathbf{A}_{1I} & \mathbf{B}_{1I} & 0 \\ \mathbf{A}_{I1} & \mathbf{A}_{II} & \mathbf{B}_{II} & 0 \\ 0 & \bar{\mathbf{A}}_{2I} & -\bar{\mathbf{B}}_{2I} & \bar{\mathbf{A}}_{22} \\ 0 & \bar{\mathbf{A}}_{II} & -\bar{\mathbf{B}}_{II} & \bar{\mathbf{A}}_{I2} \end{bmatrix} \tag{5-25}$$

denotes the boundary element influence coefficient matrix. The unknown vector $\mathbf{x}$ in (5-24) can be written as

$$\mathbf{x} = \begin{bmatrix} \mathbf{u}_1 & \mathbf{u}_{1I} & \bar{\mathbf{t}}_{2I} & \bar{\mathbf{u}}_2 \end{bmatrix}^T \tag{5-26}$$

in which the superscript T denotes the transpose operator, and the known vector $\mathbf{b}$ can be written as

$$\mathbf{b} = \begin{bmatrix} \mathbf{B}_{11} & 0 \\ \mathbf{B}_{I1} & 0 \\ 0 & \bar{\mathbf{B}}_{22} \\ 0 & \bar{\mathbf{B}}_{I2} \end{bmatrix} \begin{bmatrix} \mathbf{t}_1 \\ \bar{\mathbf{t}}_2 \end{bmatrix} \tag{5-27}$$

It should be noted that even though equations (5-23) to (5-27) were shown for a traction boundary value problem which assumes that the tractions on the boundary are known, the formulation is completely general, so that the equations can be rearranged to solve problems in which the boundary displacements or a mix of boundary displacements and tractions are known.

5.2 Elastodynamic Boundary Element Formulation

The procedure for the numerical implementation of the elastodynamic boundary element formulation is similar to the elastostatic implementation, discussed in Section 5.1, with the additional introduction of a numerical time-stepping algorithm that accounts for the temporal variation in boundary displacements and tractions. The integral equations described by equation (4-12) serve as the starting point for the numerical implementation of the elastodynamic boundary element formulation.

The evaluation of the fundamental solution tensors $U_{ij}\left(\underset{\sim}{x}, t; \underset{\sim}{\xi}, 0 \mid t_j\left(\underset{\sim}{x}, t\right)\right)$ and $T_{ij}\left(\underset{\sim}{x}, t; \underset{\sim}{\xi}, 0 \mid u_j\left(\underset{\sim}{x}, t\right)\right)$ in (4-12) occurs at time t and includes the action of the boundary displacements $u_j\left(\underset{\sim}{x}, t\right)$ and tractions $t_j\left(\underset{\sim}{x}, t\right)$ from time 0 to t. To account for the entire loading time, the time t is divided into m intervals of duration Δt, so that the left-hand side of (4-12) can be written as

$$\int_S U_{ij}\left(\underset{\sim}{x}, t; \underset{\sim}{\xi}, 0 \mid t_j\left(\underset{\sim}{x}, t\right)\right) ds\left(\underset{\sim}{x}\right) = \sum_{k=1}^{m} \int_S U_{ij}\left(m\Delta t; (k-1)\Delta t, t_{j(k)}\right) ds \tag{5-28}$$

and the right-hand side as

$$\int_S T_{ij}\left(\underset{\sim}{x}, t; \underset{\sim}{\xi}, 0 \mid u_j\left(\underset{\sim}{x}, t\right)\right) ds\left(\underset{\sim}{x}\right) = \sum_{k=1}^{m} \int_S T_{ij}\left(m\Delta t; (k-1)\Delta t, u_{j(k)}\right) ds \tag{5-29}$$

In equations (5-28) and (5-29) the loading point $\underline{\xi}$ and the receiving point $\underline{x}$ have been omitted for simplicity of presentation and $t_{j(k)}$ and $u_{j(k)}$ are the boundary displacements and tractions over the time interval $(k-1)\,\Delta t$ to $k\Delta t$. Combining (5-28) and (5-29) in accordance with (4-12) results in

$$\sum_{k=1}^{m}\int_{S} U_{ij}\left(m\Delta t;(k-1)\,\Delta t,t_{j(k)}\right)ds=\sum_{k=1}^{m}\int_{S} T_{ij}\left(m\Delta t;(k-1)\,\Delta t,u_{j(k)}\right)ds \tag{5-30}$$

The unknown displacements $u_j\left(\underline{x},t\right)$ for time step m can be written as

$$\begin{aligned}\int_{S} T_{ij}\left(m\Delta t;(m-1)\,\Delta t,u_{j(k)}\right)ds \;=\; & \sum_{k=1}^{m}\int_{S} U_{ij}\left(m\Delta t;(k-1)\,\Delta t,t_{j(k)}\right)ds\\ & -\sum_{k=1}^{m}\int_{S} T_{ij}\left(m\Delta t;(k-1)\,\Delta t,u_{j(k)}\right)ds\end{aligned} \tag{5-31}$$

To simplify the calculations of displacements in (5-31) at time step m, the time translation property (3-29) is used to shift the loading and evaluation times of the fundamental solutions by time $(k-1)\,\Delta t$. This means that all the loading times $(k-1)\,\Delta t$ become zero and all the evaluation times $m\Delta t$ become $(m-k+1)\,\Delta t$, in which k ranges from 2 to m. Finally, just as in the elastostatic formulation (5-1), the boundary contour S of the elastic body is divided into N straight-line elements, denoted by S_b, $b=1,\ldots N$, resulting in

$$\begin{aligned}\sum_{b=1}^{N}\int_{S_b} T_{ij}\left(\Delta t;0,u_{j(k)}\right)ds \;=\; & \sum_{k=1}^{m}\sum_{b=1}^{N}\int_{S_b} U_{ij}\left((m-k+1)\,\Delta t;0,t_{j(k)}\right)ds\\ & -\sum_{k=1}^{m-1}\sum_{b=1}^{N}\int_{S_b} T_{ij}\left((m-k+1)\,\Delta t;0,u_{j(k)}\right)ds\end{aligned} \tag{5-32}$$

in which the unknown displacements at each time step m are written in terms of the time history of displacements and tractions.

At each time step m, equation (5-32) can be used to formulate a system of

T_{ij} in (5-33) are obtained from definitions (3-25), (3-26) and (3-20) by using the coordinate transformation formulas (5-2), and can be written as

$$
\begin{aligned}
U_{xx} &= \frac{1}{2\pi\rho}\bigg\{H\left(t-r/c_1\right)\frac{1}{c_1^3}\bigg[\bigg(\frac{u^2-v^2}{6r^4}\cos 2\beta-\frac{uv}{3r^4}\sin 2\beta\bigg)\left(c_1^2t^2-r^2\right)^{3/2} \\
&\quad +\frac{1}{2}\left(c_1t\cosh^{-1}\left(\frac{c_1t}{r}\right)-\sqrt{c_1^2t^2-r^2}\right)\bigg] \\
&\quad -H\left(t-r/c_2\right)\frac{1}{c_2^3}\bigg[\bigg(\frac{u^2-v^2}{6r^4}\cos 2\beta-\frac{uv}{3r^4}\sin 2\beta\bigg)\left(c_2^2t^2-r^2\right)^{3/2} \\
&\quad -\frac{1}{2}\left(c_2t\cosh^{-1}\left(\frac{c_2t}{r}\right)-\sqrt{c_2^2t^2-r^2}\right)\bigg]\bigg\}
\end{aligned}
$$

$$
\begin{aligned}
U_{xy} &= \frac{1}{2\pi\rho}\bigg\{H\left(t-r/c_1\right)\frac{1}{c_1^3}\bigg(\frac{u^2-v^2}{6r^4}\sin 2\beta+\frac{uv}{3r^4}\cos 2\beta\bigg)\left(c_1^2t^2-r^2\right)^{3/2} \\
&\quad -H\left(t-r/c_2\right)\frac{1}{c_2^3}\bigg(\frac{u^2-v^2}{6r^4}\sin 2\beta+\frac{uv}{3r^4}\cos 2\beta\bigg)\left(c_2^2t^2-r^2\right)^{3/2}
\end{aligned}
\tag{5-34}
$$

$$
U_{yx} = U_{xy}
$$

$$
\begin{aligned}
U_{yy} &= \frac{1}{2\pi\rho}\bigg\{H\left(t-r/c_1\right)\frac{1}{c_1^3}\bigg[-\bigg(\frac{u^2-v^2}{6r^4}\cos 2\beta-\frac{uv}{3r^4}\sin 2\beta\bigg)\left(c_1^2t^2-r^2\right)^{3/2} \\
&\quad +\frac{1}{2}\left(c_1t\cosh^{-1}\left(\frac{c_1t}{r}\right)-\sqrt{c_1^2t^2-r^2}\right)\bigg] \\
&\quad -H\left(t-r/c_2\right)\frac{1}{c_2^3}\bigg[-\bigg(\frac{u^2-v^2}{6r^4}\cos 2\beta-\frac{uv}{3r^4}\sin 2\beta\bigg)\left(c_2^2t^2-r^2\right)^{3/2} \\
&\quad -\frac{1}{2}\left(c_2t\cosh^{-1}\left(\frac{c_2t}{r}\right)-\sqrt{c_2^2t^2-r^2}\right)\bigg]\bigg\}
\end{aligned}
$$

and

$$
\begin{aligned}
T_{xx} &= \frac{1}{2\pi}\bigg\{H\left(t-r/c_1\right)\frac{c_{21}^2}{c_1}\bigg[\cos 2\beta\bigg(\frac{8c_1^2t^2v^3}{3r^6}-\frac{2v\left(3c_1^2t^2+v^2\right)}{3r^4} \\
&\quad +\frac{v}{2c_{21}^2r^2}\bigg)\sqrt{c_1^2t^2-r^2}+\sin 2\beta\bigg(\frac{8c_1^2t^2v^2u}{3r^6}-\frac{2u\left(c_1^2t^2+v^2\right)}{3r^4} \\
&\quad -\frac{u}{3r^2}+\frac{u}{2c_{21}^2r^2}\bigg)\sqrt{c_1^2t^2-r^2}-\frac{v}{2c_{21}^2r^2}\sqrt{c_1^2t^2-r^2}\bigg]
\end{aligned}
$$

algebraic equations in which the unknowns are the boundary displacements at that time step. These algebraic equations are obtained through the analytical evaluation of the integrals in (5-32). To facilitate this integration process, it is necessary to assume a functional variation in time and space for these parameters, because the true temporal and spatial distributions of the boundary displacements and tractions are not known a priori.

In this study, the boundary displacements and tractions are assumed to change linearly over each time step. At each time step, the displacements and tractions are assumed to be distributed piecewise quadratically over each straight-line boundary element of the body, just as in the elastostatic case, discussed in Section 5.1. Once the integrals have been evaluated and the desired system of algebraic equations has been established, the unknown boundary displacements for each current time step m can be obtained. This allows the dynamic history of displacements to be established in a step-by-step fashion as time progresses.

The analytical evaluation of the integrals in (5-32) involves the spatial integration of U_{ij} and T_{ij} over straight-line elements. The evaluation of these integrals can be simplified greatly by writing them in terms of local element coordinates, rather than global coordinates, as discussed for the elastostatic case in Section 5.1. Following the same procedure as described in Section 5.1 for the elastostatic case, the transformation formulas (5-2) are used to write the fundamental displacement and traction tensors U_{ij} and T_{ij} in the global coordinate system, with space variables expressed in terms of the local coordinate system, allowing (5-32) to be re-written as

$$\begin{aligned}\sum_{b=1}^{N}\int_{S_b} T_{ij}\left(\Delta t;0,u_{j(k)}\right)d\bar{x} \;=\;& \sum_{k=1}^{m}\sum_{b=1}^{N}\int_{S_b} U_{ij}\left((m-k+1)\,\Delta t;0,t_{j(k)}\right)d\bar{x}\\ &-\sum_{k=1}^{m-1}\sum_{b=1}^{N}\int_{S_b} T_{ij}\left((m-k+1)\,\Delta t;0,u_{j(k)}\right)d\bar{x}\end{aligned} \tag{5-33}$$

where U_{ij} and T_{ij} are in the global coordinate system (x, y). The integral variable $\bar{x}$ is in the local coordinate system, as well as the omitted $\underline{x}$ and $\underline{\xi}$. The quantities U_{ij} and

$$-H\left(t-r/c_2\right)\frac{1}{c_2}\left[\cos 2\beta\left(\frac{8c_2^2t^2v^3}{3r^6}-\frac{2v\left(3c_2^2t^2+v^2\right)}{3r^4}+\frac{v}{2r^2}\right)\sqrt{c_1^2t^2-r^2}\right.$$
$$+\sin 2\beta\left(\frac{8c_2^2t^2v^2u}{3r^6}-\frac{2u\left(c_2^2t^2+v^2\right)}{3r^4}+\frac{u}{6r^2}\right)\sqrt{c_1^2t^2-r^2}$$
$$\left.\left.+\frac{v}{2r^2}\sqrt{c_1^2t^2-r^2}\right]\right\}$$

$$T_{yx} = \frac{1}{2\pi}\left\{H\left(t-r/c_1\right)\frac{c_{21}^2}{c_1}\left[\cos 2\beta\left(-\frac{8c_1^2t^2v^2u}{3r^6}+\frac{2u\left(c_1^2t^2+v^2\right)}{3r^4}\right.\right.\right.$$
$$\left.+\frac{u}{3r^2}-\frac{u}{2c_{21}^2r^2}\right)\sqrt{c_1^2t^2-r^2}+\sin 2\beta\left(\frac{8c_1^2t^2v^3}{3r^6}\right.$$
$$\left.\left.-\frac{2v\left(3c_1^2t^2+v^2\right)}{3r^4}+\frac{v}{2c_{21}^2r^2}\right)\sqrt{c_1^2t^2-r^2}+\frac{u}{r^2}\sqrt{c_1^2t^2-r^2}\left(\frac{1}{2c_{21}^2}-1\right)\right]$$
$$-H\left(t-r/c_2\right)\frac{1}{c_2}\left[\cos 2\beta\left(-\frac{8c_2^2t^2v^2u}{3r^6}+\frac{2u\left(c_2^2t^2+v^2\right)}{3r^4}-\frac{u}{6r^2}\right)\sqrt{c_2^2t^2-r^2}\right.$$
$$+\sin 2\beta\left(\frac{8c_2^2t^2v^3}{3r^6}-\frac{2v\left(3c_2^2t^2+v^2\right)}{3r^4}+\frac{v}{2r^2}\right)\sqrt{c_2^2t^2-r^2}$$
$$\left.\left.+\frac{u}{2r^2}\sqrt{c_2^2t^2-r^2}\right]\right\} \qquad (5\text{-}35)$$

$$T_{xy} = \frac{1}{2\pi}\left\{H\left(t-r/c_1\right)\frac{c_{21}^2}{c_1}\left[\cos 2\beta\left(-\frac{8c_1^2t^2v^2u}{3r^6}+\frac{2u\left(c_1^2t^2+v^2\right)}{3r^4}\right.\right.\right.$$
$$\left.+\frac{u}{3r^2}-\frac{u}{2c_{21}^2r^2}\right)\sqrt{c_1^2t^2-r^2}+\sin 2\beta\left(\frac{8c_1^2t^2v^3}{3r^6}\right.$$
$$\left.\left.-\frac{2v\left(3c_1^2t^2+v^2\right)}{3r^4}+\frac{v}{2c_{21}^2r^2}\right)\sqrt{c_1^2t^2-r^2}-\frac{u}{r^2}\sqrt{c_1^2t^2-r^2}\left(\frac{1}{2c_{21}^2}-1\right)\right]$$
$$-H\left(t-r/c_2\right)\frac{1}{c_2}\left[\cos 2\beta\left(-\frac{8c_2^2t^2v^2u}{3r^6}+\frac{2u\left(c_2^2t^2+v^2\right)}{3r^4}-\frac{u}{6r^2}\right)\sqrt{c_2^2t^2-r^2}\right.$$
$$+\sin 2\beta\left(\frac{8c_2^2t^2v^3}{3r^6}-\frac{2v\left(3c_2^2t^2+v^2\right)}{3r^4}+\frac{v}{2r^2}\right)\sqrt{c_2^2t^2-r^2}$$
$$\left.\left.-\frac{u}{2r^2}\sqrt{c_2^2t^2-r^2}\right]\right\}$$

$$T_{yy} = \frac{1}{2\pi}\left\{H\left(t-r/c_1\right)\frac{c_{21}^2}{c_1}\left[\cos 2\beta\left(-\frac{8c_1^2t^2v^3}{3r^6}+\frac{2v\left(3c_1^2t^2+v^2\right)}{3r^4}\right.\right.\right.$$

$$
\begin{aligned}
&- \frac{v}{2c_{21}^2 r^2}\Bigg) \sqrt{c_1^2 t^2 - r^2} + \sin 2\beta \Bigg(-\frac{8c_1^2 t^2 v^2 u}{3r^6} + \frac{2u\left(c_1^2 t^2 + v^2\right)}{3r^4} \\
&+ \frac{u}{3r^2} - \frac{u}{2c_{21}^2 r^2}\Bigg) \sqrt{c_1^2 t^2 - r^2} - \frac{v}{2c_{21}^2 r^2} \sqrt{c_1^2 t^2 - r^2}\Bigg] \\
&-H\left(t - r/c_2\right) \frac{1}{c_2} \Bigg[\cos 2\beta \left(-\frac{8c_2^2 t^2 v^3}{3r^6} + \frac{2v\left(3c_2^2 t^2 + v^2\right)}{3r^4} - \frac{v}{2r^2} \right) \sqrt{c_1^2 t^2 - r^2} \\
&+ \sin 2\beta \left(-\frac{8c_2^2 t^2 v^2 u}{3r^6} + \frac{2u\left(c_2^2 t^2 + v^2\right)}{3r^4} - \frac{u}{6r^2} \right) \sqrt{c_1^2 t^2 - r^2} \\
&+ \frac{v}{2r^2} \sqrt{c_1^2 t^2 - r^2}\Bigg]\Bigg\}
\end{aligned}
$$

in which $u = \bar{x} - \bar{\xi}$, $v = \bar{y} - \bar{\eta}$, and $c_{21} = c_2^2/c_1^2$.

5.2.1 Temporal Interpolations of Boundary Parameters

Implementation of the time stepping algorithm in (5-33) requires assumptions about the temporal distribution of boundary displacements and tractions from one time step to another. As stated previously, it is assumed that the boundary displacements and tractions for any given node on the boundary are piecewise linear over each time step (Figure 5-4). The formulation of the temporal interpolation functions for the boundary parameters follows Tian's (1990) work, in which the boundary displacements $u_{j(k)}$ and

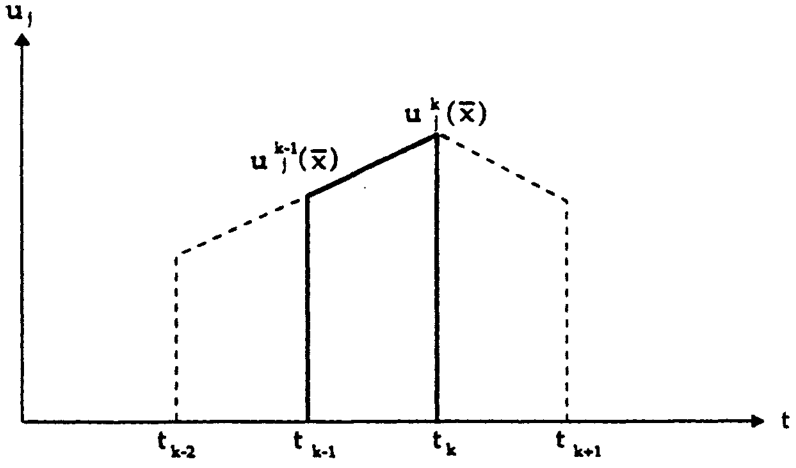

Figure 5-4: Variation of displacements between time steps.

tractions $t_{j(k)}$ were modeled as a series of triangle-shaped pulses with the local nodal values $u_j^k(\bar{x})$ and $t_j^k(\bar{x})$ as peak pulse values (Figure 5-5). Each triangular pulse with peak value u_j^k or t_j^k stretches over two time steps from $(k-1)\Delta t$ to $(k+1)\Delta t$, with the peak value centered at $k\Delta t$ (Figure 5-6). Tian (1990) illustrated that the simplest way to perform the integrations required in (5-33) is when the triangular boundary displacement and traction pulses are written in terms of linear combinations of functions of the form $H(t)\,t/\Delta t$, where $H(t)$ is the Heaviside function. The piecewise linear formulation is then obtained by combining three such functions, staggered at successive time steps, resulting in

$$u_{j(k)} = \left[H(t-t_{k-1})\frac{\tau_{k-1}}{\Delta t} - 2H(t-t_k)\frac{\tau_k}{\Delta t} + H(t-t_{k+1})\frac{\tau_{k+1}}{\Delta t}\right] u_j^k(\bar{x}) \qquad (5\text{-}36)$$

and

$$t_{j(k)} = \left[H(t-t_{k-1})\frac{\tau_{k-1}}{\Delta t} - 2H(t-t_k)\frac{\tau_k}{\Delta t} + H(t-t_{k+1})\frac{\tau_{k+1}}{\Delta t}\right] t_j^k(\bar{x}) \qquad (5\text{-}37)$$

where $t_k = k\Delta t$, and $\tau_k = t - t_k$. The fundamental solution tensors due to these triangle-shaped displacement and traction loading pulses can be obtained directly from

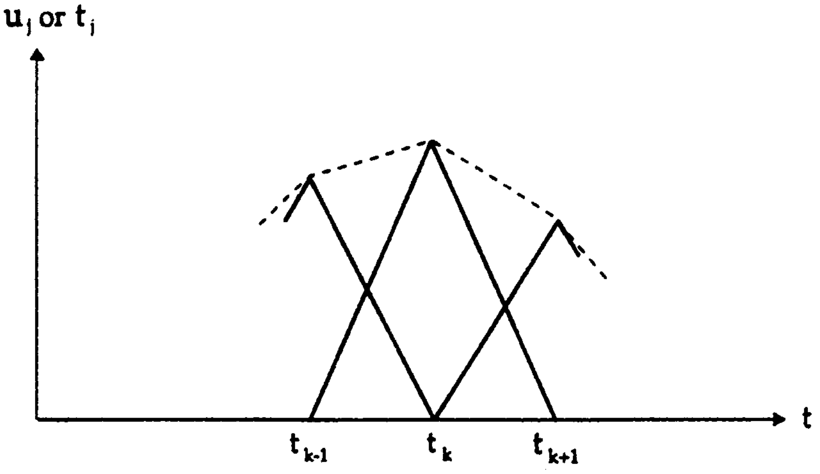

Figure 5-5: Temporal interpolation with triangular hat functions.

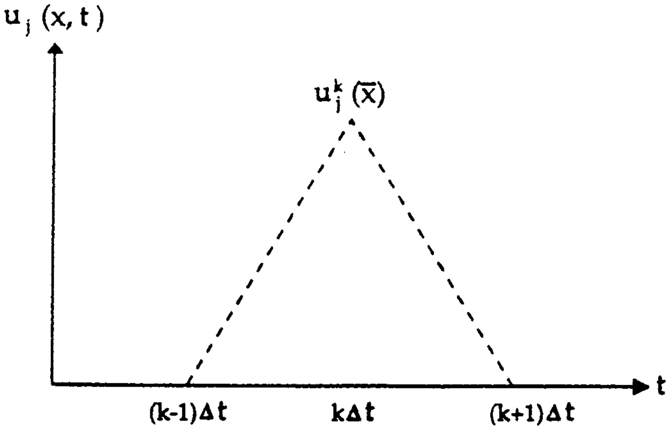

Figure 5-6: Triangular pulse at time step k.

(5-34) and (5-35). Keeping the loading time zero by using the time translation property (3-29) to shift the evaluation times to correspond with the pulses in (5-36) and (5-37) results in

$$\begin{aligned} U_{ij}\left((m-k+1)\,\Delta t; 0, t_{j(k)}\right) = & \left[U_{ij}\left((m-k+1)\,\Delta t; 0, H(t)\,\frac{t}{\Delta t}\right)\right. \\ & -2U_{ij}\left((m-k)\,\Delta t; 0, H(t)\,\frac{t}{\Delta t}\right) \\ & \left.+\,U_{ij}\left((m-k-1)\,\Delta t; 0, H(t)\,\frac{t}{\Delta t}\right)\right] t_j^k(\bar{x}) \end{aligned} \tag{5-38}$$

and

$$\begin{aligned} T_{ij}\left((m-k+1)\,\Delta t; 0, u_{j(k)}\right) = & \left[T_{ij}\left((m-k+1)\,\Delta t; 0, H(t)\,\frac{t}{\Delta t}\right)\right. \\ & -2T_{ij}\left((m-k)\,\Delta t; 0, H(t)\,\frac{t}{\Delta t}\right) \\ & \left.+\,T_{ij}\left((m-k-1)\,\Delta t; 0, H(t)\,\frac{t}{\Delta t}\right)\right] u_j^k(\bar{x}) \end{aligned} \tag{5-39}$$

Substituting (5-38) and (5-39) into (5-33) and summing over the nodal values of boundary displacements $u_j^k(\bar{x})$ and tractions $t_j^k(\bar{x})$, with k ranging from 1 to m, results in

$$\begin{aligned}
&\sum_{b=1}^{N} \int_{S_b} T_{ij}\left(\Delta t; 0, H(t)\frac{t}{\Delta t}\right) u_j^m(\bar{x})\, d\bar{x} \\
=\; &\sum_{k=1}^{m} \sum_{b=1}^{N} \int_{S_b} \left[U_{ij}\left((m-k+1)\Delta t; 0, H(t)\frac{t}{\Delta t}\right)\right. \\
&\left. - 2U_{ij}\left((m-k)\Delta t; 0, H(t)\frac{t}{\Delta t}\right) + U_{ij}\left((m-k-1)\Delta t; 0, H(t)\frac{t}{\Delta t}\right)\right] t_j^k(\bar{x})\, d\bar{x} \\
&- \sum_{k=1}^{m-1} \sum_{b=1}^{N} \int_{S_b} \left[T_{ij}\left((m-k+1)\Delta t; 0, H(t)\frac{t}{\Delta t}\right)\right. \\
&\left. - 2T_{ij}\left((m-k)\Delta t; 0, H(t)\frac{t}{\Delta t}\right) + T_{ij}\left((m-k-1)\Delta t; 0, H(t)\frac{t}{\Delta t}\right)\right] u_j^k(\bar{x})\, d\bar{x}
\end{aligned} \tag{5-40}$$

To simplify the notation, (5-40) can be written as

$$\begin{aligned}
\sum_{b=1}^{N} \int_{S_b} LT_{ij}^{1} u_j^m(\bar{x})\, d\bar{x} \;=\; &\sum_{k=1}^{m} \sum_{b=1}^{N} \int_{S_b} LU_{ij}^{m-k+1} t_j^k(\bar{x})\, d\bar{x} \\
&- \sum_{k=1}^{m-1} \sum_{b=1}^{N} \int_{S_b} LT_{ij}^{m-k+1} u_j^k(\bar{x})\, d\bar{x}
\end{aligned} \tag{5-41}$$

in which

$$\begin{aligned}
LT_{ij}^{k} &= T_{ij}\left(k\Delta t; 0, H(t)\frac{t}{\Delta t}\right) - 2T_{ij}\left((k-1)\Delta t; 0, H(t)\frac{t}{\Delta t}\right) \\
&+ T_{ij}\left((k-2)\Delta t; 0, H(t)\frac{t}{\Delta t}\right) \\
LU_{ij}^{k} &= U_{ij}\left(k\Delta t; 0, H(t)\frac{t}{\Delta t}\right) - 2U_{ij}\left((k-1)\Delta t; 0, H(t)\frac{t}{\Delta t}\right) \\
&+ U_{ij}\left((k-2)\Delta t; 0, H(t)\frac{t}{\Delta t}\right)
\end{aligned} \tag{5-42}$$

The foregoing results illustrate that the fundamental solution for triangle-shaped temporal displacement or traction pulses can be obtained by simple addition or subtraction of the fundamental solutions U_{ij} and T_{ij} given by (5-34) and (5-35), applied at different times. It should be noted that the terms in (5-41) and (5-42) are always non-negative because of the causality property of the fundamental solution tensors. U_{ij} and T_{ij}, which states that whenever the evaluation times $k\Delta t$, $(k-1)\Delta t$ and $(k-2)\Delta t$ in (5-41) and (5-42) are less than zero, the fundamental solutions are equal to zero.

5.2.2 Spatial Interpolations of Boundary Parameters

As stated previously, the dynamic boundary displacements and tractions are assumed to vary linearly in time between successive time steps. At each time step these boundary displacements and tractions are evaluated at each boundary element node. To complete the analysis, some functional variation of these parameters over the boundary elements must also be assumed. In this study, the dynamic displacements and tractions are assumed to vary quadratically in space over each boundary element, just as in the elastostatic implementation discussed previously.

The quadratic variation of boundary parameters across each element is taken with respect to the left ($\bar{x} = -a$), right ($\bar{x} = +a$) and center ($\bar{x} = 0$) boundary element nodal points, in which a denotes the element half-length. The boundary displacements and tractions across an arbitrary element S_b can then be written as

$$\begin{aligned} u_j^k(\bar{x}) &= \left(u_j^k\right)_{bL}\phi_L(\bar{x}) + \left(u_j^k\right)_{bC}\phi_C(\bar{x}) + \left(u_j^k\right)_{bR}\phi_R(\bar{x}) \\ t_j^k(\bar{x}) &= \left(t_j^k\right)_{bL}\phi_L(\bar{x}) + \left(t_j^k\right)_{bC}\phi_C(\bar{x}) + \left(t_j^k\right)_{bR}\phi_R(\bar{x}) \end{aligned} \tag{5-43}$$

in which $(\quad)_{bL}$, $(\quad)_{bC}$ and $(\quad)_{bR}$ denote the nodal displacements or tractions at the left, center and right nodes of element S_b. The functions $\phi_L(\bar{x})$, $\phi_C(\bar{x})$ and $\phi_R(\bar{x})$ are the corresponding quadratic interpolation functions given by (5-8). The substitution of (5-43) into (5-41) results in the left side of (5-41) being expressed as

$$\begin{aligned} \sum_{b=1}^{N}\int_{S_b} LT_{ij}^1 u_j^m(\bar{x})\,d\bar{x} &= \sum_{b=1}^{N}\left(u_j^m\right)_{bL}\int_{S_b} LT_{ij}^1\phi_L(\bar{x})\,d\bar{x} \\ &\quad + \sum_{b=1}^{N}\left(u_j^m\right)_{bC}\int_{S_b} LT_{ij}^1\phi_C(\bar{x})\,d\bar{x} \end{aligned} \tag{5-44}$$

$$+\sum_{b=1}^{N}\left(u_j^m\right)_{bR}\int_{S_b} LT_{ij}^{1}\phi_R(\bar{x})\,d\bar{x}$$

The first term on the right-hand side of (5-41) can be written as

$$\begin{aligned}\sum_{k=1}^{m}\sum_{b=1}^{N}\int_{S_b} LU_{ij}^{m-k+1}t_j^k(\bar{x})\,d\bar{x} &= \sum_{k=1}^{m}\sum_{b=1}^{N}\left(t_j^k\right)_{bL}\int_{S_b} LU_{ij}^{m-k+1}\phi_L(\bar{x})\,d\bar{x}\\ &+\sum_{k=1}^{m}\sum_{b=1}^{N}\left(t_j^k\right)_{bC}\int_{S_b} LU_{ij}^{m-k+1}\phi_C(\bar{x})\,d\bar{x}\\ &+\sum_{k=1}^{m}\sum_{b=1}^{N}\left(t_j^k\right)_{bR}\int_{S_b} LU_{ij}^{m-k+1}\phi_R(\bar{x})\,d\bar{x}\end{aligned}\tag{5-45}$$

and the second term as

$$\begin{aligned}\sum_{k=1}^{m-1}\sum_{b=1}^{N}\int_{S_b} LT_{ij}^{m-k+1}u_j^k(\bar{x})\,d\bar{x} &= \sum_{k=1}^{m-1}\sum_{b=1}^{N}\left(u_j^k\right)_{bL}\int_{S_b} LT_{ij}^{m-k+1}\phi_L(\bar{x})\,d\bar{x}\\ &+\sum_{k=1}^{m-1}\sum_{b=1}^{N}\left(u_j^k\right)_{bC}\int_{S_b} LT_{ij}^{m-k+1}\phi_C(\bar{x})\,d\bar{x}\\ &+\sum_{k=1}^{m-1}\sum_{b=1}^{N}\left(u_j^k\right)_{bR}\int_{S_b} LT_{ij}^{m-k+1}\phi_R(\bar{x})\,d\bar{x}\end{aligned}\tag{5-46}$$

in which LU_{ij}^k and LT_{ij}^k are given by (5-42). Because of the linearity of the governing equations, it should be noted that rather than increasing the counter k on the boundary displacements and decreasing it for the kernels in the time-stepping summation in (5-45) and (5-46), the reverse form may be obtained, namely

$$\begin{aligned}\sum_{k=1}^{m}\sum_{b=1}^{N}\int_{S_b} LU_{ij}^{k}t_j^{m-k+1}(\bar{x})\,d\bar{x} &= \sum_{k=1}^{m}\sum_{b=1}^{N}\left(t_j^{m-k+1}\right)_{bL}\int_{S_b} LU_{ij}^{k}\phi_L(\bar{x})\,d\bar{x}\\ &+\sum_{k=1}^{m}\sum_{b=1}^{N}\left(t_j^{m-k+1}\right)_{bC}\int_{S_b} LU_{ij}^{k}\phi_C(\bar{x})\,d\bar{x}\\ &+\sum_{k=1}^{m}\sum_{b=1}^{N}\left(t_j^{m-k+1}\right)_{bR}\int_{S_b} LU_{ij}^{k}\phi_R(\bar{x})\,d\bar{x}\end{aligned}\tag{5-47}$$

and

$$\begin{aligned}
\sum_{k=1}^{m-1}\sum_{b=1}^{N}\int_{S_b} LT_{ij}^{m-k+1}u_j^k\left(\bar{x}\right)d\bar{x} \;=\; & \sum_{k=2}^{m}\sum_{b=1}^{N}\left(u_j^{m-k+1}\right)_{bL}\int_{S_b} LT_{ij}^{k}\phi_L\left(\bar{x}\right)d\bar{x} \qquad (5\text{-}48)\\
& +\sum_{k=2}^{m}\sum_{b=1}^{N}\left(u_j^{m-k+1}\right)_{bC}\int_{S_b} LT_{ij}^{k}\phi_C\left(\bar{x}\right)d\bar{x}\\
& +\sum_{k=2}^{m}\sum_{b=1}^{N}\left(u_j^{m-k+1}\right)_{bR}\int_{S_b} LT_{ij}^{k}\phi_R\left(\bar{x}\right)d\bar{x}
\end{aligned}$$

These forms lend themselves more easily to numerical implementation, because once the boundary element influence coefficients have been calculated for all time steps in an ascending time-stepping order and saved to a data file, they are directly accessible at each time step k, without any further manipulation. Substitution of (5-8) into (5-47) and (5-48) results in the following algebraic expressions

$$\begin{aligned}
\left(B_{xx}^{L}\right)_J^k &= \int_{S_b} LU_{xx}^{k}\phi_L\left(\bar{x}\right)d\bar{x}\\
&= \int_{-a}^{+a}\frac{1}{2}\frac{\bar{x}}{a}\left(\frac{\bar{x}}{a}-1.0\right)LU_{xx}^{k}d\bar{x}
\end{aligned}$$

$$\begin{aligned}
\left(B_{xx}^{C}\right)_J^k &= \int_{S_b} LU_{xx}^{k}\phi_C\left(\bar{x}\right)d\bar{x}\\
&= \int_{-a}^{+a}\left(1.0-\frac{\bar{x}^2}{a^2}\right)LU_{xx}^{k}d\bar{x} \qquad (5\text{-}49)
\end{aligned}$$

$$\begin{aligned}
\left(B_{xx}^{R}\right)_J^k &= \int_{S_b} LU_{xx}^{k}\phi_R\left(\bar{x}\right)d\bar{x}\\
&= \int_{-a}^{+a}\frac{1}{2}\frac{\bar{x}}{a}\left(\frac{\bar{x}}{a}+1.0\right)LU_{xx}^{k}d\bar{x}
\end{aligned}$$

and so forth for the traction coefficients, and

$$\begin{aligned}\left(A^L_{xx}\right)^k_J &= \int\limits_{S_b} LT^k_{xx}\phi_L(\bar{x})\,d\bar{x} \\ &= \int\limits_{-a}^{+a} \frac{1}{2}\frac{\bar{x}}{a}\left(\frac{\bar{x}}{a}-1.0\right) LU^k_{xx}d\bar{x}\end{aligned}$$

$$\begin{aligned}\left(A^L_{xx}\right)^k_J &= \int\limits_{S_b} LT^k_{xx}\phi_L(\bar{x})\,d\bar{x} \\ &= \int\limits_{-a}^{+a} \frac{1}{2}\frac{\bar{x}}{a}\left(\frac{\bar{x}}{a}-1.0\right) LU^k_{xx}d\bar{x} \qquad (5\text{-}50)\end{aligned}$$

$$\begin{aligned}\left(A^L_{xx}\right)^k_J &= \int\limits_{S_b} LT^k_{xx}\phi_L(\bar{x})\,d\bar{x} \\ &= \int\limits_{-a}^{+a} \frac{1}{2}\frac{\bar{x}}{a}\left(\frac{\bar{x}}{a}-1.0\right) LU^k_{xx}d\bar{x}\end{aligned}$$

and so forth for the displacement coefficients. The notation $(\quad)^k_J$ denotes that the coefficients are evaluated at the *k-th* time step and are associated with element J. Substitution of the algebraic expressions (5-49) and (5-50) into (5-44), (5-47) and (5-48) results in

$$\begin{aligned}\sum_{b=1}^{N}\int\limits_{S_b} LT^1_{ij}u^m_j(\bar{x})\,d\bar{x} &= \sum_{J=1}^{N}\Big\{\left(u^m_j\right)_{JL}\left(A^L_{ij}\right)^1_J + \left(u^m_j\right)_{JC}\left(A^L_{ij}\right)^1_J \\ &\quad + \left(u^m_j\right)_{JR}\left(A^R_{ij}\right)^1_J\Big\} \qquad (5\text{-}51)\end{aligned}$$

for (5-44), and

$$\begin{aligned}\sum_{k=1}^{m}\sum_{b=1}^{N}\int\limits_{S_b} LU^k_{ij}t^{m-k+1}_j(\bar{x})\,d\bar{x} &= \sum_{k=1}^{m}\sum_{J=1}^{N}\Big\{\left(t^{m-k+1}_j\right)_{JL}\left(B^L_{ij}\right)^k_J \qquad (5\text{-}52) \\ &\quad + \left(t^{m-k+1}_j\right)_{JC}\left(B^C_{ij}\right)^k_J + \left(t^{m-k+1}_j\right)_{JR}\left(B^R_{ij}\right)^k_J\Big\}\end{aligned}$$

for (5-47), and finally

$$\sum_{k=2}^{m}\sum_{b=1}^{N}\int_{S_b} LT_{ij}^{k}u_j^{m-k+1}(\bar{x})\,d\bar{x} = \sum_{k=2}^{m}\sum_{J=1}^{N}\left\{\left(u_j^{m-k+1}\right)_{JL}\left(A_{ij}^{L}\right)_J^k \right. \tag{5-53}$$
$$\left. + \left(u_j^{m-k+1}\right)_{JC}\left(A_{ij}^{C}\right)_J^k + \left(u_j^{m-k+1}\right)_{JR}\left(A_{ij}^{R}\right)_J^k\right\}$$

for (5-48). Subsequently, substitution of (5-51), (5-52) and (5-53) into (5-41) yields

$$\begin{aligned}
&\sum_{J=1}^{N}\left\{\left(u_j^{m}\right)_{JL}\left(A_{ij}^{L}\right)_J^1 + \left(u_j^{m}\right)_{JC}\left(A_{ij}^{C}\right)_J^1 + \left(u_j^{m}\right)_{JR}\left(A_{ij}^{R}\right)_J^1\right\} \\
= &\sum_{k=1}^{m}\sum_{J=1}^{N}\left\{\left(t_j^{m-k+1}\right)_{JL}\left(B_{ij}^{L}\right)_J^k + \left(t_j^{m-k+1}\right)_{JC}\left(B_{ij}^{C}\right)_J^k\right. \\
&\left. + \left(t_j^{m-k+1}\right)_{JR}\left(B_{ij}^{R}\right)_J^k\right\} \\
&-\sum_{k=2}^{m}\sum_{J=1}^{N}\left\{\left(u_j^{m-k+1}\right)_{JL}\left(A_{ij}^{L}\right)_J^k + \left(u_j^{m-k+1}\right)_{JC}\left(A_{ij}^{C}\right)_J^k\right. \\
&\left. - \left(u_j^{m-k+1}\right)_{JR}\left(A_{ij}^{R}\right)_J^k\right\}
\end{aligned} \tag{5-54}$$

in which $i = x, y$ and $j = x, y$.

All the integrals needed in (5-54) can be evaluated analytically. The results of the necessary integrations are listed in Appendix B. It should be noted that in evaluating these integrals analytically, a simplifying assumption was made for the case when the waves have just arrived at points between any two nodal points. In this case, it is assumed that all the terms at the wave fronts $c_1 t = r$ and $c_2 t = r$ are zero. This assumption is based on the observation that the results of the analytical integrations are all zero at the wave fronts, except possibly terms involving the arctangent function.

Finally, it should be noted that (5-54) can be rearranged so that the summations are performed over the nodal points rather than the elements. In this case, a closed boundary contour approximated by N elements, will have $2N$ nodes. Then, following the notation used in the elastostatic formulation, expression (5-54) can be rewritten as

$$\sum_{wc=1,3,..}^{2N-1}\overset{wc}{\left(u_j^m\right)}_J\overset{wc}{\left(A_{ij}^L\right)}{}_J^1 + \sum_{we=2,4,..}^{2N}\left[\overset{we}{\left(u_j^m\right)}_{J-1}\overset{we}{\left(A_{ij}^R\right)}{}_{J-1}^1\overset{we}{\left(u_j^m\right)}_J\overset{we}{\left(A_{ij}^L\right)}{}_J^1\right]$$

$$
\begin{aligned}
= & \sum_{k=1}^{m}\sum_{wc=1,3,..}^{2N-1} \overset{wc}{\left(t_j^{m-k+1}\right)_J}\overset{wc\quad k}{\left(B_{ij}^{C}\right)_J} \\
& +\sum_{k=1}^{m}\sum_{wc=2,4,..}^{2N} \left[\overset{we}{\left(t_j^{m-k+1}\right)_{J-1}}\overset{we\quad k}{\left(B_{ij}^{R}\right)_{J-1}} + \overset{we}{\left(t_j^{m-k+1}\right)_J}\overset{we\quad k}{\left(B_{ij}^{L}\right)_J}\right] \\
& -\sum_{k=2}^{m}\sum_{wc=1,3,..}^{2N-1} \overset{wc}{\left(u_j^{m-k+1}\right)_J}\overset{wc\quad k}{\left(A_{ij}^{C}\right)_J} \\
& -\sum_{k=2}^{m}\sum_{wc=2,4,..}^{2N} \left[\overset{we}{\left(u_j^{m-k+1}\right)_{J-1}}\overset{we\quad k}{\left(A_{ij}^{R}\right)_{J-1}} + \overset{we}{\left(u_j^{m-k+1}\right)_J}\overset{we\quad k}{\left(A_{ij}^{L}\right)_J}\right]
\end{aligned}
\tag{5-55}
$$

At each time step, the analytical evaluation of the boundary integrals in (5-55) results in an algebraic equation with $4N$ unknown displacements, because there are two unknown displacements $(\overset{i}{u_x^m})$ and $\left(\overset{i}{u_y^m}\right)$ at each node i. To obtain the same number of equations as unknowns, the loading point $\underline{\xi}$ is allowed to approach every node on the boundary, resulting in two algebraic equations for each node. The limiting process to the boundary is identical to the elastostatic limiting process, discussed previously. It should be pointed out that the resulting self-effect coefficients listed in Appendix B contain *no* singularities. All the singularities have been eliminated as a result of using analytical integration to evaluate the integrals. This is a fundamental reason for using analytical integration schemes, rather than numerical integration schemes in elastodynamic time domain boundary element methods.

The final system of algebraic equations resulting from this limiting process consists of $4N$ by $4N$ equations at each time step and can be written in matrix form as

$$
\mathbf{A}^1\mathbf{u}^m = \sum_{k=1}^{m}\mathbf{B}^k\mathbf{t}^{m-k+1} - \sum_{k=2}^{m}\mathbf{A}^k\mathbf{u}^{m-k+1} \tag{5-56}
$$

in which the terms under the summation signs represent the time history of the boundary displacements and tractions and the vectors $\mathbf{u}^k$ and $\mathbf{t}^k$ are the nodal displacements and tractions at time $k\Delta t$. The coefficient matrices $\mathbf{A}^k$ and $\mathbf{B}^k$at time $k\Delta t$ are defined as $\left[A_{ij}^k\right]_{pq}$ and $\left[B_{ij}^k\right]_{pq}$, in which i and j denote either the x or the y

direction, and p and q take on values from 1 to $2N$. Therefore, $\mathbf{A}^k$ can be written as

$$\mathbf{A}^k = \begin{bmatrix} \left[A_{ij}^k\right]_{11} & \cdots & \left[A_{ij}^k\right]_{12N} \\ \vdots & & \vdots \\ \left[A_{ij}^k\right]_{2N1} & \cdots & \left[A_{ij}^k\right]_{2N2N} \end{bmatrix} \tag{5-57}$$

in which

$$\left[A_{ij}^k\right]_{pq} = \begin{bmatrix} A_{xx}^k & A_{xy}^k \\ A_{yx}^k & A_{yy}^k \end{bmatrix} \tag{5-58}$$

The coefficient matrix $\mathbf{B}^k$ has the same form as in (5-57) and (5-58).

5.2.3 Piecewise Homogeneous Media in Elastodynamics

The numerical implementation of the dynamic direct boundary element method was formulated in (5-56) for homogeneous media. In the following, (5-56) is extended to include solutions of displacements and tractions at interfaces between zones of homogeneous materials with different material properties. An approach will be developed that exploits the equivalence between the static formulation, discussed previously, and the dynamic formulation at any given time step. This equivalence between the two formulations can be observed by rewriting (5-56) as

$$\sum_{k=1}^{m} \mathbf{B}^k \mathbf{t}^{m-k+1} = \sum_{k=1}^{m} \mathbf{A}^k \mathbf{u}^{m-k+1} \tag{5-59}$$

This form is closely related to the numerical formulation of the static boundary element method, expressed by (5-17). A comparison between the dynamic formulation (5-59) and the static formulation (5-17) illustrates that the main difference between the two is that the dynamic formulation requires summations over the time history of loading, whereas the static formulation is only applied once. This difference is due to the nature of the fundamental solutions in the dynamic and static formulations.

The static formulation is based on a fundamental solution due to a load that is static in time, whereas the dynamic formulation is based on a fundamental solution that is due to a load that changes with time, making it necessary to include the time history of loading in the dynamic formulation. However, at each time step, m, the dynamic coefficient matrices $\mathbf{A}^m$ and $\mathbf{B}^m$ are obtained in an equivalent way to the static coefficient matrices $\mathbf{A}$ and $\mathbf{B}$. This equivalency between the elastostatic formulation and the elastodynamic formulation at each time step allows (5-56) to be extended to solve for the interface displacements and tractions at each time step. The continuity conditions, expressed by (5-22), are applied at each time step, resulting in

$$\begin{aligned} \mathbf{u}_{1I}^m &= \bar{\mathbf{u}}_{2I}^m \\ \mathbf{t}_{1I}^m &= -\bar{\mathbf{t}}_{2I}^m \end{aligned} \tag{5-60}$$

This gives a system of equations that can be written as

$$\sum_{k=1}^{m} \mathbf{C}^k \mathbf{x}^{m-k+1} = \mathbf{b}^m \tag{5-61}$$

in which $\mathbf{C}^k$ denotes the coefficient matrix at time step $k\Delta t$. The vector $\mathbf{x}^k$ denotes the unknown boundary and interface displacements and tractions at time step k, and the vector $\mathbf{b}^m$ denotes the knowns at time step m. More specifically, $\mathbf{C}^k$ can be expressed as

$$\mathbf{C}^k = \begin{bmatrix} \mathbf{A}_{11}^k & \mathbf{A}_{1I}^k & \mathbf{B}_{1I}^k & 0 \\ \mathbf{A}_{I1}^k & \mathbf{A}_{II}^k & \mathbf{B}_{II}^k & 0 \\ 0 & \bar{\mathbf{A}}_{2I}^k & -\bar{\mathbf{B}}_{2I}^k & \bar{\mathbf{A}}_{22}^k \\ 0 & \bar{\mathbf{A}}_{II}^k & -\bar{\mathbf{B}}_{II}^k & \bar{\mathbf{A}}_{I2}^k \end{bmatrix} \tag{5-62}$$

in which the sub-matrices at each time step k are obtained in a similar way as in the elastostatic formulation, described previously. A comparison of the elastostatic boundary influence coefficient matrix in (5-24) and the current elastodynamic boundary influence coefficient matrix (5-62) clearly illustrates the equivalency of the static formulation and the elastodynamic formulation at each time step. The unknown vector $\mathbf{x}^k$ can be written as

$$\mathbf{x}^k = \begin{bmatrix} \mathbf{u}_1^k & \mathbf{u}_{1I}^k & \bar{\mathbf{t}}_{2I}^k & \bar{\mathbf{u}}_2^k \end{bmatrix}^T \tag{5-63}$$

in which the superscript T denotes the transpose operator, and the known vector $\mathbf{b}^m$ can be expanded as

$$\mathbf{b}^m = \sum_{k=1}^{m} \left\{ \begin{bmatrix} \mathbf{B}_{11}^k & 0 \\ \mathbf{B}_{I1}^k & 0 \\ 0 & \bar{\mathbf{B}}_{22}^k \\ 0 & \bar{\mathbf{B}}_{I2}^k \end{bmatrix} \begin{bmatrix} \mathbf{t}_1^{m-k+1} \\ \bar{\mathbf{t}}_2^{m-k+1} \end{bmatrix} \right\} \tag{5-64}$$

Just as in the elastostatic case, this formulation assumes for convenience of presentation that the tractions on the boundary are known. However, the formulation is completely general and by rearranging the equations appropriately, it can be used to solve problems in which the boundary displacements or a mix of boundary displacements and tractions are known.

5.3 State of Stress at the Boundary

The boundary element formulations discussed previously only provide the displacements and tractions at the boundary and interface of a given sub-region. Sometimes this is sufficient, but many engineering applications require a knowledge of displacements and the whole state of stress at the boundary and interface. In this study, the procedure for determining the normal stress parallel to a boundary or interface consists of the differentiation of the boundary displacements. This yields the local state of strain along the boundary and opens the way to the computation of the corresponding stress components. In the following, the procedure is formulated for the evaluation of the local state of strain and stress on the boundary of an statically loaded domain. Subsequently, it will be extended to any dynamically loaded region. All expressions below are formulated in terms of the *local* element coordinates $(\bar{x}, \bar{y})$, shown in Figure 5-1. The origin of these coordinates is assumed to be at the stress point under consideration.

For plane loading conditions, it follows from the kinematic relation (3-2), that the strain at the boundary or interface is

$$\epsilon_{\bar{x}\bar{x}} = \frac{\partial u_{\bar{x}}}{\partial \bar{x}} \tag{5-65}$$

in which $\epsilon_{\bar{x}\bar{x}}$ denotes the component of the local strain tensor and $u_{\bar{x}}$ the displacement in the local $\bar{x}$-direction, respectively. Now, applying Hooke's law (3-3), the following relationship between stress and strain at the boundary point in question is obtained:

$$\sigma_{\bar{x}\bar{x}} = \frac{1}{1-\nu}\left[\nu\sigma_{\bar{y}\bar{y}} + 2G\epsilon_{\bar{x}\bar{x}}\right] \tag{5-66}$$

This relationship in addition to

$$\sigma_{\bar{x}\bar{y}} = t_{\bar{x}} \quad \sigma_{\bar{y}\bar{y}} = t_{\bar{y}} \tag{5-67}$$

fully determines the plane state of strain at the boundary. In (5-67), $\sigma_{\bar{y}\bar{y}}$ is the component of the local stress tensor in the normal or $\bar{y}$ direction, which can be calculated in terms of the known boundary tractions in the global coordinate system (x, y) as

$$\sigma_{\bar{y}\bar{y}} = -t_x \sin\beta + t_y \cos\beta \tag{5-68}$$

where β is the angle of inclination of the element in question. The local strain tensor $\epsilon_{\bar{x}\bar{x}}$ can be calculated by differentiating the displacements with respect to the local variable $\bar{x}$, resulting in

$$\epsilon_{\bar{x}\bar{x}} = \frac{\partial u_{\bar{x}}}{\partial \bar{x}} = \frac{\partial}{\partial \bar{x}}\left(u_x \cos\beta + u_y \sin\beta\right) \tag{5-69}$$

The displacements on the boundary are given by (5-7) and (5-8) in terms of nodal values. Differentiating these with respect to the local variable $\bar{x}$ and evaluating the results at the center of the element, namely at $\bar{x} = 0$, results in (5-69) becoming

$$\epsilon_{\bar{x}\bar{x}} = \frac{1}{2a}\left[\left((u_x)_{bR} - (u_x)_{bL}\right)\cos\beta + \left((u_y)_{bR} - (u_y)_{bL}\right)\sin\beta\right] \tag{5-70}$$

Now, substituting (5-68) and (5-70) into (5-66) gives

$$\begin{aligned}\sigma_{\bar{x}\bar{x}} &= \frac{\nu}{1-\nu}\left(-t_x \sin\beta + t_y \cos\beta\right) \\ &\quad + \frac{G}{(1-\nu)\,a}\left[\left((u_x)_{bR} - (u_x)_{bL}\right)\cos\beta \right. \\ &\quad \left. + \left((u_y)_{bR} - (u_y)_{bL}\right)\sin\beta\right] \qquad (5\text{-}71)\end{aligned}$$

This completes the full description of stresses at the boundary of the statically loaded domain in question.

In the elastodynamic case, the stresses, tractions and displacements are obtained at the end of each time-step k, in which case the formulation is identical to the elastostatic case. Therefore, the elastostatic formulation above can be repeated exactly at each time step k, resulting in the elastodynamic version of (5-71) as

$$\begin{aligned}\sigma^k_{\bar{x}\bar{x}} &= \frac{\nu}{1-\nu}\left(-t^k_x \sin\beta + t^k_y \cos\beta\right) \\ &\quad + \frac{G}{(1-\nu)\,a}\left[\left(\left(u^k_x\right)_{bR} - \left(u^k_x\right)_{bL}\right)\cos\beta \right. \\ &\quad \left. + \left(\left(u^k_y\right)_{bR} - \left(u^k_y\right)_{bL}\right)\sin\beta\right] \qquad (5\text{-}72)\end{aligned}$$

The elastodynamic formulation can also be written in terms of mass density, ρ, and compressional and shear wave velocities c_1 and c_2, resulting in

$$\begin{aligned}\sigma^k_{\bar{x}\bar{x}} &= \left(1 - \frac{2c_2^2}{c_1^2}\right)\left(-t^k_x \sin\beta + t^k_y \cos\beta\right) \\ &\quad + 2\rho c_2^2\left(1 - \frac{c_2^2}{c_1^2}\right)\left[\left(\left(u^k_x\right)_{bR} - \left(u^k_x\right)_{bL}\right)\cos\beta \right. \\ &\quad \left. + \left(\left(u^k_y\right)_{bR} - \left(u^k_y\right)_{bL}\right)\sin\beta\right] \qquad (5\text{-}73)\end{aligned}$$

5.4 Interior Displacements, Stresses and Velocities

The numerical formulation presented up to this point has focused on calculating the unspecified displacements and tractions on the boundary S of an arbitrary domain Ω. If it is desired to calculate the displacements and stresses at points inside the domain Ω

then use has to be made of the discretized form of the integral equations in Chapter 4. For example, if it is desired to calculate displacements at interior points, then the discretized forms of equations (4-4) for the elastostatic case and (4-7) for the elastodynamic case have to be used. In the following, a brief review is provided of the algebraic expressions that result from the discretization of the elastostatic and elastodynamic displacement equations, (4-4) and (4-7), and a procedure for obtaining interior stresses is developed.

The discretized form of (4-4) can be written as

$$\begin{aligned} u_i\left(\underset{\sim}{\xi}\right) &= \sum_{J=1}^{N}\left\{(t_j)_{JL}\left(B_{ij}^{L}\right)_J + (t_j)_{JC}\left(B_{ij}^{C}\right)_J + (t_j)_{JR}\left(B_{ij}^{R}\right)_J\right\} \qquad (5\text{-}74) \\ &\quad - \sum_{J=1}^{N}\left\{(u_j)_{JL}\left(A_{ij}^{L}\right)_J + (u_j)_{JC}\left(A_{ij}^{C}\right)_J + (u_j)_{JR}\left(A_{ij}^{R}\right)_J\right\} \end{aligned}$$

in which J denotes element number, and where, for example, $(t_j)_{JL}$ and $(u_j)_{JL}$ denote the traction and displacement in the j-th direction at the left-hand node on element J, and the coefficients $\left(A_{ij}^{L}\right)_J$ and $\left(B_{ij}^{L}\right)_J$ denote the boundary element influence coefficients at the same node. A comparable formulation for the interior stresses can be obtained by applying the kinematic equations (3-2) and Hooke's law (3-3) to both sides of (5-74). Because all the necessary differentiations are with respect to $\underset{\sim}{\xi}$, they can be carried out directly inside the integrals. Therefore, it is instructive to first re-write (5-74) in an alternative form, namely

$$\begin{aligned} u_i\left(\underset{\sim}{\xi}\right) &= \sum_{b=1}^{N}\left\{(t_j)_{JL}\int_{S_b} U_{ij}\phi_L(\bar{x})\,d\bar{x} + (t_j)_{JC}\int_{S_b} U_{ij}\phi_C(\bar{x})\,d\bar{x}\right. \\ &\quad \left. + (t_j)_{JR}\int_{S_b} U_{ij}\phi_R(\bar{x})\,d\bar{x}\right\} \\ &\quad - \sum_{b=1}^{N}\left\{(u_j)_{JL}\int_{S_b} T_{ij}\phi_L(\bar{x})\,d\bar{x} + (u_j)_{JC}\int_{S_b} T_{ij}\phi_C(\bar{x})\,d\bar{x}\right. \\ &\quad \left. + (u_j)_{JR}\int_{S_b} T_{ij}\phi_R(\bar{x})\,d\bar{x}\right\} \qquad (5\text{-}75) \end{aligned}$$

Now, introducing a counter $wn = 1, 2, 3$ for the nodes on the *left* (L), *center* (C) and *right* (R) hand sides of the element J gives

$$u_i\left(\underline{\xi}\right) = \sum_{b=1}^{N}\sum_{wn=1}^{3}(t_j)_{wn}\int_{S_b} U_{ij}\phi_{wn}(\bar{x})\,d\bar{x} - \sum_{b=1}^{N}\sum_{wn=1}^{3}(u_j)_{wn}\int_{S_b} T_{ij}\phi_{wn}(\bar{x})\,d\bar{x} \tag{5-76}$$

Substitution of (5-76) into the kinematic equation (3-2) and Hooke's law (3-3), results in

$$\begin{aligned}\sigma_{ij}\left(\underline{\xi}\right) &= \sum_{b=1}^{N}\sum_{wn=1}^{3}(t_k)_{wn}\int_{S_b}\left[\lambda U_{mk,m}\delta_{ij} + G\left(U_{ik,j} + U_{jk,i}\right)\right]\phi_{wn}(\bar{x})\,d\bar{x} \\ &\quad -\sum_{b=1}^{N}\sum_{wn=1}^{3}(u_k)_{wn}\int_{S_b}\left[\lambda\, T_{mk,m}\delta_{ij} + G\left(T_{ik,j} + T_{jk,i}\right)\right]\phi_{wn}(\bar{x})\,d\bar{x}\end{aligned} \tag{5-77}$$

The procedure for calculating internal displacements and stresses in the elastodynamic formulation is similar to the elastostatic formulation, presented above. To calculate the displacements at interior points, the discretized version of (4-7) is used. It can be written as

$$\begin{aligned}u_i\left(\underline{\xi}, t\right) &= \sum_{k=1}^{m}\sum_{b=1}^{N}\sum_{wn=1}^{3}\left(t_j^k\right)_{wn}\int_{S_b} U_{ij}^{m-k+1}\phi_{wn}(\bar{x})\,d\bar{x} \\ &- \sum_{k=1}^{m}\sum_{b=1}^{N}\sum_{wn=1}^{3}\left(u_j^k\right)_{wn}\int_{S_b} T_{ij}^{m-k+1}\phi_{wn}(\bar{x})\,d\bar{x}\end{aligned} \tag{5-78}$$

The interior stresses can be obtained by substituting (5-78) into the kinematic equation (3-2) and Hooke's law (3-3), resulting in

$$\begin{aligned}\sigma_{ij}\left(\underline{\xi}, t\right) &= \sum_{k=1}^{m}\sum_{b=1}^{N}\sum_{wn=1}^{3}\left(t_l^k\right)_{wn}\int_{S_b}\left[\lambda U_{rl,r}^{m-k+1}\delta_{ij}\right. \\ &\quad \left. + G\left(U_{il,j}^{m-k+1} + U_{jl,i}^{m-k+1}\right)\right]\phi_{wn}(\bar{x})\,d\bar{x} \\ &\quad -\sum_{k=1}^{m}\sum_{b=1}^{N}\sum_{wn=1}^{3}\left(u_l^k\right)_{wn}\int_{S_b}\left[\lambda\, T_{rl,r}^{m-k+1}\delta_{ij}\right.\end{aligned} \tag{5-79}$$

$$+\, G\left(T^{m-k+1}_{il,j} + T^{m-k+1}_{jl,i}\right)\Big]\, \phi_{wn}\left(\bar{x}\right) d\bar{x}$$

It should be noted that in the above elastostatic and elastodynamic formulations, both u_i and σ_{ij} are in terms of the global coordinate system, whereas all the space variables inside the boundary element influence coefficients are evaluated in the local coordinate system $(\bar{x}, \bar{y})$ originating at the midpoint of the j-th boundary element. The point $\underline{\xi}$ has coordinates (ξ, η) in the global coordinate system and coordinates $(\bar{\xi}, \bar{\eta})$ in the local coordinate system (Figure 5-1). Therefore, the chain rule for partial differentiation has to be used to perform the necessary differentiations. Using the transformation formulas

$$\begin{aligned} \bar{\xi} &= \xi \cos\beta + \eta \sin\beta \\ \bar{\eta} &= -\xi \sin\beta + \eta \cos\beta \end{aligned} \qquad (5\text{-}80)$$

allows a relationship to be established between the global and the local coordinates. Now, using the chain rule for partial differentiation results in

$$\begin{aligned} \frac{\partial}{\partial \xi} &= \frac{\partial \bar{\xi}}{\partial \xi}\frac{\partial}{\partial \bar{\xi}} + \frac{\partial \bar{\eta}}{\partial \xi}\frac{\partial}{\partial \bar{\eta}} = \cos\beta \frac{\partial}{\partial \bar{\xi}} - \sin\beta \frac{\partial}{\partial \bar{\eta}} \\ \frac{\partial}{\partial \eta} &= \frac{\partial \bar{\xi}}{\partial \eta}\frac{\partial}{\partial \bar{\xi}} + \frac{\partial \bar{\eta}}{\partial \eta}\frac{\partial}{\partial \bar{\eta}} = \sin\beta \frac{\partial}{\partial \bar{\xi}} + \cos\beta \frac{\partial}{\partial \bar{\eta}} \end{aligned} \qquad (5\text{-}81)$$

These relationships relate differentiations with respect to global coordinates to differentiations with respect to local coordinates. Once the differentiations have been carried out, all integrations in the above expressions can be performed analytically. All integrations necessary to evaluate (5-76) and (5-77) are presented in Appendix A, and all integrals necessary to evaluate (5-78) are presented in Appendix B. Similarly, all the differentiations necessary to obtain (5-79) from substituting (5-78) into the kinematic equation (3-2) and Hooke's law (3-3) were originally evaluated by Tian (1990) and are listed in Appendix C for completeness.

The elastostatic and elastodynamic displacements and stresses in piecewise homogeneous media can be computed from the above expressions by using only the influence coefficients and the boundary parameters that are associated with the sub-region in which the interior point is located.

Once the time history of displacements has been obtained at any interior point $\underline{\xi}$ by using (5-78), then the particle velocities at $\underline{\xi}$ may be calculated using the simple differencing scheme

$$v_i^m = \frac{u_i^m - u_i^{m-1}}{\Delta t} \tag{5-82}$$

Because the variation in time between each time step is linear, (5-82) is equivalent to the analytical evaluation of particle velocities by using

$$\begin{aligned} v_i\left(\underline{\xi}, t\right) &= \sum_{b=1}^{N} \sum_{wn=1}^{3} \left(t_j^k\right)_{wn} \frac{\partial B_{ij}^{m-k+1}}{\partial t} \\ &\quad - \sum_{k=1}^{m} \sum_{b=1}^{N} \sum_{wn=1}^{3} \left(u_j^k\right)_{wn} \frac{\partial A_{ij}^{m-k+1}}{\partial t} \end{aligned} \tag{5-83}$$

in which B_{ij}^k and A_{ij}^k are the algebraic expressions given by (5-49) and (5-50), respectively, and since $B_{ij}\left(t = 0\right) = A_{ij}\left(t = 0\right) = 0$.

Chapter 6

Verification and Examples

A number of example problems are presented below to demonstrate the accuracy and versatility of the elastostatic and elastodynamic boundary element implementations. These problems include examples for both homogenous and piecewise homogeneous materials. Both the elastostatic and the elastodynamic problem categories include comparative studies with analytical solutions as well as with problems solved by previous researchers. Also, a number of problems of general practical interest are included. Those problems range from the elastostatic load responses of homogeneous half-planes and layered materials to the generation of surface waves in an elastic half-plane, wave propagation through layered soils, and a study of the surface displacements generated by an underground explosion in a multi-layered soil. The question of the causality of the elastodynamic boundary element scheme is addressed through a simple case study of wave propagation around a v-shaped ditch in a half-plane. Finally, the stability of the elastodynamic boundary element implementation presented in this study is discussed briefly.

Most of the solutions in this chapter are presented in a normalized form, unless the problem being studied was presented by a previous researcher in a given format. In these cases the format of the previous presentation was kept for ease of comparison.

6.1 Elastostatic Problems

In this section, a number of elastostatic problems are presented. These include the loading response of an annulus inside a large plate, a strip loaded homogenous half-plane, a layer resting on a half-plane and a three-layered material.

6.1.1 Annulus Inside a Circular Hole in a Plate

A simple example of a boundary value problem for a piecewise homogenous body is shown in Figure 6.1. This problem was studied previously with boundary elements by Crouch and Starfield (1983), who used a stress discontinuity boundary element formulation with straight-line boundary elements and a constant variation of the unknown stress discontinuities over each element. The region of interest consists of an annulus $a \leq r \leq b$ with a Poisson's ratio ν_1 and a shear modulus G_1 inside a circular hole of radius $r = b$ in an infinite plate with a Poisson's ratio ν_2 and shear modulus G_2.

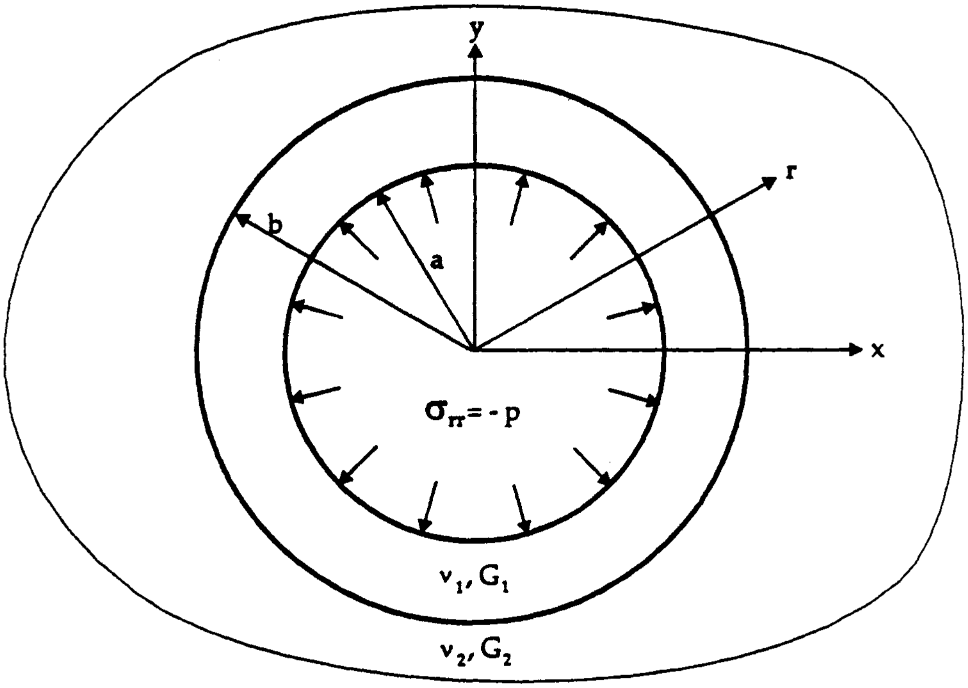

Figure 6-1: Annulus inside a circular hole in a plate.

As shown in the Figure, the inside wall of the annulus is subjected to a normal stress $\sigma_{rr} = -p$, and the plate is unstressed at infinity. Crouch and Starfield (1983) provide the analytical solution to this problem, by assuming that the continuity of radial stress and displacement holds at the interface $r = b$. For the region $a \leq r \leq b$, the radial and tangential stresses are

$$\begin{aligned} \sigma_{rr} &= \frac{1}{1 - a^2/b^2}\left[\left(pa^2/b^2 - \bar{p}\right) - (p - \bar{p})\, a^2/r^2\right] \\ \sigma_{\theta\theta} &= \frac{1}{1 - a^2/b^2}\left[\left(pa^2/b^2 - \bar{p}\right) + (p - \bar{p})\, a^2/r^2\right] \end{aligned} \tag{6-1}$$

and for the region $r \geq b$, the stresses are

$$\begin{aligned} \sigma_{rr} &= -\bar{p}b^2/r^2 \\ \sigma_{\theta\theta} &= +\bar{p}b^2/r^2 \end{aligned} \tag{6-2}$$

in which

$$\bar{p} = \frac{2(1 - \nu_1)pa^2/b^2}{2(1 - \nu_1) + (G_1/G_2 - 1)(1 - a^2/b^2)} \tag{6-3}$$

In this study, a numerical solution to the problem was obtained for the same input parameters as used by Crouch and Starfield (1983): $\nu_1 = \nu_2 = 0.25$, $G_1/G_2 = 2$ and $p/G_1 = 10^{-3}$. The circular boundary $r = a$ and each side of the interface $r = b$ were divided into 32 straight-line elements. Figure 6-2 shows the comparison of the numerical and analytical results. The differences between the numerical and analytical values of both the radial and tangential stresses were less than 0.25 percent. This shows that circular and irregular geometries can be approximated well with a sufficient number of straight-line elements.

6.1.2 A Strip-Loaded Half-plane

Many practical problems in linear elasticity involve bodies that can be idealized as half-planes. Examples of such problems are layered pavement systems resting on an idealized half-plane, and problems in mining and tunneling, where the boundary of a half-plane represents the surface of the earth. The analytical solution to strip-loaded

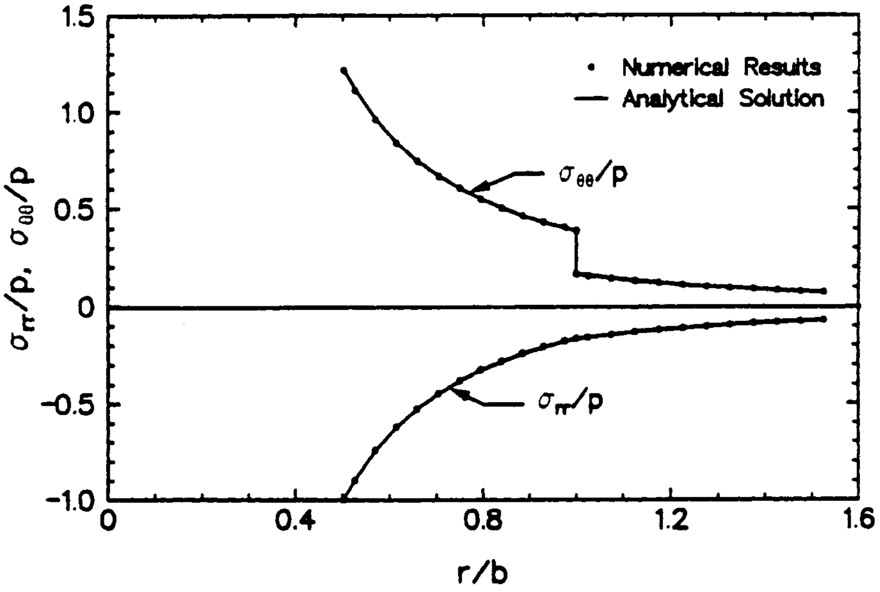

Figure 6-2: Radial and tangential stresses in annulus and plate.

half-planes is readily available in many texts on solid mechanics (see, for example, Crouch and Starfield, 1983). This analytical solution is based on Flamant's problem, which is the problem of a line of concentrated force applied perpendicular to an isotropic elastic half-plane. Flamant's problem can be generalized by the principle of superposition to obtain the solution of a strip load over a limited extent on a half-plane.

By recognizing that the influence of loads far away from their points of action is often negligible, it is possible to approximate the loading response of a half-plane by assuming that it is of limited spatial extent. To test this assumption, the numerical model shown in Figure 6-3 was constructed. The model consists of 44 straight-line elements each of length $b = 10$ m, along the top and bottom surfaces of the "idealized" half-plane, and of 10 elements on each of its sides. The boundary conditions at the bottom and side surfaces of the "idealized" body were taken to be displacement boundary conditions with both the normal and tangential displacement components at each node specified to be equal to zero. The material properties are represented by

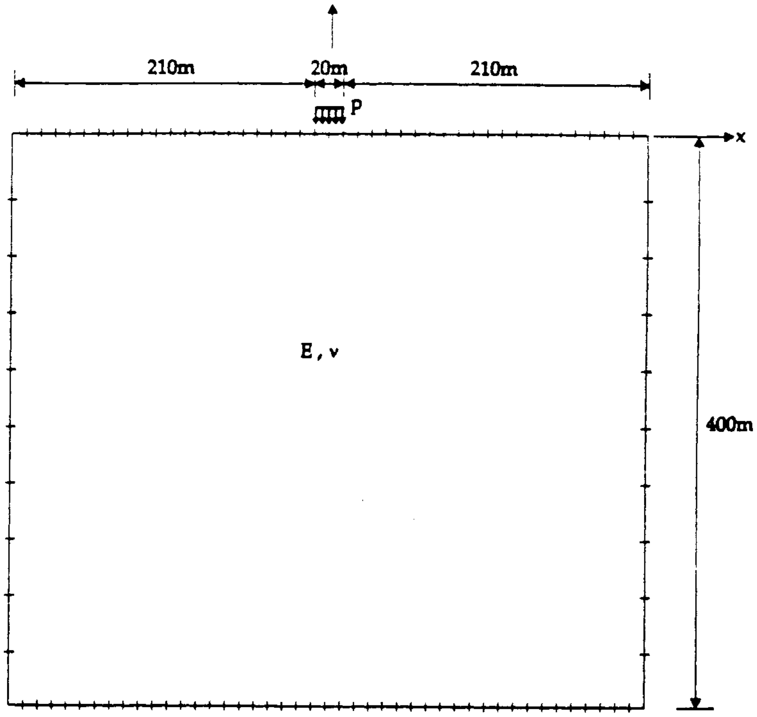

Figure 6-3: Homogeneous half-plane.

Young's modulus $E = 330$ MPa and Poisson's ratio $\nu = 0.25$, and the strip load was taken to be $p = 100$ kPa.

The numerical results obtained for the problem were compared to the analytical solution for a strip loaded homogeneous half-plane. Figures 6-4 and 6-5 show the variation of vertical stresses with depth below the centerline and the edge of the of the strip loaded area. The analytical solution for the vertical stress, σ_{yy}, is given by (e.g. Crouch and Starfield, 1983):

$$\sigma_{yy} = \frac{-p}{\pi}\left[\theta_1 - \theta_2 - y\,(x-a)\,/r_1^2 + y\,(x+a)\,/r_2^2\right] \tag{6-4}$$

in which

$$\begin{array}{lcl} \theta_1 = \arctan \frac{y}{x-a} & \text{and} & \theta_2 = \arctan \frac{y}{x+a} \\ r_1^2 = (x-a)^2 + y^2 & \text{and} & r_2^2 = (x+a)^2 + y^2 \end{array} \tag{6-5}$$

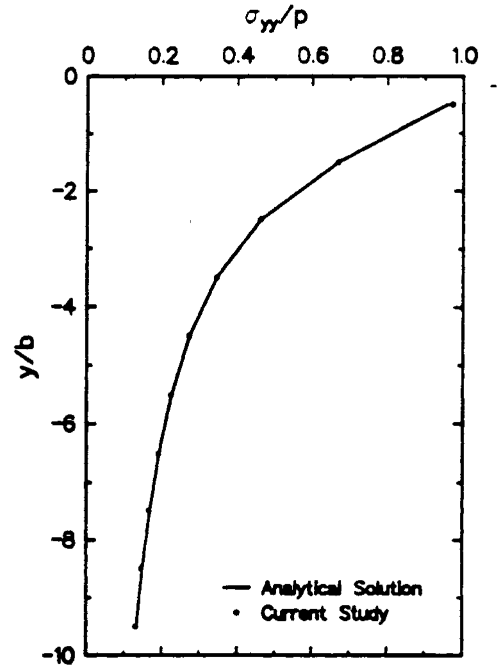

Figure 6-4: Vertical stress below centerline of strip loaded area.

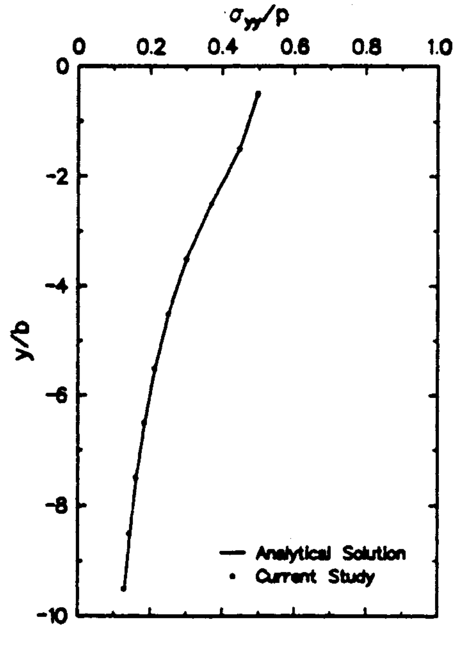

Figure 6-5: Vertical stress below edge of strip loaded area.

The numerical results match the analytical solution very well, with the difference between the numerical and analytical values less than 0.5 percent for both cases. Therefore, it can be concluded that half-plane problems can be modeled for many practical applications by assuming that the half-plane is of limited spatial extent.

It should be noted that volume-based numerical methods such as finite element and finite difference methods also assume that the half-plane is of limited spatial extent. These methods require many more elements than a comparable boundary element discretization, because the internal volume of the body needs to be discretized, whereas with boundary elements only the external surfaces of the body of interest need to be discretized.

6.1.3 A Strip-Loaded Layered Half-Plane

As stated previously, many problems of practical interest in linear elasticity involve one or more layers of finite thickness resting on a half-plane. To establish the validity of the elastostatic boundary element formulation presented in this study for modeling such layer problems, a number of comparisons were made with other existing numerical boundary element formulations and existing analytical solutions. The "idealized" geometry used in this study is shown in Figure 6-6, which is essentially the same as the geometry used for the homogenous half-plane problem discussed previously (Figure 6-3), except for the introduction of an interface at depth $y = -30$ m. Each side of this interface is modeled a row of 44 straight-line elements, each of length $b = 10$ m.

Three distinct cases are studied: (1) the elastic constants for the layer and half-plane are the same, namely $E_1 = E_2 = 330$ MPa and $\nu_1 = \nu_2 = 0.25$ in which the subscripts 1 and 2 denote the layer and the half-plane, respectively, (2) $E_1 = 0.25E_2 = 330$ MPa and $\nu_1 = \nu_2 = 0.25$, such that the half-plane is stiffer than the layer, and (3) $E_1 = 4E_2 = 1320$ Mpa and $\nu_1 = \nu_2 = 0.25$, in which the layer is stiffer than the half-plane. This problem is modeled numerically by two boundary element methods, - the boundary element formulation presented in this study, and a formulation developed by Selcuk (1992), which assumes that the interface connects two bonded half-planes where the interface continuity conditions are satisfied analytically.

Figure 6-7 shows the discretization used for modeling the strip-loaded half-plane with a bonded half-plane boundary element formulation. The surface of the idealized half-plane is modeled with 44 displacement discontinuity elements, each of length $b = 10$ m. The normal and tangential displacement discontinuities are assumed to vary quadratically over each element.

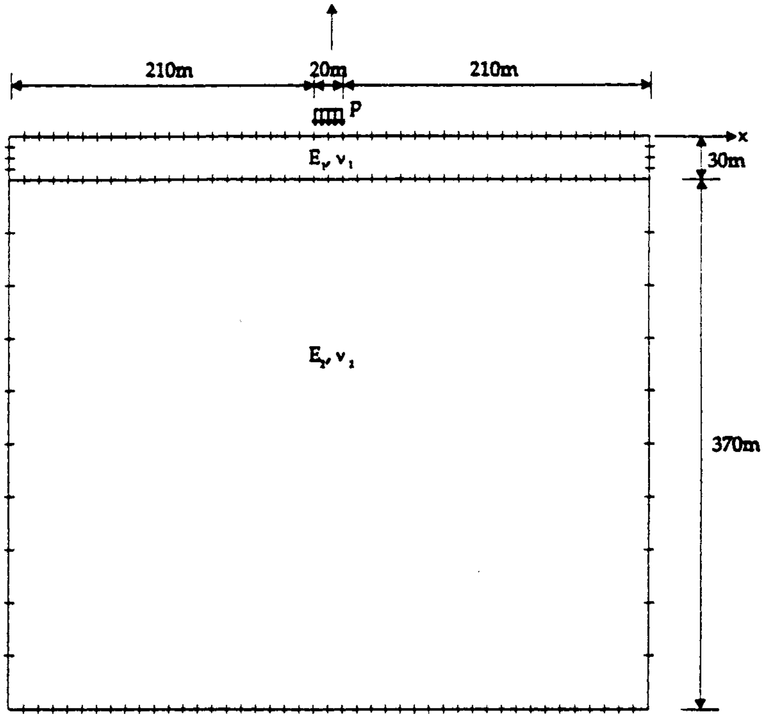

Figure 6-6: Strip-loaded half-plane.

Figure 6-8 compares the vertical stresses along the interface obtained with these two boundary element formulations to the analytical solution given by (6-4). The numerical results obtained by both boundary element methods compare favorably with the analytical solution. Similarly, the variation of vertical stress with depth underneath the centerline of the loaded area is shown in Figure 6-9 and Figure 6-10 for the two formulations. Figure 6-9 shows the case for which the half-plane is stiffer than the layer ($E_2 = 4E_1$). Figure 6-10 shows the stiff layer case ($E_1 = 4E_2$). In both cases, the difference in results between the two boundary element formulations is negligible.

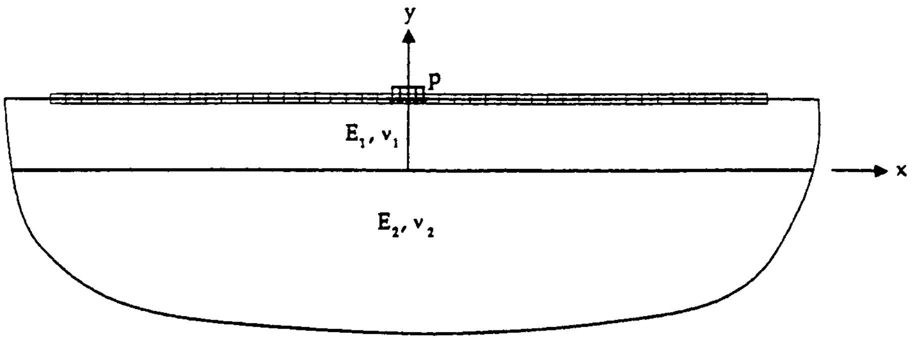

Figure 6-7: Bonded half-plane model.

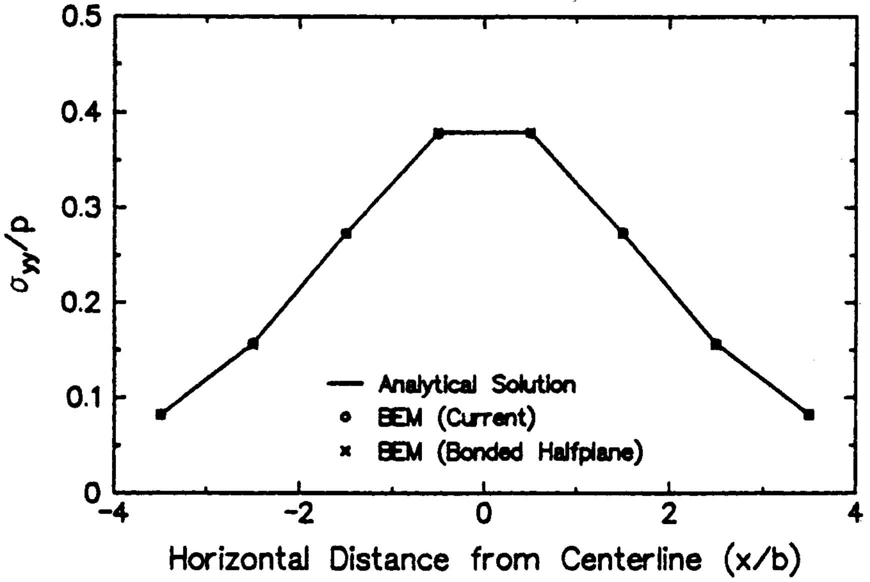

Figure 6-8: Vertical stresses along interface.

Figures 6-8 to 6-10 illustrate clearly that interfaces between two different piecewise homogeneous regions can be modeled quite satisfactorily by either boundary element formulation.

Looking at Figures 6-9 and 6-10, it is worth noticing how the vertical stress dissipates more rapidly with depth for the stiff upper layer case (Figure 6-10). To illustrate this effect further, the vertical stresses along a vertical centerline underneath the loaded area were obtained with the current numerical formulation for the three cases $E_1 = 0.25E_2$, $E_1 = E_2$, and $E_1 = 4E_2$. The results shown in Figure 6-11, clearly show that the higher the relative stiffness ratio (E_1/E_2) between the upper layer and the half-plane, the more pronounced is the associated drop in vertical stress with depth.

6.1.4 A Three-Layered Soil System

The last example given in this study for the elastostatic boundary element formulation is a three-layered problem. Figure 6-12 shows the geometry and the discretization of each layer. Each side boundary is placed at $x = \pm 170$ m and is divided into 12 boundary elements with fixed boundary conditions at each node. The horizontal boundary at $y = -90$ m is also assumed to be fixed. The mesh of 26 elements along each interface has been chosen symmetric with respect to $x = 0$ and is depicted at the bottom of Figure 6-12. The loads on the half-plane are taken as $p' = 150$ kPa and $p'' = 250$ kPa and the elastic constants are $\nu = 0.3$, $E_t = 1.0 \times 10^5$ kPa and $E_b = 5.5 \times 10^5$ kPa. The linear variation in the Young's modulus with depth, depicted in Figure 6-12 is approximated by assuming that the Young's modulus for each layer is the average of its values at the relevant interfaces.

This problem was first studied by Maier and Novati (1987), who used straight-line boundary elements with constant variation in displacements and tractions across each element. An interesting aspect of their analysis is that they specifically exploit the chain-like pattern of the system, by developing a recursive formula which generates a 'stiffness matrix' of the first n layers (from bottom) at the upper interface with the subsequent layer ($n = 1, \ldots, L$). This method is essentially a special case of a more general method to deal with chain-like structures that was proposed by Linkov and

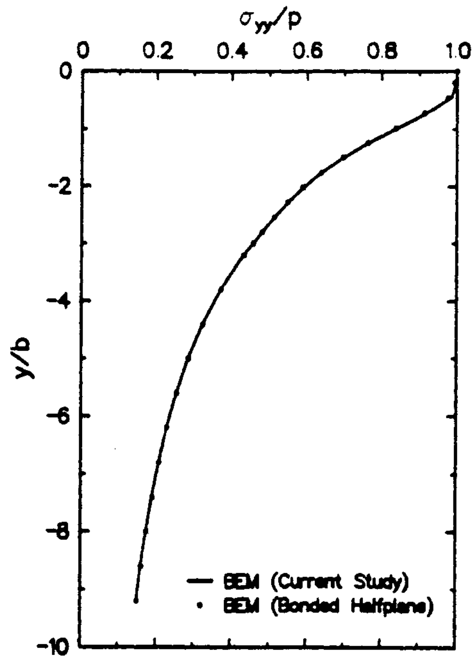

Figure 6-9: Half-plane stiffer than layer of finite thickness.

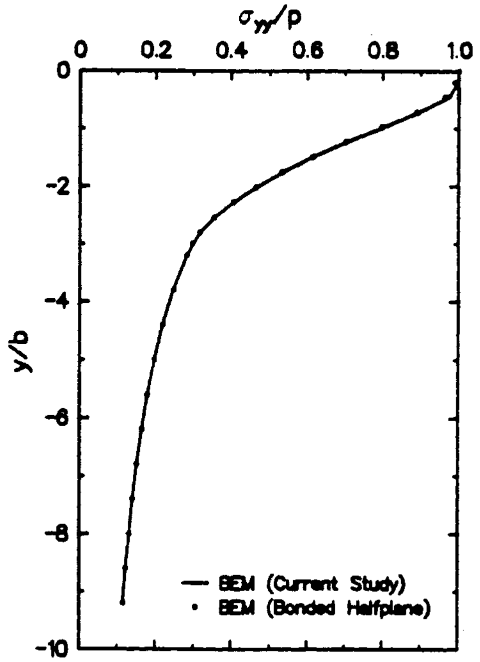

Figure 6-10: Half-plane softer than layer of finite thickness.

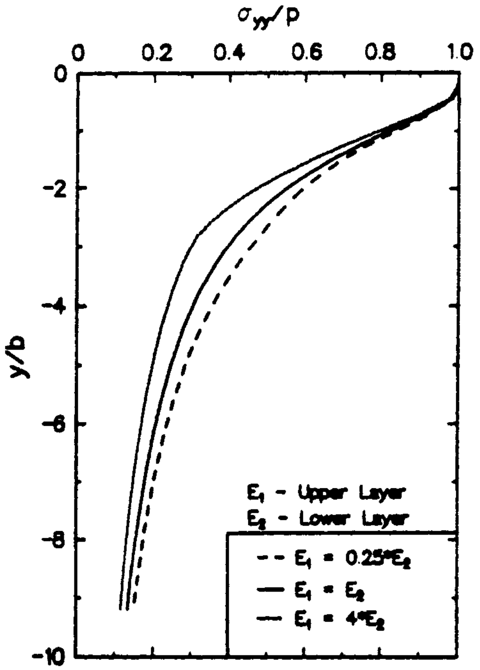

Figure 6-11: Effects of relative stiffness on the vertical stress below centerline of a strip-loaded area.

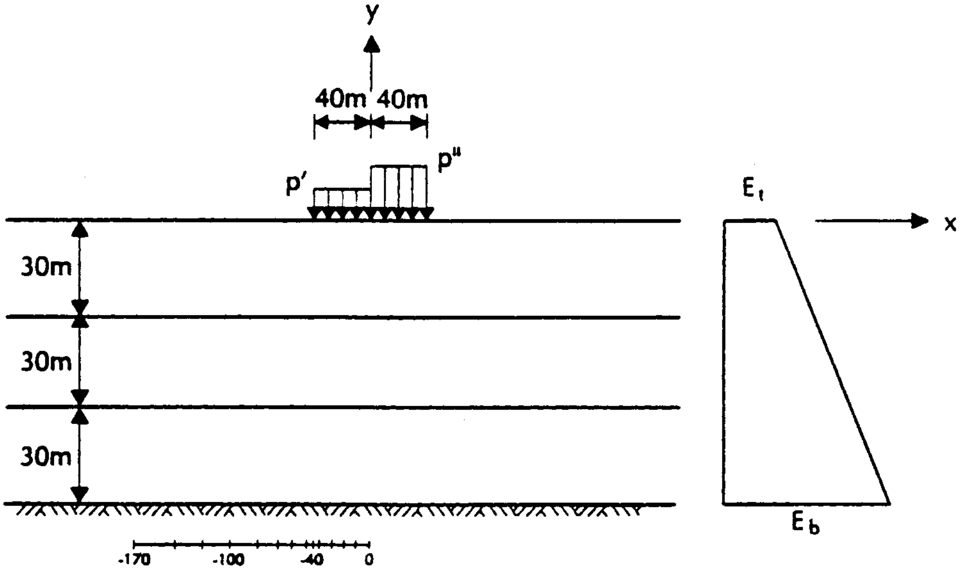

Figure 6-12: A three-layered half-plane.

Filippov (1991).

Figures 6-13 to 6-15 compare the results from the current numerical formulation to the results reported by Maier and Novati (1987). Figure 6-13 shows the variation of vertical stress σ_{yy} along $x = 0$ and Figure 6-14 shows the variation of the horizontal stress σ_{xx} along $x = 0$. The two methods show a close comparison for the variation in vertical stress with depth, but the horizontal stress obtained by the two methods varies considerably between the two methods. This difference in the horizontal stress profiles can possibly be explained by the fact that Maier and Novati use constant boundary elements which may not be appropriate for modeling horizontal stresses in layered systems, and these horizontal stresses also turn out to be very sensitive to the piecewise-constant approximations of the linear variation of Young's modulus with depth, as pointed out by Maier and Novati themselves.

Figure 6-15 shows the variation in vertical displacements u_y along $y = 0$ (lower set of curves) and $y = -30$ m (upper set of curves). The vertical displacements obtained from the two numerical methods compare reasonably well to each other, even though the current study results in slightly greater displacements than the constant boundary element method of Maier and Novati.

It can be concluded from this example that the elastostatic analysis of layered material can be conducted with reasonable accuracy for complex problems of realistic geometries. Common examples of such problems are pavements and layered deposits and formations of soil and rock.

6.2 Elastodynamic Problems

In this section, several examples and applications of the elastodynamic boundary element implementation are discussed. A number of well-known examples are included from the literature, as well as some new applications and examples that illustrate the power and usefulness of the current approach.

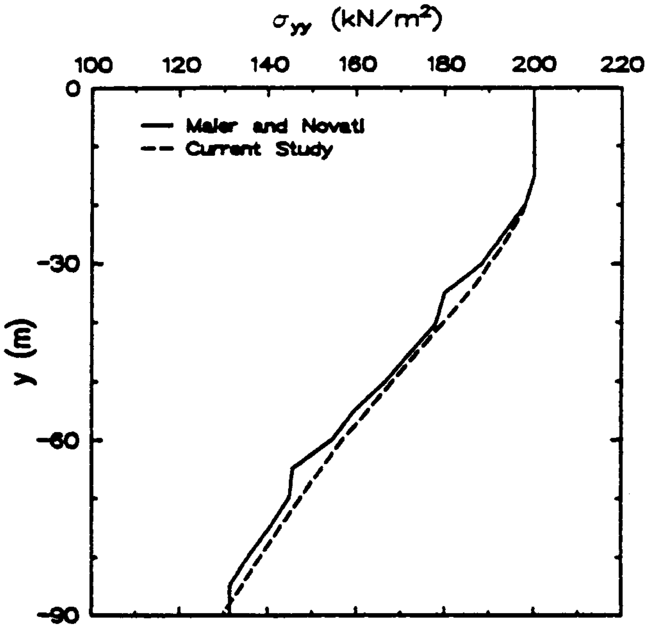

Figure 6-13: Vertical stress along x = 0.

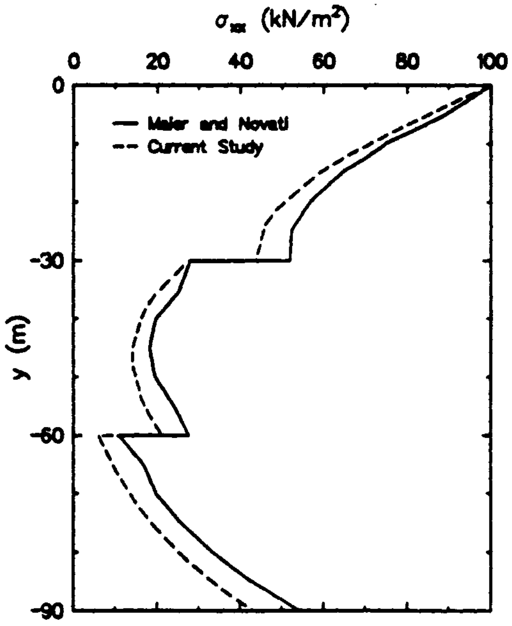

Figure 6-14: Horizontal stress along x = 0.

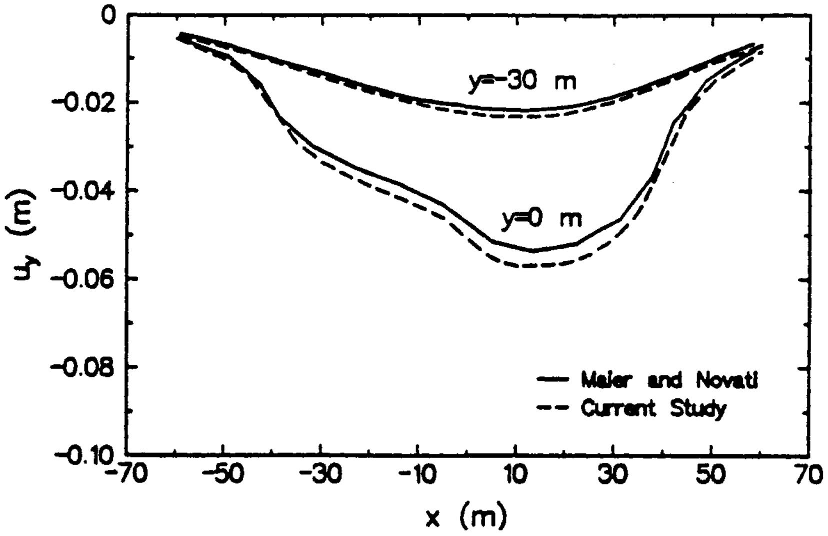

Figure 6-15: Variation of vertical displacements along y = 0 and y = -30 m.

6.2.1 Suddenly Loaded Half-plane

The half-plane shown in Figure 6-16 is initially at rest. Then at time $t = 0$ a part of its surface is disturbed by a vertical traction that is continuous in time and space, as shown in Figure 6-17. The problem is modeled with 26 elements, each of length $\Delta x = 40$ ft. The elastic constants of the half-plane are $E = 2 \times 10^5$ lb/in^2 and $\nu = 0.15$. The longitudinal and shear wave velocities are $c_1 = 3.288 \times 10^4$ in/sec and $c_2 = 2.112 \times 10^4$ in/sec, and the load, $p_o = 1 \times 10^3$ lb/in^2 has a rise time of $t_r = 20 \times 10^{-3}$ seconds. The size of time step was taken as $\Delta t = 0.005$ seconds.

This problem was first solved with an elastodynamic time-domain direct boundary element method by Mansur (1983). The boundaries were approximated by straight-line elements and constant interpolation functions were used to approximate the variation of the tractions and displacements over each boundary element. The temporal variation between subsequent time-steps was taken to be constant for displacements and linear for tractions. The spatial integrations were carried out numerically by using Gauss quadrature and the time integrations were performed analytically. The interior

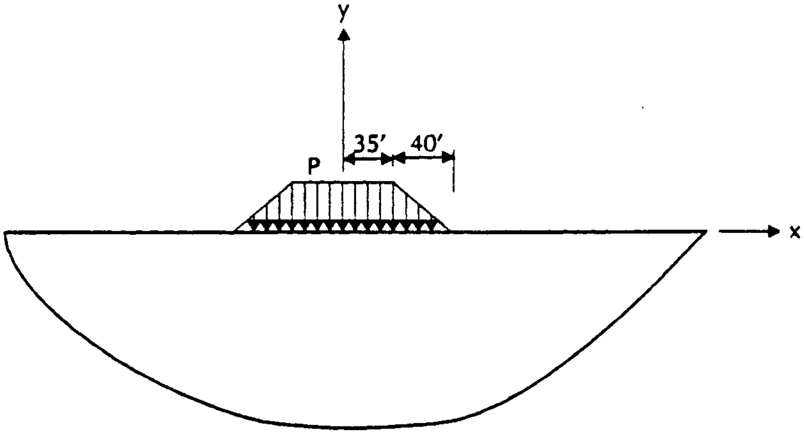

Figure 6-16: Load for the half-plane under continuous prescribed stress distribution.

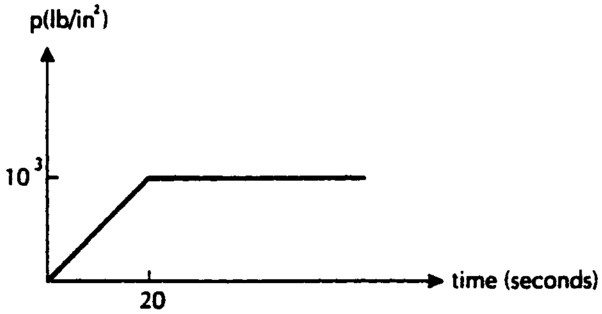

Figure 6-17: Time history for prescribed load on a half-plane.

stresses were obtained by a finite element type approximation. Triangular internal cells were used and stresses at their centroids were computed from displacements which were linearly interpolated inside each cell as a function of the displacements at the cell nodes.

Israil and Banerjee (1990a) also used a time-domain direct boundary element method to solve this problem. The geometry was modeled with isoparametric quadratic elements and linear temporal interpolation functions were used. Again, the spatial and temporal integrations were evaluated numerically and analytically, respectively. It should be noted that the formulation by Israil and Banerjee (1990a) does not allow for exterior boundary value problems. Their formulation requires that all problems be modeled as interior boundary value problems. To approximate exterior boundary value problems, they introduce what they refer to as "enclosing elements," which appear to be some kind of non-reflecting boundary elements. Unfortunately, none of their published work describes the mathematical details of these "enclosing elements."

Figures 6-18 and 6-19 show comparisons with published results for the vertical displacements at interior points $F\,(80', -60')$ and $G\,(150', -10')$ obtained by the present formulation. Overall, the results from the current study give similar results to other published results, except for the first arrival time of the longitudinal wave at point G. Mansur (1983) reports the arrival time to be 0.62 seconds and Israil and Banerjee (1990a) found it to be 0.27 seconds. The present solution also shows the arrival time to be about 0.27 seconds which corresponds well with the physics of the problem, namely the given distance to point G from the edge of the loaded area (908 in) and the given longitudinal wave velocity of 3.288×10^4 in/sec. It should be noted, though, that it is difficult to determine an exact value for the arrival time for this problem, because of the rather long rise time (t_r) of loading.

The vertical stresses, σ_{yy} at points $B\,(75', -75')$ and $C\,(5', -75')$ are shown in Figures 6-20 and 6-21. Again, the current numerical results compare reasonably well with the other published results, except for the increased waviness at late times in the solution by Mansur for both displacements and interior stresses. This behavior could possibly be explained by the fact that constant elastodynamic boundary element formulations have been shown to lead to numerical instabilities at late times (see, for

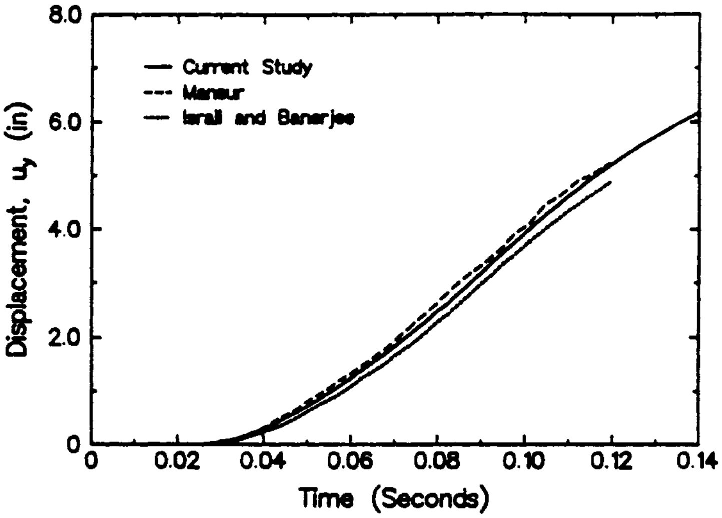

Figure 6-18: Vertical displacments at point F(80', -60').

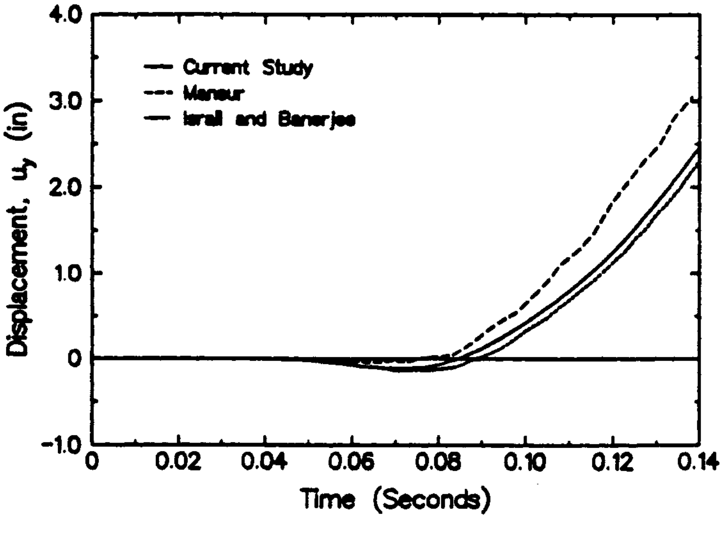

Figure 6-19: Vertical displacements at point G(150', -10').

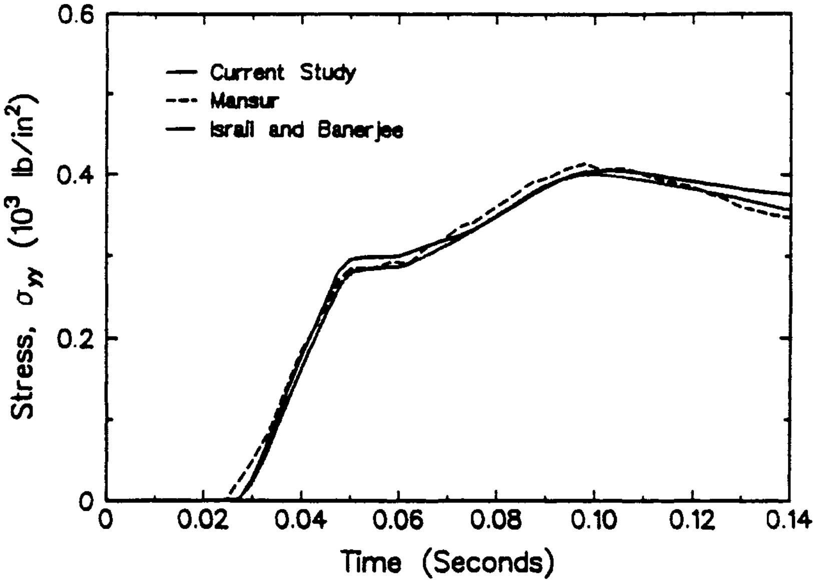

Figure 6-20: Vertical stress at point B(75', -75').

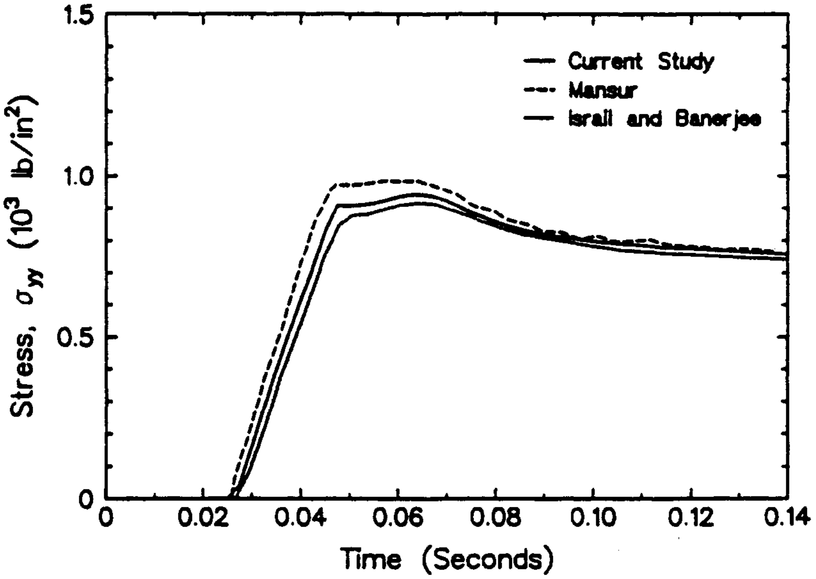

Figure 6-21: Vertical stress at point C(5', 5').

example, Tian, 1991; Siebrits, 1992).

6.2.2 Triangular Open Trench in a Half-plane

The issue of causality of elastodynamic time-domain boundary element methods has been a topic of discussion in the literature for the last decade. Siebrits (1992) defines causality as the relation between a cause and its effect. In a properly implemented time-domain elastodynamic computer code, the receiver point cannot experience any dynamic motion until the longitudinal wave arrives from the nearest source position. If an obstacle such as a ditch or a cavity is located directly between a source and a receiver point, then the receiver point should not experience any dynamic effect from the source position until the wave has traveled around the ditch or cavity.

During their work on wave diffraction by trenches with the aid of a time-domain boundary element method, certain researchers have persistently observed an apparent violation of the causality principle in their results. Antes and von Estorff (1987) were the first to observe this apparent violation of causality in the wave diffraction problem shown in Figure 6-22. They reported significant numerical discrepancy in the vertical displacements at point B in Figure 6-22 depending on whether the problem was discretized as a single or a two-region model. Figure 6-23 shows these reported differences in the vertical displacement at point B. Antes and von Estorff (1987) observed that the response at point B due to an impulse load at point A started earlier than at the time required for the longitudinal wave to travel around the ditch from A to B. They also found that this causality problem disappears if the domain is modeled as a two region system. The same phenomenon was observed by Triantafyllidis and Dasgupta (1990) and Leung et al. (1990) in the frequency domain, and the difficulty was again circumvented by substructuring. Von Estorff and Kausel (1989) and von Estorff and Prabucki (1990) were able to obtain causal solutions with a hybrid boundary element and finite element method for trench diffraction problems, thus leading them to conclude that the causality problem is only associated with boundary element formulations.

Antes and Meise (1990), von Estorff et al. (1990) and Israil and Banerjee (1990a),

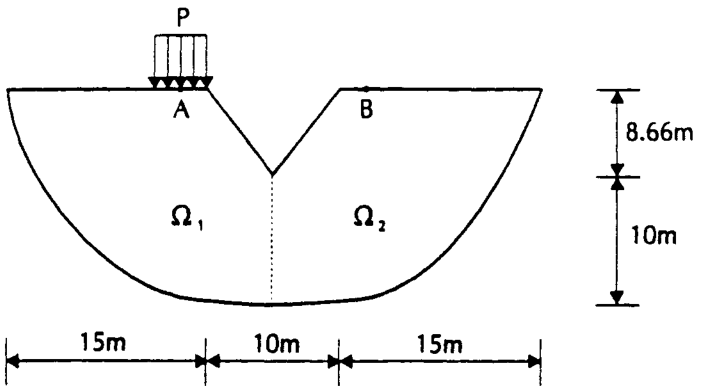

Figure 6-22: Geometry of a triangular open trench.

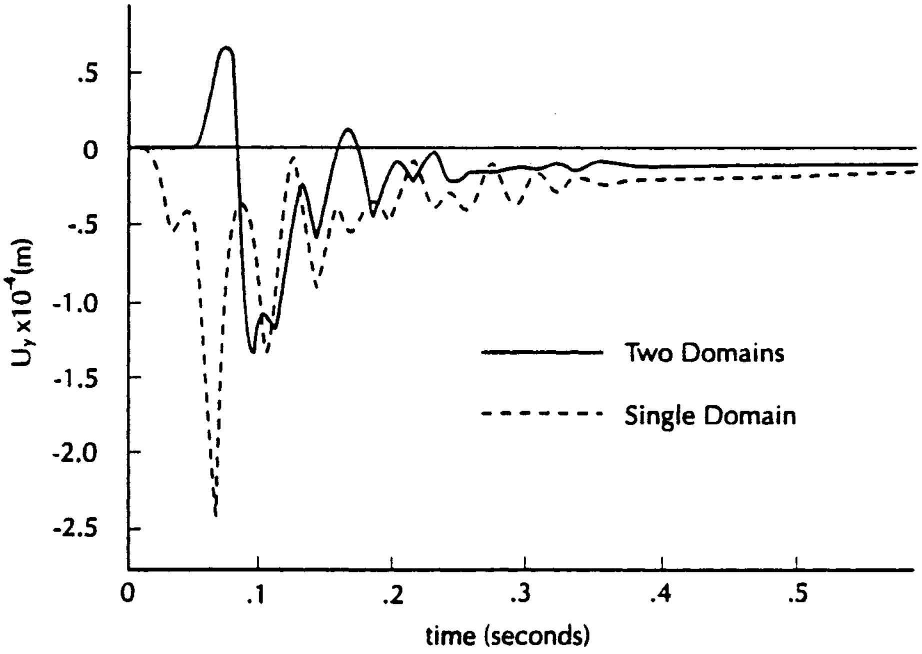

Figure 6-23: Time history of the vertical response at point B as reported by Antes and Von Estorff (1987).

through anti-plane and plane frequency and time-domain boundary element formulations, concluded that any violations of causality reported previously are the results of insufficient discretization of the boundary and the use of low order elements. Tian (1990) and Siebrits (1992) also concluded that boundary element methods can model non-convex domains and that methods that violate causality simply do not have sufficiently accurate integrations along the boundaries. However, Triantifyllidis (1993) brought up the causality problem again in a study where both direct and indirect boundary element methods were applied analytically to the problem of diffraction of SH-waves by a cylindrical cavity in an infinite space. The results of the indirect boundary element method were identical to the analytical solution, but the results obtained with the direct boundary element method were not. This conclusion is in direct opposition with the results obtained by Tian (1990), who used the time-domain direct boundary element formulation. Tian (1990) used quadratic and linear spatial and temporal interpolation functions, respectively. All integrals were carried out analytically, and the boundary element formulation was tested on a non-convex domain. The results clearly show that the direct boundary element method *does not* violate causality.

Because of all the previous discussion in the literature, it was felt that the current implementation should be used to model a non-convex domain problem. The problem of a v-shaped ditch in an elastic half-plane shown in Figure 6-22 provides a good check on the issue of causality. The half-plane has a mass density $\rho = 2000$ kg/m^3, a Poisson's ratio $\nu = 0.33$ and a Young's modulus $E = 2.66 \times 10^5$ kPa. The corresponding propagational wave velocities are $c_1 = 443.9$ m/s and $c_2 = 223.6$ m/s. The time step in this study was taken to be $\Delta t = 0.002815$ seconds.

Israil and Banerjee (1990a) found a small discrepancy at late times in the time history of the vertical displacement at point B, which they attributed to the limited spatial extent of the original discretization by Antes and von Estorff (Figure 6-22). They suggested that the interface discretization for the two-region case should be extended to such a distance as is reached by the longitudinal wave during the desired time-history. The current study extends the interface and surface discretizations

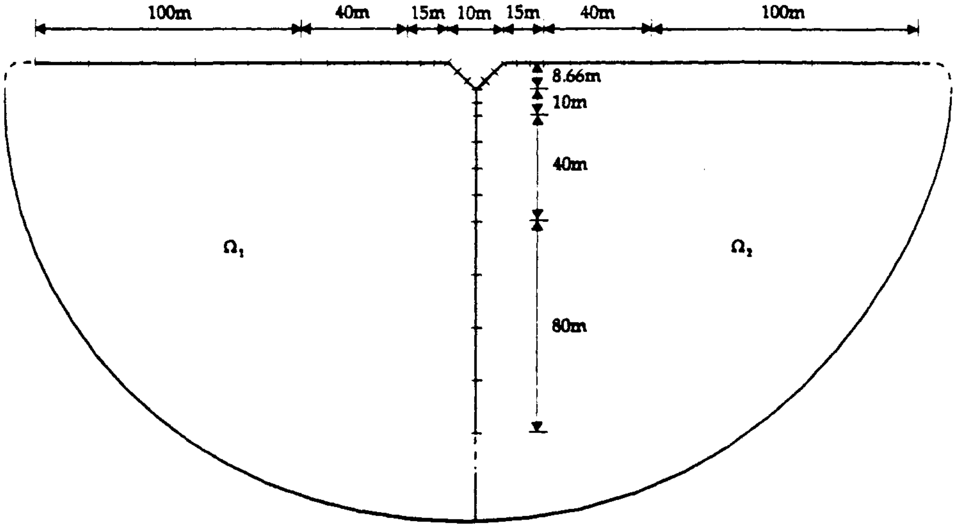

Figure 6-24: Discretization of v-shaped ditch used in this study.

beyond the distance reached by the longitudinal wave during the desired time-history (see Figure 6-24). The discretization used in this study is shown in Figure 6-24 for the two region case. The discretization used for the single region case is identical, except that the interface between regions Ω_1 and Ω_2 is removed. Figure 6-25 compares the time history of vertical displacements at point B for both the single and two region cases. The arrival time of the longitudinal wave from the right end of the loaded element to point B is about 0.0474 seconds and it is correctly produced for both discretization cases. The time histories at later times for both cases also are almost identical.

It is therefore concluded that a properly implemented direct boundary element formulation satisfies the principle of causality for non-convex domains and that the results do not depend on whether the mesh is of a single or multiple region. The so-called causality problem is a numerical artifact and certainly disappears with a

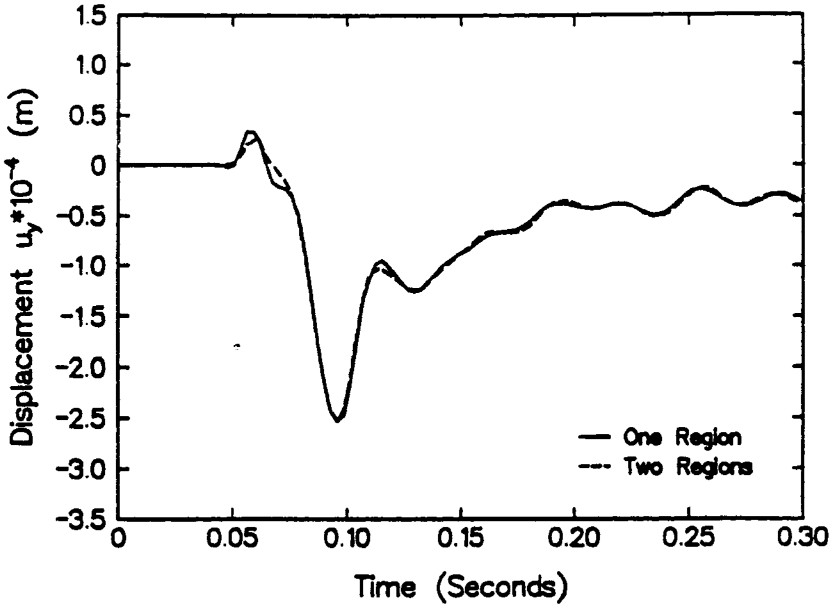

Figure 6-25: Time history of vertical displacement at point B using extended discretization pattern.

proper implementation in which both the spatial and temporal integrals are evaluated analytically.

6.2.3 Lamb's Problem

This example illustrates the generation of a Rayleigh wave in a half-plane that is suddenly loaded with a concentrated line load. A complete analytical solution was presented by Lamb (1904) for the vertical component of the surface displacement, but the analytical solution for the horizontal component was given only until the arrival of the shear wave. Lamb's (1904) formulation of the horizontal and vertical displacements due to a concentrated vertical load $Q(t)$ can be written as

$$
\begin{aligned}
u_0 &= -\frac{B}{G} Q(t - cx) \\
&\quad -\frac{2}{\pi G} \int_a^b \frac{b^2\theta\left(2\theta^2 - b^2\right)\sqrt{\left(\theta^2 - a^2\right)}\sqrt{\left(b^2 - \theta^2\right)}}{\left(2\theta^2 - b^2\right)^4 + 16\theta^4\left(\theta^2 - a^2\right)\left(b^2 - \theta^2\right)} Q(t - \theta x)\, d\theta \qquad (6\text{-}6)
\end{aligned}
$$

$$
\begin{aligned}
v_0 \;=\; & -\frac{1}{\pi G}\int\limits_{a}^{b}\frac{b^2\left(2\theta^2-b^2\right)^2\sqrt{\left(\theta^2-a^2\right)}}{\left(2\theta^2-b^2\right)^4+16\theta^4\left(\theta^2-a^2\right)\left(b^2-\theta^2\right)}Q\left(t-\theta x\right)d\theta \\
& -\frac{1}{\pi G}\int\limits_{b}^{\infty}\frac{b^2\sqrt{\left(\theta^2-a^2\right)}}{\left(2\theta^2-b^2\right)^2-4\theta^2\sqrt{\left(\theta^2-a^2\right)}\sqrt{\left(\theta^2-b^2\right)}}Q\left(t-\theta x\right)d\theta
\end{aligned}
\tag{6-7}
$$

where $a = 1/c_1$, $b = 1/c_2$ and $c = 1/c_R$, in which c_1, c_2 and c_R denote the longitudinal, shear and Rayleigh wave velocities. The first term in the horizontal displacement component also contains the following term,

$$
B = \frac{K^2\left(2k^2-K^2\right)^3}{16K^6k^2\left\{1-\left(6-4\frac{h^2}{K^2}\right)\frac{k^2}{K^2}+6\left(1-\frac{h^2}{K^2}\right)\frac{k^4}{K^4}\right\}}
\tag{6-8}
$$

where $h^2 = p^2a^2$, $K^2 = p^2b^2$ and $k^2 = p^2c^2$, in which p denotes the frequency of the disturbance.

Right after the shear wave arrives at the point of interest, all horizontal displacement wave activity ceases, until the arrival of the horizontal Rayleigh wave component, which is represented by the first term in (6-6). This solitary Rayleigh wave of short duration is said to be of unchanging type, because it does not decay with distance away from the source. This non-decaying nature makes it very difficult to model with any numerical method, because the solution matrices tend to become ill-conditioned, with off-diagonal elements of about the same size as the diagonal terms. Numerical treatment of this problem was attempted by Israil and Banerjee (1990b). Unfortunately, the authors did not provide information about problem discretization, load magnitude and load duration, time step and body wave velocities, so it is not possible to compare the current implementation to their results.

In this study, the elastic half-plane shown in Figure 6-26 is used to approximate Lamb's problem. The half-plane is discretized with 50 equal-size elements of length $b = 10$ m. To approximate a line load on the half-plane, the load $p(t)$ is applied as a triangular load over two elements, with an apex value $p_0 = 100$ kPa applied at $x = 0$. Similarly, to approximate a delta pulse in time, the load is assumed to have the triangular load distribution shown in Figure 6-27. The rise time of the load is $t_r = 0.02$

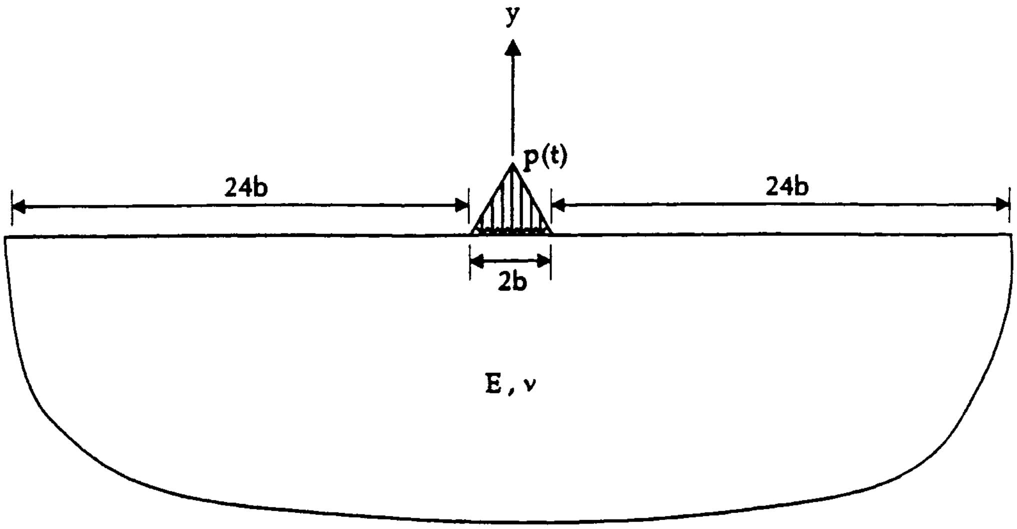

Figure 6-26: Triangular load on a half-plane.

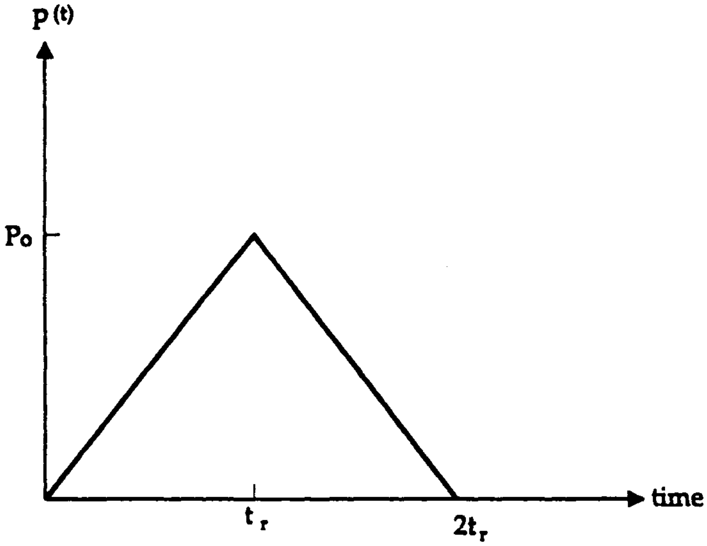

Figure 6-27: Time history of applied load.

seconds and the size of the time step is $\Delta t = 0.005$ seconds. The elastic constants for the half-plane are $E = 330$ MPa, $\nu = 0.25$ and the mass density, $\rho = 1783.9$ kg/m^3. The wave velocities are $c_1 = 471$ m/s and $c_2 = 272$ m/s. Field point displacement vectors are also presented in Appendix D for a field point window defined by the following four corner nodes: $(60m, -2m)$, $(150m, -2m)$, $(150m, -32m)$ and $(60m, -32m)$. This window was deemed far enough from the origin so that the effects of the applied load would be "felt" to be closer to the delta pulse load approximation, discussed previously. At distances very close to the origin of the applied load, this assumption is clearly not valid, because of the finite spatial extent of the applied load.

Figures 6-28 and 6-29 show the surface displacements obtained by the current implementation at a normalized distance $x/b = 12$. This distance was assumed to be far enough away from the point of load application for the approximation of a suddenly applied line load to be reasonable. The normalization parameter Q is simply the magnitude of the triangular load. Figure 6-28 shows how the horizontal disturbance at the point of interest begins after a time $t = x/c_1$, which is the time it takes the longitudinal wave to travel that distance. The disturbance lasts until time $t = x/c_2$, which is the time it takes the shear wave to travel to the point of interest, and then ceases, until the arrival of the non-decaying horizontal Rayleigh wave component, after which the horizontal displacements return to zero.

Figure 6-29 shows the vertical displacements at the point of interest. The most important part of the vertical displacement component is that corresponding to $t = x/c_R$, when the integrand in the second term in (6-7) changes signs by passing through infinity. This is the epoch of the main shock; the relatively minor disturbance which starts at time $t = x/c_1$ leads continuously up to this, and only dies out gradually after it. The results shown in Figure 6-29 show good agreement with Lamb's solution, considering the fact that the analytical solution for the vertical displacement component predicts a singularity upon the arrival of the Rayleigh wave at the point of interest, and considering also the difficulty in matching the loadings. It should be noted that at later times the numerical results match the analytical results quite well, despite the primary wave activity having reached the edges of the discretized area quite

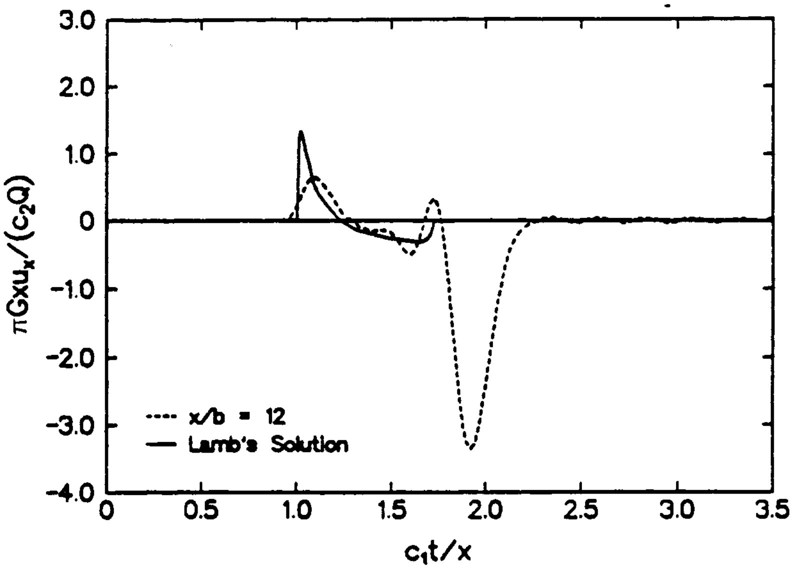

Figure 6-28: Horizontal displacement at the surface of a loaded half-plane.

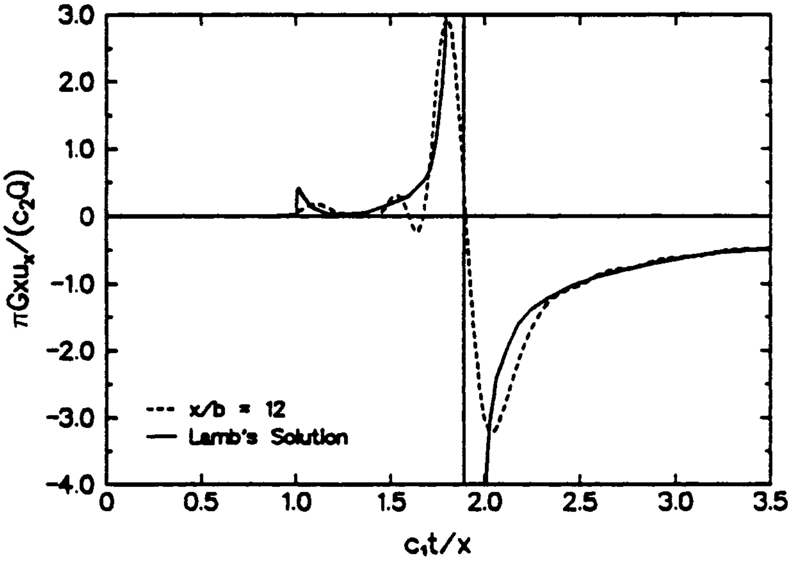

Figure 6-29: Vertical displacement at the surface of a loaded half-plane.

some time previously.

The displacement vectors shown in Figures D-1 to D-11 illustrate the expected (see e.g. Eringen and Suhubi, 1975) vertically elongated counterclockwise elliptical movement of points within the body of interest as the Rayleigh wave passes through the field point window. After the Rayleigh wave has passed, the horizontal displacement component disappears as expected and the downward vertical component illustrates the slow decrease in magnitude observed in Figure 6-29.

6.2.4 Selberg's Problem

This example deals with the load response of a cylindrical cavity, shown in Figure 6-30, which is suddenly loaded with a pressure loading. The cavity has a radius $r = a$ and the applied pressure load is expressed as $p(t) = p_o H(t)$, where $p_0/G_1 = 10^{-3}$. The material properties used in this study are $\rho = 2700$ kg/m^3, longitudinal wave velocity, $c_1 = 5367$ m/s, shear wave velocity $c_2 = 3287$ m/s, Poisson's ratio $\nu = 0.20$ and shear modulus $G = 29.17 \times 10^6$ kPa. The time step Δt was selected so that the longitudinal wave would travel exactly one-quarter of an element length at each time step. This can be expressed by a dimensionless parameter

$$Q_1 = 0.5 = \frac{c_1 \Delta t}{a_l} \tag{6-9}$$

where a_l = element half-length. The boundary of the cavity was discretized by 16 straight-line elements and the number of time steps was 85.

Selberg (1952) presented an analytical solution for the hoop stress along the wall of the cylindrical cavity. The hoop stress $\sigma_{\theta\theta}$ can be written as

$$\sigma_{\theta\theta} = \frac{2(\lambda + \mu)}{\lambda} \sigma_{zz} - \sigma_{rr} \tag{6-10}$$

where λ and μ are Lamé's constants and σ_{zz} is the axial stress acting in the direction along the length of the cavity and σ_{rr} is the radial stress. Using Laplace transforms, the analytical expressions for the radial and axial stresses can be written in terms of

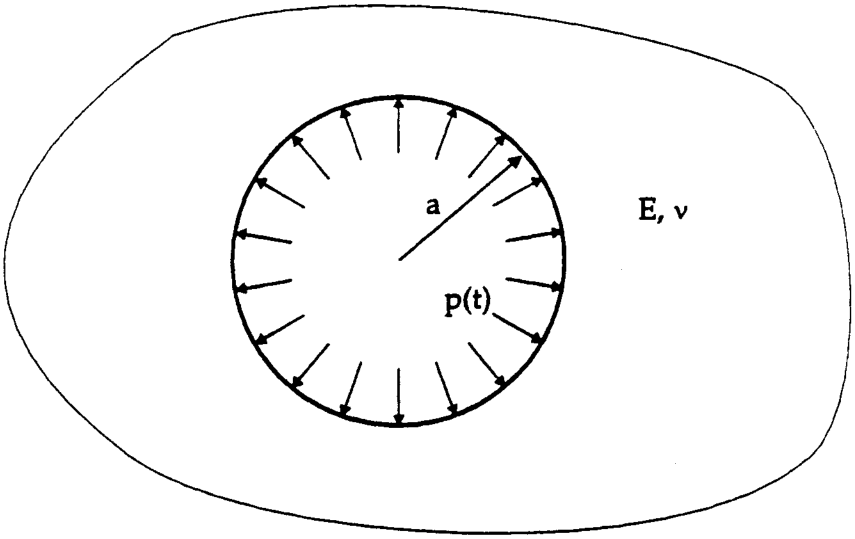

Figure 6-30: Suddenly loaded circular cavity.

the n-th order Hankel functions of the first kind $H_n^1(\xi)$as

$$\sigma_{rr} = \frac{1}{\pi}\Im \int_0^{-\infty} \frac{F(\xi r/a)\exp\{c_1 t\xi/a\}}{\xi F(\xi)} d\xi + 2\Re \frac{F(r\xi_0/a)\exp\{c_1 t\xi_0/a\}}{\xi_0 F'(\xi_0)} + \left(\frac{a}{r}\right)^2 \tag{6-11}$$

$$\sigma_{zz} = \frac{\lambda}{\pi}\Im \int_0^{-\infty} \frac{K_0(\xi r/a)\exp\{c_1 t\xi/a\}}{\xi F(\xi)} d\xi + 2\lambda\Re \frac{K_0(\xi_0 r/a)\exp\{c_1 t\xi_0/a\}}{\xi_0 F'(\xi_0)} \tag{6-12}$$

where $\Im$ and $\Re$ denote the imaginary and real parts, and

$$K_n(\xi) = \frac{\pi i}{2}\exp\{1/2n\pi i\} H_n^1(i\xi) \tag{6-13}$$

and

$$F(\xi) = (\lambda + 2\mu) K_0(\xi) + 2\mu/\xi K_1(\xi) \tag{6-14}$$

and $\xi_0 = a + i\beta$ is the solution of the equation $F(\xi) = 0$ in the half-plane $\beta \geq 0$. To obtain a solution for the tangential stress at the wall of the cavity, Selberg (1952) approximated the root ξ_0 by numerical iteration.

Figure 6-31 shows a comparison between the current numerical results and Selberg's solution. The normalized time $c_1 t/a$ presents the time that it takes the compressional wave to travel multiples of the distance a. The results show good agreement with the Selberg solution (solid line), both at early and late times.

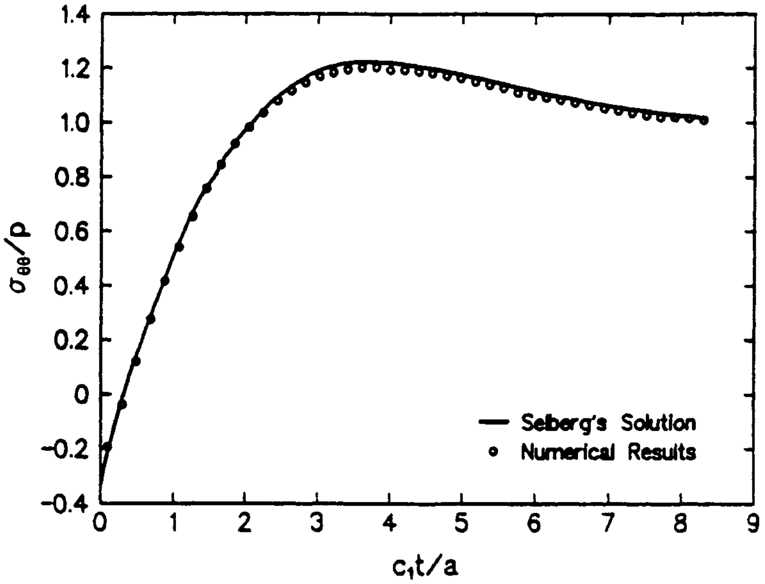

Figure 6-31: Hoop stress at the wall of a single cavity.

6.2.5 Suddenly Loaded Annulus

This example extends the problem shown in Figure 6-1 to dynamics. The region of interest consists of an annulus $a \leq r \leq b$ with Poisson's ratio ν_1 and shear modulus G_1 inside a hollow circular hole of radius $r = b$ in an infinite plate with Poisson's ratio ν_2

and shear modulus G_2. Insight into the dynamic response of this problem may be obtained from Selberg's problem discussed previously, which can be viewed as a special case in which the material properties of the plate and the annulus are the same. Also, (6-1) to (6-3) provide the static solution for the problem, to which the dynamic solution should tend at later times.

The cases of $G_1/G_2 = 1$, $G_1/G_2 = 2$ and $G_1/G_2 = 4$ were studied. In all cases the material properties of the plate were taken to be the same as the material properties used in the Selberg problem, namely, longitudinal wave velocity, $c_1 = 5367$ m/s, shear wave velocity $c_2 = 3287$ m/s, and shear modulus $G_2 = 29.17 \times 10^6$ kPa. The Poisson's ratio $\nu = 0.20$, and the mass density $\rho = 2700$ kg/m^3 were assumed to be the same for both the plate and the annulus. The time step Δt was again selected as $0.5a_l/c_{\max}$, where a_l is the element half-length and $c_{\max}$ is defined as the maximum compressional wave velocity in the problem. The circular boundary $r = a$ and each side of the interface $r = b$ were divided into 16 straight-line elements, and the number of time steps was again taken as 85.

Case I: $G_1/G_2 = 1$

This particular case allows for an evaluation of the effects of introducing an artificial numerical interface at $r = b$. First, the time histories of hoop stresses and radial displacements are evaluated for the cases with and without a numerical interface. Second, the effects of the rise time (t_r) of loading are evaluated for the numerical interface case.

Figure 6-32 shows the hoop stress at the circular boundary $r = a$ for the cases with and without (solid line) a numerical interface. The case without a numerical interface is exactly the same as that presented for the Selberg problem in Figure 6-30 and the applied pressure $p(t)$ at the circular boundary $r = a$ is applied in the form of the Heaviside ramp load, shown in Figure 6-33. Therefore, it can be concluded that the introduction of a numerical interface at $r = b$ does not appreciably affect the hoop stresses at the boundary $r = a$. Similarly, Figure 6-34 shows the time history of normalized radial displacements at $r = b$, due to a suddenly applied Heaviside load at

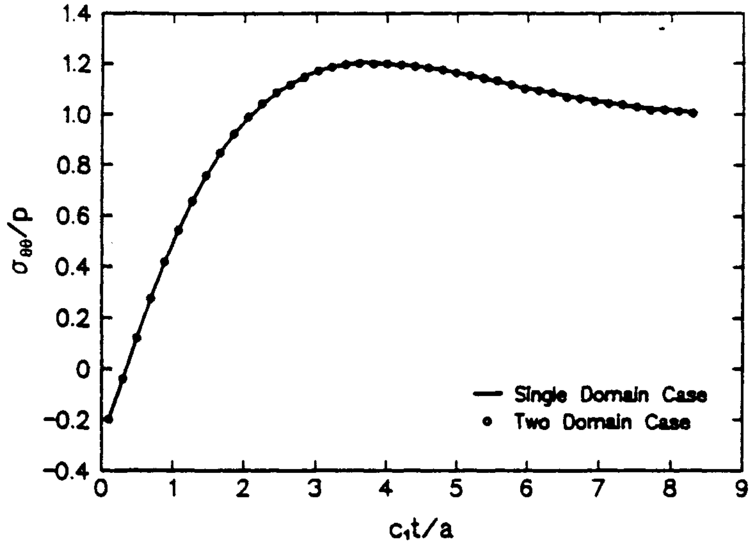

Figure 6-32: Hoop stress at the circular boundary r = a.

$r = a$. The results show that the introduction of a numerical interface at $r = b$ does not significantly affect the radial displacements at $r = b$.

To evaluate the effects of the rise time t_r, the hoop stress at $r = b$ was compared for the two loading cases shown in Figures 6-33a and 6-33b. The first case assumes that the pressure applied at the circular boundary $r = a$ is in the form of a Heaviside ramp load (Figure 6-33a), whereas the second case (Figure 6-33b) assumes that the pressure is applied as a ramp-step load with a rise time of one time step ($t_r = \Delta t$). The results of the comparison are shown in Figure 6-35. Small perturbations are seen in the Heaviside load response (solid line) at normalized times $c_1 t/a = 3, 5$ and 7, whereas these perturbations are not seen in the ramp-step load case (broken line). These perturbations are likely due to a minor wave reflection activity at the artificial interface, indicating that the use of linear time variation of tractions and displacements may not work well for multiple domain problems with a suddenly applied Heaviside loading at the boundary. However, Figure 6-35 clearly illustrates that the loading response due to a Heaviside load can be approximated with a load that is applied with a rise time of one time step. It is of interest to note that Love (1906) also concluded

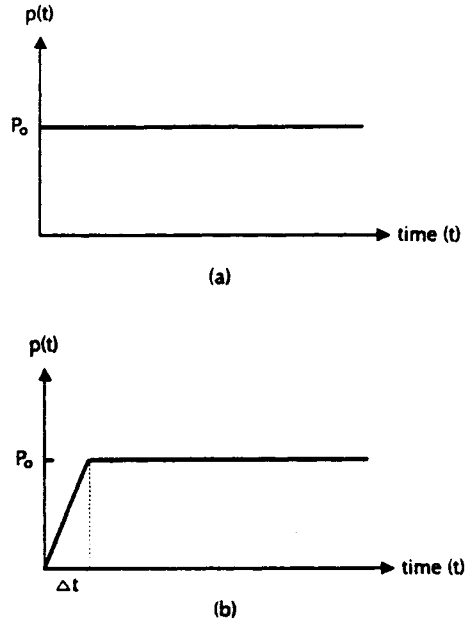

Figure 6-33: Time history of prescribed load: (a) Heaviside type, (b) Ramp-step type.

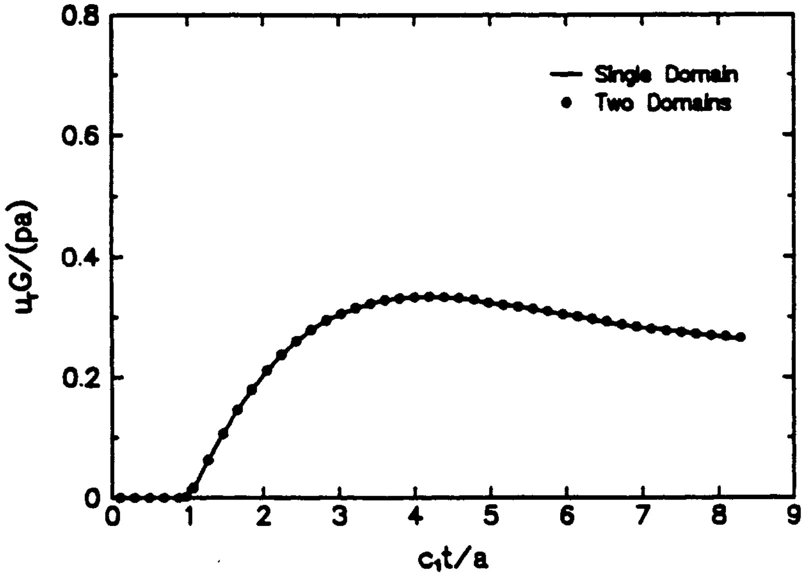

Figure 6-34: Radial displacements at the interface r = b.

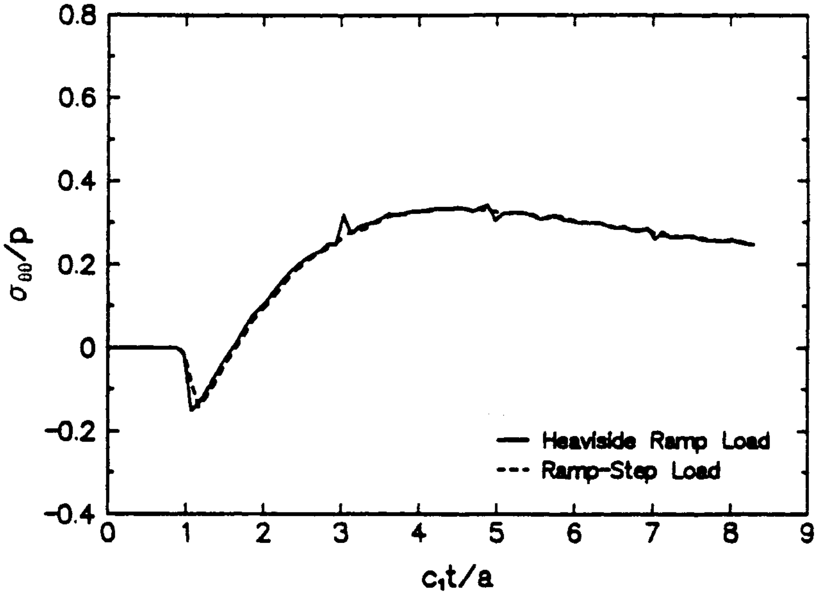

Figure 6-35: Hoop stress at the material interface r = b.

after an extensive study of the three-dimensional displacement fundamental solution that it yields correct results only when the input quantities are continuous at the propagating wave front. This also implies that if the input excitation is a Heaviside step load, then it must be modeled as a ramp-step load with a finite rise time.

Case II: $G_1/G_2 = 2$

For this case, the ramp-step loading (Figure 6-33b) was used. The material parameters were $G_1 = 29.17 \times 10^6$ kPa, $G_2 = 14.585 \times 10^6$ kPa and the Poisson's ratio was $\nu = 0.2$ for both regions. The wave velocities were $c_1 = 5367$ m/s and $c_2 = 3287$ m/s for the annulus, and $c_1 = 3795.5$ m/s and $c_2 = 2324.2$ m/s for the outer plate. The time was divided into 85 time steps, each of size $0.5a_l/c_{\max}$.

Figures 6-36 and 6-37 show the normalized hoop stress at both sides of the material interface at radial distance $r = b$. Both cases show a small perturbation in the solution at normalized times $c_1t/a = 3, 5$ and 7, indicating waves that have reflected off the $r = b$ interface and traveled to the circular boundary $r = a$ and back to $r = b$. This

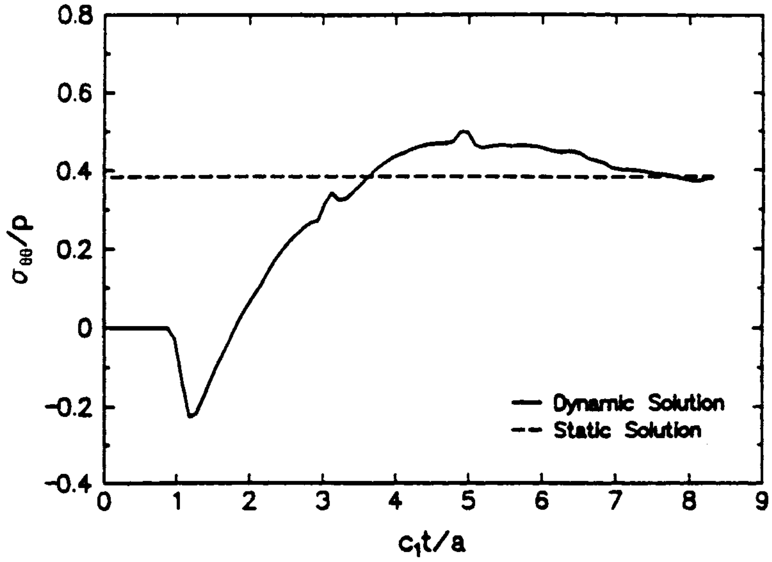

Figure 6-36: Hoop stress at r = b-.

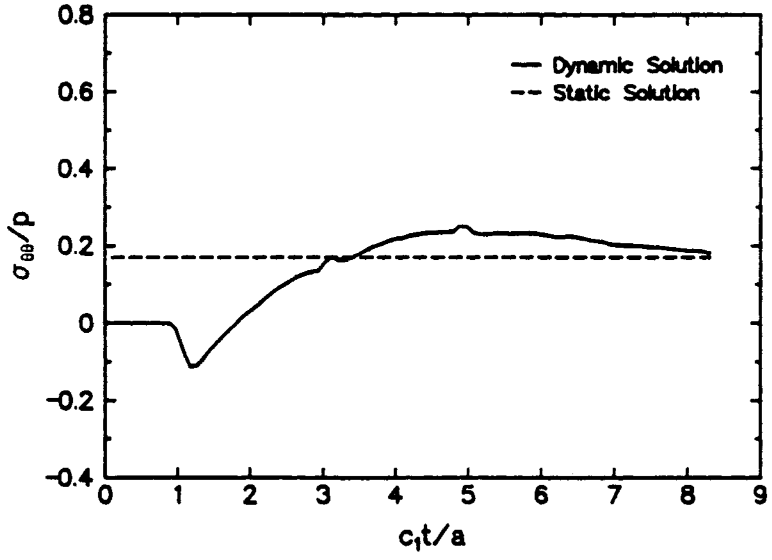

Figure 6-37: Hoop stress at r = b+.

wave reflection phenomenon can also be seen in Figure 6-38, which shows the normalized radial displacement at the interface. It should be noted that in all three cases, the dynamic solution approaches the static solution at later times. Finally, Figure 6-39 shows a comparison of the normalized hoop stress on each side of the material interface $r = b$. The distinct perturbations at normalized times $c_1 t/a = 3, 5$ and 7 are quite distinct and clearly take place at exactly the same times.

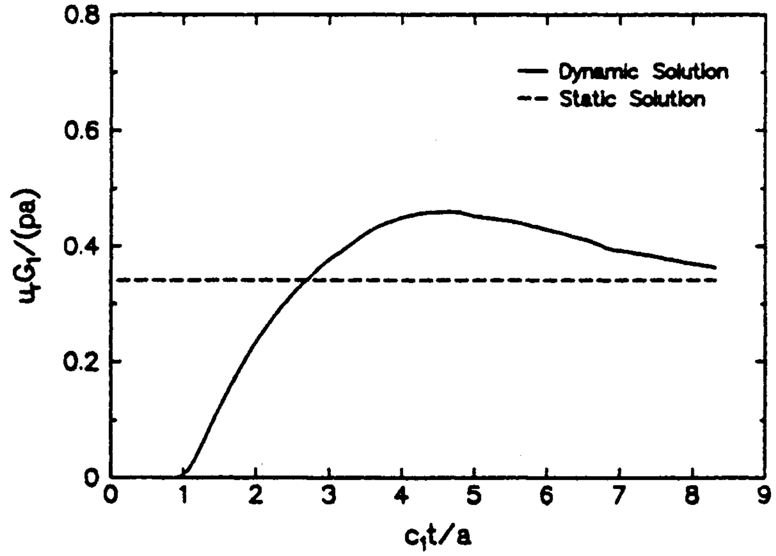

Figure 6-38: Radial stress at the interface.

Case III: $G_1/G_2 = 4$

Figures 6-40 and 6-41 show the normalized hoop stress at both sides of the material interface at radial distance $r = b$. As in the $G_1/G_2 = 2$ case, the dynamic solution tends to the static solution at later times, but the perturbations at normalized times $c_1 t/a = 3, 5$ and 7 are now more distinct than for the $G_1/G_2 = 2$ case. The normalized radial displacements shown in Figure 6-42 also show small perturbations at these times, even though this reflection effect is much harder to detect for the displacements.

Figure 6-43 shows a comparison between the normalized hoop stress on each side of

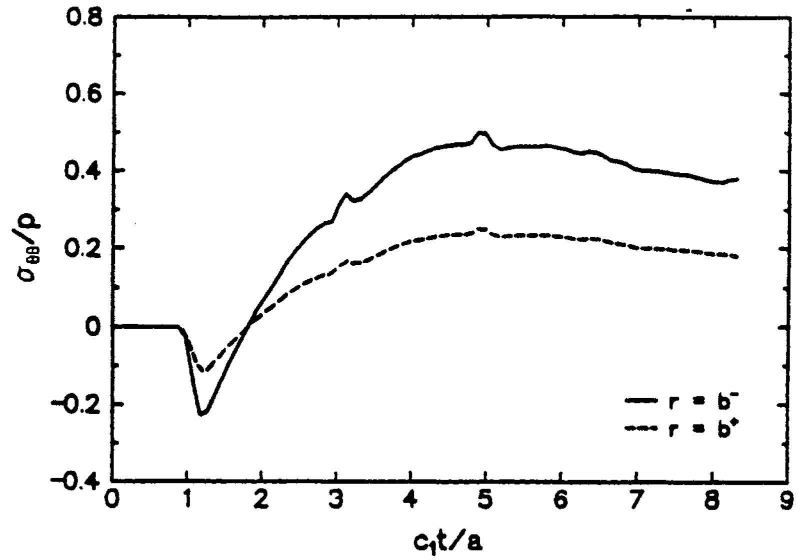

Figure 6-39: Comparison of hoop stresses at the interface.

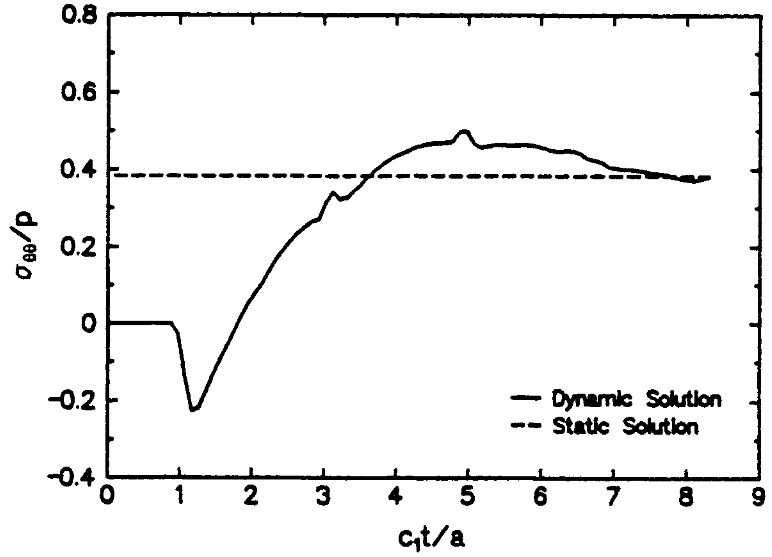

Figure 6-40: Hoop stress at interface r = b-.

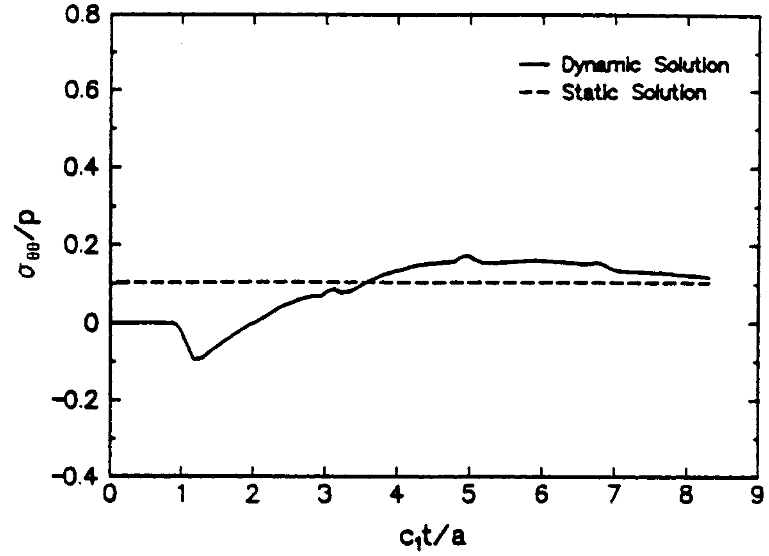

Figure 6-41: Hoop stress at interface r = b+.

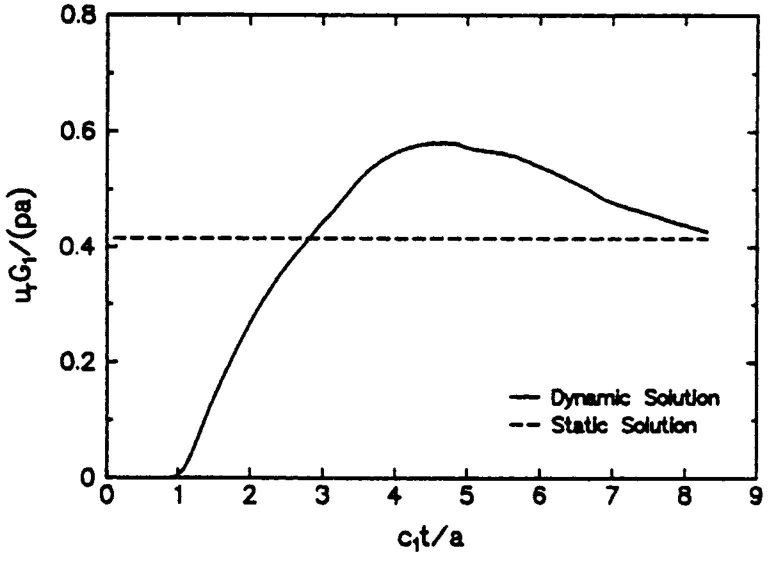

Figure 6-42: Radial stress at interface r = b.

the material interface $r = b$. It is interesting to note that as the material properties between the annulus (region 1) and the plate (region 2) diverge, the dynamic behavior in the stiff annulus (solid line) becomes more abrupt as compared to the softer plate (broken line), and the jump in hoop stress at the interface grows larger. This effect is illustrated in Figures 6-44 and 6-45, which show respectively the normalized hoop stresses and radial displacements for all three cases, namely $G_1/G_2 = 1$, $G_1/G_2 = 2$ and $G_1/G_2 = 4$. The initial negative stress, corresponding to a dynamic compression effect, shows a significant increase with the ratio of the shear moduli (G_1/G_2) between the annulus and plate. The dynamic reflection phenomenon at normalized times $c_1t/a = 3, 5$ and 7 also increases significantly with an increase in the G_1/G_2 ratio. It should also be observed that as the G_1/G_2 ratio increases and the dynamic reflection behavior becomes more distinct, the dynamic stresses and displacements approach the static solution more rapidly at later times, because the waves lose energy at a faster rate due to increased interference and scattering activity.

It can be concluded that the current numerical implementation is capable of modeling complicated multi-domain geometries with straight-line elements and that the results approach the static solution as time tends to infinity.

6.2.6 Wave Propagation Through Layered Material

Realistic description of both natural and man-made materials should include changes in material stiffness with depth. Soil and rock profiles can almost never be assumed to be completely homogeneous with depth. Rather, the profiles are stratified with softer layers overlying stiffer ones, or sometimes there is a hard crust overlying softer material. Examples of man-made materials include concrete and asphalt pavements, where a stiff layer of concrete or asphalt overlies a softer base material. The presence of layers of finite thicknesses affects the dynamic loading response significantly. As explained in Section 3.4.3, waves originating from a loaded boundary will reflect and refract at the interface between layers and the resulting surface and interface waves will become dispersive in character. Waves are considered to be dispersive when the phase velocity depends on the frequency. Correspondingly, Rayleigh waves traveling along the

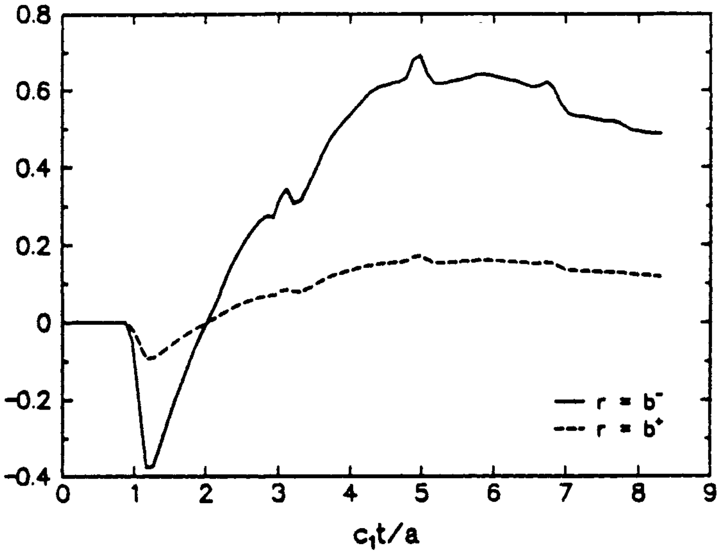

Figure 6-43: Comparison of hoop stresses at the interface.

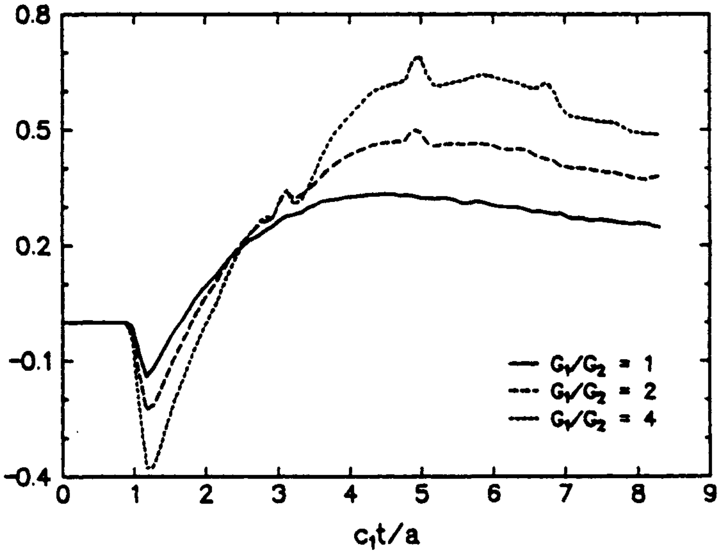

Figure 6-44: Comparison of hoop stresses at interface.

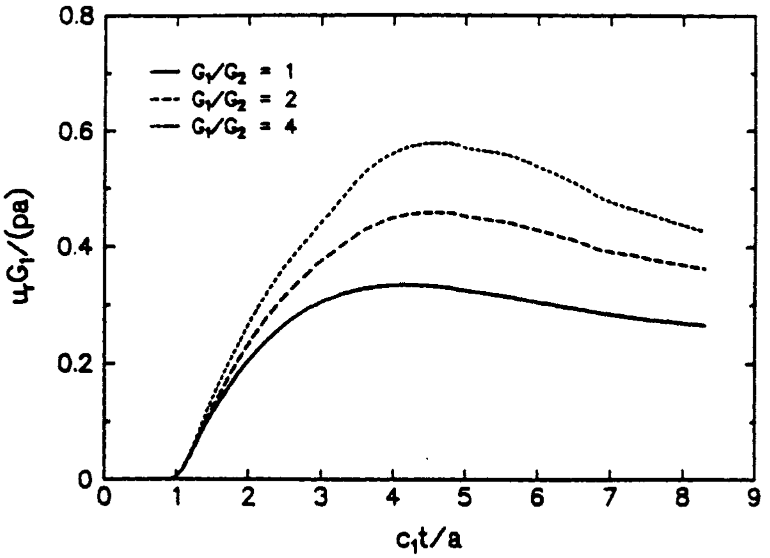

Figure 6-45: Comparison of radial displacements at interface.

surface of a half-plane and Stoneley waves moving along the interface between two homogenous bonded half-planes are non-dispersive, because of the absence of a length dimension in the problem.[1]

The present study involves a homogenous half-plane underlying a layer of finite thickness H. The geometry and time history of loading for the problem are shown in Figure 6-46. The depth of the upper layer is $H = 2b$, where b is the length of each surface and interface element. Both the surface and each side of the interface are modeled with 48 straight-line boundary elements, each of length $b = 10$ m. The ratio of the shear moduli G_1/G_2 is varied, with all other properties remaining the same in the two layers. The Poisson's ratio and mass density for both layers are $\nu = 0.25$ and $\rho = 1783.9$ kg/m^3. The applied transient load shown in Figure 6-46 has a finite rise time $t_r = 0.02$ seconds, with a total time of applied loading of $3t_r$. The number of time

---

[1] It should be noted here that it is only possible to obtain dispersive in-plane surface waves for plane strain elastodynamic problems. It is not possible to obtain Love waves, which are out-of-plane dispersive surface waves, despite claims to the contrary by Israil and Banerjee (1990b).

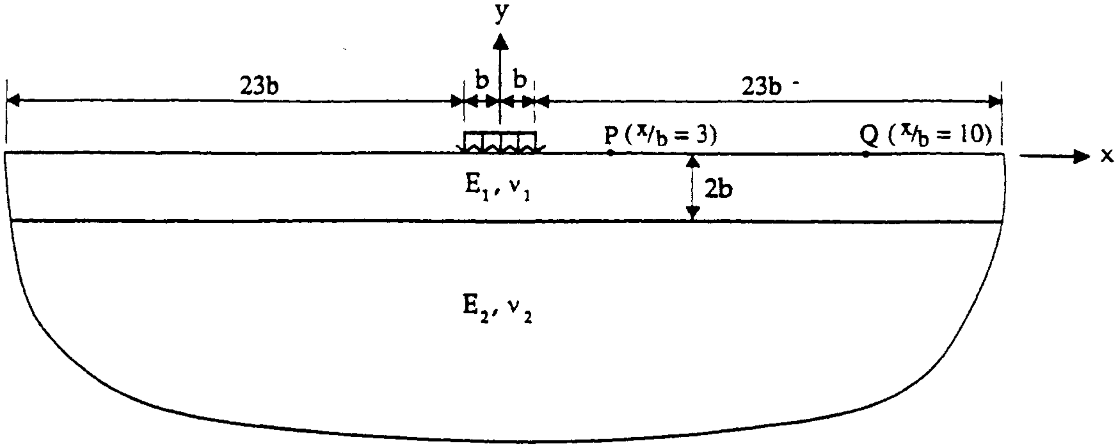

Figure 6-46: Discretization of layered half-plane.

steps for all cases was 220, with each time-step of size $\Delta t = 0.005$ seconds. The ratio of shear moduli was taken as $G_1/G_2 = 0.2, 0.5, 1, 2, 5$, ranging from a very stiff half-plane to a very stiff layer. The corresponding values for the dimensionless parameter $Q_1 = c_{\max}\Delta t/a_l$ ($c_{\max} = \max(c_1, \bar{c}_1)$, where c_1 and $\bar{c}_1$ denote the compressional wave velocities in the layer and the half-plane) are $Q_1 = 1.0535, 0.6663, 0.471, 0.6663, 1.0535$.

In the current study, the vertical displacements for the case of a stiffer half-plane were monitored at Stations $P\,(x/b = 3)$ and $Q\,(x/b = 10)$. The results are shown in Figures 6-47 and 6-48 in terms of normalized vertical displacements versus normalized time c_2t/b, where the value of c_2 corresponds to the shear wave velocity in the layer. The wave velocities in the layer are $c_1 = 471$ m/s and $c_2 = 272$ m/s. The wave velocities for the half-plane corresponding to the various G_1/G_2 ratios are

$G_1/G_2 = 1$:	$\bar{c}_1 = 471.0$ m/s;	$\bar{c}_2 = 272.0$ m/s
$G_1/G_2 = 1/2$:	$\bar{c}_1 = 666.3$ m/s;	$\bar{c}_2 = 384.7$ m/s
$G_1/G_2 = 1/5$:	$\bar{c}_1 = 1053.5$ m/s;	$\bar{c}_2 = 608.3$ m/s

The results show that as the half-plane becomes stiffer, the wave activity in the overlying layer increases until the displacement becomes oscillatory for the case $G_1/G_2 = 1/5$. Also, Figure 6-48 illustrates how the waves reach Station Q at progressively earlier times as the lower medium becomes stiffer, because the waves in

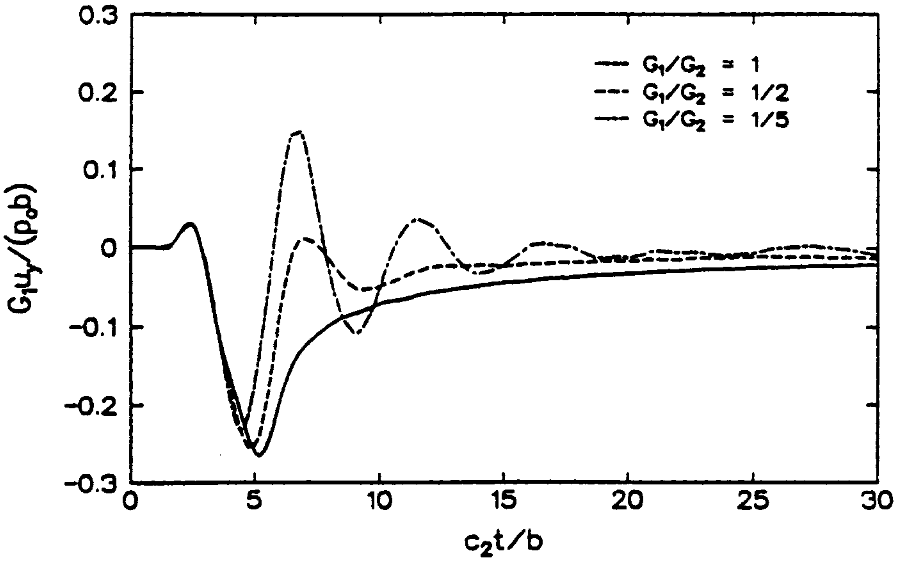

Figure 6-47: Vertical displacements at point P (x/b = 3) for the case of a stiffer half-plane.

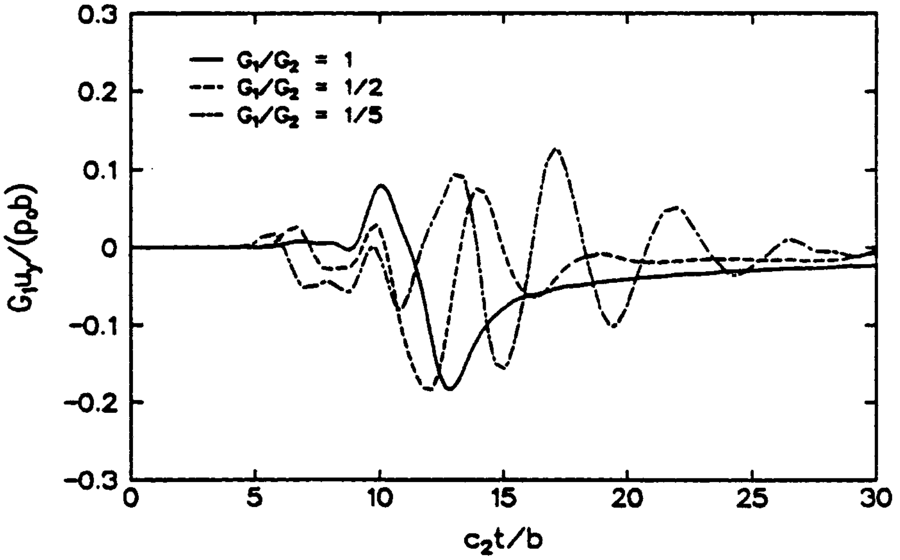

Figure 6-48: Vertical displacements at point Q (x/b = 10) for the case of a stiffer half-plane.

the half-plane will travel along the interface faster than the waves in the upper layer and arrive sooner at Station Q. These waves also interfere with the slower moving waves in the upper medium, resulting in a change in the initial form of the time-history of displacements at location Q.

To illustrate how the displacements change with horizontal distance between Stations P and Q, the time history of both horizontal and vertical displacements for the representative case of $G_1/G_2 = 1/5$ is presented in Figures 6-49 and 6-50. The results show how the amplitude and the frequency of oscillations in the horizontal displacements increase with the distance between Stations P and Q. The frequency of oscillations in the vertical component of displacements also increases with distance from Station P to Station Q, as shown in Figure 6-50, but the amplitude decreases.

The vertical displacements for the case of a stiff layer overlying a softer half-plane are shown in Figures 6-51 and 6-52. The shear wave velocity in the normalized time $\bar{c}_2 t/b$ is now the shear wave velocity in the half plane. The wave velocities in the half-plane are $\bar{c}_1 = 471$ m/s and $\bar{c}_2 = 272$ m/s. The wave velocities for the layer corresponding to the various G_1/G_2 ratios are

$$G_1/G_2 = 1: \quad c_1 = 471.0 \text{ m/s}; \quad c_2 = 272.0 \text{ m/s}$$
$$G_1/G_2 = 2: \quad c_1 = 666.3 \text{ m/s}; \quad c_2 = 384.7 \text{ m/s}$$
$$G_1/G_2 = 5: \quad c_1 = 1053.5 \text{ m/s}; \quad c_2 = 608.3 \text{ m/s}$$

The results show that as the overlying layer becomes stiffer the time histories of displacements at Stations P and Q become less sharp, and more spread out in time. Also, Figure 6-52 illustrates how the waves reach Station Q at progressively earlier times as the layer becomes stiffer. The waveforms at early arrival times do not include the interference effect shown in Figure 6-50, because now the waves traveling in the underlying half-plane are slower than the waves in the layer. However, a slight increase in oscillations at later times for the case $G_1/G_2 = 5$ can possibly be explained by refractive effects from the half-plane.

A significant difference in the observed behavior of the response between the stiffer half-plane and stiffer upper layer cases can be observed from Figures 6-49 to 6-52. The stiff overlying layer cases do not show the oscillatory behavior that is observed for the

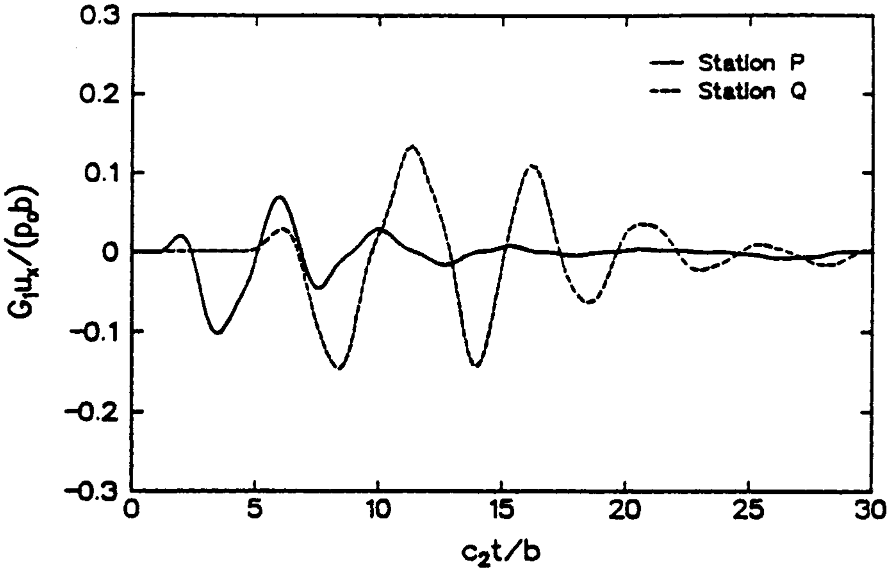

Figure 6-49: Variation in horizontal displacements with distance along surface of layered half-plane.

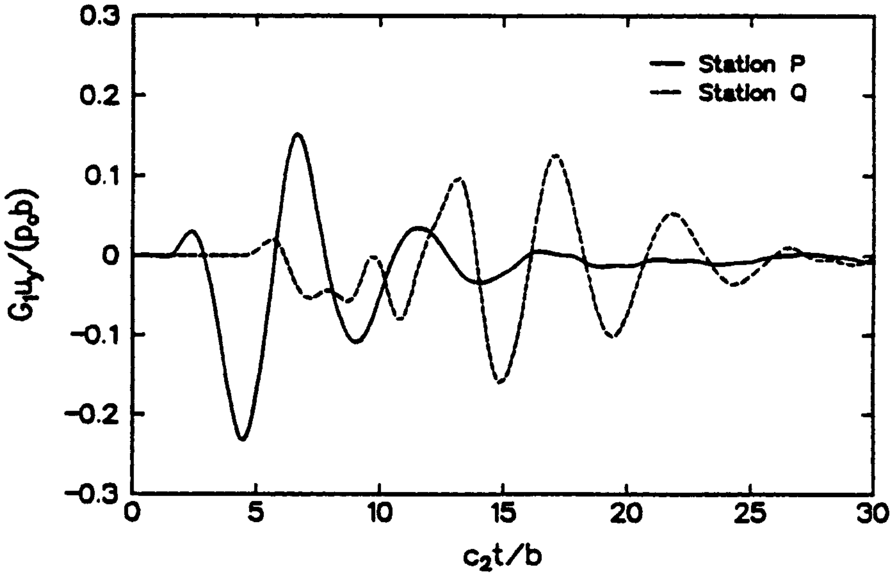

Figure 6-50: Variation in vertical displacements along surface of a layered half-plane.

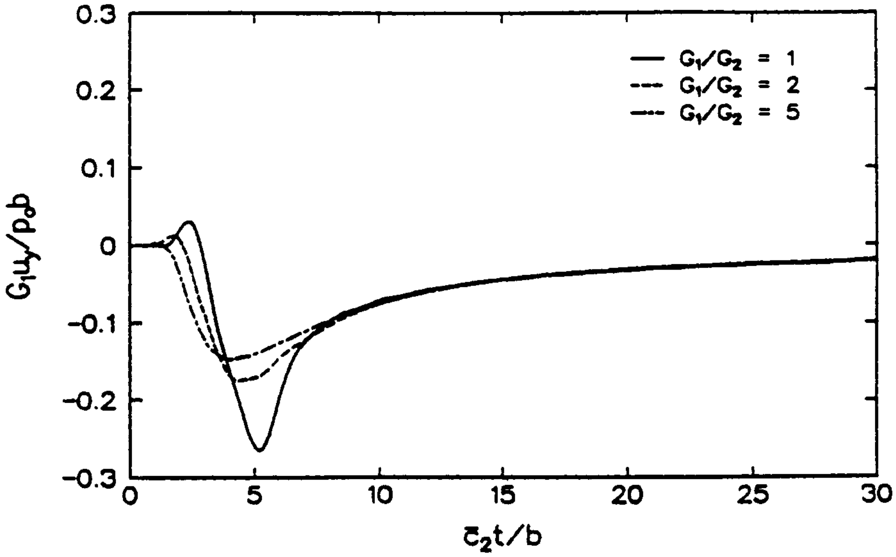

Figure 6-51: Vertical displacements at point P (x/b = 3) for the case of a stiffer upper layer.

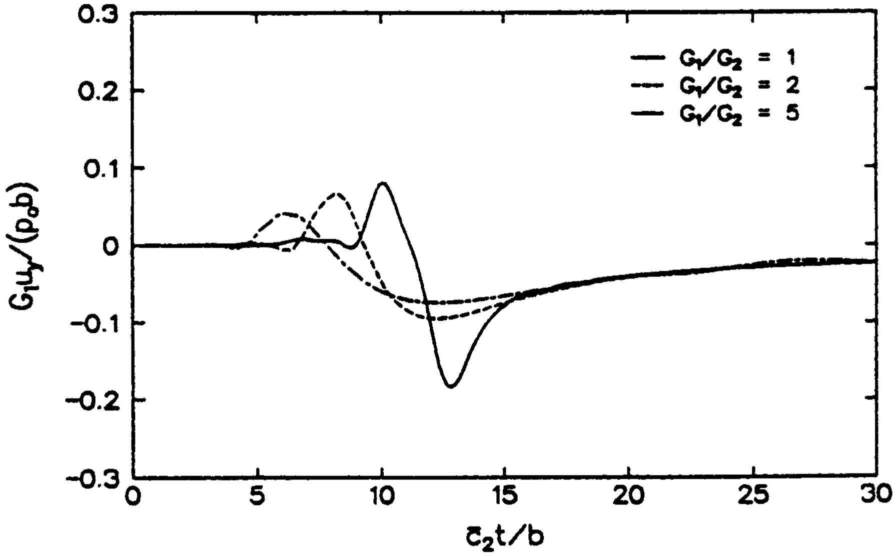

Figure 6-52: Vertical displacements at point Q (x/b = 10) for the case of a stiffer upper layer.

stiff half-plane case in Figures 6-49 and 6-50. To explain this difference in response adequately, it is necessary to review some of the basics of wave scattering phenomena in elastodynamics. A detailed discussion of the very complicated mathematical expressions involved is beyond the scope of this study. Interested readers can find some of the highlights of the necessary mathematical derivations in Eringen and Suhubi (1975) and Achenbach (1973), and a detailed description of the mathematics in Ewing et al. (1957, Section 3-1).

Surface waves occur under plane strain conditions because of a constructive interference between dilatational and shear waves (P- and S-waves). To understand the behavior of surface waves it is necessary to first review the scattering behavior of incident plane P- and S- waves in the presence of a material interface. In the simple case where the incident wave is either a pure P-wave or S-wave, the interface will generate four waves of two types propagating into each medium. Each incident wave will generate reflected and refracted P- and S-waves. Correspondingly, if the incident wave is composed of P- and S-waves, then eight waves will be generated at the interface. These refracted and reflected waves are always excited in their totality if the following inequality holds:

$$c_1 > c_2 > \bar{c}_1 > \bar{c}_2$$

where c_1 and c_2 are the wave velocities in the material containing the incident wave and $\bar{c}_1$ and $\bar{c}_2$ are the wave velocities in the adjacent medium. This inequality guarantees that all angles of reflection and refraction are real. If two media violate this inequality, some, or all, of the refracted waves are extinguished beyond a certain critical angle of incidence, which depends on the relative magnitude of wave velocities in the two media.

To give an example, the case of a stiffer half-plane is of particular interest, namely

$$\bar{c}_1 > \bar{c}_2 > c_1 > c_2$$

Then, it can be shown (Eringen and Suhubi, 1975) that an angle of incidence i greater that a critical angle i_{cr}, where

$$\sin i_{cr} = c_1/\bar{c}_2$$

results in all angles of refractions being imaginary and both components of the incident wave will be totally reflected (see Figure 6-53). This special case is a condition for the existence of oscillatory surface waves, sometimes termed generalized Rayleigh waves, which are generated by the constructive interference of plane waves trapped in the overlying (softer) layer and undergoing multiple and total reflections at the free surface and the interface. Therefore, surface waves in a layered half-plane can only occur if the velocity of wave propagation along the layer is less than the wave velocities of the substratum. Physically significant results may be obtained only when $\bar{c}_2 > c_1$. If this is the case, then the layer undergoes oscillatory motion in the vertical y-direction propagating in the horizontal x-direction with a surface wave velocity c, which is confined to the following inequality:

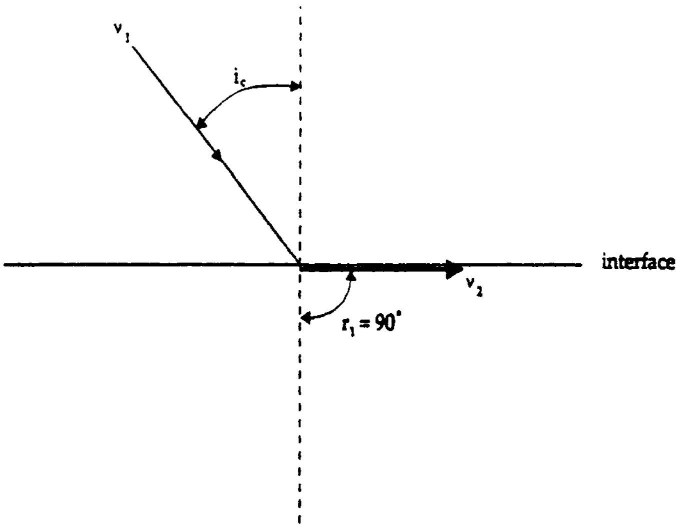

Figure 6-53: Total internal reflection.

$$\bar{c}_1 > \bar{c}_2 > c > c_1 > c_2$$

The disturbances in the layer decay exponentially with depth in the underlying half-plane. Hence, the generalized Rayleigh wave is confined to the upper layer. This surface wave is dispersive, unlike ordinary Rayleigh waves in a half-plane. It should be noted that the dispersion is simply an interface phenomenon and not a physical property of the material and it is strictly a result of introducing a finite length scale in the form of a finite layer thickness into the problem.

With this background, the wave scattering behavior of the cases shown in Figures 6-49 to 6-52 can be explained. The first case of $G_1/G_2 = 1$ shows a non-dispersive Rayleigh wave, because of the absence of a finite length scale or a characteristic length, such as a finite layer thickness. This is verified by the observation in Figures 6-49 to 6-52 that the shape of the wave form is not altered significantly as it travels from Station P to Station Q. Likewise, the case of $G_1/G_2 = 1/2$ does not meet the requirements for an oscillatory surface wave to occur, because $c_1 > \bar{c}_2$. Rather, some refraction into the half-plane will occur, which could possibly explain the interference observed at early times in Figure 6-50. The remaining stiffer half-plane case, described by $G_1/G_2 = 1/5$, fulfills the requirement for total reflection and should therefore show the oscillatory surface wave behavior observed in Figures 6-49 and 6-50.

The stiff layer case $G_1/G_2 = 5$ does not fulfill the requirements for an oscillatory surface wave to be generated, but all reflected and refracted waves should always be excited in their totality. Similarly, the case $G_1/G_2 = 2$ should not show any oscillatory surface wave effect, but some reflection and refraction will take place. Because of the wave scattering at the interface for these last three cases, energy associated with the refracted waves will be lost from the upper layer, going into the half-plane. This energy transfer away from the layer could possibly explain the observed reduction of displacement amplitudes in the upper layer, shown in Figures 6-51 and 6-52.

Because of the rather complicated nature of the case $G_1/G_2 = 1/5$, the time histories of displacement and velocity vectors were found to be of interest. The field point window is defined by the following four corner nodes: $(0m, -2m)$, $(120m, -2m)$, $(120m, -42m)$ and $(0m, -42m)$. Figures D-12 to D-24 show the time history of displacement vectors. Most of the displacement activity takes place in the upper layer, which is consistent with what should be expected for the case of total internal reflection. It is interesting to note the sharp turn in the displacement vectors from vertical right underneath the load to almost horizontal along the material interface for time steps 12 and 15. At time step 21, the surface oscillation observed in Figures 6-49 and 6-50 is clearly visible in the displacement vector plots. This surface oscillation is mostly confined to the upper layer and manifests itself in clearly oscillatory wave-like pattern that becomes quite visible at time step 30 and beyond. Similar oscillatory behavior is noticeable in the velocity vector plots shown in Figures D-25 to D-37. The velocity vectors are almost only noticeable in the upper layer, which again is consistent with what is expected for the case of total internal reflection.

It can be concluded from this example that the present numerical formulation is capable of modeling the complicated wave interaction phenomena associated with the scattering of waves in layered material.

6.2.7 Underground Explosion in a Two-Layered Rock

This final example deals with the surface vibration of a rock mass due to an underground explosion. The rock is modeled by an elastic rock layer overlying an elastic half-plane. The explosion is simulated by a suddenly applied pressure on the walls of a cylindrical cavity in the half-plane. The problem geometry and the time history of the applied pressure are shown in Figure 6-54. The surface and each side of the interface are modeled with 30 elements each of length 10 and the wall of the cavity is modeled with 16 straight-line elements. The unitless material properties (taken from a study by Israil and Banerjee, 1990b) are as follows:

Top layer: $G_1 = 647,200$, $\nu_1 = 0.35$, $\rho_1 = 3.25$, $c_1 = 928.9$, $c_2 = 446.2$

Half-plane: $G_2 = 1,991,150$, $\nu_2 = 0.30$, $\rho_2 = 2.85$, $c_1 = 1563.7$, $c_2 = 835.8$

The number of time steps was 175, each of size $\Delta t = 1.208 a_l / c_{\max}$, where $c_{\max} = 1563.7$. The time history of the vertical displacements is monitored at three selected points $A\,(0,0)$, $B\,(2a,0)$ and $C\,(4a,0)$ on the free surface, where $a = 10$ is the radius of the cavity. The corresponding results for the horizontal displacements are monitored at points $B\,(2a,0)$ and $C\,(4a,0)$.

This problem was first solved by a time domain boundary element method by Israil and Banerjee (1990b), in which a higher order boundary element formulation was used with isoparametric elements and with all integrals evaluated numerically. The

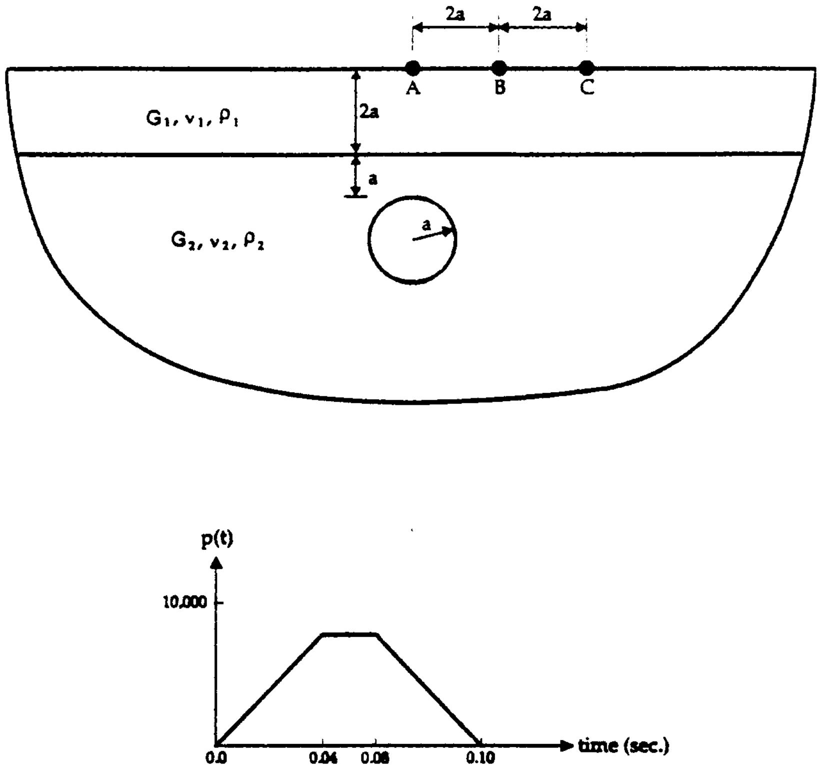

Figure 6-54: Underground explosion in a two-layered soil.

semi-infinite region was modeled as a closed domain with non-reflecting "enclosing elements" at an unspecified distance away from the boundaries of the problem. Figures 6-55, 6-56 and 6-57 compare the vertical displacements at Stations A and C and the horizontal displacements at Station C to the results obtained by Israil and Banerjee (1990b). The current results show very close agreement with the solution obtained by Israil and Banerjee (1990b). Again, it should be pointed out that the results are not significantly affected by the use of straight-line elements to model the boundary of the hole.

Figure 6-58 shows the vertical displacements at Stations A, B and C obtained by the current numerical implementation. The corresponding results for the horizontal displacements at Stations B and C are presented in Figure 6-59. The results show that the vertical displacements attenuate with distance as expected. However, the horizontal displacements do not attenuate significantly with distance, and at Station C

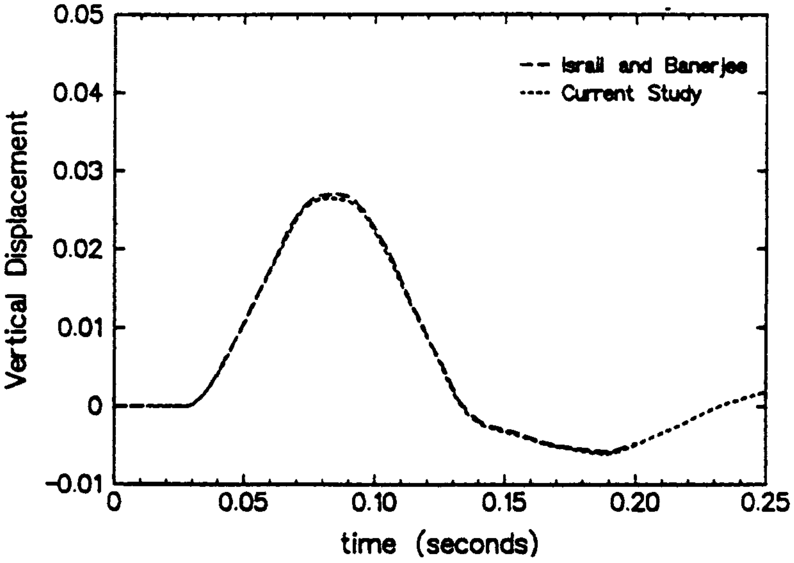

Figure 6-55: Vertical displacement at Station A.

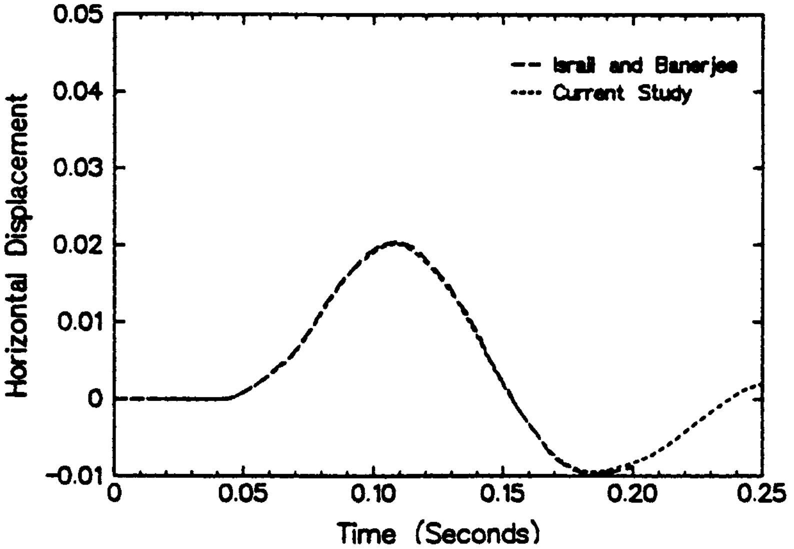

Figure 6-56: Vertical displacement at Station B.

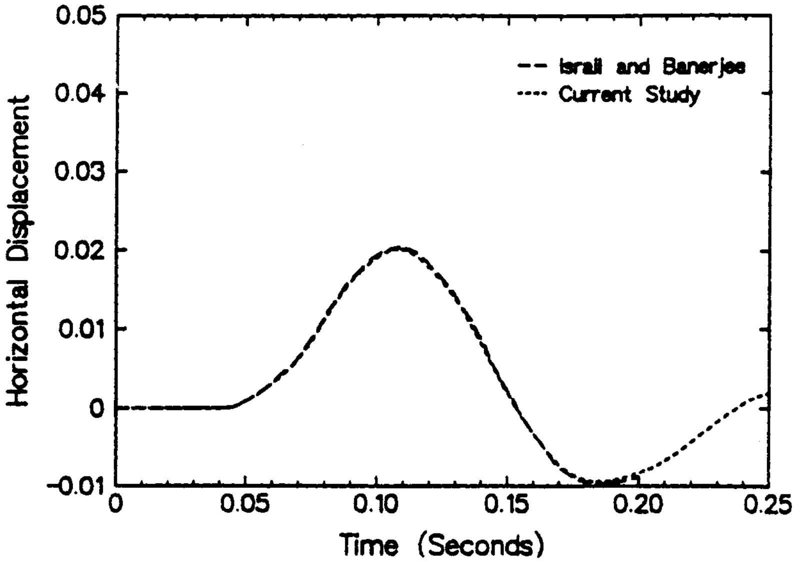

Figure 6-57: Vertical displacement at Station C.

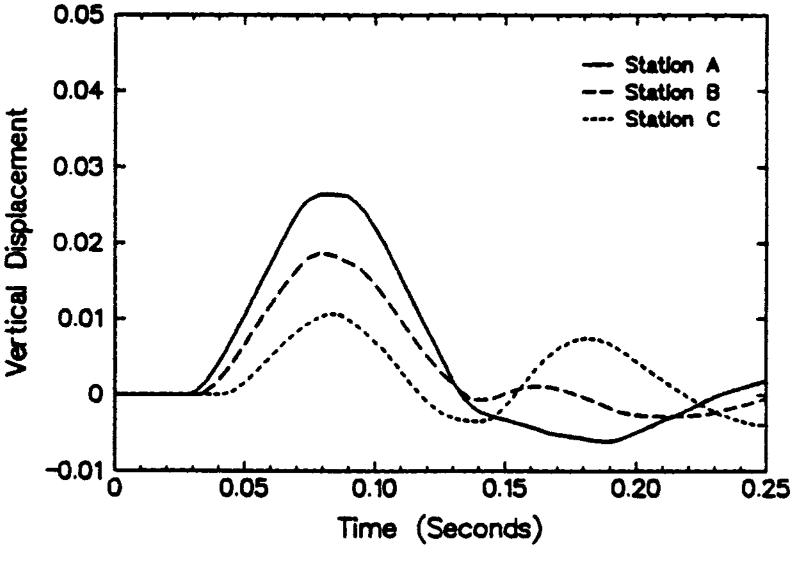

Figure 6-58: Vertical displacements at Stations A, B and C.

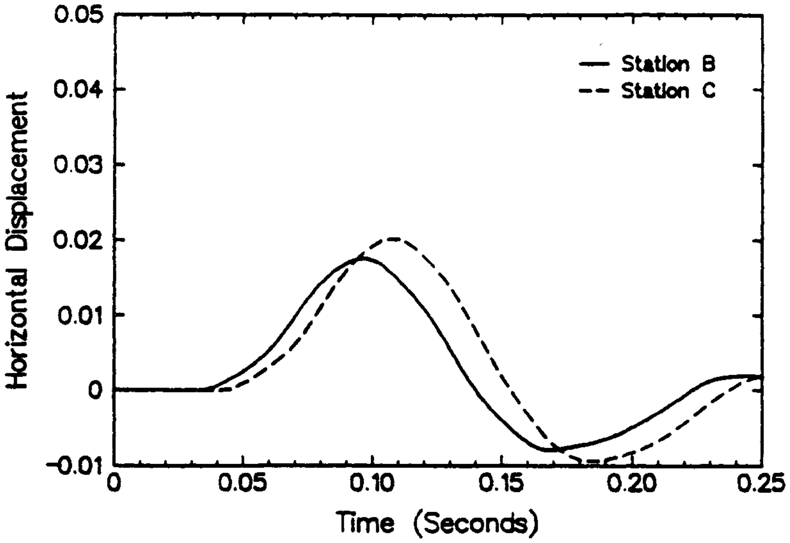

Figure 6-59: Horizontal displacements at Stations B and C.

the peak horizontal displacement is significantly higher that the corresponding vertical component, which clearly illustrates the complexity of scattering problems in layered and piecewise homogeneous media.

The time histories of displacement and velocity vectors are presented in Appendix D for a field point window defined by the following four corner nodes: $(0,-2)$, $(120,-2)$, $(120,-42)$ and $(0,-42)$. Figures D-38 to D-52 show how the displacements radiate away from the underground cavity, right after the explosion, until the wave front reaches the surface. Once the wave front has reached the surface, circular to slightly elliptical counterclockwise eddies are gradually formed in the upper layer, propagate along the surface and eventually disappear out of the field point window as expected. Another interesting point is how the velocity vectors shown in Figures D-53 to D-67 change their direction towards the hole as the magnitude of the applied load begins to decrease after time step 40. Both the displacement and velocity vectors show how the horizontal displacements and velocities become more and more dominant in comparison with their vertical components as the distance from the hole is increased. This is consistent with the observations made in Figures 6-58 and 6-59 that show how the vertical displacements at the surface attenuate with distance, while the horizontal displacements do not attenuate significantly with distance away from the hole.

6.3 Numerical Stability and the Size of Time-Step

Little discussion appears in the literature regarding the stability properties of elastodynamic boundary element methods. This lack of analysis is somewhat puzzling given the relatively large number of publications discussing the stability properties of both finite element and finite difference methods. This general lack of detailed stability analysis may be explained partly by repeated suggestions by a number of workers, such as for example, Ahmad and Banerjee (1988),and Israil and Banerjee (1990a, 1990b), that implicit time-marching formulations in boundary element methods are unconditionally stable. This is an erroneous conclusion as shown by the results obtained by Siebrits (1992) and Loken (1992). Rather, it appears that instabilities have been observed in virtually all elastodynamic time-domain boundary element implementations to date.

Numerical instabilities occur in various direct and indirect boundary element formulations. The direct boundary element formulations presented by Mansur (1983), Antes (1985) and Fukui (1986) illustrate increased oscillations at late times, indicating instabilities for some of their results. The results obtained by Tian (1990) and Wang (1991), who both use a direct formulation with quadratic spatial and linear temporal elements, and analytical integrations for all integrals, show instabilities at later times. A more recently published direct boundary element code, QUADPLET, by Dominguez (1994), which uses isoparametric quadratic spatial and linear temporal elements, also has been shown to go unstable (Siebrits and Peirce, 1995). Elastodynamic indirect boundary element formulations by Mack (1991) and Siebrits (1992) have been observed to have numerical stability problems for both three-dimensional and two-dimensional displacement discontinuity formulations. Also, Tian (1990) and Loken (1992) noted numerical instabilities in their two-and three-dimensional fictitious stress codes.

It can be concluded that numerical instability represents a persistent problem in elastodynamic time domain boundary element formulations, irrespective of whether the codes use two- or three-dimensional fundamental solutions, and irrespective of whether the integrals are performed analytically or evaluated numerically. A mathematical analysis of the stability properties of the direct boundary element method for elastodynamic problems in the time domain is beyond the scope of this study. However, some intuitive observations can be made regarding stability. In particular, it should be clear to the reader at this point that the results presented in this study certainly appear stable for all "practical purposes."

The stability of elastodynamic boundary element methods depends on the properties of fundamental solutions used in the formulation and the order of spatial and temporal interpolation functions used in the numerical formulation. As stated in Chapter 3, the fundamental solutions used in dynamic boundary element formulations are solutions to the equations of motion. The equations of motion conserve energy; no energy is lost and none is gained. The only way that a disturbance can dissipate is through geometric damping and through diffraction and scattering, which may lead to energy being scattered into adjacent media.

The requirement for the conservation of energy can in some cases lead to the fundamental solution not decaying with space and time. Close-coupling between neighboring and even remote elements can lead to a situation in which the response of neighboring elements to a stimulus by a given element will involve more energy than the original signal. This results in off-diagonal elements in the boundary element influence coefficient matrix being of the same magnitude or greater than the diagonal self-effects. A good example, discussed previously, is the case of a Rayleigh wave generation along a suddenly loaded homogeneous half-plane, where the horizontal component of the surface displacements given by (6-6) contains a non-decaying part. Also, a Rayleigh wave propagating along a free crack surface does not decay with distance from the source (Graff, 1975). These cases have in common the lack of a macroscopic length scale, such as the thickness of a finite layer resting on a half-plane or the thickness of a layer in which the crack is embedded. The introduction of a characteristic length into a problem changes the nature of energy propagation significantly. Any surface waves that are generated become dispersive and thereby distribute the energy associated with the initial disturbance over a number of elements, because waves of different frequencies have different phase velocities and different energy transport velocities. This may in some cases lead to a reduction in the amplitudes of disturbances away from the source, when compared to non-dispersive surface waves.

The other issue that influences the stability of boundary element formulations is the order of spatial and temporal interpolation functions used in the numerical formulation. Any errors introduced into the discretization scheme, because of the polynomial approximations of the tractions and displacements, can cause the total energy to increase, eventually leading to unstable results at later times. Therefore, accurate analytical integrations with higher order spatial and temporal interpolation functions should be used to minimize the possibility of the accumulation of discretization errors in the system. The use of higher order temporal interpolation functions should be encouraged at all times, unless the problem involves Heaviside loading. In these cases, the resulting displacement field is continuous, but the stresses will have a finite jump that is not adequately modeled by a linear approximation. The use of linear time interpolations to model the load response of Heaviside loading can result in artificial reflections taking place as discussed previously for the case of a suddenly loaded annulus. Therefore, two possibilities remain: (a) change the Heaviside loading to a ramp-step loading in which the load is applied with a finite rise time of one time-step, or (b) use a mixed time variation, in which the traction is assumed to stay constant, while the displacement is taken to be linear over each time step. In this study, approach (a) was selected, because it was felt that a linear approximation in time would generally provide more accurate results than a constant approximation in time.

The size of the time step also plays an important role in the stability properties of boundary element methods. An algorithm for which stability imposes a time step restriction is called *conditonally stable.* An algorithm for which there is no time step restriction imposed by stability is called *unconditionally stable.* All elastodynamic boundary element formulations appear to be at best conditionally stable. A convenient factor measuring the size of the time step Δt is the factor $Q_1 = c_1 \Delta t / a_l$, previously defined in Equation 6-6. This factor indicates how far the longitudinal wave travels in a single time step in terms of the half-length of a boundary element. In this study, it was found that stable results could be obtained for values of Q_1 ranging from $0.05 \leq Q_1 \leq 1.6$. In some cases, even a larger time-step was found to produce stable results. As the time step becomes larger, the self-effects are distributed over a greater number of nodes. This may result in a situation in which off diagonal elements are of the same magnitude as the diagonal elements in the boundary element influence matrices. Also, in cases where the loading response due to a suddenly applied load is changing very rapidly, it was found that smaller time-steps were needed to adequately predict the time histories of displacements and tractions. The linear temporal variation in displacements and tractions results in "choppy" time-histories for very large time steps in these cases. Therefore, it was found that $Q_1 \leq 1.0$ generally produces accurate and stable results. The lower limit of $Q_1 \geq 0.05$ can also be explained by an observation made by Manolis and Beskos (1988) that very small time steps result in non-vanishing dilations and rotations at the wave front and should therefore not be used.

Chapter 7

Conclusions and Recommendations for Future Work

Two direct boundary element methods for the analysis of elastostatic and elastodynamic problems associated with two-dimensional homogeneous or piecewise homogeneous problems have been developed. These methods have been verified for a variety of problems, ranging in scope from well-defined homogeneous planar half-plane and layered problems to cases in which curved geometries and complicated loadings are common, such as found in the underground blasting of circular openings in layered rock. Both methods assume piecewise quadratic in space interpolation functions between element nodes and, in addition, the elastodynamic method assumes piecewise linear temporal interpolation functions. Both methods assume the boundary to be composed of a number of straight-line elements and both methods are currently limited to linearly elastic problems where the material is piecewise homogeneous within any given subregion. Two or more subregions can be connected together at an interface to form a body with an arbitrary number of connected subregions. Currently, the methods assume that each subregion is held together at an interface in a welded contact, meaning that no slip or openings can exist at the interface between two subregions. Also, it can be concluded from the examples presented in this study that the elastodynamic boundary element method is stable for "practical purposes."

The advantages of using analytical integration rather than numerical integration include an increase in the numerical accuracy and stability of solutions, with an associated reduction in computer time and memory requirements. Another reason for using analytical integration is to capture the singular behavior of the self-effects better than is possible with the numerical integration schemes reported in the literature.

The methods presented in this thesis are ideally suited for studying of wave scattering phenomena associated with complicated layer and inclusion problems, such as those encountered in pavement engineering and mining. One of the limitations of the elastodynamic method presented in this study is that it does not easily lend itself to the modeling of crack-like geometries, such as those associated with the presence of faults, joints or cracks. This feature can be incorporated by a coupling of the current methods with displacement discontinuity methods, such as those developed by Siebrits (1992). Other features that would improve upon the current methods are the introduction of computer program restart options and a more efficient calculation and storage of influence coefficients. Other possible improvements of the methods include the coupling with finite element methods that allow for the modeling of non-linear behavior and the inclusion of interfaces on which limited slip is allowed and the incorporation of spring supports on the interfaces. Finally, despite the substantial amount of work involved, there is merit in the extension of the elastodynamic method to three dimensions to allow for a more realistic modeling of wave scattering phenomena around layers and inclusions.

References

Abascal, R. and J. Dominguez 1986. "Vibrations of Footings on Zoned Viscoelastic Soils," *J. Eng. Mech.* Vol. 112, pp. 433-447.

Achenbach, J. D. 1973. *Wave Propagation in Elastic Solids.* Amsterdam: North-Holland.

Ahmad, S. and P. K. Banerjee 1988. "Time-Domain Transient Elastodynamic Analysis of 3-D Solids by BEM," *Int. J. Numer. Methods Eng.* Vol. 26, pp. 1709-1728.

Aki, K. and P. G. Richards 1980. *Quantitative Seismology: Theory and Methods.* New York: Freeman and Company.

Antes, H. 1985. "A Boundary Element Procedure for Transient Wave Propagation in Two-Dimensional Isotropic Elastic Media," *Finite Elem. Anal. and Design* Vol. 1, pp. 313-322.

Antes, H. and T. Meise 1990. "Coping with Non-Convex Domains in the Boundary Element Analysis," *Comput. Mech.* Vol. 6, pp. 47-53.

Antes, H. and O. von Estorff 1986. "Transient Behavior of Strip Foundations Resting on Differential Soil Profiles by a Time Domain BEM," in: *Proc. Int'l Conf. Soil Dynamics Earth. Eng.* Ed.: A. S. Cakmak. Princeton.

Antes, H. and O. von Estorff 1987. "On Causality in Dynamic Response Analysis by

Time-Dependent Boundary Element Methods," *Earthquake Eng. Struct. Dyn.* Vol. 15, pp. 865-870.

Banaugh, R. P. and W. Goldsmith 1963. "Diffraction of Steady Elastic Waves by Surfaces of Arbitrary Shape," *J. Appl. Mech.* Vol. 30, pp. 589-597.

Banerjee, P. K. 1976. "Integral Equation Methods for Analysis of Piece-wise Non-homogeneous Three-dimensional Elastic Solids of Arbitrary Shape," *Int. J. Mech. Sci.* Vol. 18, pp. 293-303.

Banerjee, P. K. and R. Butterfield 1981. *Boundary Element Methods in Engineering Science*, London and New York: McGraw-Hill.

Banerjee, P. K., S. Ahmad, and G. D. Manolis 1986. "Transient Elastodynamic Analysis of Three-Dimensional Problems by Boundary Element Method," *Earthquake Eng. Struct. Dyn.* Vol. 4, pp. 933-949.

Banerjee, P. K., S. Ahmad, and G. D. Manolis 1987. "Advanced Elastodynamic Analysis," In: *Boundary Element Methods in Mechanics,* pp. 257-284. Amsterdam: North-Holland.

Banerjee, P. K., S. Ahmad and H. C. Wang 1989. "Advanced Development of BEM for Elastic and Inelastic Dynamic Analysis of Solids," in: *Developments in Boundary Element Methods-5.* Ed.: P. K. Banerjee and R. B. Wilson, pp. 77-117. London: Elsevier.

Benjumea, R. and D. L. Sikarskie 1972. "On the Solution of Plane, Orthotropic Elasticity Problems by an Integral Method," *J. Appl. Mech.* Vol. 39, pp. 801-808.

Beskos, D. E. (Editor) 1987. *Boundary Element Methods in Mechanics.* Amsterdam: North-Holland.

Beskos, D. E. 1993. "Wave Propagation Through Ground," in: *Boundary Element Techniques in Geomechanics*, Ed.: G. D. Manolis and T. G. Davies, pp. 359-406. Southampton: Computational Mechanics Publications.

Beskos, D. E., K. L. Leung and I. G. Vardoulakis 1986. "Vibration Isolation of Structures from Surface Waves in Layered Soil," in: *Recent Advances in Computational Mechanics*, Ed.: D. L. Karabalis, pp. 125-140. New York: ASCE.

Betti, E. 1876. Teoria dell Elasticita, *Il Nuovo Ciemento*, tome 7-10.

Brady, B. H. G. and J. W. Bray 1978. "The Boundary Element Method for Elastic Analysis of Tabular Orebody Extraction, Assuming Complete Plane Strain," *Int. J. Rock Mech. and Min. Sci. and Geomech. Abstr.* Vol. 15, pp. 29-37.

Brebbia, C. A., J. C. F. Telles and L. C. Wrobel 1984. *Boundary Element Techniques.* Berlin: Springer-Verlag.

Brebbia, C. A. and J. Dominguez 1992. *Boundary Elements: An Introductory Course.* New York: McGraw-Hill.

Brekhovskikh, L. M. 1980. *Waves in Layered Media*, 2nd edn. New York: Academic Press.

Butterfield, R. and G. R. Tomlin 1972. "Integral Techniques for Solving Zoned Anisotropic Continuum Problems," *Variational Methods in Eng.* 9/30-9/50, Southampton: University of Southampton.

Cagniard, L. 1939. *Réflexion et Réfraction des Ondes Séismiques Progressive.* Paris: Gauthier-Villard. English Translation in 1962: *Reflection and Refraction of Progressive Seismic Waves*, translated by E. A. Flinn and C. H. Dix. New York: McGraw-Hill.

Chouw, N., R. Le and G. Schmid 1991. "Propagation of Vibration in a Soil Layer Over Bedrock," *Eng. Anal. Boundary Elem.* Vol. 8, pp. 125-131.

Cole, D. M., D. D. Kosloff, and J. B. Minster 1978. "A Numerical Boundary Integral Equation Method for Elastodynamics," *Bull. Seism. Soc. Am.* Vol. 68, pp. 1331-1357.

Crouch, S. L. 1976. "Solution of Plane Elasticity Problems by the Displacement-Discontinuity Method," *Int. J. Numer. Methods Eng.* Vol. 10, pp. 301-343.

Crouch, S. L. and A. M. Starfield 1983. *Boundary Element Methods in Solid Mechanics.* London: George Allen and Unwin.

Cruse, T. A. 1968. "A Direct Formulation and Numerical Solution of the General Transient Elastodynamic Problem. II," *J. Math. Anal. Appl.* Vol. 22, pp. 341-355.

Cruse, T. A. 1974. "An Improved Boundary-Integral Equation Method for Three-Dimensional Elastic Stress Analysis," *Comput. and Struct.* Vol. 4, pp. 741-54.

Cruse, T. A. 1987. "Recent Advances in Boundary Element Analysis Methods," *Comput. Methods Appl. Mech. and Eng.* Vol. 62, pp. 227-244.

Cruse, T. A. 1988. *Boundary Element Analysis in Computational Fracture Mechanics.* Dordrecht: Kluwer Academic Publishers.

Cruse, T. A. and F. J. Rizzo 1968. "A Direct Formulation and Numerical Solution of the General Transient Elastodynamic Problem. I," *J. Math. Anal. Appl.* Vol. 22, pp. 244-259.

Cundall, P. A. 1971. "A Computer Model for Simulating Progressive Large Scale Movements in Blocky Rock Systems," In: *Rock Fracture*, Proc. Int'l Symp. on Rock

Fracture, Paper 2-8. Nancy.

Dominguez, J. 1994. *Boundary Elements in Dynamics.* Southampton: Computational Mechanics Publications.

Dominguez, J. and T. Meise 1991. "On the Use of the BEM for Wave Propagation in Infinite Domains," *Eng. Anal. Boundary Elem.* Vol. 8, pp. 132-138.

Dravinski, M. and T. M. Mossessian 1987. "Scattering of Plane Harmonic P, SV, and Rayleigh Waves by Dipping Layers of Arbitrary Shape," *Bull. Seism. Soc. Am.* Vol. 77, pp. 212-235.

Durbin, F. 1974. "Numerical Inversion of Laplace Transforms by Relating them to the Finite Cosine Transform," *J. Assoc. Comp. Mech.* Vol. 15, pp. 115-123.

Emperador, J. M. and J. Dominguez 1989. "Dynamic Response of Axisymmetric Embedded Foundations," *Earthquake Eng. Struct. Dyn.* Vol. 18, pp. 1105-1117.

Eringen, A. C. and E. S. Suhubi 1975. *Elastodynamics.* New York: Academic Press.

Ewing, W. M., W. S. Jardetsky and F. Press 1957. *Elastic Waves in Layered Media.* New York: McGraw-Hill.

Fredholm, I. 1903. "Sur Une Classe D'Equations Fonctionelles," *Acta Math.* Vol. 27, pp. 365-390.

Friedman, M. B. and R. P. Shaw 1962. "Diffraction of Pulses by Cylindrical Obstacles of Arbitrary Cross-Section," *J. Appl. Mech.* Vol. 29, pp. 40-46.

Fukui, T. 1986. "Time Marching Analysis of Boundary Integral Equations in Two Dimensional Elastodynamics," in: *Innovative Numerical Methods in Engineering*, Ed. : R. P. Shaw et al., pp. 405-410. New York: Springer-Verlag.

Gaul, L. P. Klein and M. Plenge 1991. "Simulation of Wave Propagation in Irregular Soil Domains by BEM and Associated Small Scale Experiments," *Eng. Anal. Boundary Elem.* Vol. 8, pp. 200-205.

Gonsalves, I. R., D. J. Shippy and F. J. Rizzo 1990. "Direct Boundary Integral Equations for Elastodynamics in 3-D Half-spaces," *Comput. Mech.* Vol. 6, pp. 279-292.

Graff, K. F. 1975. *Wave Motion in Elastic Solids.* Oxford: Clarendon Press.

Graffi, D. 1947. "Sul Teorema di Reciprocita nella Dinamica dei Corpi Elastici," Memoria della Academia della Scienze, Bologna, Ser. 10 Vol. 4, pp. 103-111.

Habault, D. 1990. "Propagation of Vibrations in a Layer of Ground," in: *Boundary Elements in Mechanical and Electrical Engineering*, Ed.: C. A. Brebbia and A. Chaudouet-Miranda, pp. 169-178. Berlin: Springer-Verlag.

Hadley, P. K., A. Askar and A. S. Cakmak 1991. "Earthquake Wave Propagation in Layered Media by Boundary Integral Methods," *Soil Dyn. Earthquake Eng.* Vol. 10, pp. 130-140.

Jaswon, M. A. 1963. "Integral Equation Methods in Potential Theory. I," *Proc. Royal Soc. London Series A* Vol. 275, pp. 23-32.

Israil, A. S. M. and P. K. Banerjee 1990a. "Advanced Time-Domain Formulation of BEM for Two-Dimensional Transient Elastodynamics," *Int. J. Numer. Methods Eng.* Vol. 29, pp. 1421-1440.

Israil, A. S. M. and P. K. Banerjee 1990b. "Two-Dimensional Transient Wave-Propagation Problems by Time-Domain BEM," *Int. J. Solids and Struct.* Vol. 26, No. 8, pp. 851-864.

Karabalis, D. L. and D. E. Beskos 1984. "Dynamic Response of 3-D Rigid Surface Foundations by Time Domain Boundary Element Method," *Earthquake Eng. Struct. Dyn.* Vol. 12, pp. 73-93.

Karabalis, D. L. and D. E. Beskos 1990. "Time-Domain Transient Elastodynamic Analysis of 3-D Solids by BEM," *Int. J. Numer. Methods Eng.* Vol. 29, pp. 211-215.

Kellogg, O. D. 1954. *Foundations of Potential Theory.* New York: Dover.

Kobayashi, S. 1987. "Elastodynamics," in: *Boundary Element Methods in Mechanics*, pp. 192-255. Amsterdam: North-Holland.

Kobayashi, S. and N. Nishimura 1982. "Transient Stress Analysis of Tunnels and Cavities of Arbitrary Shape due to Traveling Waves," in: *Developments in Boundary Element Methods*, Vol. 2, pp. 177-210. London: Appl. Sci. Publ.

Kolsky, H. 1953. *Stress Waves in Solids.* Oxford: Clarendon Press.

Koppe, H. 1948. "Über Rayleigh-Wellen an den Oberfläche zweier Medien," *Z. Angew. Math. und Mech.* Vol. 28, pp. 355-360.

Kuhn, G. 1988. "Boundary Element Technique in Elastostatics and Linear Fracture Mechanics: Theory and Engineering Application," in: *Finite Element and Boundary Element Techniques from Mathematical and Engineering Point of View*, Ed.: E. Stein and W. L. Wendland. New York: Springer-Verlag.

Kupradze, V. D. 1965. *Potential Methods in the Theory of Elasticity.* London: Oldbourne Press.

Lachat, J. C. and J. O. Watson 1976. "Effective Numerical Treatment of Boundary-Integral Equations: A Formulation for Three-Dimensional Elastostatics," *Int. J. Numer. Methods Eng.* Vol. 10, pp. 991-1005.

Lamb, H. 1904. "On the Propagation of Tremors over the Surface of an Elastic Solid," *Philos. Trans. Roy. Soc. London Ser. A* Vol. 203, pp. 1-42.

Leung, K. L., D. E. Beskos and I. G. Vardoulakis 1990. "Vibration Isolation Using Open or Filled Trenches, Part 3: 2-D Non-homogeneous Soil By the BEM," *Comput. Mech.* Vol. 7, pp. 137-148.

Linkov, A. and N. Filippov 1991. "Difference Equations Approach to the Analysis of Layered Systems," *Meccanica* Vol. 26, pp. 195-209.

Loken, M. C. 1992. *A Three-Dimensional Boundary Element Method for Linear Elastodynamics.* Ph. D. Thesis. University of Minnesota.

Love, A. E. H. 1906. *A Treatise on the Mathematical Theory of Elasticity,* 2nd edn.Cambridge: University Press.

Mack, M. G. 1991. *A Three-Dimensional Boundary Element Method for Elastodynamics.* Ph.D. Thesis. University of Minnesota.

Maier, G. and G. Novati 1987. "Boundary Element Elastic Analysis of Layered Soils by a Successive Stiffness Method," *Int. J. Numer. Anal. Methods Geomech.* Vol. 11, pp. 435-447.

Manolis, G. D. 1980. *Dynamic Responses of Underground Structures.* Ph.D. Thesis. University of Minnesota.

Manolis, G. D. 1983. "A Comparative Study on Three Boundary Element Method Approaches to Problems in Elastodynamics," *Int. J. Numer. Methods Eng.* Vol. 19, pp. 71-93.

Manolis, G. D. and D. E. Beskos 1981. "Dynamic Stress Concentration Studies by Boundary Integrals and Laplace Transformations," *Int. J. Numer. Methods Eng.* Vol. 17, pp. 573-599.

Mansur, W. J. 1983. *A Time-Stepping Technique to Solve Wave Propagation Problems Using the Boundary Element Method.* Ph.D. Thesis. University of Southampton.

Massonet, C. E. 1966. "Numerical Use of Integral Procedures," in: *Stress Analysis,* Ed.: O. C. Zienkiewicz and G. S. Hollister. London: Wiley.

Mikhlin, S. G. 1957. *Integral Equations.* Oxford: Pergamon Press.

Miklowitz, J. 1977. *The Theory of Elastic Waves and Wave Guides.* Amsterdam: North-Holland Publishing.

Muskhelishivili, N. I. 1953. *Singular Integral Equations.* Groningen: Noordhoff Publishing.

Muskhelishivili, N. I. 1963. *Some Basic Problems of the Mathematical Theory of Elasticity.* Groningen: Noordhoff Publishing.

Niwa, Y., S. Kobayashi and N. Azuma 1975. "An Analysis of Transient Stresses Produced Around Cavities of Arbitrary Shape During the Passage of Traveling Waves," *Mem. Fac. Eng. Kyoto Univ.* Vol. 37, pp. 28- 46.

Niwa, Y., S. Kobayashi and T. Fukui 1976. "Applications of Integral Equation Methods to Some Geomechanical Problems," in: *Numerical Methods in Geomechanics,* Ed.: C. S. Desai, pp. 120-131. New York: ASCE.

Niwa, Y., T. Fukui, S. Sato, and L. Fujiki 1980. "An Application of the Integral Equation Method to Two-Dimensional Elastodynamics," *Theor. Appl. Mech.* Vol. 28, pp. 281-290.

Papoulis, A. 1957. "A New Method of Inversion of the Laplace Transform," *Quart. Appl. Math.* Vol. 14, No. 4, pp. 405-414.

Pao, Y. H. and C. C. Mow 1973. *Diffraction of Elastic Waves and Dynamic Stress Concentrations.* New York: Crane Russak.

Rizzo, F. J. 1967. "An Integral Equation Approach to Boundary Value Problems of Classical Elastostatics," *Q. Appl. Math.* Vol. 25, pp. 83-95.

Rizzo, F. J. and D. J. Shippy 1968. "A Formulation and Solution of the General Non-homogeneous Elastic Inclusion Problem," *Int. J. Solids and Struct.* Vol. 4, pp. 1161-1179.

Rizzo, F. J. and D. J. Shippy 1970. "A Method for Stress Determination in Plane Anisotropic Elastic Bodies," *J. Compos. Mater.* Vol. 4, pp. 36-61.

Rizzo, F. J., D. J. Shippy and M. Rezayat 1985. "A Boundary Integral Equation Method for Radiation and Scattering of Elastic Waves in Three Dimensions," *Int. J. Numer. Methods Eng.* Vol. 21, pp. 115-129.

Rudolphi, T. J. 1983. "An Implementation of the Boundary Element Method Method for Zoned Media with Stress Discontinuities," *Int. J. Numer. Methods Eng.* Vol. 19, pp 1-15.

Scholte, J. G. 1947. "The Range of Existence of Rayleigh and Stoneley Waves," *Mon. Not. R. Astron. Soc. Geophys. Suppl.* Vol. 5, pp. 120-126.

Selberg, H. L. 1952. "Transient Compression Waves from Spherical and Cylindrical Cavities," *Ark. Fys.* Vol. 5, No. 7, pp. 97-108.

Selcuk, S. 1992. *A Higher-Order Boundary Integral-Displacement Discontinuity Method for Fracture Propagation in Layered Elastic Media.* Ph.D. Thesis. University of Minnesota.

Sezawa, K. and K. Kanai 1939. "The Range of Possible Existence of Stoneley Waves and Some Related Problems," *Bull. Earthquake Res. Inst. Univ. Tokyo* Vol 17, pp. 1-18.

Siebrits, E. 1992. *Two-Dimensional Time Domain Elastodynamic Displacement Discontinuity Method with Mining Applications.* Ph.D. Thesis. University of Minnesota.

Siebrits, S. and A. P. Peirce 1995. "Stability Properties of Time Domain Elastodynamic Boundary Element Methods," in: *Boundary Element Methods 17.* Southampton: Computational Mechanics Publications.

Smirnov, V. J. 1964. "Integral Equations and Partial Differential Equations," in: *A Course in Higher Mathematics*, Vol. IV. London: Addison-Wesley.

Sokolnikoff, I. S. 1956. *Mathematical Theory of Elasticity*, 2nd Edn. New York: McGraw-Hill.

Somigliana, V. 1885. "Sopra l'equilibrio di us corpo elastico isotropo," *Il Nuovo Ciemento*, tome 17-19.

Stokes, G. G. 1883. "On the Dynamical Theory of Diffraction," in: *Mathematical and Physical Papers*, Vol. II, Ed.: G. B. Stokes, pp. 243-290. Cambridge: University Press.

Symm, G. T. 1963. "Integral Equations in Potential Theory. II," *Proc. Royal Soc. London Series A* Vol. 275, pp. 33-46.

Swedlow, J. L. and T. A. Cruse 1971. "Formulation of Boundary Integral Equations for Three Dimensional Elastoplastic Flow," *Int. J. Solids and Struct.* Vol. 5, pp. 1259-1274.

Tian, Y. 1990. *A Two-Dimensional Direct Boundary Integral Method for Elastodynamics.* Ph.D. Thesis. University of Minnesota.

Tian, Y., M. C. Loken, and S. L. Crouch 1990. "Elastodynamic Simulation of Mining," in: *Proc. of the ISRM Int. Symp. on Static and Dynamic Considerations in Rock Engineering.* Swaziland.

Triantafyllidis, T. 1993. "Über die Anwendung der Randelementmethoden auf Probleme der Wellendiffraktion," *Z. Angew. Math. und Mech.* Vol. 73, pp. 15-26.

Triantafyllidis, T. and B. Dasgupta 1987. "The Causality of the Boundary Element Method in Elastodynamics," *University of Minnesota Supercomputer Institute Report 87/112.* Minneapolis.

Triantafyllidis, T. and B. Dasgupta 1990. "The Causality of the Boundary Element Method in Elastodynamics," *Soil Dyn. Earthquake Eng.* Vol. 9, pp. 78-84.

von Estorff, O. and M. J. Prabucki 1990. "Dynamic Response in the Time Domain by Coupled Boundary and Finite Elements," *Comput. Mech.* Vol. 6, pp. 35-46.

von Estorff, O. and E. Kausel 1989. "Coupling of Boundary and Finite Elements for Soil-Structure Interaction Problems," *Earthquake Eng. Struct. Dyn.* Vol. 18, pp. 1065-1075.

von Estorff, O., A. L. Pais and E. Kausel 1990. "Some Observations on Time Domain and Frequency Domain Boundary Elements," *Int. J. Numer. Methods Eng.* Vol. 29, pp. 785-800.

von Estorff, O. and G. Schmid 1984. "Application of the Boundary Element Method to the Analysis of the Vibration Behavior of Strip Foundations on a Soil Layer," in: *Dynamic Soil-Structure Interaction*, Ed.: D. E. Beskos, T. Krauthammer and I. Vardoulakis, pp. 11-17. Rotterdam: A. A. Balkema.

Wang, C. Y. 1991. *A New Approach to Time Domain Boundary Element Method and Application to Wave Propagation and Scattering Problems.* Ph.D. Thesis. Okayama University.

Wardle, L. J. and J. M. Crotty 1978."Two-dimensional Boundary Integral Equation Analysis for Non-homogeneous Mining Applications," in: *Recent Advances in Boundary Element Methods*, Ed.: C. A. Brebbia, pp. 233-249. London: Pentech Press.

Wheeler, L. T. and E. Sternberg 1968. "Some Theorems in Classical Elastodynamics," *Arch. Rational Mech. Anal.* Vol. 31, pp. 51-90.

Zienkiewicz, O. C. 1977. *The Finite Element Method*, 3rd edn. London: McGraw-Hill.

Appendix A

Elastostatic Integrations

The integrals needed for the development of the boundary influence coefficients from algebraic expressions (5-11) and (5-12) are presented below. These integrals are given in terms of the local variables $u = \bar{x} - \bar{\xi}$ and $v = \bar{y} - \bar{\eta}$. (The transformation of local variables to global variables is given by (5-2) and shown in Figure 5-1.) These integrals are:

$$\int g du = e_1 \int \ln r du = e_1 \left[u \ln r - u + v \arctan \frac{u}{v} \right] \tag{A-1}$$

$$\int u \ln r du = e_1 \int u g du = e_1 \frac{r^2}{2} \left[\ln r - \frac{1}{2} \right] \tag{A-2}$$

$$\int u^2 g du = e_1 \int u^2 \ln r du = e_1 \left[\frac{u^3}{3} \ln r - \frac{1}{9} u^3 + \frac{1}{3} v^2 u - \frac{1}{3} v^3 \arctan \left(\frac{u}{v} \right) \right] \tag{A-3}$$

$$\int g_{,u} du = \int \frac{u}{r^2} du = e_1 \frac{-1}{4\pi (1-\nu)} \ln r \tag{A-4}$$

$$\int u g_{,u} du = \int u \frac{u}{r^2} du = e_1 \frac{-1}{4\pi (1-\nu)} \left[u - v \arctan \left(\frac{u}{v} \right) \right] \tag{A-5}$$

$$\int u^2 g_{,u} du = \int u^2 \frac{u}{r^2} du = e_1 \frac{-1}{4\pi (1-\nu)} \left[\frac{r^2}{2} - v^2 \ln r \right] \tag{A-6}$$

$$\int g_{,v} du = \int \frac{v}{r^2} du = e_1 \frac{-1}{4\pi (1-\nu)} \arctan \left(\frac{u}{v} \right) \tag{A-7}$$

$$\int u g_{,v} du = \int u \frac{v}{r^2} du = e_1 \frac{-1}{4\pi (1-\nu)} v \ln r \tag{A-8}$$

$$\int u^2 g_{,v} du = \int u^2 \frac{v}{r^2} du = e_1 \frac{-1}{4\pi(1-\nu)} v \left[u - v \arctan\left(\frac{u}{v}\right)\right] \tag{A-9}$$

$$\int g_{,uv} du = \int g_{,uv} du = e_1 \frac{-1}{4\pi(1-\nu)} \frac{v}{r^2} \tag{A-10}$$

$$\int u g_{,uv} du = \int u g_{,uv} du = e_1 \left[\frac{uv}{r^2} - \arctan\left(\frac{u}{v}\right)\right] \tag{A-11}$$

$$\int u^2 g_{,uv} du = \int u^2 g_{,uv} du = e_1 v \left[\frac{u^2}{r^2} - 2 \ln r \right] \tag{A-12}$$

$$\int g_{,uu} du = \int g_{,uu} du = e_1 \frac{u}{r^2} \tag{A-13}$$

$$\int u g_{,uu} du = \int u g_{,uu} du = e_1 \left[\frac{u^2}{r^2} - \ln r \right] \tag{A-14}$$

$$\int u^2 g_{,uu} du = \int u^2 g_{,uu} du = e_1 \left[\frac{u^3}{r^2} - 2u + 2v \arctan\left(\frac{u}{v}\right)\right] \tag{A-15}$$

in which

$$e_1 = -\frac{1}{4\pi(1-\nu)} \tag{A-16}$$

and $r^2 = u^2 + v^2$.

Additionally, the following integrals are needed for the calculation of the internal stresses by (5-77):

$$\int g_{,uuv} du = \int g_{,uuv} du = e_1 \left[-2\frac{uv}{r^4} \right] \tag{A-17}$$

$$\int u g_{,uuv} du = \int u g_{,uuv} du = e_1 \left[\frac{-v}{r^2} - 2\frac{vu^2}{r^4} \right] \tag{A-18}$$

$$\int u^2 g_{,uuv} du = \int u^2 g_{,uuv} du = e_1 \left[-2\frac{vu^3}{r^4} - 2\frac{uv}{r^2} + 2 \arctan\left(\frac{u}{v}\right)\right] \tag{A-19}$$

$$\int g_{,vvu} du = \int g_{,vvu} du = e_1 \left[\frac{u^2 - v^2}{r^4} \right] \tag{A-20}$$

$$\int u g_{,vvu} du = \int u g_{,vvu} du = e_1 \left[2\frac{u^3}{r^4} \right] \tag{A-21}$$

$$\int u^2 g_{,vvu} du = \int u^2 g_{,vvu} du = e_1 \left[\frac{u^2}{r^2} + 2\frac{u^4}{r^4} - 2 \ln r \right] \tag{A-22}$$

The traction self-effect boundary influence coefficients for $\underline{\xi} \rightarrow \underline{x}$ are:

$$\left(B^{R}_{xx}\right)_J = \int U_{xx}\varphi_R d\bar{x} = -\frac{a\,(3-4\nu)}{8\pi\,(1-\nu)}\left\{2\frac{\ln{(2a)}}{3} - \frac{17}{9}\right\} \tag{A-23}$$

$$\left(B^{R}_{xy}\right)_J = \int U_{xy}\phi_R d\bar{x} = 0 \tag{A-24}$$

$$\left(B^{R}_{yx}\right)_J = \int U_{yx}\phi_R d\bar{x} = 0 \tag{A-25}$$

$$\left(B^{R}_{yy}\right)_J = \int U_{yy}\phi_R d\bar{x} = -\frac{a\,(3-4\nu)}{8\pi\,(1-\nu)}\left\{2\frac{\ln{(2a)}}{3} - \frac{17}{9}\right\} \tag{A-26}$$

$$\left(B^{C}_{xx}\right)_J = \int U_{xx}\varphi_C d\bar{x} = -\frac{a\,(3-4\nu)}{8\pi\,(1-\nu)}\left\{4\frac{\ln{(a)}}{3} + \frac{2}{9}\right\} \tag{A-27}$$

$$\left(B^{C}_{xy}\right)_J = \int U_{xy}\phi_C d\bar{x} = 0 \tag{A-28}$$

$$\left(B^{C}_{yx}\right)_J = \int U_{yx}\phi_C d\bar{x} = 0 \tag{A-29}$$

$$\left(B^{C}_{yy}\right)_J = \int U_{yy}\phi_C d\bar{x} = -\frac{a\,(3-4\nu)}{8\pi\,(1-\nu)}\left\{4\frac{\ln{(a)}}{3} + \frac{2}{9}\right\} \tag{A-30}$$

$$\left(B^{L}_{xx}\right)_J = \int U_{xx}\phi_L d\bar{x} = -\frac{a\,(3-4\nu)}{8\pi\,(1-\nu)}\left\{2\frac{\ln{(2a)}}{3} - \frac{17}{9}\right\} \tag{A-31}$$

$$\left(B^{L}_{xy}\right)_J = \int U_{xy}\phi_L d\bar{x} = 0 \tag{A-32}$$

$$\left(B^{L}_{yx}\right)_J = \int U_{xy}\phi_L d\bar{x} = 0 \tag{A-33}$$

$$\left(B^{L}_{yy}\right)_J = \int U_{xx}\phi_L d\bar{x} = -\frac{a\,(3-4\nu)}{8\pi\,(1-\nu)}\left\{2\frac{\ln{(2a)}}{3} - \frac{17}{9}\right\} \tag{A-34}$$

Similarly, the displacement self-effect boundary influence coefficients for $\underline{\xi} \rightarrow \underline{x}$ are:

$$\begin{aligned}\left(A^{R}_{xx}\right)_J &= \int T_{xx}\phi_R d\bar{x} = 0.25\left(1+\frac{\gamma}{\pi}\right)\\ &\quad -\frac{1}{8\pi\,(1-\nu)}\left\{(1+\cos\gamma)\sin 2\beta + \sin\gamma\cos 2\beta\right\}\end{aligned} \tag{A-35}$$

$$\begin{aligned}\left(A^{R}_{xy}\right)_J &= \int T_{xy}\phi_R d\bar{x} = -\frac{1}{8\pi\,(1-\nu)}\left\{-(1-2\nu)\left[4-2\ln{(2a)}\right]\right.\\ &\quad \left.-(1+\cos\gamma)\cos 2\beta + \sin\gamma\sin 2\beta\right\}\end{aligned} \tag{A-36}$$

$$\begin{aligned}\left(A^{R}_{yx}\right)_{J} &= \int T_{yx}\phi_{R}d\bar{x} = -\frac{1}{8\pi\left(1-\nu\right)}\left\{\left(1-2\nu\right)\left[4-2\ln\left(2a\right)\right]\right.\\ &\left.-\left(1+\cos\gamma\right)\cos 2\beta+\sin\gamma\sin 2\beta\right\}\end{aligned} \tag{A-37}$$

$$\begin{aligned}\left(A^{R}_{yy}\right)_{J} &= \int T_{yy}\phi_{R}d\bar{x} = 0.25\left(1+\frac{\gamma}{\pi}\right)\\ &-\frac{1}{8\pi\left(1-\nu\right)}\left\{-\left(1+\cos\gamma\right)\sin 2\beta-\sin\gamma\cos 2\beta\right\}\end{aligned} \tag{A-38}$$

$$\left(A^{C}_{xx}\right)_{J} = \int T_{xx}\phi_{C}d\bar{x} = \frac{1}{2} \tag{A-39}$$

$$\left(A^{C}_{xy}\right)_{J} = \int T_{xy}\phi_{C}d\bar{x} = 0 \tag{A-40}$$

$$\left(A^{C}_{yx}\right)_{J} = \int T_{yx}\phi_{C}d\bar{x} = 0 \tag{A-41}$$

$$\left(A^{C}_{yy}\right)_{J} = \int T_{yy}\phi_{C}d\bar{x} = \frac{1}{2} \tag{A-42}$$

$$\begin{aligned}\left(A^{L}_{xx}\right)_{J} &= \int T_{xx}\phi_{L}d\bar{x} = 0.25\left(1+\frac{\gamma}{\pi}\right)\\ &-\frac{1}{8\pi\left(1-\nu\right)}\left\{-\left(1+\cos\gamma\right)\sin 2\beta+\sin\gamma\cos 2\beta\right\}\end{aligned} \tag{A-43}$$

$$\begin{aligned}\left(A^{L}_{xy}\right)_{J} &= \int T_{xy}\phi_{L}d\bar{x} = -\frac{1}{8\pi\left(1-\nu\right)}\left\{-\left(1-2\nu\right)\left[2\ln\left(2a\right)-4\right]\right.\\ &\left.+\left(1+\cos\gamma\right)\cos 2\beta+\sin\gamma\sin 2\beta\right\}\end{aligned} \tag{A-44}$$

$$\begin{aligned}\left(A^{L}_{yx}\right)_{J} &= \int T_{yx}\phi_{L}d\bar{x} = -\frac{1}{8\pi\left(1-\nu\right)}\left\{\left(1-2\nu\right)\left[2\ln\left(2a\right)-4\right]\right.\\ &\left.+\left(1+\cos\gamma\right)\cos 2\beta+\sin\gamma\sin 2\beta\right\}\end{aligned} \tag{A-45}$$

$$\begin{aligned}\left(A^{L}_{yy}\right)_{J} &= \int T_{yy}\phi_{L}d\bar{x} = 0.25\left(1+\frac{\gamma}{\pi}\right)\\ &-\frac{1}{8\pi\left(1-\nu\right)}\left\{\left(1+\cos\gamma\right)\sin 2\beta+\sin\gamma\cos 2\beta\right\}\end{aligned} \tag{A-46}$$

Appendix B

Elastodynamic Integrations

All the integrations needed to develop the elastodynamic boundary influence coefficients can be expressed in terms of a set of 12 basic, recurring integrals. In the following, these integrals are presented in terms of the local variables $u = \bar{x} - \bar{\xi}$ and $v = \bar{y} - \eta$. (The transformation of local variables to global variables is given by (5-2) and shown in Figure 5-1.) The integrals are:

$$\begin{aligned}\int \cosh^{-1}\left(\frac{ct}{r}\right) du &= u\cosh^{-1}\left(\frac{ct}{r}\right) + ct\arcsin\left(\frac{u}{\sqrt{c^2t^2 - v^2}}\right) \\ &\quad -v\arctan\left(\frac{ctu}{v\sqrt{c^2t^2 - r^2}}\right)\end{aligned} \tag{B-1}$$

$$\int u\cosh^{-1}\left(\frac{ct}{r}\right) du = \frac{r^2}{2}\cosh^{-1}\left(\frac{ct}{r}\right) - \left(\frac{ct}{2}\sqrt{c^2t^2 - r^2}\right) \tag{B-2}$$

$$\begin{aligned}\int u^2\cosh^{-1}\left(\frac{ct}{r}\right) du &= \frac{u^3}{3}\cosh^{-1}\left(\frac{ct}{r}\right) \\ &\quad +ct\left(\frac{c^2t^2}{6} - \frac{1}{2}v^2\right)\arcsin\left(\frac{u}{\sqrt{c^2t^2 - v^2}}\right) \\ &\quad -\frac{v^3}{3}\arctan\left(\frac{ctu}{v\sqrt{c^2t^2 - r^2}}\right) - \frac{ct}{6}u\sqrt{c^2t^2 - r^2}\end{aligned} \tag{B-3}$$

$$\int \sqrt{c^2t^2 - r^2} = \frac{u}{2}\sqrt{c^2t^2 - r^2} + \frac{c^2t^2 - v^2}{2}\arcsin\left(\frac{u}{\sqrt{c^2t^2 - v^2}}\right) \tag{B-4}$$

$$\int u\sqrt{c^2t^2 - r^2} = -\frac{1}{3}\left(c^2t^2 - r^2\right)^{3/2} \tag{B-5}$$

$$\begin{aligned}\int u^2\sqrt{c^2t^2 - r^2} &= \frac{1}{8}\left(c^2t^2 - v^2\right)^2 \arcsin\left(\frac{u}{\sqrt{c^2t^2 - v^2}}\right) \\ &\quad -\frac{u}{8}\left(c^2t^2 - r^2\right)^{3/2} + \frac{u^3}{8}\sqrt{c^2t^2 - r^2}\end{aligned} \tag{B-6}$$

$$\int \frac{1}{r^2}\sqrt{c^2t^2 - r^2} = \frac{ct}{v}\arctan\left(\frac{ctu}{v\sqrt{c^2t^2 - r^2}}\right) - \arcsin\left(\frac{u}{\sqrt{c^2t^2 - v^2}}\right) \tag{B-7}$$

$$\int \frac{u}{r^2}\sqrt{c^2t^2 - r^2} = \sqrt{c^2t^2 - r^2} - ct\cosh^{-1}\left(\frac{ct}{r}\right) \tag{B-8}$$

$$\int \frac{1}{r^4}\sqrt{c^2t^2 - r^2} = \frac{c^2t^2 - v^2}{2ctv^3}\arctan\left(\frac{ctu}{v\sqrt{c^2t^2 - r^2}}\right) + \frac{u}{2v^2r^2}\sqrt{c^2t^2 - r^2} \tag{B-9}$$

$$\int \frac{u}{r^4}\sqrt{c^2t^2 - r^2} = \frac{1}{2ct}\cosh^{-1}\left(\frac{ct}{r}\right) - \frac{1}{2r^2}\sqrt{c^2t^2 - r^2} \tag{B-10}$$

$$\begin{aligned}\int \frac{1}{r^6}\sqrt{c^2t^2 - r^2} &= \frac{u}{4c^2t^2v^2r^4}\left(c^2t^2 - r^2\right)^{3/2} \\ &\quad + \frac{u}{2c^2t^2v^2r^2}\sqrt{c^2t^2 - r^2} + \frac{3u\left(c^2t^2 - v^2\right)}{8c^2t^2r^2v^4}\sqrt{c^2t^2 - r^2} \\ &\quad + \left(\frac{3ct}{8v^5} - \frac{1}{4ctv^3} - \frac{1}{8c^3t^3v}\right)\arctan\left(\frac{ctu}{v\sqrt{c^2t^2 - r^2}}\right)\end{aligned} \tag{B-11}$$

$$\int \frac{u}{r^6}\sqrt{c^2t^2 - r^2} = \left(\frac{1}{8c^2t^2r^2} - \frac{1}{4r^4}\right)\sqrt{c^2t^2 - r^2} + \frac{1}{8c^3t^3}\cosh^{-1}\left(\frac{ct}{r}\right) \tag{B-12}$$

Certain simplifications of the terms in (5-34) and (5-35) are needed to obtain the above integrals. First, the components of the displacement tensor (5-34) and the associated integrals will be listed and simplified term by term. Subsequently, the components of the traction tensor (5-35) and the associated integrals will be listed. All of these algebraic manipulations are based on repeated use of the following identities:

$$r^2 = u^2 + v^2 \tag{B-13}$$

and

$$\left(c^2t^2 - r^2\right)^{3/2} = c^2t^2\sqrt{c^2t^2 - r^2} - r^2\sqrt{c^2t^2 - r^2} \tag{B-14}$$

Integrals needed for the displacement boundary influence calculations are of the form $\int \overline{u} U_{ij} d\overline{u}$, $\int \overline{u} U_{ij} d\overline{u}$, $\int \overline{u}^2 U_{ij} d\overline{u}$. Now, evaluating each distinct term in (5-34) results in

$$\int \frac{u^2}{r^4}\left(c^2t^2 - r^2\right)^{3/2} du = \int \left\{\left(c^2t^2 + v^2\right)\frac{1}{r^2} - c^2t^2v^2\frac{1}{r^2} - 1\right\}\sqrt{c^2t^2 - r^2}du \tag{B-15}$$

$$\int \frac{u^2}{r^4}\left(c^2t^2 - r^2\right)^{3/2} udu = \int \left\{c^2t^2\frac{u}{r^2} - c^2t^2v^2\frac{u}{r^4} - u + v^2\frac{u}{r^2}\right\}\sqrt{c^2t^2 - r^2}du \tag{B-16}$$

$$\begin{aligned}\int \frac{u^2}{r^4}\left(c^2t^2 - r^2\right)^{3/2} u^2du &= \int \left\{\left(c^2t^2 + v^2\right)\frac{u^2}{r^2} - u^2 - c^2t^2v^2\frac{1}{r^2}\right.\\ &\qquad \left. + c^2t^2v^4\frac{1}{r^4}\right\}\sqrt{c^2t^2 - r^2}du\end{aligned} \tag{B-17}$$

$$\int \frac{v^2}{r^4}\left(c^2t^2 - r^2\right)^{3/2} du = \int \left(c^2t^2v^2\frac{1}{r^4} - v^2\frac{1}{r^2}\right)\sqrt{c^2t^2 - r^2}du \tag{B-18}$$

$$\int \frac{v^2}{r^4}\left(c^2t^2 - r^2\right)^{3/2} udu = \int \left\{c^2t^2v^2\frac{u}{r^4} - c^2t^2v^2\frac{1}{r^2}\right\}\sqrt{c^2t^2 - r^2}du \tag{B-19}$$

$$\begin{aligned}\int \frac{v^2}{r^4}\left(c^2t^2 - r^2\right)^{3/2} u^2du &= \int \left\{\left(c^2t^2v^2 + v^4\right)\frac{1}{r^2}\right.\\ &\qquad \left. - c^2t^2v^4\frac{1}{r^4} - v^2\right\}\sqrt{c^2t^2 - r^2}du\end{aligned} \tag{B-20}$$

$$\int \frac{uv}{r^4}\left(c^2t^2 - r^2\right)^{3/2} du = \int \left(c^2t^2v\frac{u}{r^4} - v\frac{u}{r^2}\right)\sqrt{c^2t^2 - r^2}du \tag{B-21}$$

$$\int \frac{uv}{r^4}\left(c^2t^2 - r^2\right)^{3/2} udu = \int \left\{\left(c^2t^2v + v^3\right)\frac{1}{r^2} - c^2t^2v^3\frac{1}{r^4} - v\right\}\sqrt{c^2t^2 - r^2}du \tag{B-22}$$

$$\begin{aligned}\int \frac{uv}{r^4}\left(c^2t^2 - r^2\right)^{3/2} u^2du &= \int \left\{\left(c^2t^2v + v^3\right)\frac{u}{r^2}\right.\\ &\qquad \left. - c^2t^2v^3\frac{u}{r^4} - vu\right\}\sqrt{c^2t^2 - r^2}du\end{aligned} \tag{B-23}$$

Similarly, the integrals needed for the traction boundary influence calculations are of the form $\int \overline{u} U_{ij} d\overline{u}$, $\int \overline{u} U_{ij} d\overline{u}$, $\int \overline{u}^2 U_{ij} d\overline{u}$. The required integrals not already listed above are:

$$\int \frac{u^2}{r^4}\sqrt{c^2t^2 - r^2}du = \int \left\{ \frac{1}{r^2} - \frac{v^2}{r^4} \right\} \sqrt{c^2t^2 - r^2}du \tag{B-24}$$

$$\int \frac{u^3}{r^4}\sqrt{c^2t^2 - r^2}du = \int \left\{ \frac{u}{r^2} - v^2\frac{u}{r^4} \right\} \sqrt{c^2t^2 - r^2}du \tag{B-25}$$

$$\int \frac{u^2}{r^6}\sqrt{c^2t^2 - r^2}du = \int \left\{ \frac{1}{r^4} - v^2\frac{1}{r^6} \right\} \sqrt{c^2t^2 - r^2}du \tag{B-26}$$

$$\int \frac{u^3}{r^6}\sqrt{c^2t^2 - r^2}du = \int \left\{ \frac{u}{r^4} - v^2\frac{u}{r^6} \right\} \sqrt{c^2t^2 - r^2}du \tag{B-27}$$

This completes the listing of all integrals that are necessary to obtain the dynamic displacement and traction boundary influence coefficients.

The self-effects for the displacement coefficients for the case $\underline{\xi} \to \underline{x}$ are:

$$\int U_{xx}\phi_L d\bar{x} = \frac{1}{2\pi\rho c_2^2}\left\{\cos 2\beta\,(GG1) + FFA1\right\} \tag{B-28}$$

$$\int U_{xy}\phi_L d\bar{x} = \frac{1}{2\pi\rho c_2^2}\left\{\sin 2\beta\,(GG1)\right\} \tag{B-29}$$

$$\int U_{yx}\phi_L d\bar{x} = \frac{1}{2\pi\rho c_2^2}\left\{\sin 2\beta\,(GG1)\right\} \tag{B-30}$$

$$\int U_{yy}\phi_L d\bar{x} = \frac{1}{2\pi\rho c_2^2}\left\{-\cos 2\beta\,(GG1) + FFA1\right\} \tag{B-31}$$

$$\int U_{xx}\phi_C d\bar{x} = \frac{1}{2\pi\rho c_2^2}\left\{\cos 2\beta\,(GG2) + FFA3\right\} \tag{B-32}$$

$$\int U_{xy}\phi_C d\bar{x} = \frac{1}{2\pi\rho c_2^2}\left\{\sin 2\beta\,(GG2)\right\} \tag{B-33}$$

$$\int U_{yx}\phi_C d\bar{x} = \frac{1}{2\pi\rho c_2^2}\left\{\sin 2\beta\,(GG2)\right\} \tag{B-34}$$

$$\int U_{yy}\phi_C d\bar{x} = \frac{1}{2\pi\rho c_2^2}\left\{-\cos 2\beta\,(GG1) + FFA2\right\} \tag{B-35}$$

$$\int U_{xx}\phi_R d\bar{x} = \frac{1}{2\pi\rho c_2^2}\left\{\cos 2\beta\,(GG1) + FFA1\right\} \tag{B-36}$$

$$\int U_{xy}\phi_R d\bar{x} = \frac{1}{2\pi\rho c_2^2}\left\{\sin 2\beta\,(GG1)\right\} \tag{B-37}$$

$$\int U_{yx}\phi_R d\bar{x} = \frac{1}{2\pi\rho c_2^2}\left\{\sin 2\beta\,(GG1)\right\} \tag{B-38}$$

$$\int U_{yy}\phi_R d\bar{x} = \frac{1}{2\pi\rho c_2^2}\left\{-\cos 2\beta\,(GG1) + FFA1\right\} \tag{B-39}$$

in which

$$\begin{aligned} GG1 \;=\;& \frac{c_2^2 t^3}{4a\Delta t}\ln\left(\sqrt{Q_1^2-1}\right) + \frac{c_2^2 t^2}{4ac_1\Delta t}\left(\frac{c_1^2 t^2}{8a^2}-1\right)\left(\arctan\left(\frac{\sqrt{Q_1^2-1}}{-a}\right)-\frac{\pi}{2}\right) \\ & -\frac{5c_2^2 a^2}{2c_1^3\Delta t}\left(Q_1^2-1\right)^{3/2} - \frac{5c_2^2 a^2}{2c_1^3\Delta t}\sqrt{Q_1^2-1} + \frac{c_2^2 t^3}{3a\Delta t} - \frac{c_2^2 t^3}{4a\Delta t}\ln\left(\sqrt{Q_2^2-1}\right) \\ & -\frac{c_2 t^2}{4a\Delta t}\left(\frac{c_2^2 t^2}{8a^2}-1\right)\left(\arctan\left(\frac{\sqrt{Q_2^2-1}}{-a}\right)-\frac{\pi}{2}\right) + \frac{5a^2}{2c_2\Delta t}\left(Q_2^2-1\right)^{3/2} \\ & +\frac{5a^2}{2c_2\Delta t}\sqrt{Q_2^2-1} - \frac{c_2^2 t^3}{3a\Delta t} \end{aligned} \tag{B-40}$$

$$\begin{aligned} FFA1 \;=\;& \frac{ta}{\Delta t}\frac{c_2^2 t}{6c_1^2}\ln\left(\sqrt{Q_1^2-1}\right) + \frac{c_2^2 t^2}{4c_1\Delta t}\left(\frac{c_1^2 t^2}{24a^2}+1\right)\left(\arctan\left(\frac{\sqrt{Q_1^2-1}}{-a}\right)-\frac{\pi}{2}\right) \\ & +\frac{5c_2^2 a^2}{6c_1^3\Delta t}\left(Q_1^2-1\right)^{3/2} + \frac{5c_2^2 a^2}{6c_1^3\Delta t}\sqrt{Q_1^2-1} - \frac{c_2^2 t^3}{8a\Delta t} \\ & +\frac{ta}{6\Delta t}\ln\left(\sqrt{Q_2^2-1}\right) + \frac{c_2 t^2}{4\Delta t}\left(\frac{c_2^2 t^2}{24a^2}+1\right)\left(\arctan\left(\frac{\sqrt{Q_2^2-1}}{-a}\right)-\frac{\pi}{2}\right) \\ & +\frac{5a^2}{6c_2\Delta t}\left(Q_2^2-1\right)^{3/2} + \frac{5a^2}{6c_2\Delta t}\sqrt{Q_2^2-1} - \frac{c_2^2 t^3}{8a\Delta t} \end{aligned} \tag{B-41}$$

$$\begin{aligned} GG2 \;=\;& -\frac{c_2^2 t^2}{4c_1\Delta t}\left(\frac{c_1^2 t^2}{4a^2}+1\right)\left\{\arctan\left(\frac{\sqrt{Q_1^2-1}}{-a}\right) - \arctan\left(\frac{\sqrt{Q_1^2-1}}{a}\right)\right\} \\ & +\frac{c_2 t^2}{4\Delta t}\left(\frac{c_2^2 t^2}{4a^2}+1\right)\left\{\arctan\left(\frac{\sqrt{Q_2^2-1}}{-a}\right) - \arctan\left(\frac{\sqrt{Q_2^2-1}}{a}\right)\right\} \\ & -\frac{13a^2}{24c_1\Delta t}\frac{c_2^2}{c_1^2}\left(Q_1^2-1\right)^{3/2} - \frac{5a^2}{8c_1\Delta t}\frac{c_2^2}{c_1^2}\sqrt{Q_1^2-1} \end{aligned}$$

$$+\frac{13a^2}{24c_2\Delta t}\left(Q_2^2-1\right)^{3/2}+\frac{5a^2}{8c_2\Delta t}\sqrt{Q_2^2-1} \tag{B-42}$$

$$\begin{aligned} FFA2 \;=\;& \frac{2ta}{3\Delta t}\frac{c_2^2}{c_1^2}\ln\left(Q_1+\sqrt{Q_1^2-1}\right)+\frac{a^2}{24c_1\Delta t}\frac{c_2^2}{c_1^2}\left(Q_1^2-1\right)^{3/2} \\ & -\frac{c_2^2t^2}{4c_1\Delta t}\left(\frac{c_1^2t^2}{12a^2}-1\right)\left\{\arctan\left(\frac{\sqrt{Q_1^2-1}}{-a}\right)-\arctan\left(\frac{\sqrt{Q_1^2-1}}{a}\right)\right\} \\ & +\frac{2ta}{3\Delta t}\ln\left(Q_2+\sqrt{Q_2^2-1}\right)+\frac{a^2}{24c_2\Delta t}\left(Q_2^2-1\right)^{3/2} \\ & -\frac{c_2t^2}{4\Delta t}\left(\frac{c_2^2t^2}{12a^2}-1\right)\left\{\arctan\left(\frac{\sqrt{Q_2^2-1}}{-a}\right)-\arctan\left(\frac{\sqrt{Q_2^2-1}}{a}\right)\right\} \\ & -\frac{5a^2}{24c_1\Delta t}\frac{c_2^2}{c_1^2}\sqrt{Q_1^2-1}-\frac{5a^2}{24c_2\Delta t}\sqrt{Q_2^2-1} \end{aligned} \tag{B-43}$$

in which $Q1 = 1.0$ if $c_1t/r < 1.0$, $Q1 = c_1t/r$ if $c_1t/r > 1.0$, $Q2 = 1.0$ if $c_2t/r < 1.0$, $Q2 = c_2t/r$ if $c_2t/r > 1.0$, a is the half-length of each element and Δt is the size of each time step.

Similarly, self-effects for the traction coefficients for the case $\underline{\xi} \rightarrow \underline{x}$ are:

$$\int T_{xx}\phi_L d\bar{x} = \frac{1}{2\pi}\left\{\cos 2\beta\,(FF1) - \sin 2\beta\,(GL1) - HHA1\right\} \tag{B-44}$$

$$\int T_{xy}\phi_L d\bar{x} = \frac{1}{2\pi}\left\{\cos 2\beta\,(GL1) + \sin 2\beta\,(FF1) - LLA1\right\} \tag{B-45}$$

$$\int T_{yx}\phi_L d\bar{x} = \frac{1}{2\pi}\left\{\cos 2\beta\,(GL1) + \sin 2\beta\,(FF1) + LLA1\right\} \tag{B-46}$$

$$\int T_{yy}\phi_L d\bar{x} = \frac{1}{2\pi}\left\{-\cos 2\beta\,(FF1) + \sin 2\beta\,(GL1) - HHA1\right\} \tag{B-47}$$

$$\int T_{xx}\phi_C d\bar{x} = \frac{t}{2\Delta t} \tag{B-48}$$

$$\int T_{xy}\phi_C d\bar{x} = 0 \tag{B-49}$$

$$\int T_{yx}\phi_C d\bar{x} = 0 \tag{B-50}$$

$$\int T_{yy}\phi_C d\bar{x} = \frac{t}{2\Delta t} \tag{B-51}$$

$$\int T_{xx}\phi_R d\bar{x} = \frac{1}{2\pi}\left\{\cos 2\beta\,(FF1) + \sin 2\beta\,(GL1) - HHA1\right\} \tag{B-52}$$

$$\int T_{xy}\phi_R d\bar{x} = \frac{1}{2\pi}\left\{-\cos 2\beta\,(GL1) + \sin 2\beta\,(FF1) + LLA1\right\} \tag{B-53}$$

$$\int T_{yx}\phi_R d\bar{x} = \frac{1}{2\pi}\left\{-\cos 2\beta\,(GL1) + \sin 2\beta\,(FF1) - LLA1\right\} \tag{B-54}$$

$$\int T_{yy}\phi_R d\bar{x} = \frac{1}{2\pi}\left\{-\cos 2\beta\,(FF1) - \sin 2\beta\,(GL1) - HHA1\right\} \tag{B-55}$$

in which

$$FF1 = \frac{t}{2\Delta t}\left(\frac{c_2^2}{c_1^2} - 1\right)\sin(\pi - \gamma) \tag{B-56}$$

$$HHA1 = -\frac{t}{2\Delta t}(\pi + \gamma) \tag{B-57}$$

$$\begin{aligned} GL1 \;=\;& \frac{t}{2\Delta t}\left(\frac{2c_2^2t^2}{3a^2} - 1\right)\ln\left(\sqrt{Q_1^2 - 1}\right) + \frac{2a}{9\Delta t}\left(3 + 25\frac{c_2^2}{c_1^2}\right)\left(Q_1^2 - 1\right)^{3/2} \\ & - \frac{56a}{9\Delta t}\sqrt{Q_1^2 - 1} + \frac{a}{6\Delta t}\left(3 + 34\frac{c_2^2}{c_1^2}\right)\sqrt{Q_1^2 - 1} - \frac{37a}{6\Delta t}\sqrt{Q_2^2 - 1} \\ & + \frac{t}{\Delta t}\frac{c_1^2t^2}{a^2}\left(\frac{c_2^2}{c_1^2} - 1\right) + \frac{3c_2^2t^2}{8a\Delta t}\left(\frac{c_1^2}{c_2^2} + 2\right)\left(\frac{\pi}{2} - \arctan\left(\frac{\sqrt{Q_1^2 - 1}}{a}\right)\right) \\ & - \frac{9c_2^2t^2}{8a\Delta t}\left(\frac{\pi}{2} - \arctan\left(\frac{\sqrt{Q_2^2 - 1}}{a}\right)\right) + \frac{t}{2\Delta t}\left(\frac{c_2^2}{c_1^2} - 1\right)\cos(\pi - \gamma) \end{aligned} \tag{B-58}$$

$$\begin{aligned} LLA1 \;=\;& \left(2\frac{c_2^2}{c_1^2} - 1\right)\frac{t}{\Delta t}\Bigg\{\frac{1}{2}\ln\left(\sqrt{Q_1^2 - 1}\right) + \frac{3c_1t}{8a}\left(\arctan\left(\frac{\sqrt{Q_1^2 - 1}}{a}\right) - \frac{\pi}{2}\right) \\ & + \frac{1}{2} - \frac{1}{12}\frac{c_1^2t^2}{a^2} + \frac{2a}{3c_1t}\left(Q_1^2 - 1\right)^{3/2} + \frac{a}{2c_1t}\sqrt{Q_1^2 - 1}\Bigg\} \\ & + \frac{t}{\Delta t}\Bigg\{\frac{1}{2}\ln\left(\sqrt{Q_2^2 - 1}\right) + \frac{3c_2t}{8a}\left(\arctan\left(\frac{\sqrt{Q_2^2 - 1}}{a}\right) - \frac{\pi}{2}\right) \end{aligned}$$

$$+\frac{1}{2}-\frac{1}{12}\frac{c_2^2t^2}{a^2}+\frac{2a}{3c_2t}\left(Q_2^2-1\right)^{3/2}+\frac{a}{2c_2t}\sqrt{Q_2^2-1}\Bigg\} \tag{B-59}$$

in which $Q1$ and $Q2$ are as defined previously, and $\gamma = \beta^J - \beta^{J-1}$ is the difference of the inclinations of elements J and $J-1$.

Appendix C

Derivatives for the Calculation of Interior Dynamic Stresses

The derivatives necessary to obtain the interior dynamic stresses from (5-79) by substituting (5-78) into the kinematic equation (3-2) and Hooke's law (3-3) are listed below. These results are due to Tian (1990). Because the integrals in (5-78) are all evaluated in the local coordinate system $(\bar{x}, \bar{y})$, whereas the required derivatives are with respect to the global coordinate system, it is necessary to use (5-81), which is the chain rule for partial differentiation to establish a relationship between the global and local coordinates. The following differentiations are with respect to the local variables and have to be transformed into differentiations with respect to global variables with the use of (5-81).

All the integrals necessary to evaluate (5-78) are listed in Appendix B, and they are all in terms of the local variables $u = \bar{x} - \bar{\xi}$ and $v = \bar{y} - \bar{\eta}$ (see also Figure 5-1). To obtain (5-79) it is necessary to evaluate the derivatives of these integrals with respect to $\bar{\xi}$ and $\bar{\eta}$, rather than u and v, which leads to the relationships

$$\begin{aligned}\frac{\partial}{\partial \bar{\xi}} &= -\frac{\partial}{\partial u}\\ \frac{\partial}{\partial \bar{\eta}} &= -\frac{\partial}{\partial v}\end{aligned} \tag{C-1}$$

In the following, the necessary derivatives of the individual terms in (B-1) to (B-12) are listed. First, the derivatives with respect to $\bar{\xi}$ are listed, followed by the derivatives with respect to $\bar{\eta}$.

The derivatives with respect to $\bar{\xi}$ that are necessary to evaluate (5-79) are:

$$\frac{\partial}{\partial \bar{\xi}} \left(r^2\right) = -2u \tag{C-2}$$

$$\frac{\partial}{\partial \bar{\xi}} \left(\frac{1}{r^2}\right) = \frac{2v}{r^4} \tag{C-3}$$

$$\frac{\partial}{\partial \bar{\xi}} \left(\frac{1}{r^4}\right) = 4\frac{u}{r^6} \tag{C-4}$$

$$\frac{\partial}{\partial \bar{\xi}} \left(\sqrt{c^2t^2 - r^2}\right) = \frac{u}{\sqrt{c^2t^2 - r^2}} \tag{C-6}$$

$$\frac{\partial}{\partial \bar{\xi}} \left(c^2t^2 - r^2\right)^{3/2} = 3u\sqrt{c^2t^2 - r^2} \tag{C-7}$$

$$\frac{\partial}{\partial \bar{\xi}} \cosh^{-1}\left(\frac{ct}{r}\right) = \frac{uct}{r^2\sqrt{c^2t^2 - r^2}} \tag{C-8}$$

$$\frac{\partial}{\partial \bar{\xi}} \arctan\left(\frac{ctu}{v\sqrt{c^2t^2 - r^2}}\right) = -\frac{vct}{r^2\sqrt{c^2t^2 - r^2}} \tag{C-9}$$

$$\frac{\partial}{\partial \bar{\xi}} \arcsin\left(\frac{u}{\sqrt{c^2t^2 - v^2}}\right) = -\frac{1}{\sqrt{c^2t^2 - r^2}} \tag{C-10}$$

Similarly, the derivatives with respect to $\bar{\xi}$ that are necessary to evaluate (5-79) are:

$$\frac{\partial}{\partial \bar{\eta}} \left(r^2\right) = -2v \tag{C-11}$$

$$\frac{\partial}{\partial \bar{\eta}} \left(\frac{1}{r^2}\right) = \frac{2v}{r^4} \tag{C-12}$$

$$\frac{\partial}{\partial \bar{\eta}} \left(\frac{1}{r^4}\right) = 4\frac{v}{r^6} \tag{C-13}$$

$$\frac{\partial}{\partial \bar{\eta}} \left(\sqrt{c^2t^2 - r^2}\right) = \frac{v}{\sqrt{c^2t^2 - r^2}} \tag{C-14}$$

$$\frac{\partial}{\partial \bar{\eta}} \left(c^2t^2 - r^2\right)^{3/2} = 3v\sqrt{c^2t^2 - r^2} \tag{C-15}$$

$$\frac{\partial}{\partial \bar{\eta}} \cosh^{-1}\left(\frac{ct}{r}\right) = \frac{vct}{r^2\sqrt{c^2t^2 - r^2}} \tag{C-16}$$

$$\begin{aligned} \frac{\partial}{\partial \bar{\eta}} \arctan\left(\frac{ctu}{v\sqrt{c^2t^2 - r^2}}\right) &= \frac{uct}{r^2\sqrt{c^2t^2 - r^2}} \\ &\quad - \frac{uct}{\left(c^2t^2 - v^2\right)\sqrt{c^2t^2 - r^2}} \end{aligned} \tag{C-17}$$

$$\frac{\partial}{\partial \bar{\eta}} \arcsin\left(\frac{u}{\sqrt{c^2t^2 - v^2}}\right) = -\frac{uv}{\left(c^2t^2 - v^2\right)\sqrt{c^2t^2 - r^2}} \tag{C-18}$$

Appendix D

Additional Results for Dynamic Problems

This appendix contains supplemental graphical results for the following three cases presented in Chapter 6: Lamb's problem (Section 6.2.3), wave propagation through layered material (Section 6.2.6) and underground explosion in a two-layered rock (Section 6.2.7). The displacement and velocity time histories are listed for all three problems, except Lamb's problem, for which only the displacements are given. All results are calculated in "field-point windows" which are defined by four corner nodes. These nodes are for (a) Lamb's Problem: $(60m, -2m)$, $(150m, -2m)$, $(150m, -32m)$ and $(60m, -32m)$, (b) wave propagation through layered material: $(0m, -2m)$, $(120m, -2m)$, $(120m, -42m)$ and $(0m, -42m)$, and finally (c) the underground explosion problem: $(0, -2)$, $(120, -2)$, $(120, -42)$ and $(0, -42)$.

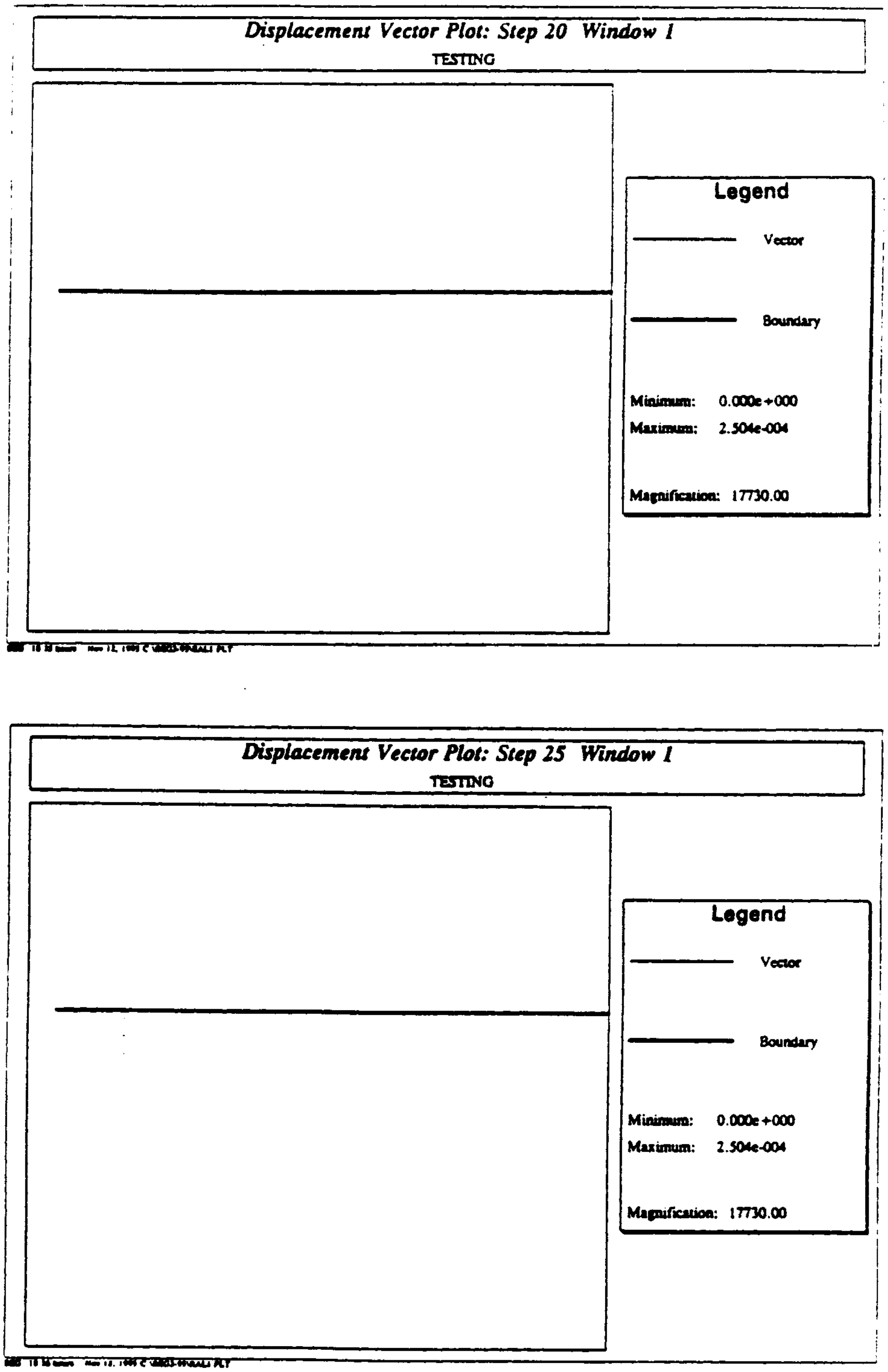

Figure D-1: Displacement vectors at times $20\Delta t$ and $25\Delta t$ for Lamb's problem.

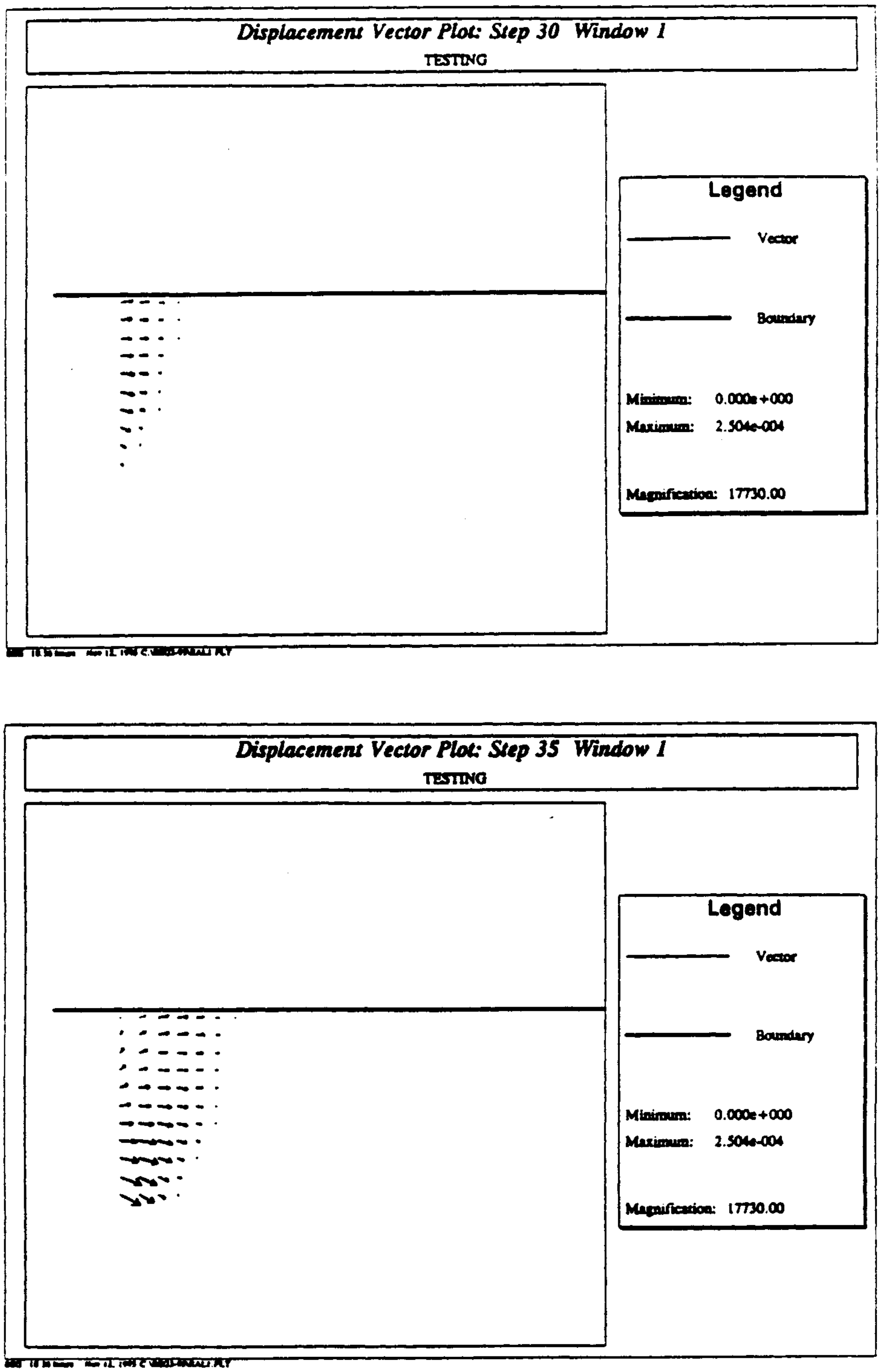

Figure D-2: Displacement vectors at times $30\Delta t$ and $35\Delta t$ for Lamb's problem.

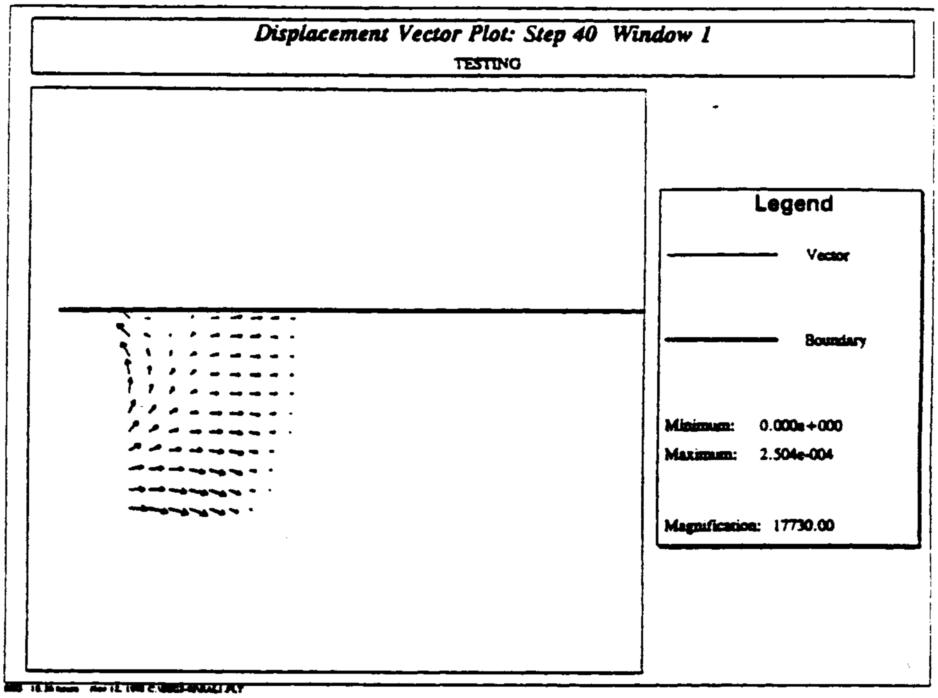

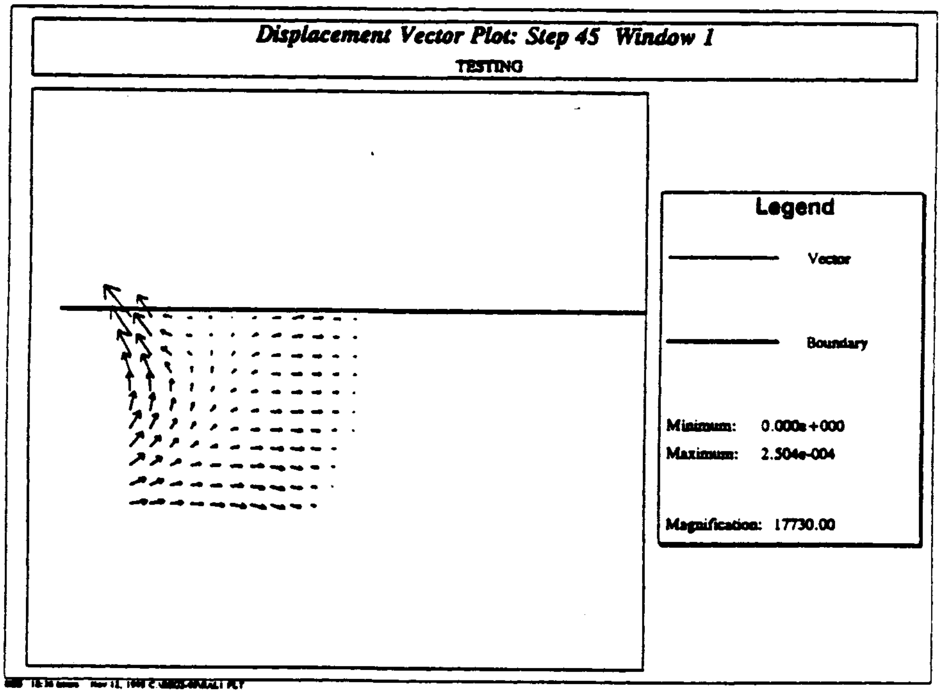

Figure D-3: Displacement vectors at times $40\Delta t$ and $45\Delta t$ for Lamb's problem.

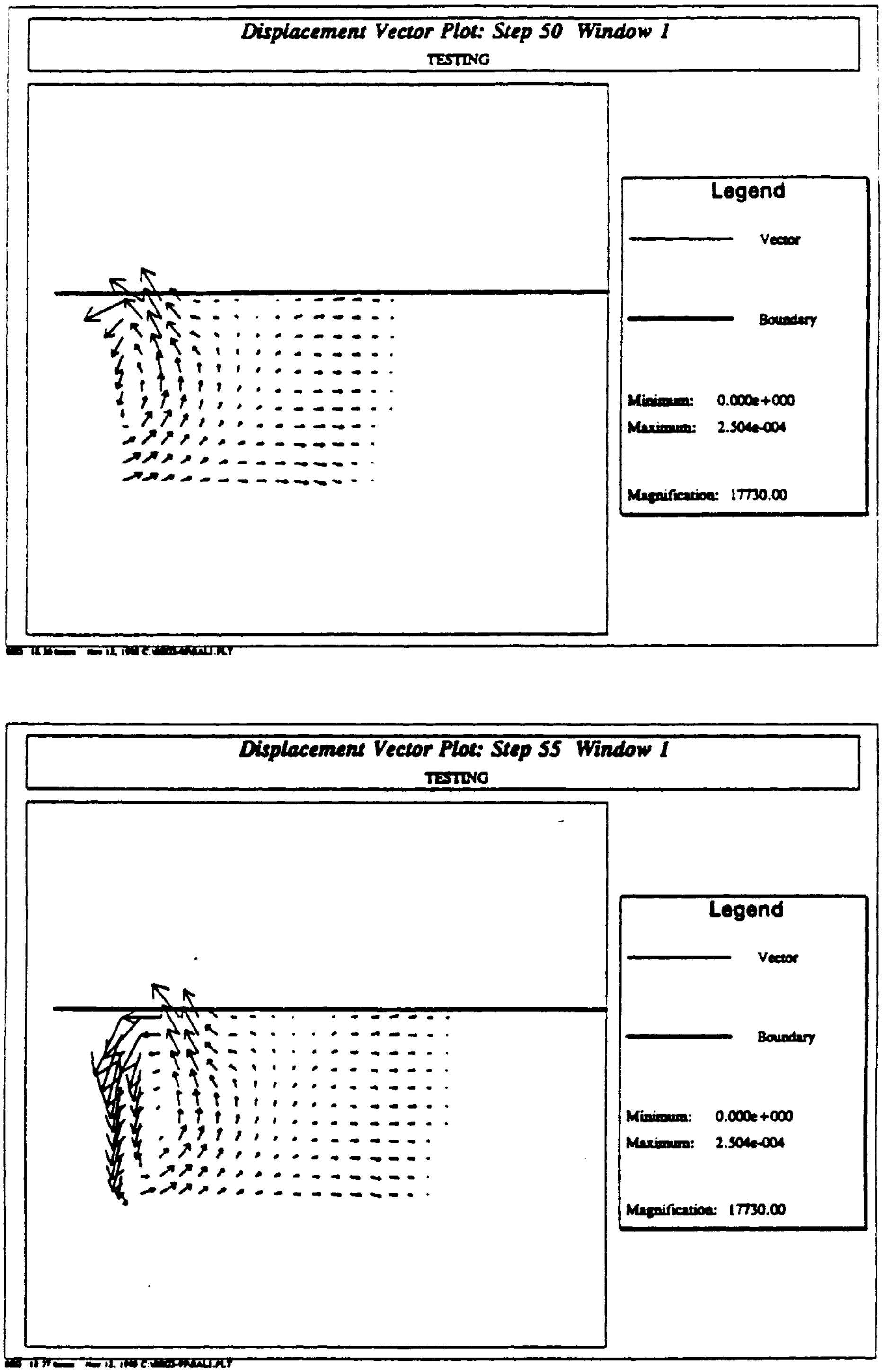

Figure D-4: Displacement vectors at times $50\Delta t$ and $55\Delta t$ for Lamb's problem.

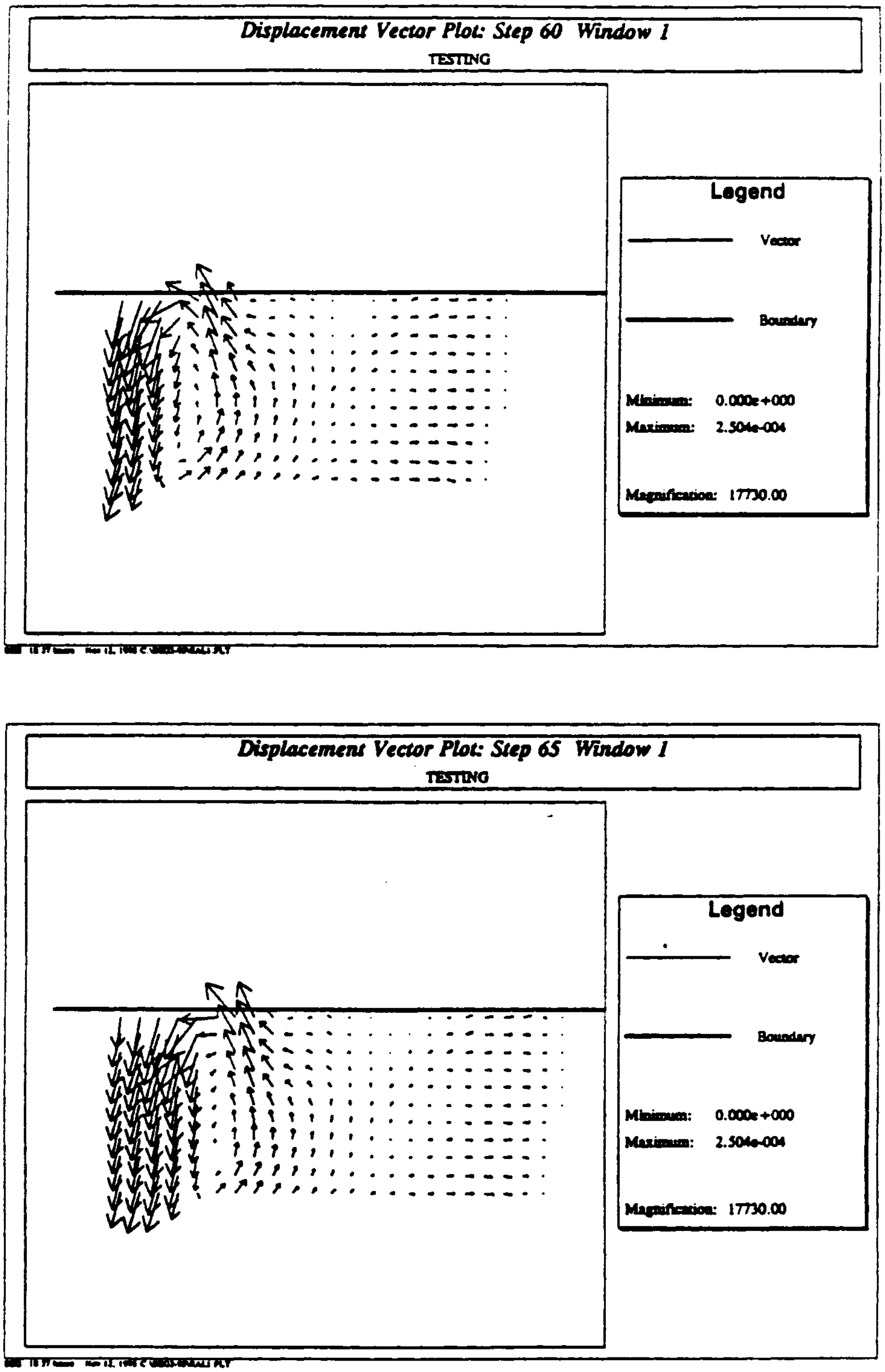

Figure D-5: Displacement vectors at times $60\Delta t$ and $65\Delta t$ for Lamb's problem.

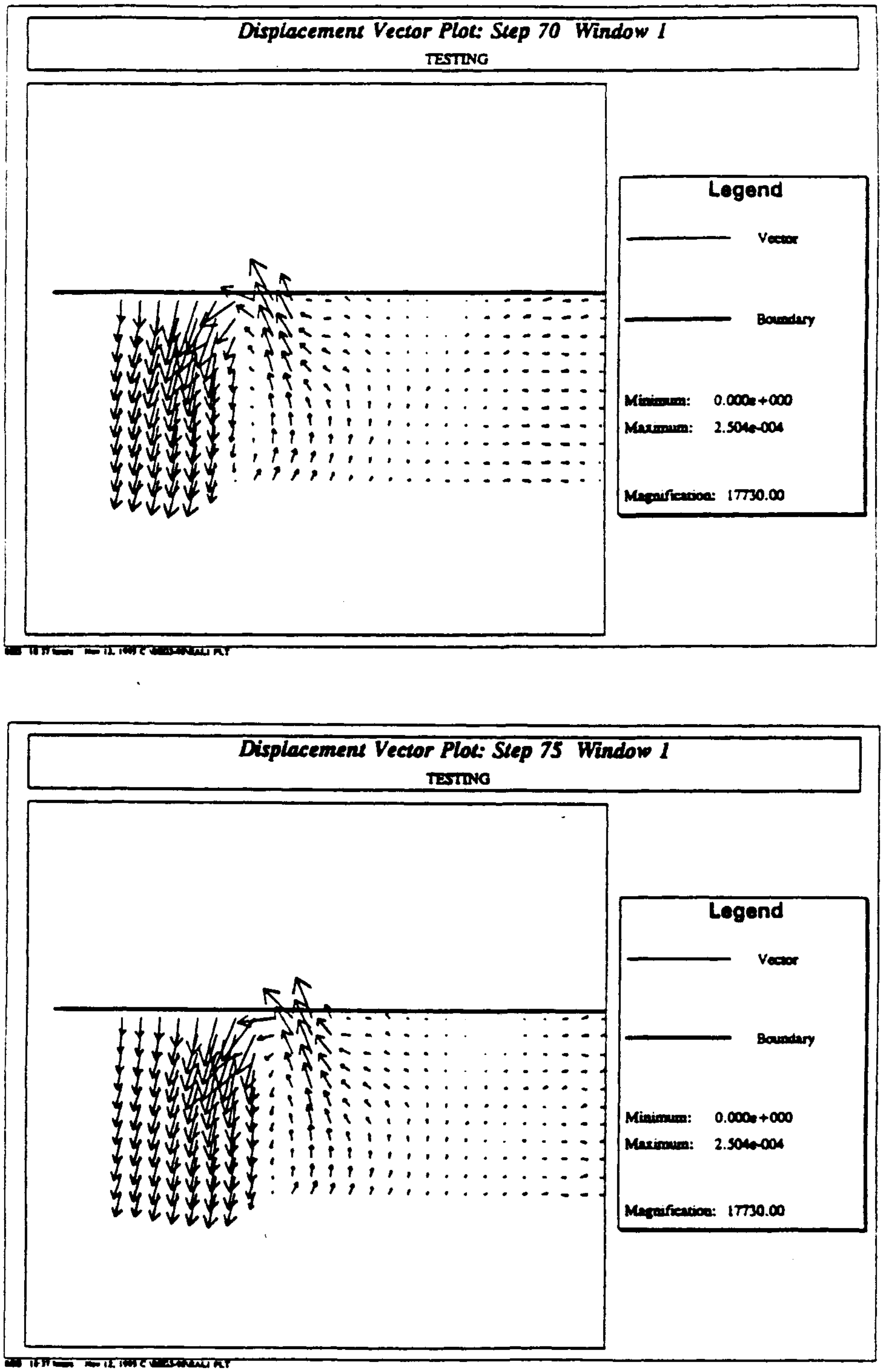

Figure D-6: Displacement vectors at times $70\Delta t$ and $75\Delta t$ for Lamb's problem.

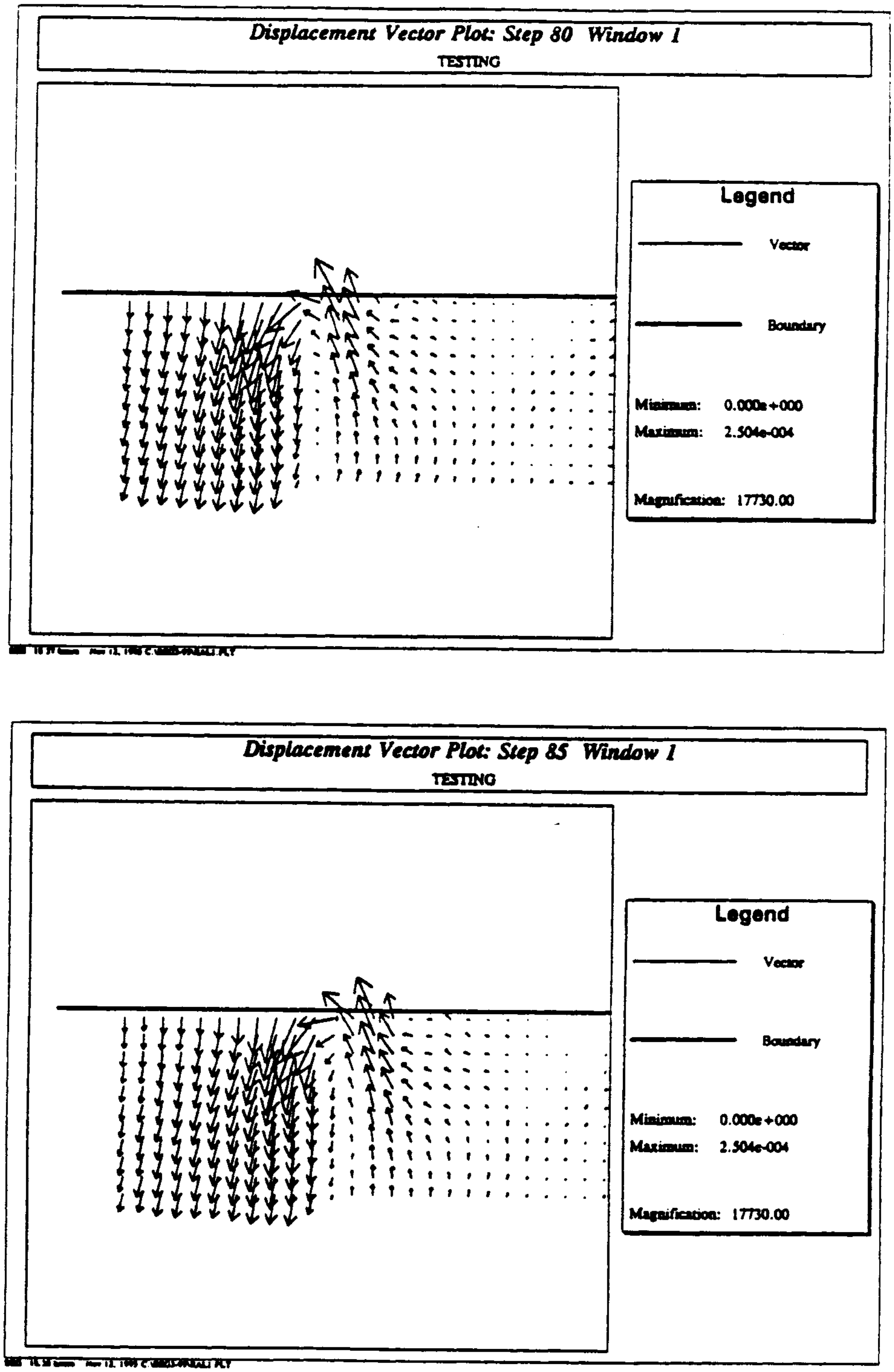

Figure D-7: Displacement vectors at times $80\Delta t$ and $85\Delta t$ for Lamb's problem.

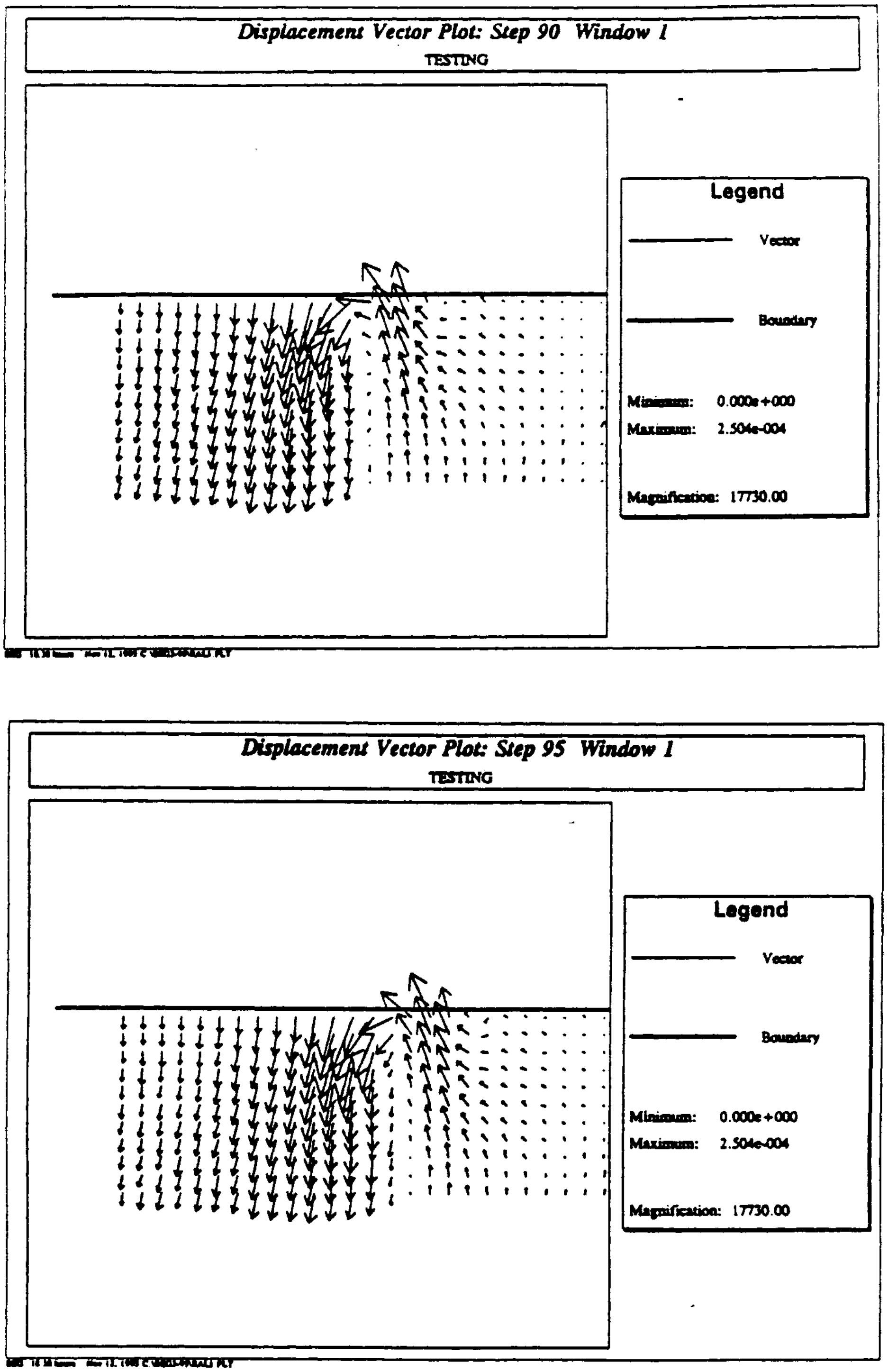

Figure D-8: Displacement vectors at times $90\Delta t$ and $95\Delta t$ for Lamb's problem.

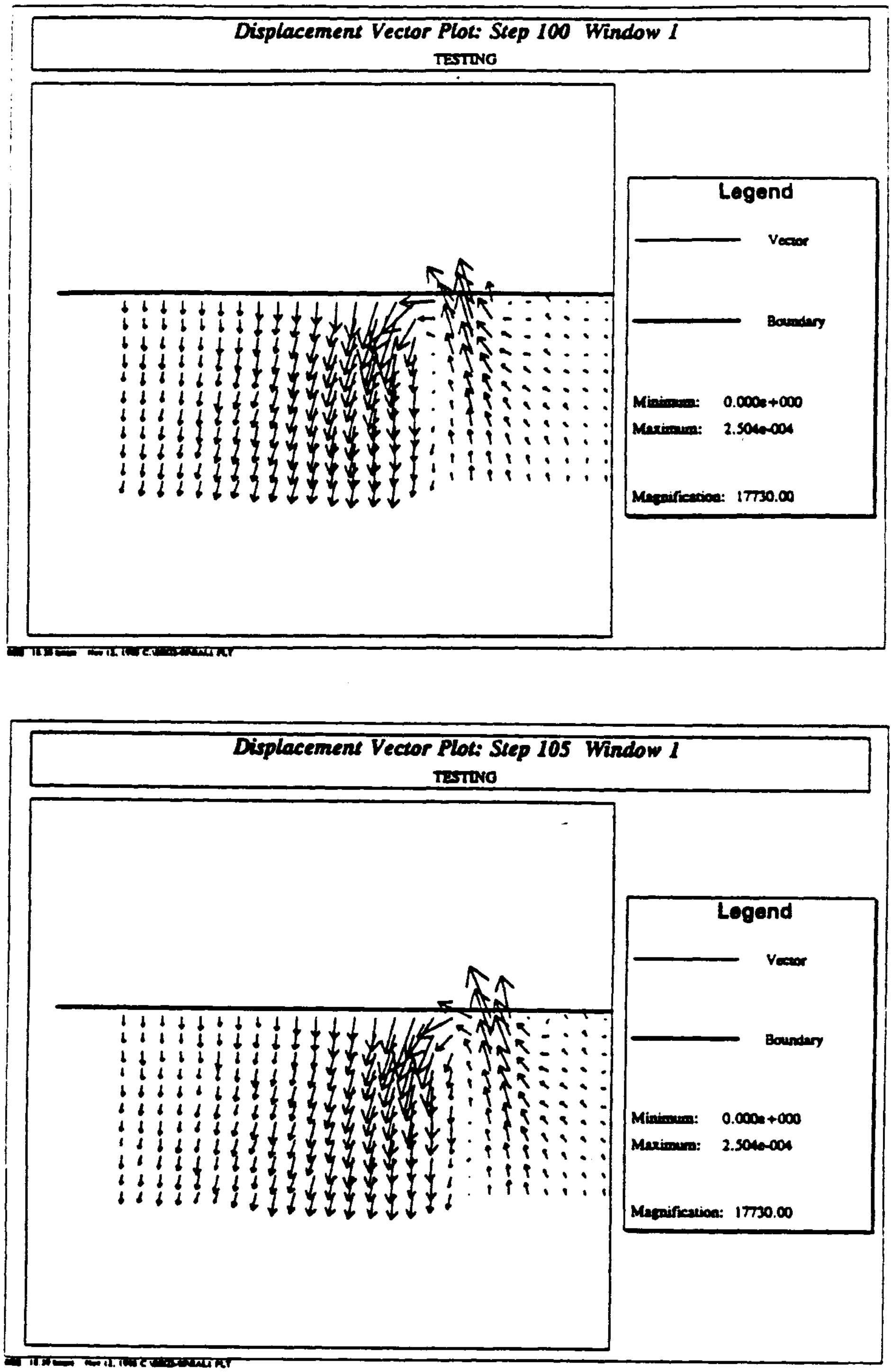

Figure D-9: Displacement vectors at times $100\Delta t$ and $105\Delta t$ for Lamb's problem.

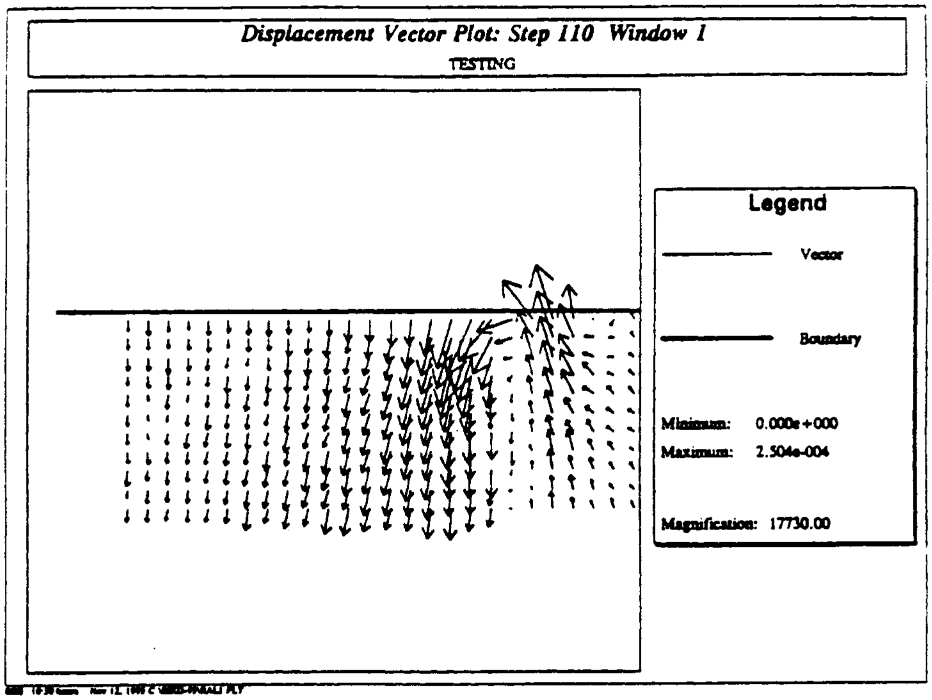

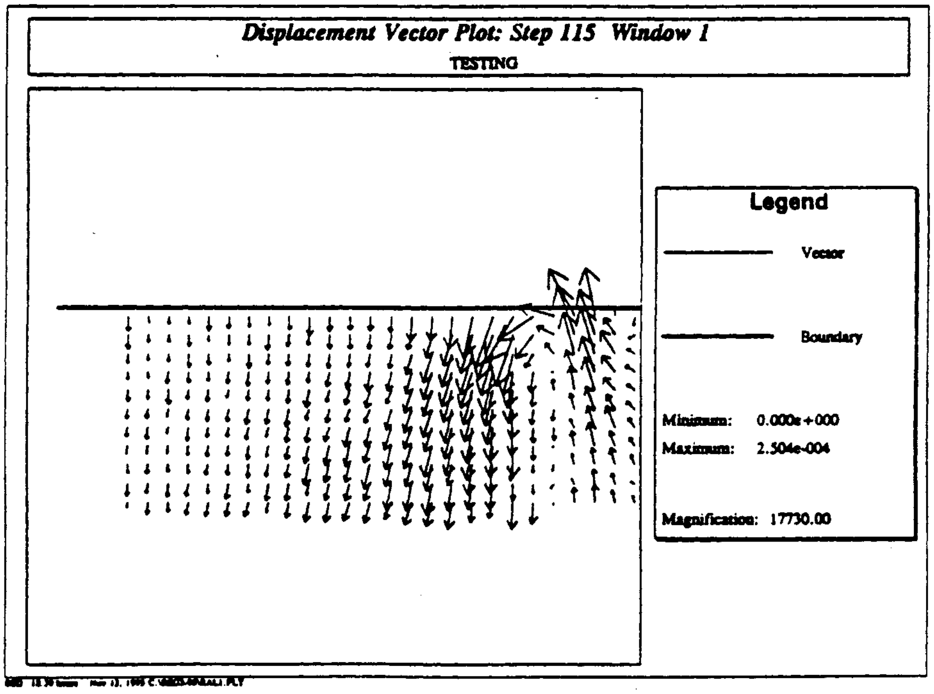

Figure D-10: Displacement vectors at times $110\Delta t$ and $115\Delta t$ for Lamb's problem.

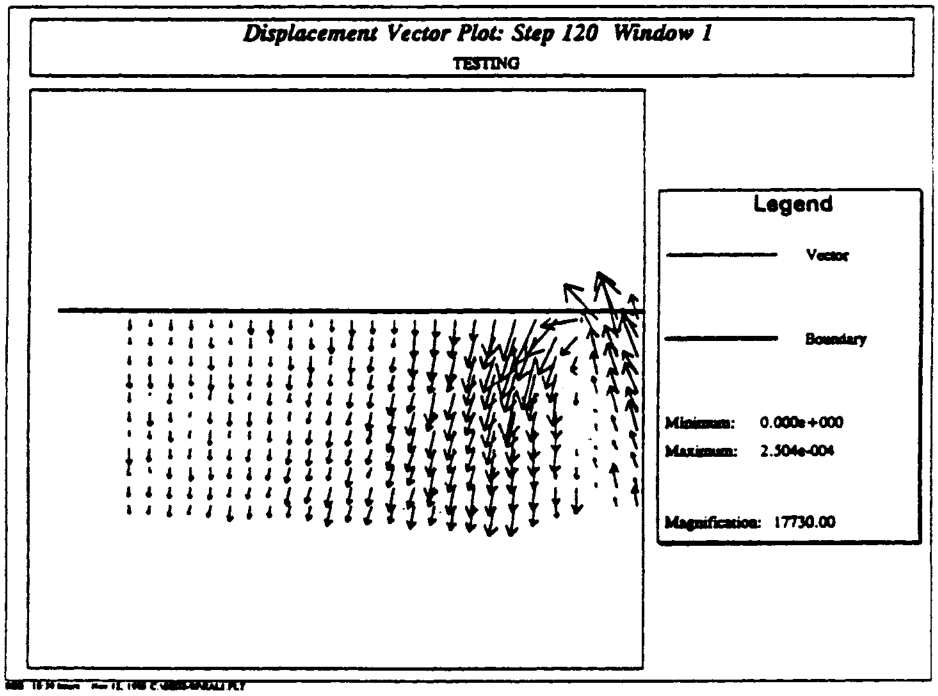

Figure D-11: Displacement vectors at time $120\Delta t$ for Lamb's problem.

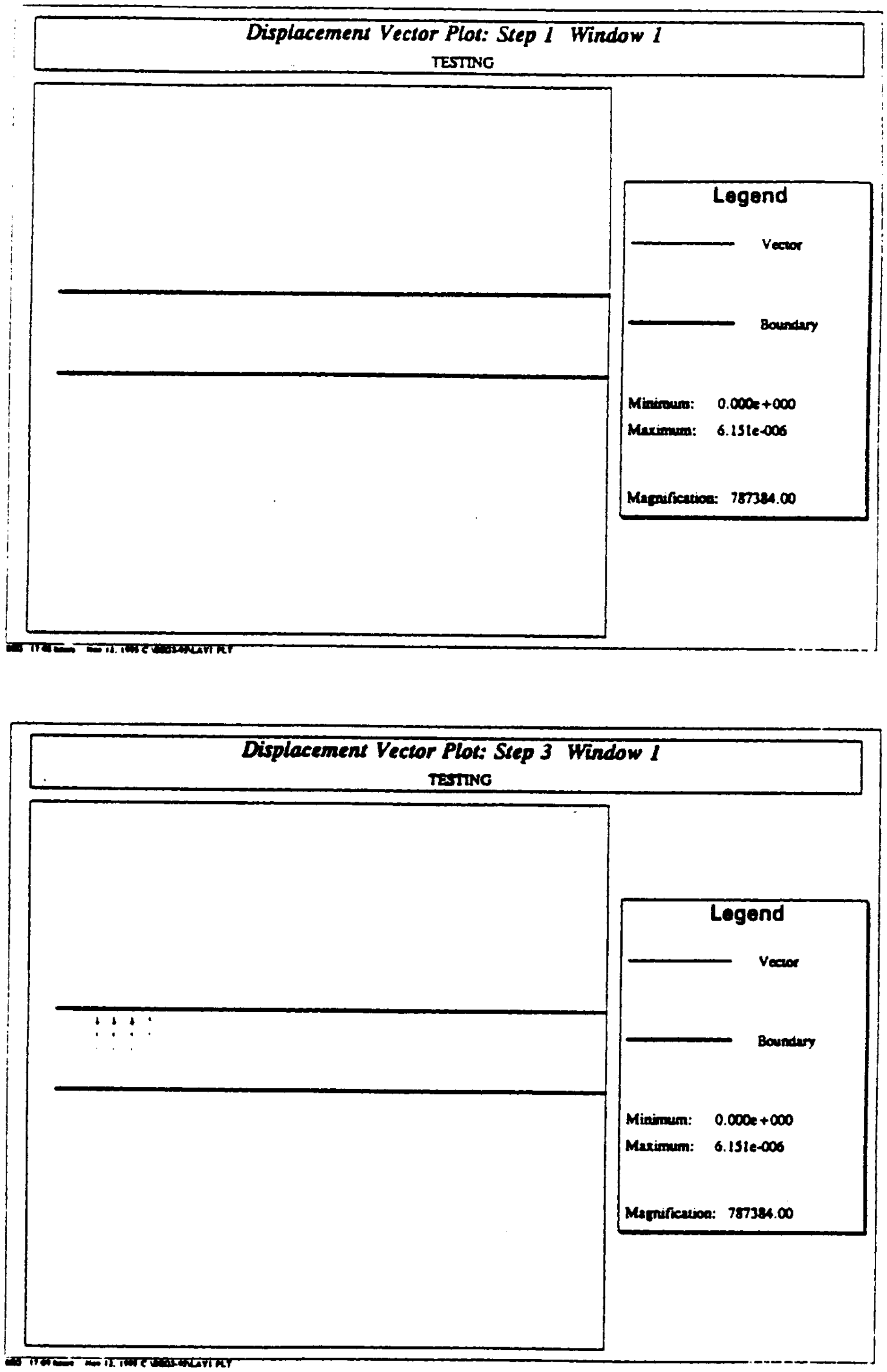

Figure D-12: Displacement vectors at times $1\Delta t$ and $3\Delta t$ for the wave propagation through layered material problem.

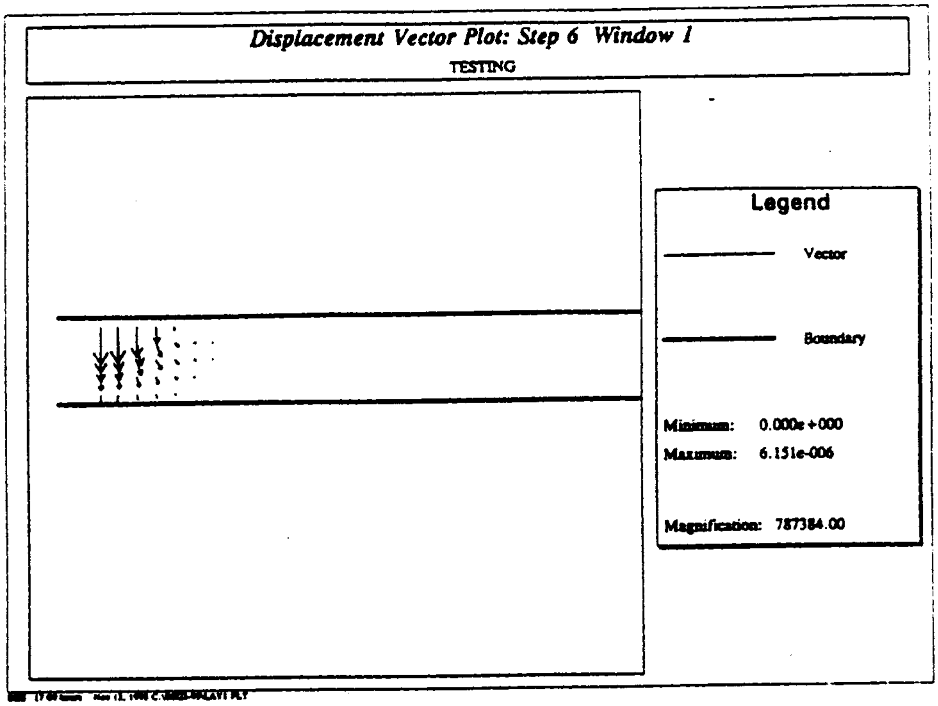

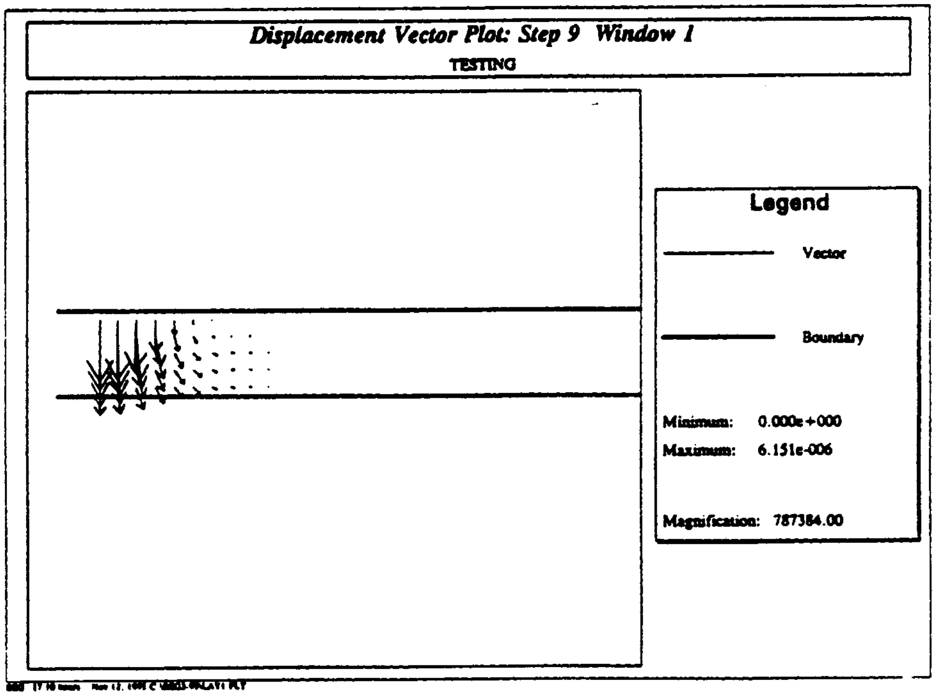

Figure D-13: Displacement vectors at times $6\Delta t$ and $9\Delta t$ for the wave propagation through layered material problem.

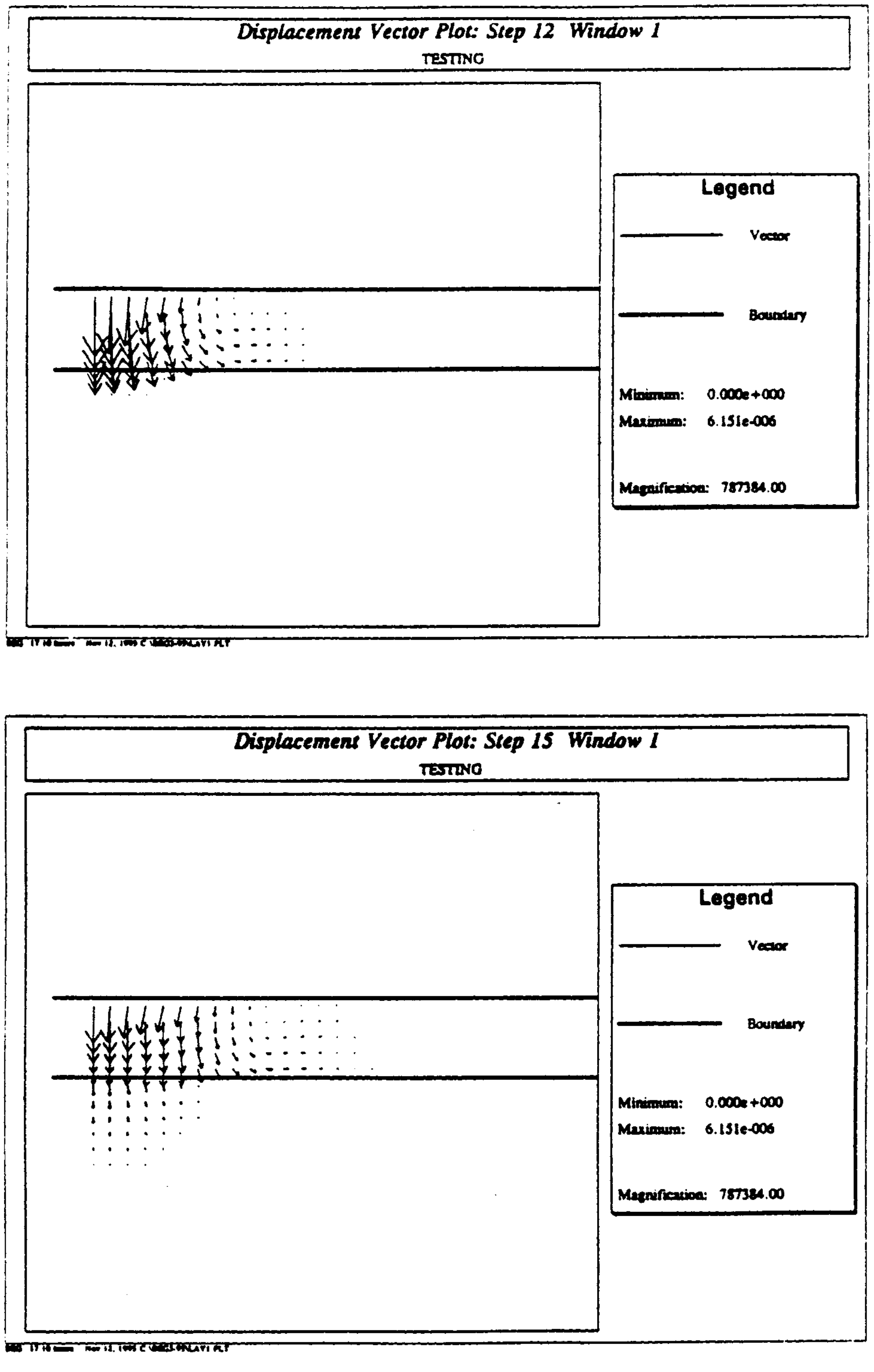

Figure D-14: Displacement vectors at times $12\Delta t$ and $15\Delta t$ for the wave propagation through layered material problem.

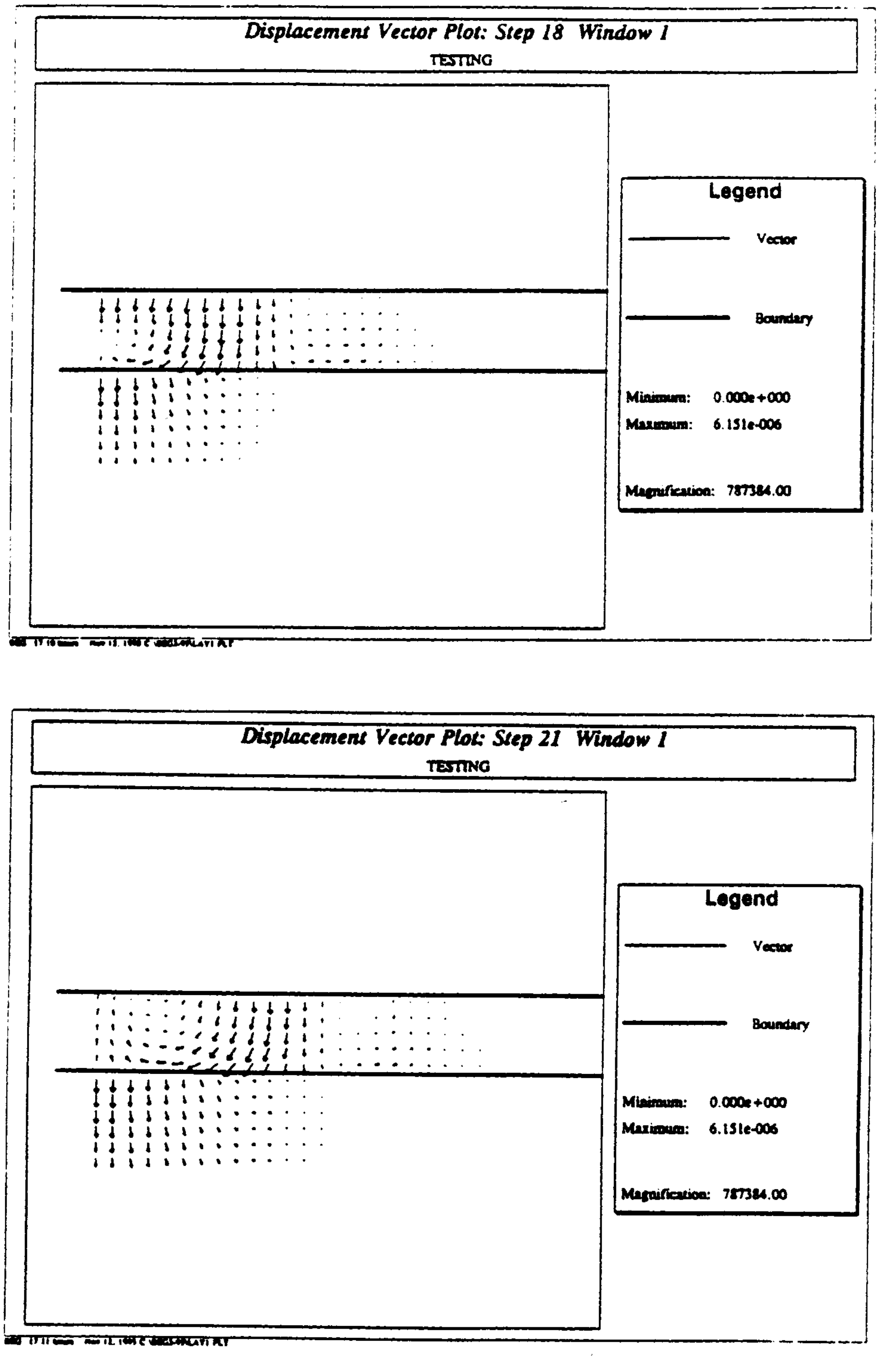

Figure D-15: Displacement vectors at times $18\Delta t$ and $21\Delta t$ for the wave propagation through layered material problem.

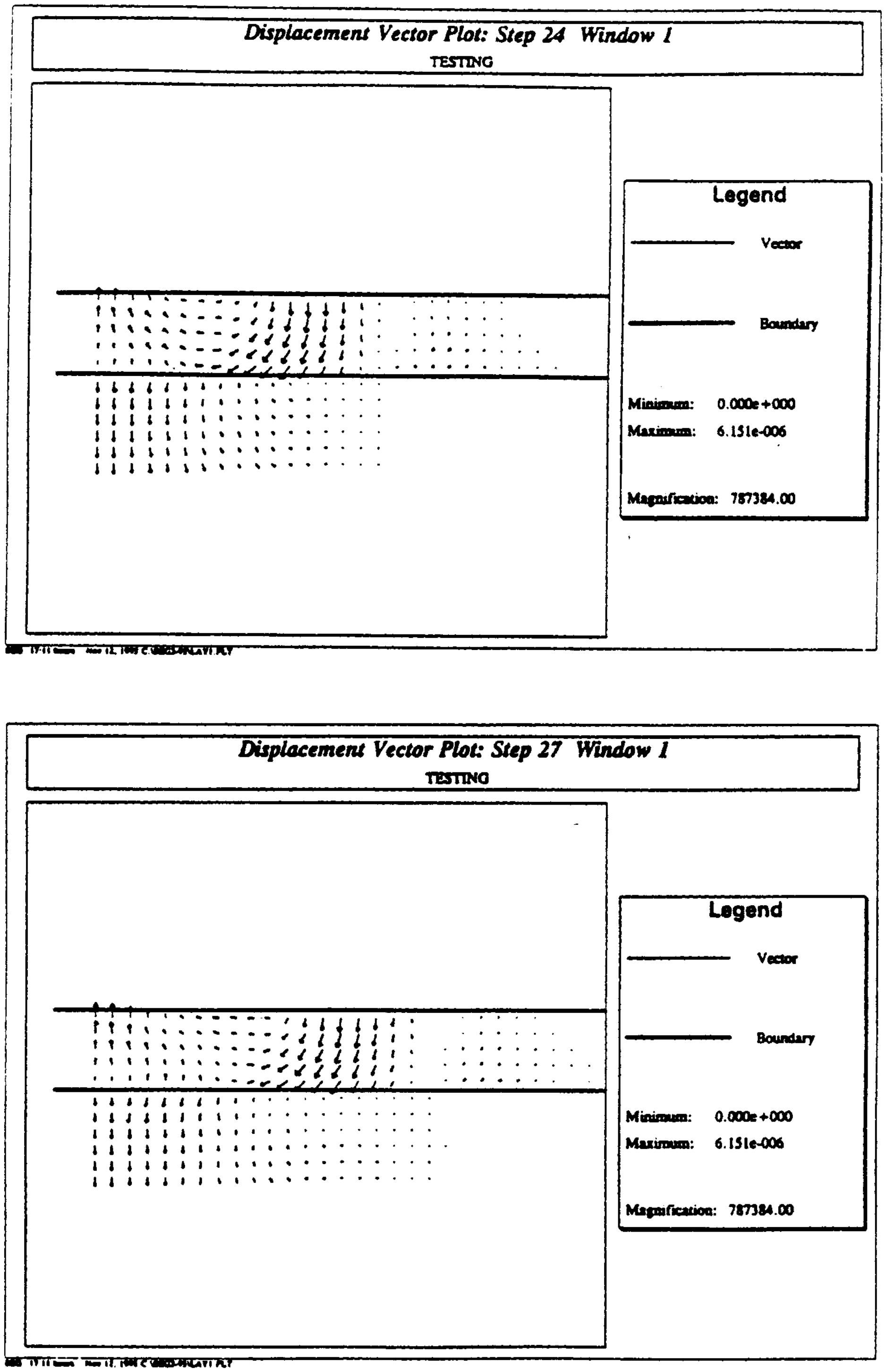

Figure D-16: Displacement vectors at times $24\Delta t$ and $27\Delta t$ for the wave propagation through layered material problem.

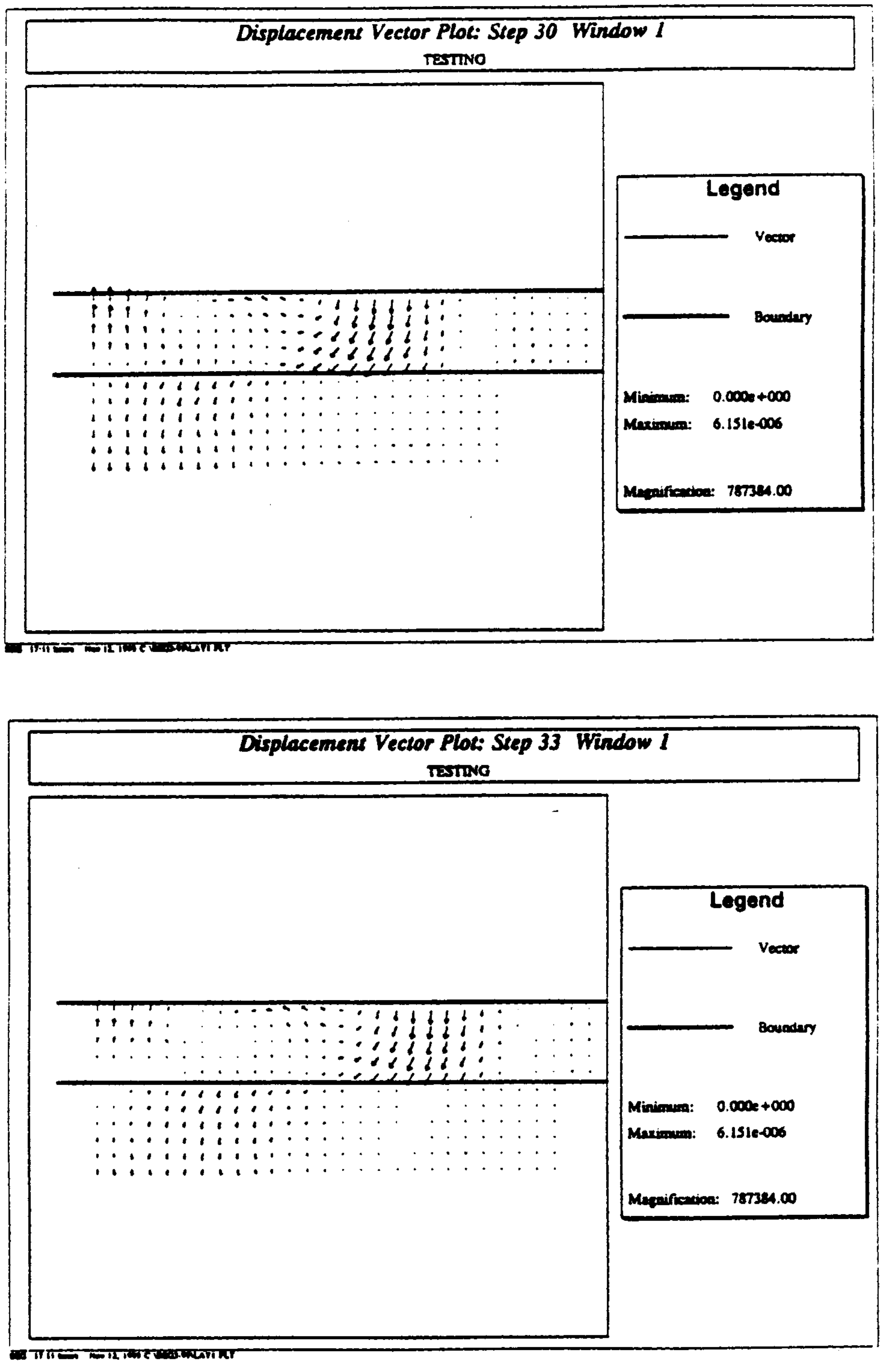

Figure D-17: Displacement vectors at times $30\Delta t$ and $33\Delta t$ for the wave propagation through layered material problem.

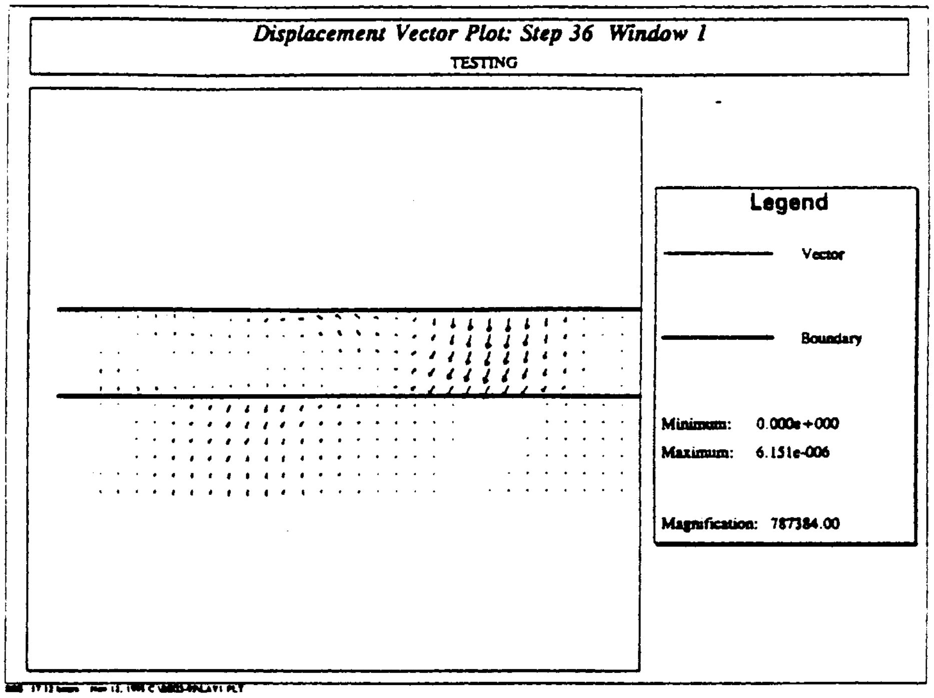

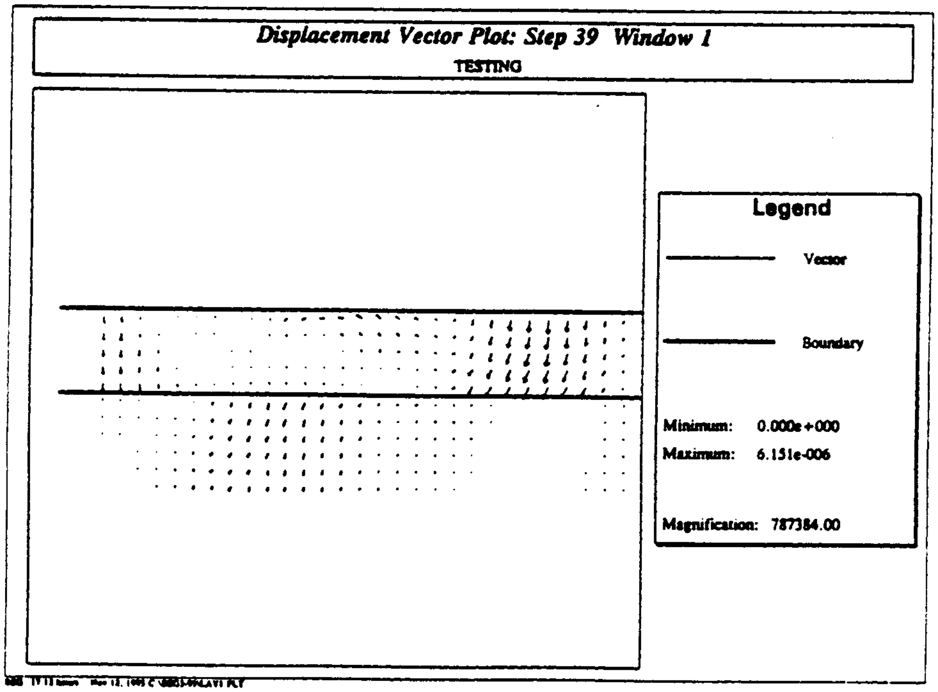

Figure D-18: Displacement vectors at times $36\Delta t$ and $39\Delta t$ for the wave propagation through layered material problem.

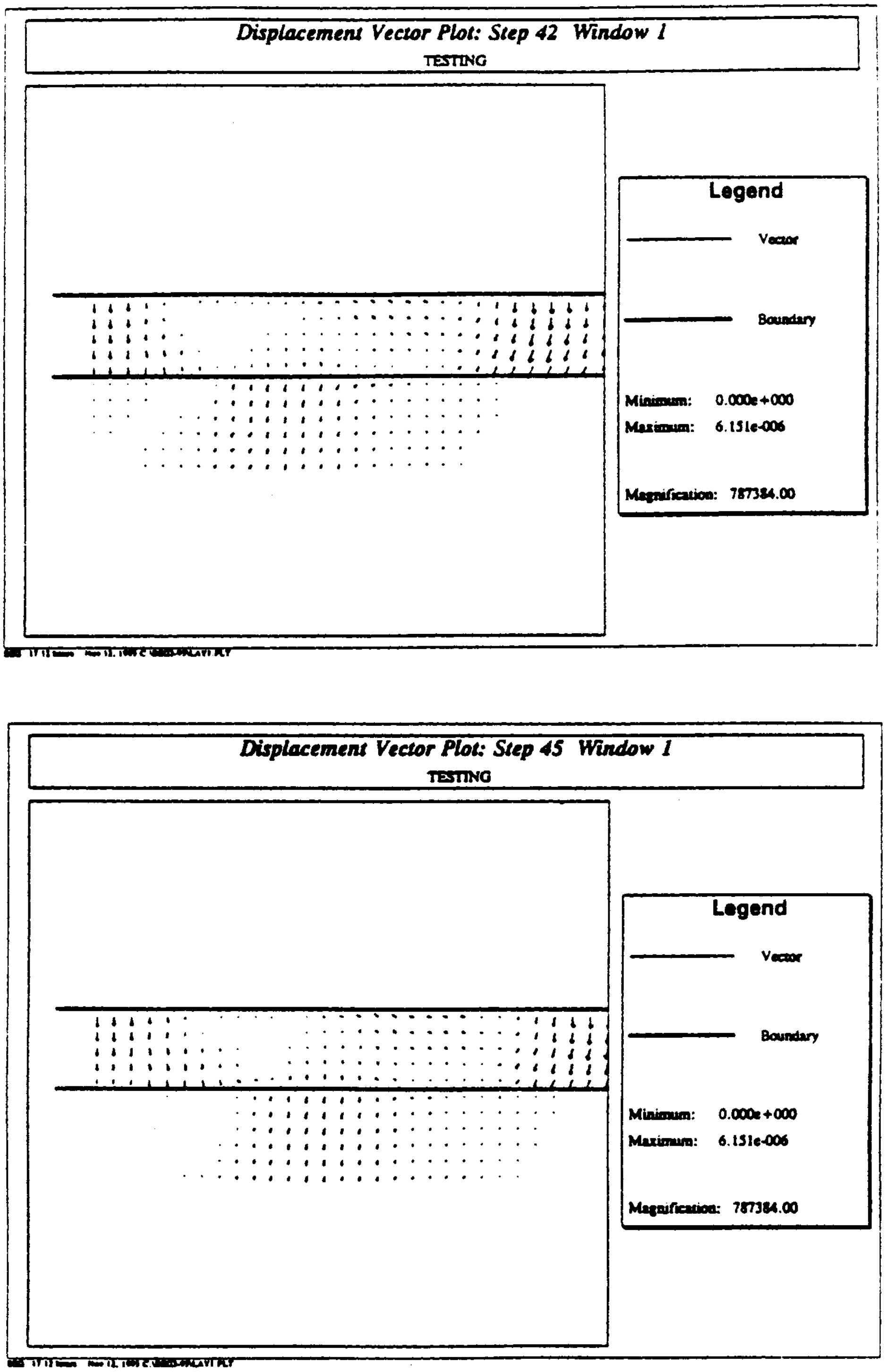

Figure D-19: Displacement vectors at times $42\Delta t$ and $45\Delta t$ for the wave propagation through layered material problem.

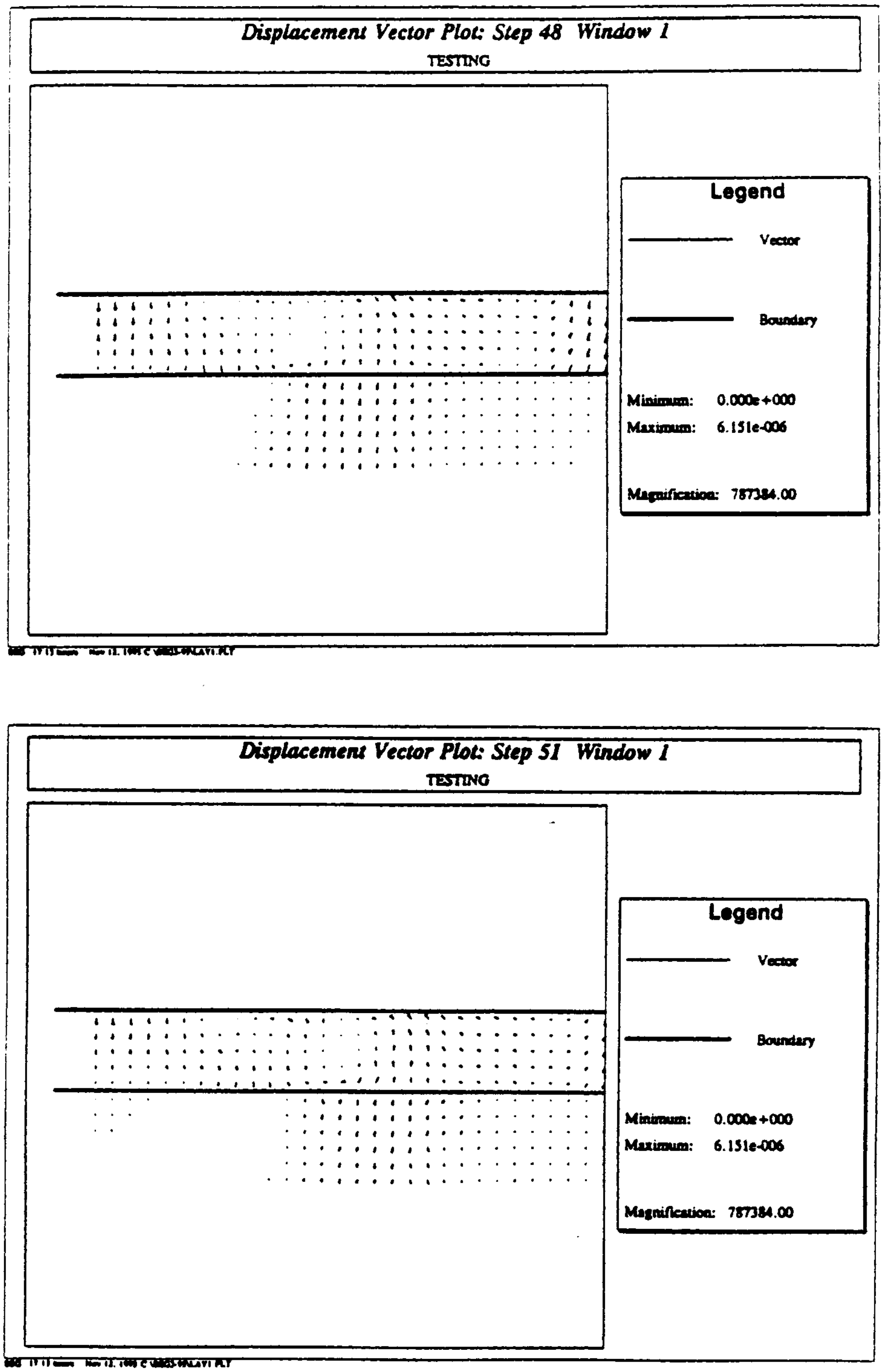

Figure D-20: Displacement vectors at times $48\Delta t$ and $51\Delta t$ for the wave propagation through layered material problem.

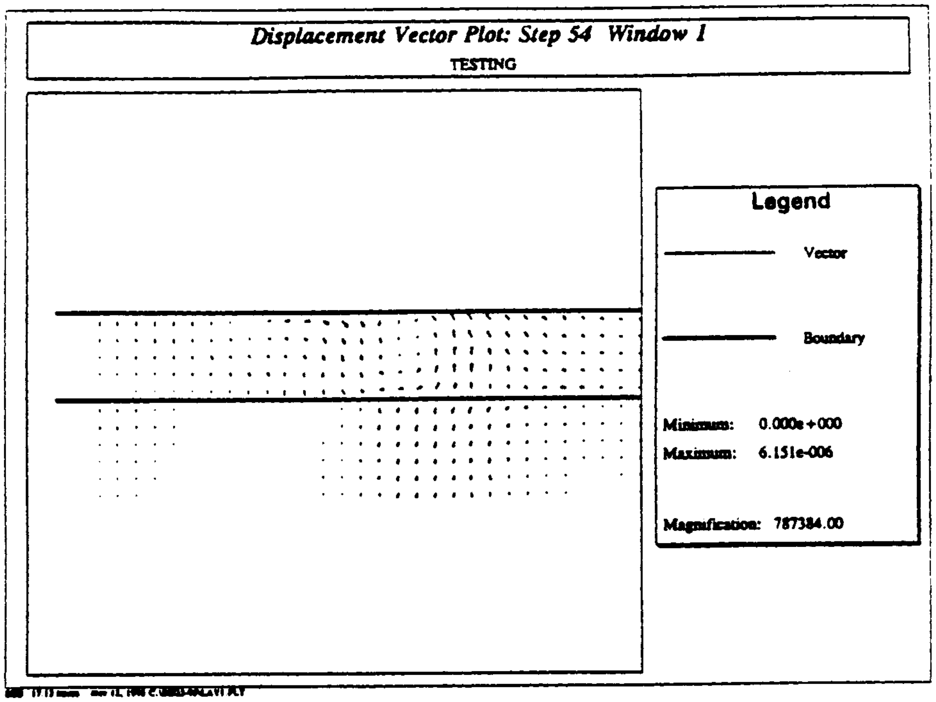

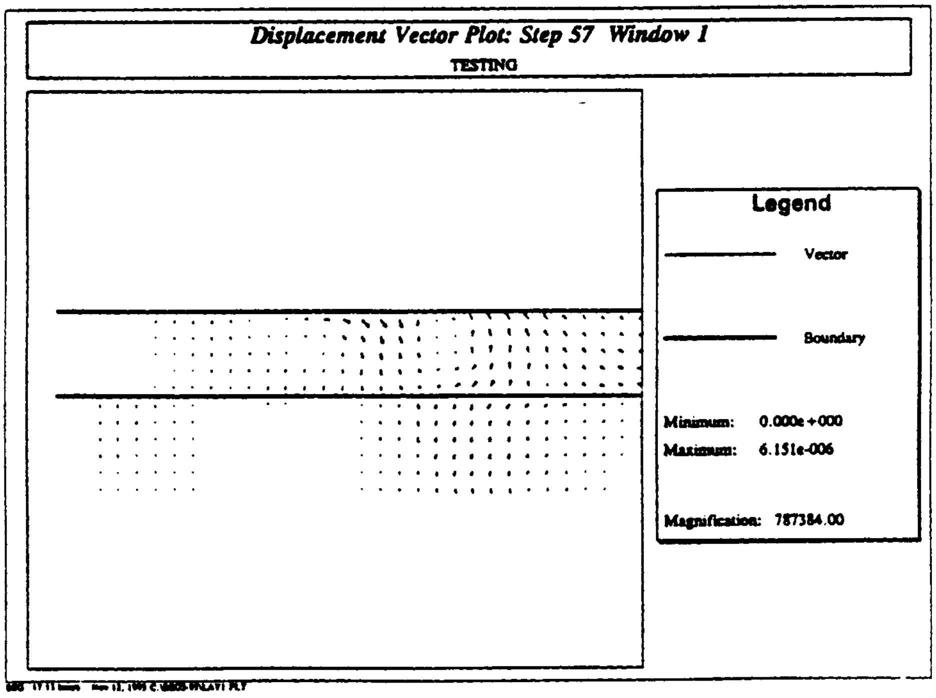

Figure D-21: Displacement vectors at times 54Δt and 57Δt for the wave propagation through layered material problem.

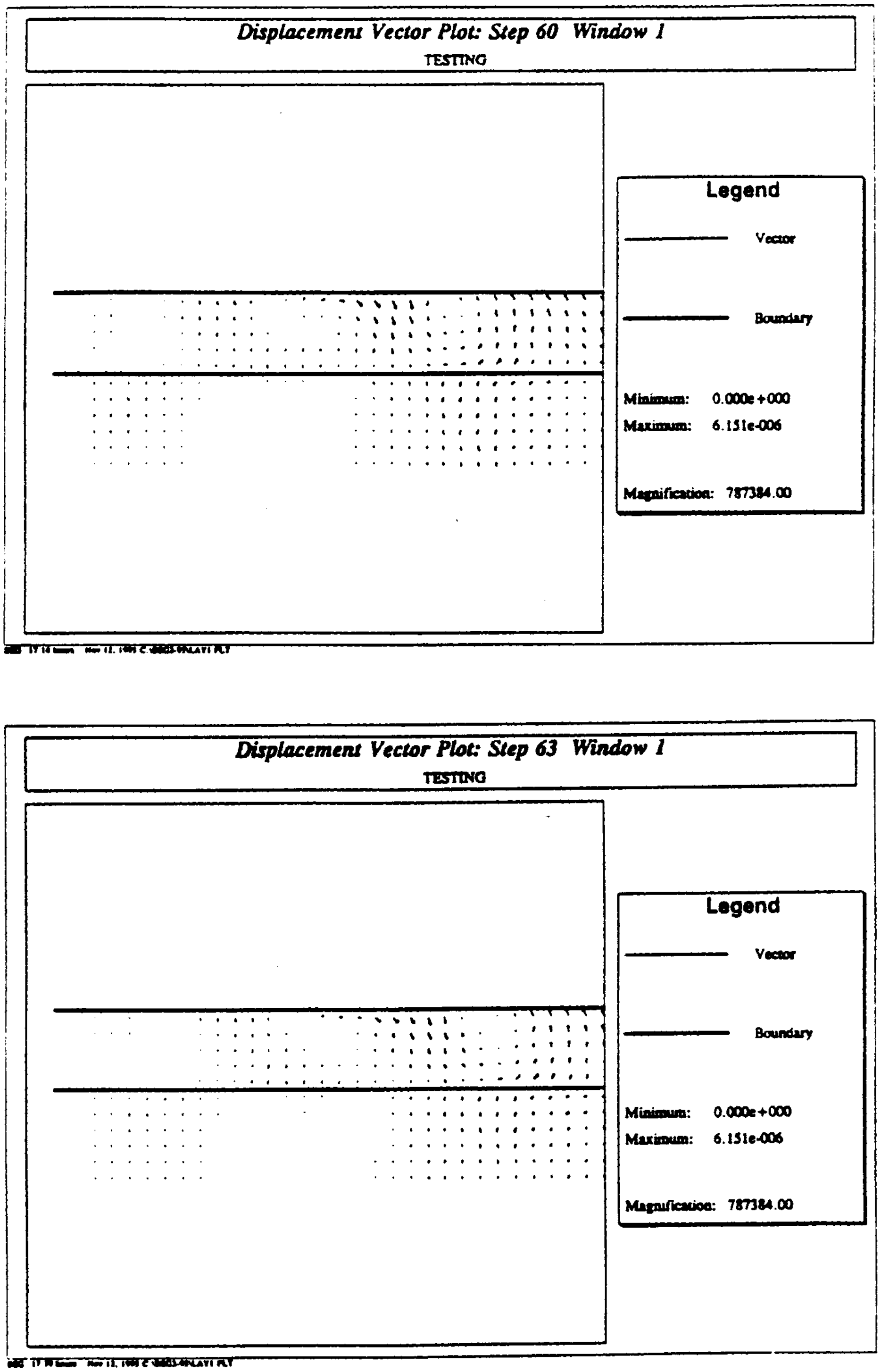

Figure D-22: Displacement vectors at times $60\Delta t$ and $63\Delta t$ for the wave propagation through layered material problem.

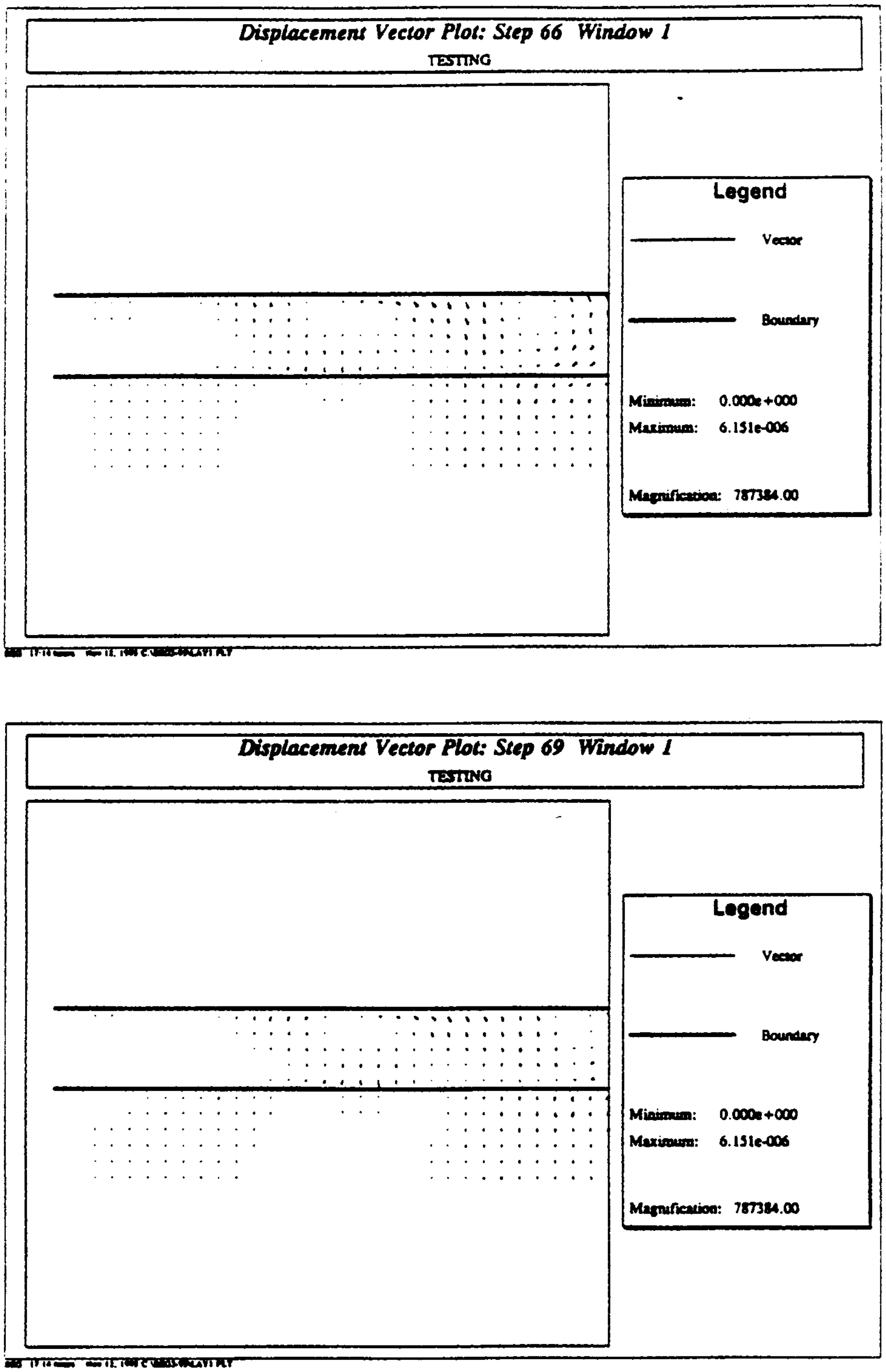

Figure D-23: Displacement vectors at times $66\Delta t$ and $69\Delta t$ for the wave propagation through layered material problem.

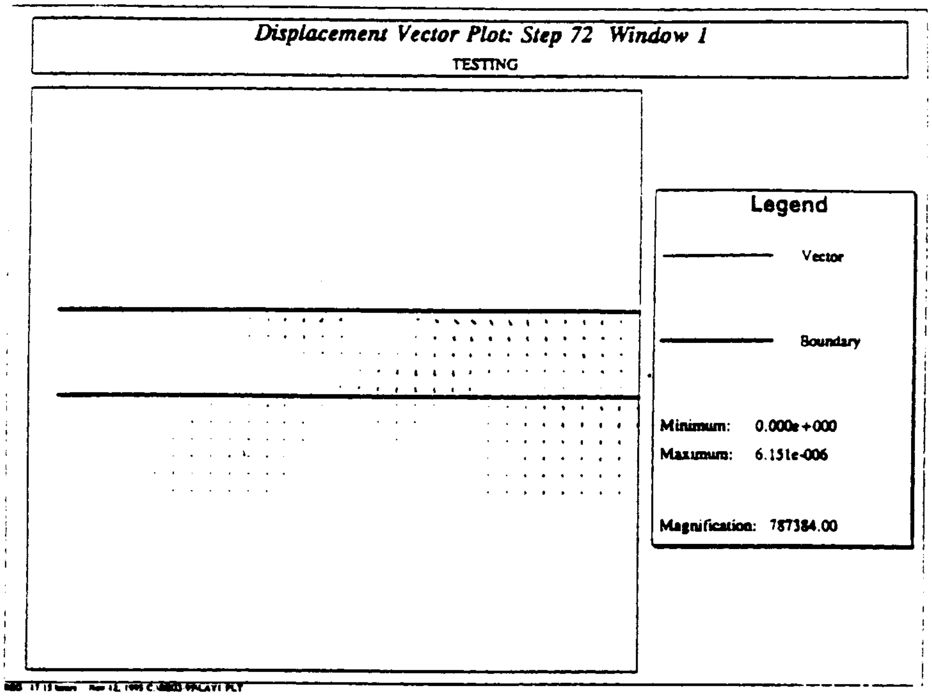

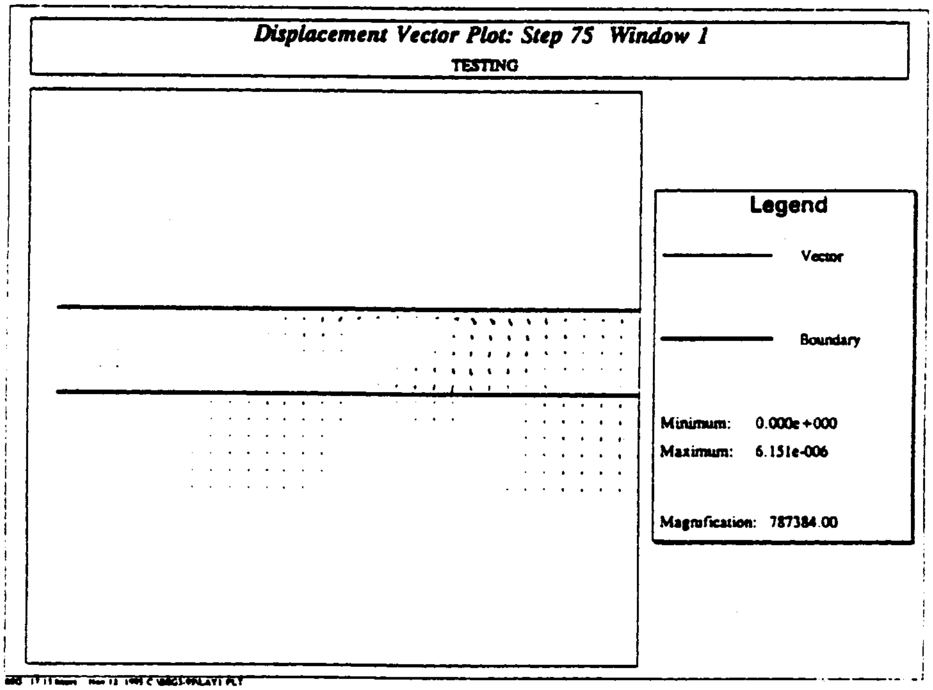

Figure D-24: Displacement vectors at times $72\Delta t$ and $75\Delta t$ for the wave propagation through layered material problem.

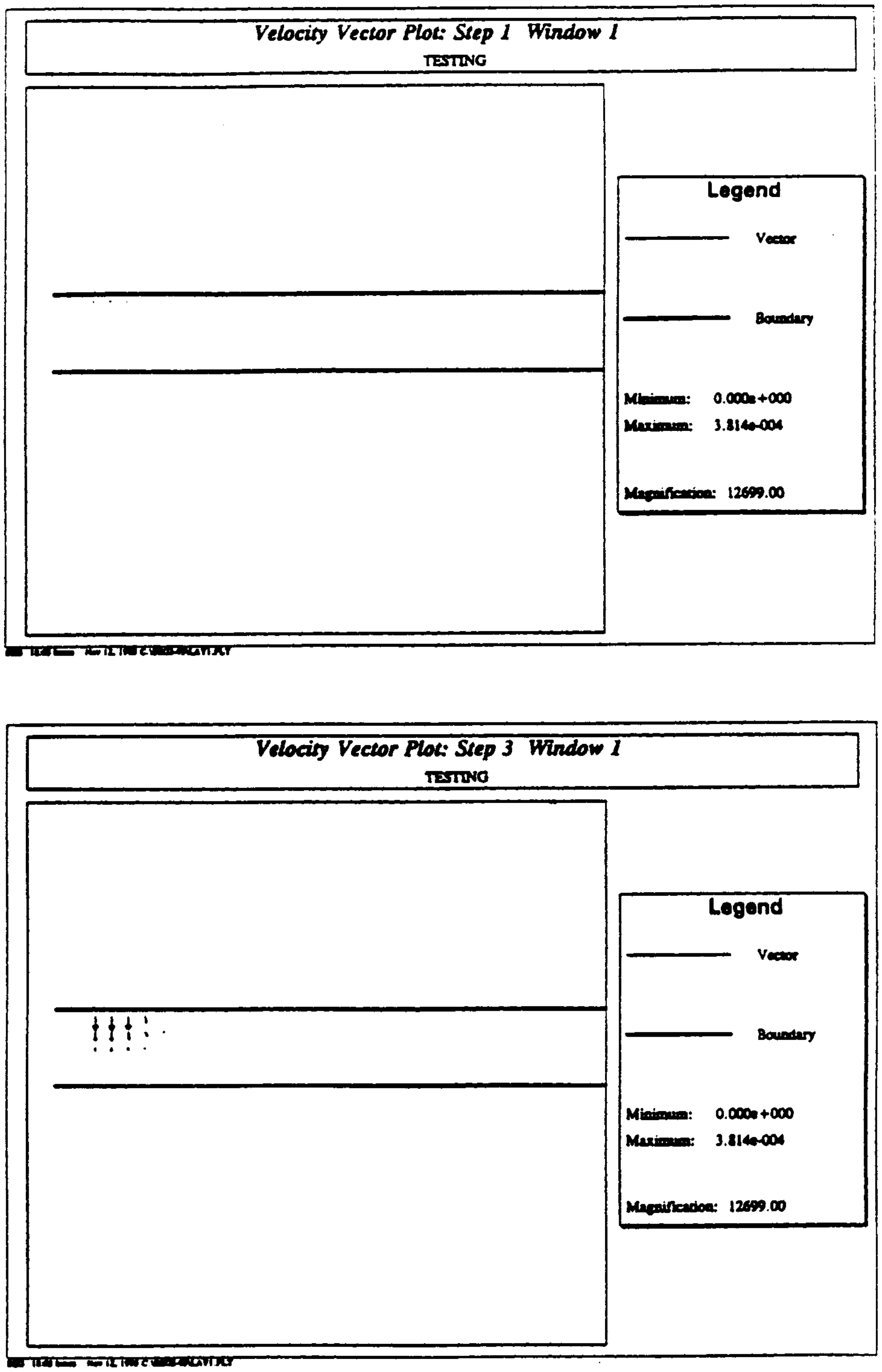

Figure D-25: Velocity vectors at times $1\Delta t$ and $3\Delta t$ for the wave propagation through layered material problem.

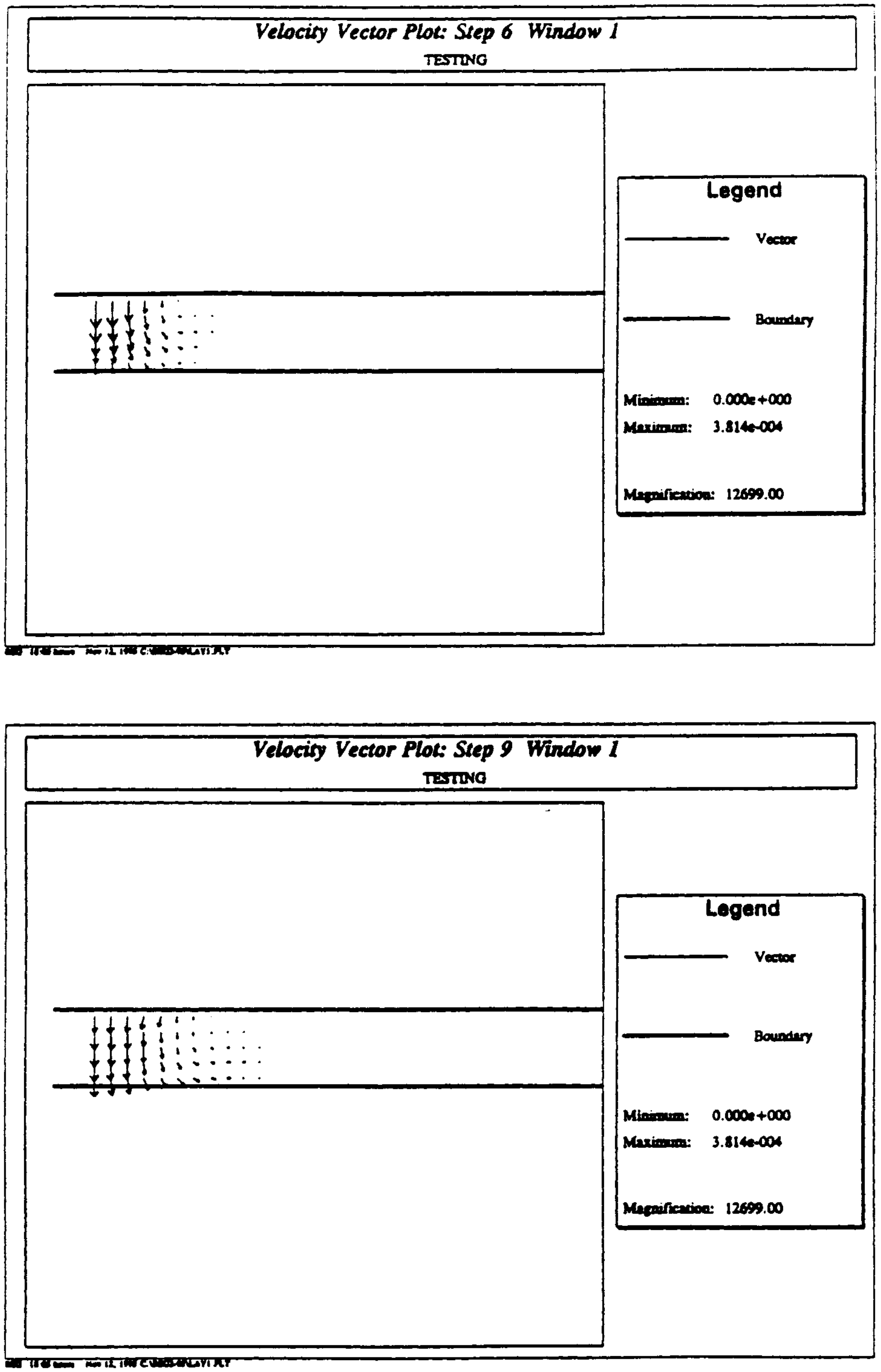

Figure D-26: Velocity vectors at times $6\Delta t$ and $9\Delta t$ for the wave propagation through layered material problem.

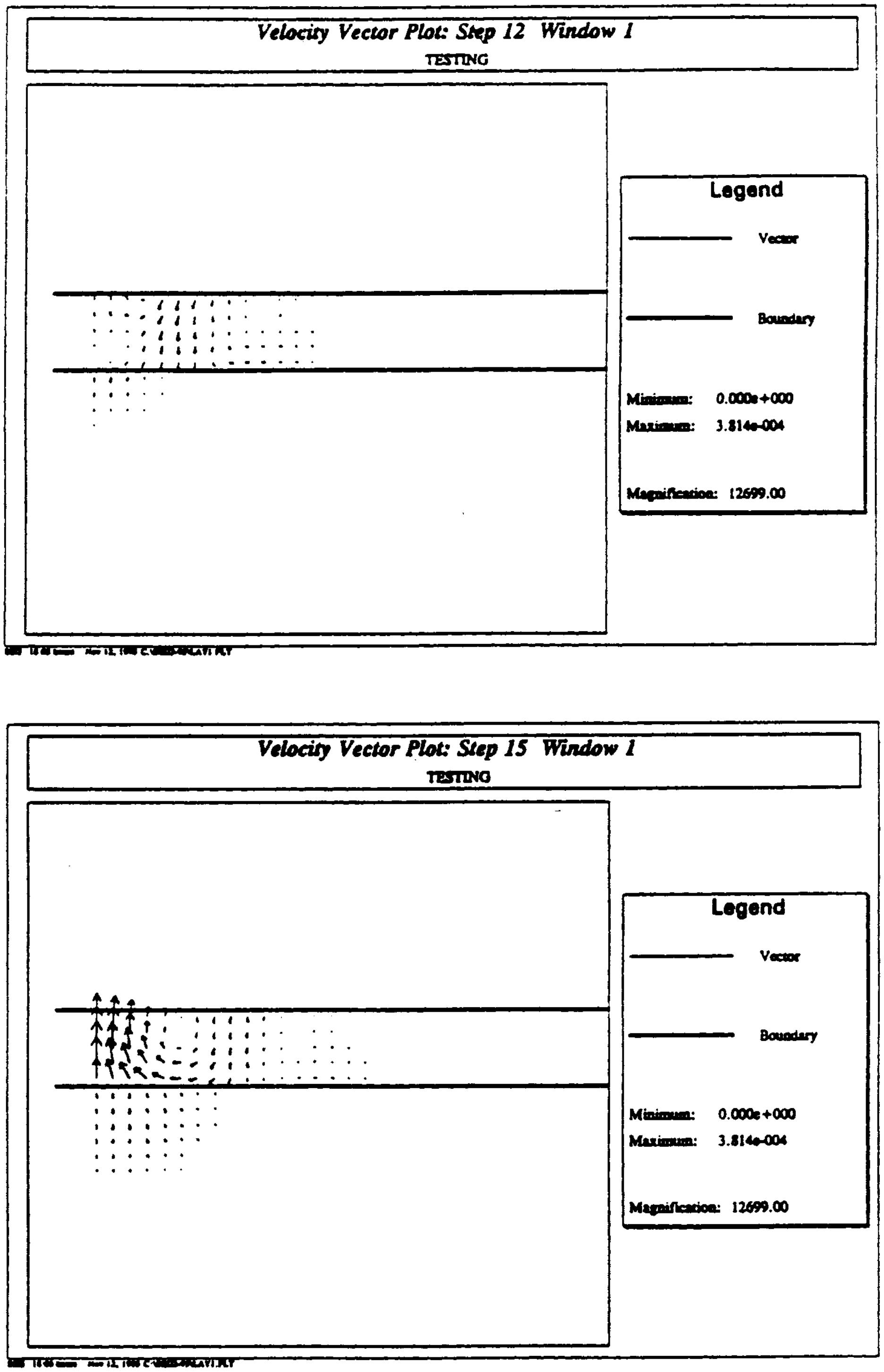

Figure D-27: Velocity vectors at times $12\Delta t$ and $15\Delta t$ for the wave propagation through layered material problem.

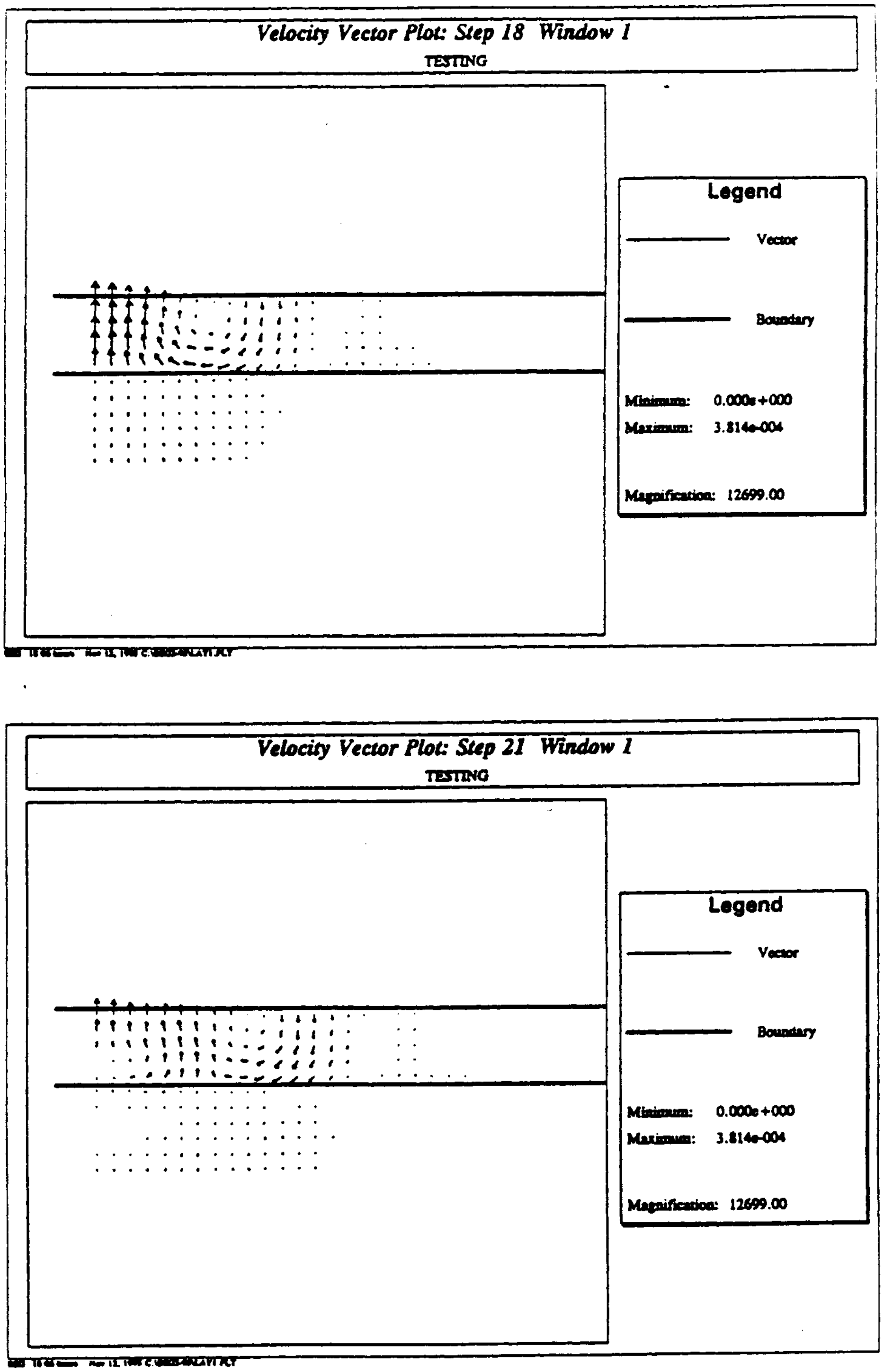

Figure D-28: Velocity vectors at times 18Δt and 21Δt for the wave propagation through layered material problem.

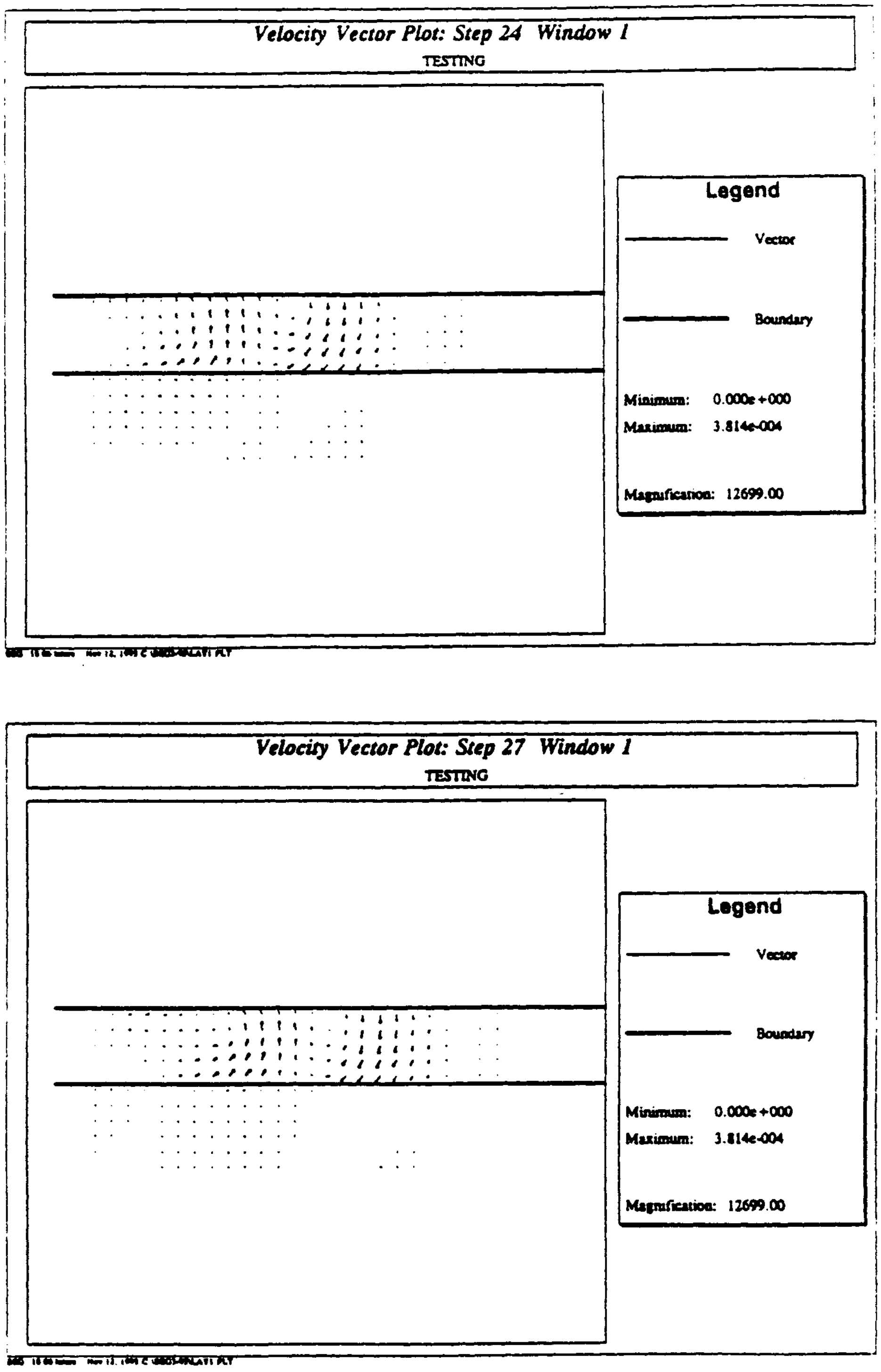

Figure D-29: Velocity vectors at times $24\Delta t$ and $27\Delta t$ for the wave propagation through layered material problem.

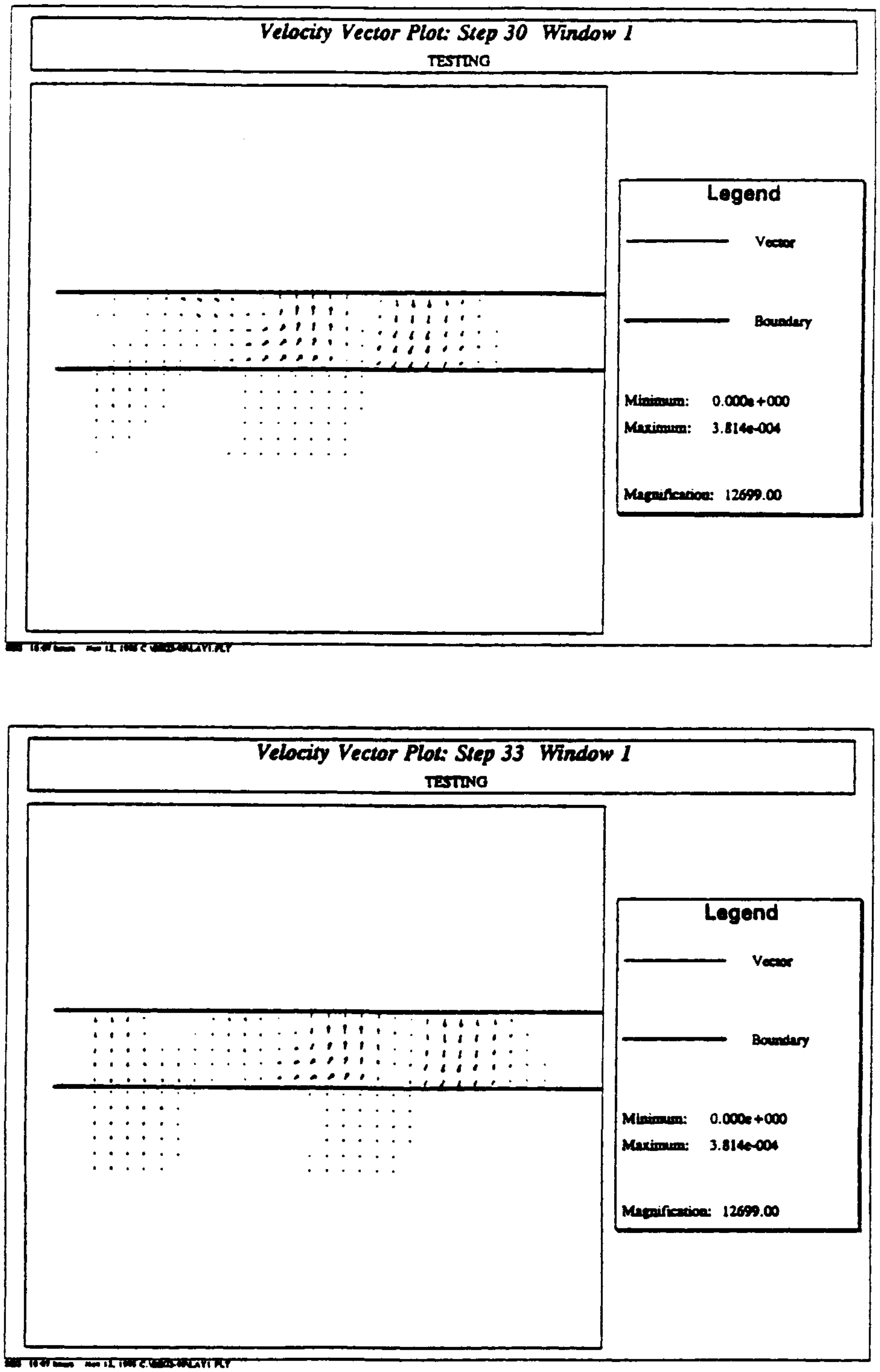

Figure D-30: Velocity vectors at times $30\Delta t$ and $33\Delta t$ for the wave propagation through layered material problem.

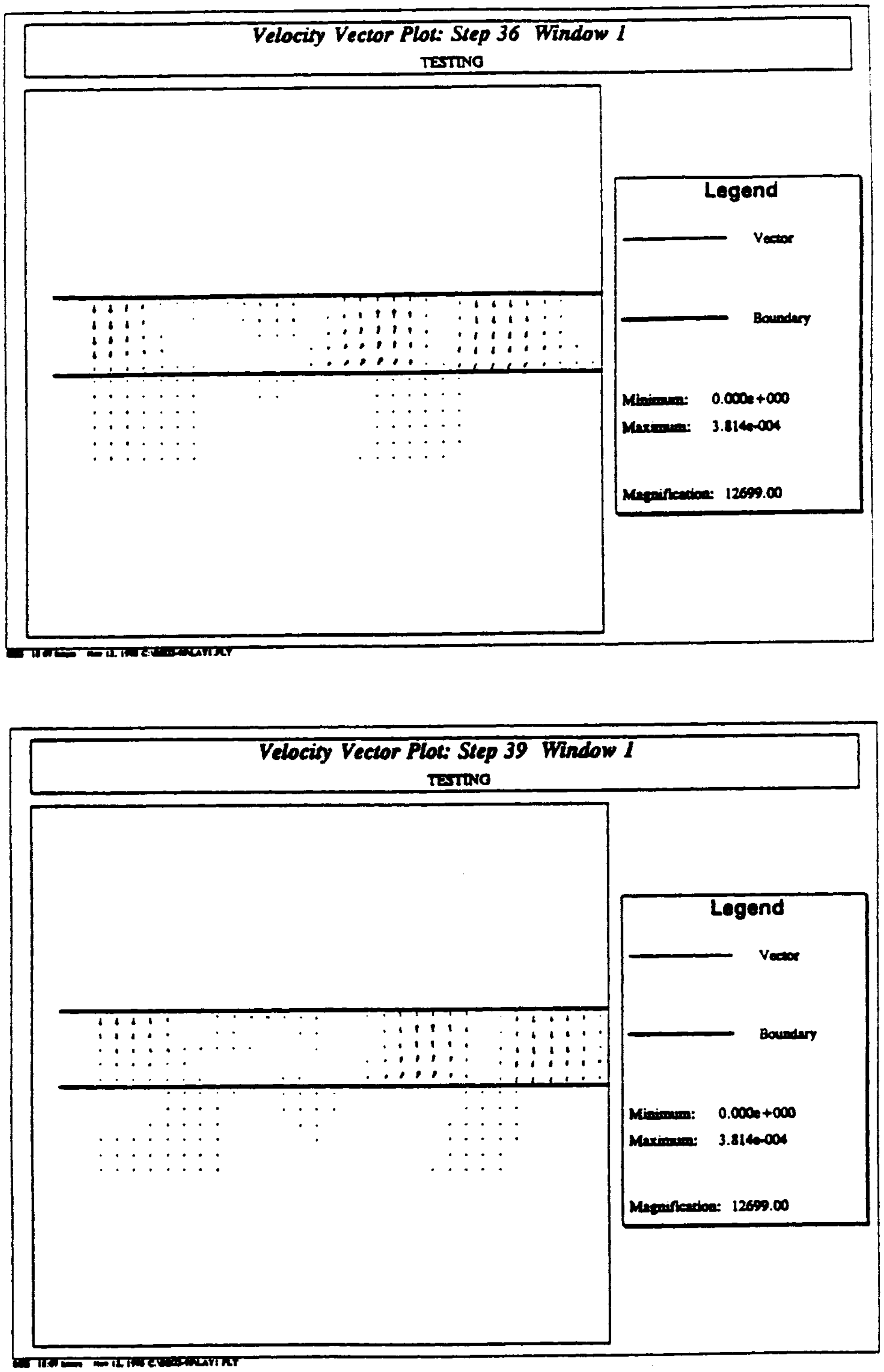

Figure D-31: Velocity vectors at times $36\Delta t$ and $39\Delta t$ for the wave propagation through layered material problem.

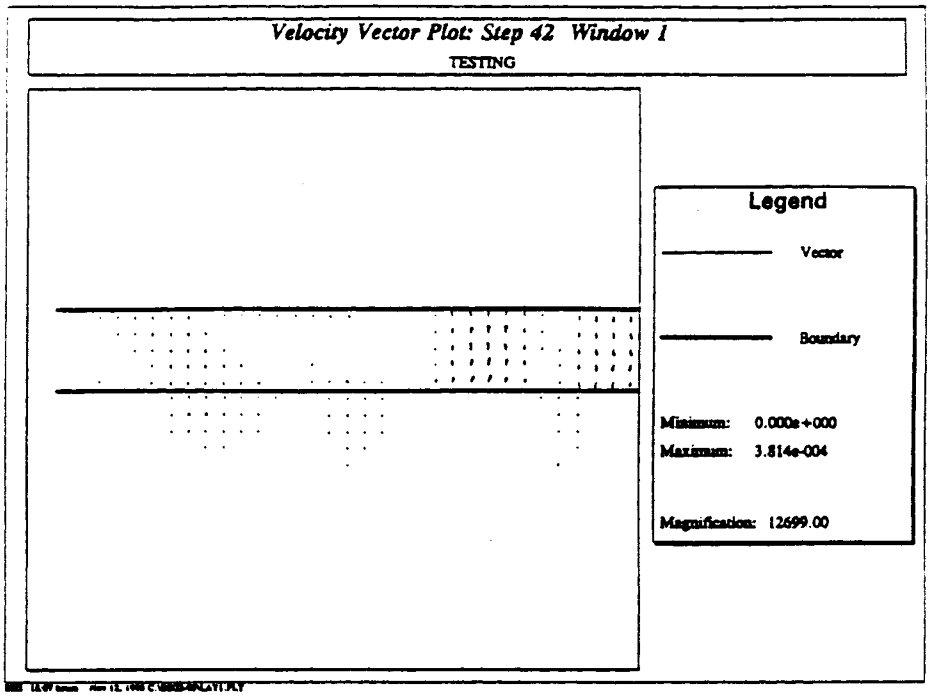

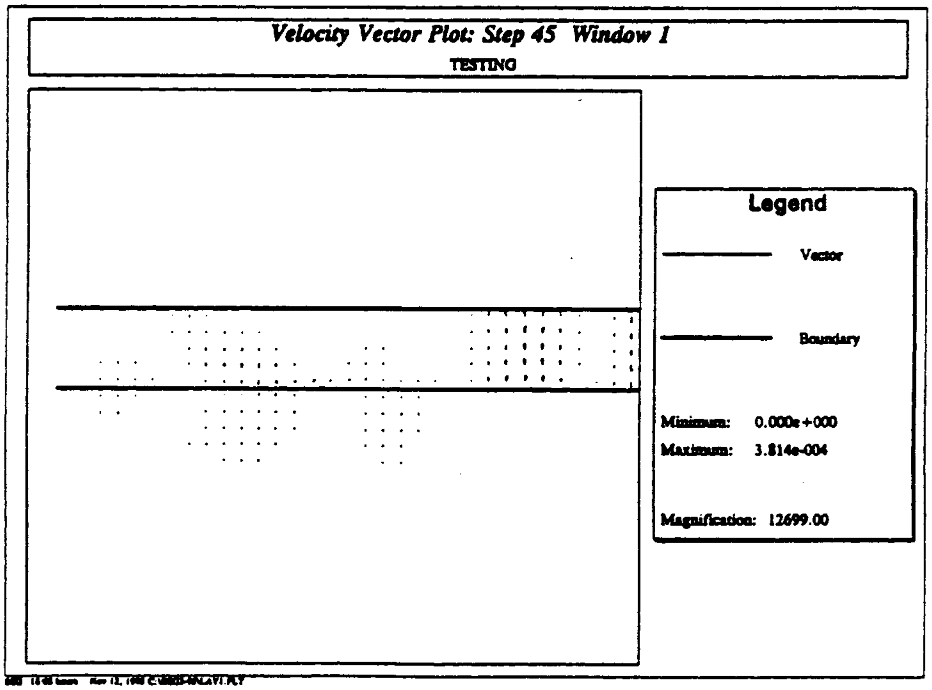

Figure D-32: Velocity vectors at times $42\Delta t$ and $45\Delta t$ for the wave propagation through layered material problem.

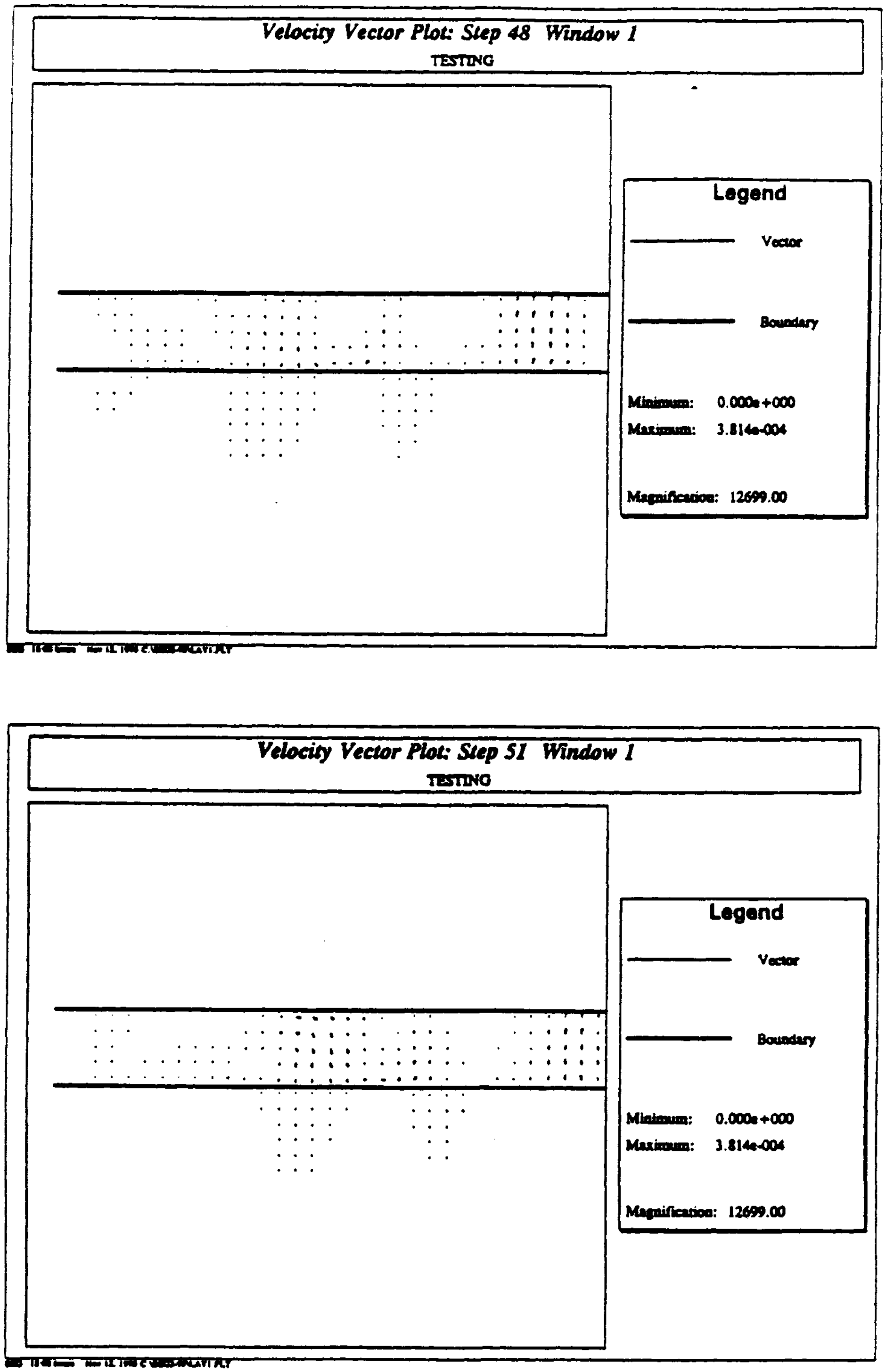

Figure D-33: Velocity vectors at times $48\Delta t$ and $51\Delta t$ for the wave propagation through layered material problem.

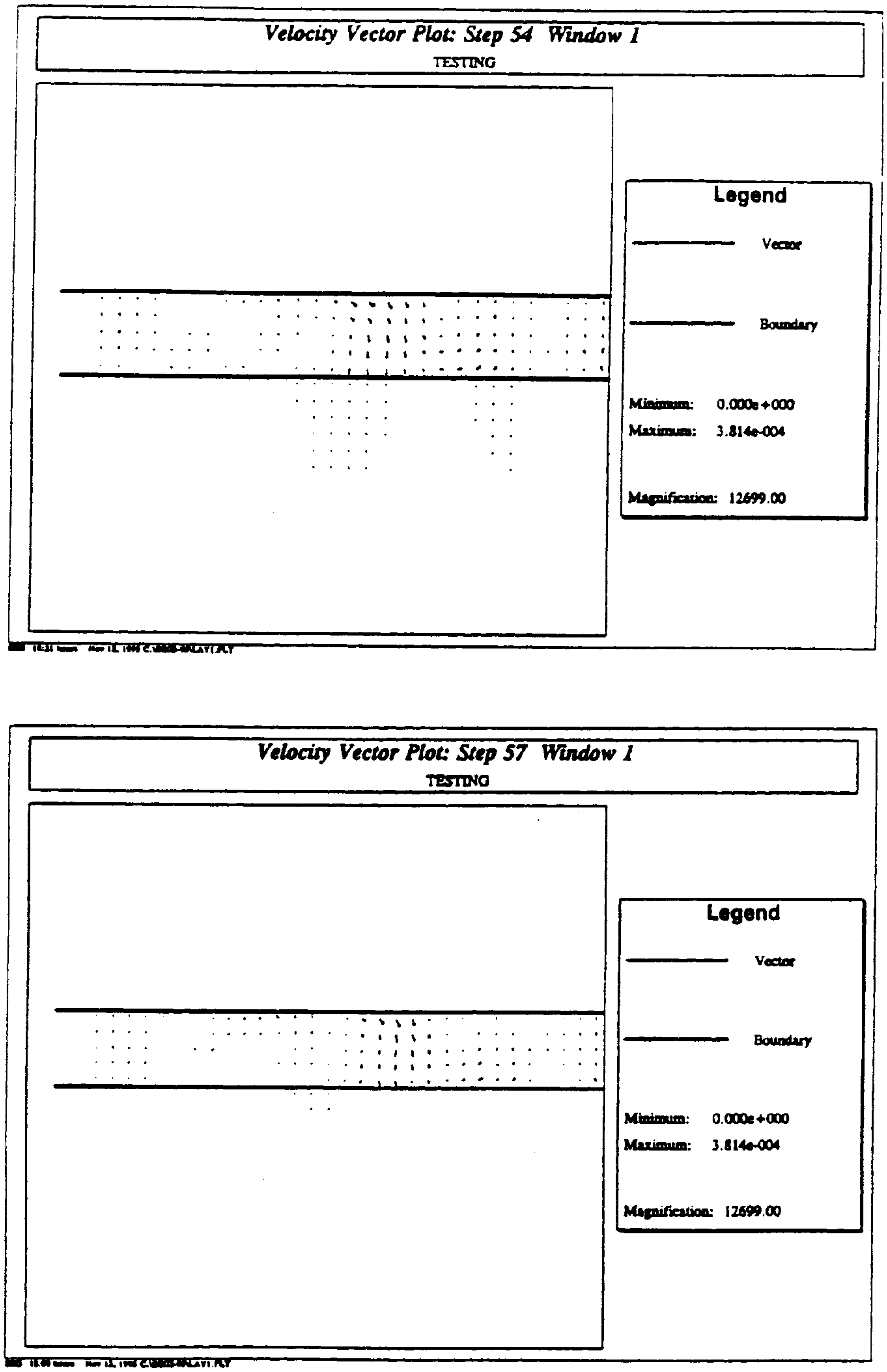

Figure D-34: Velocity vectors at times $54\Delta t$ and $57\Delta t$ for the wave propagation through layered material problem.

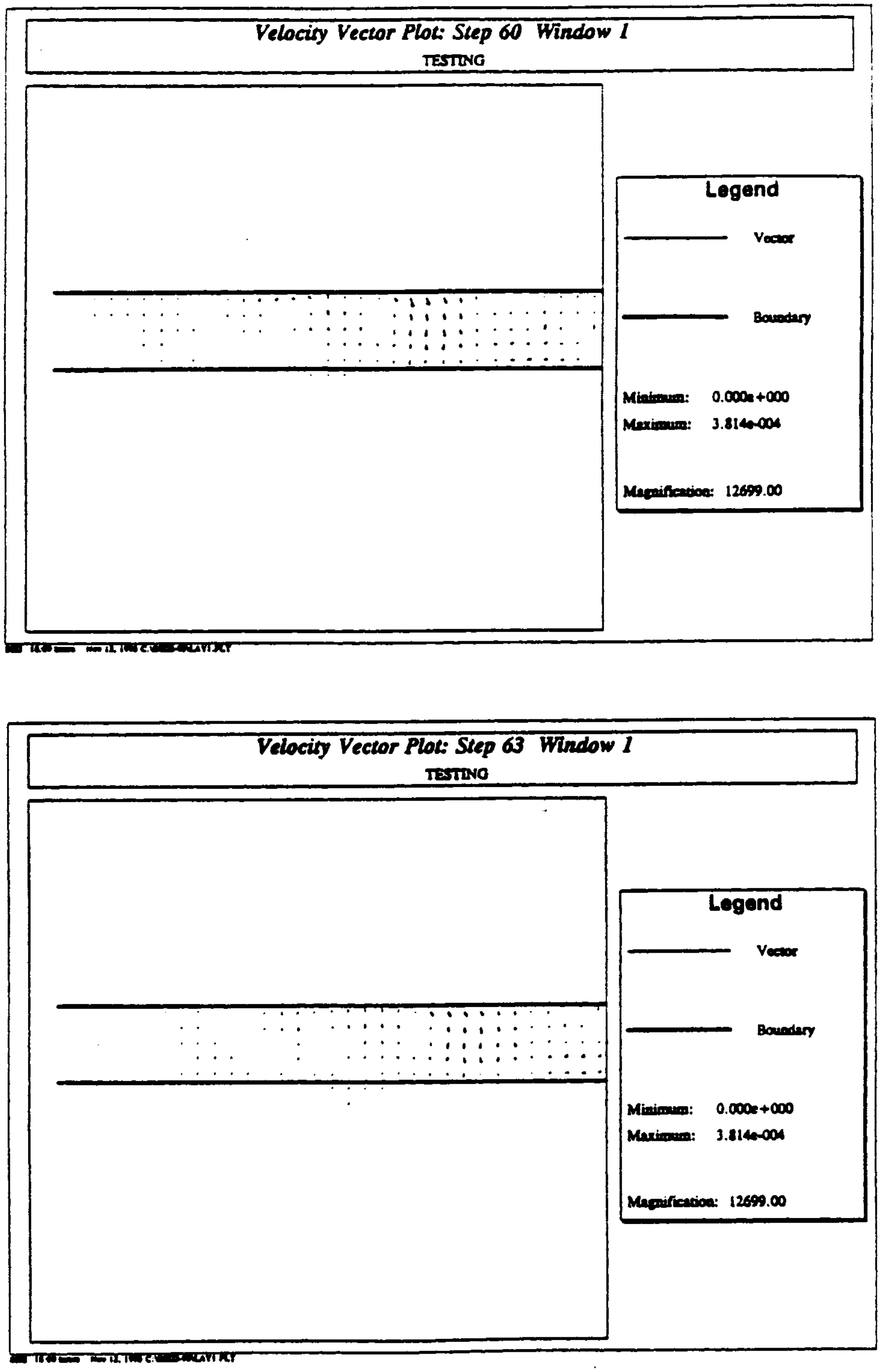

Figure D-35: Velocity vectors at times $60\Delta t$ and $63\Delta t$ for the wave propagation through layered material problem.

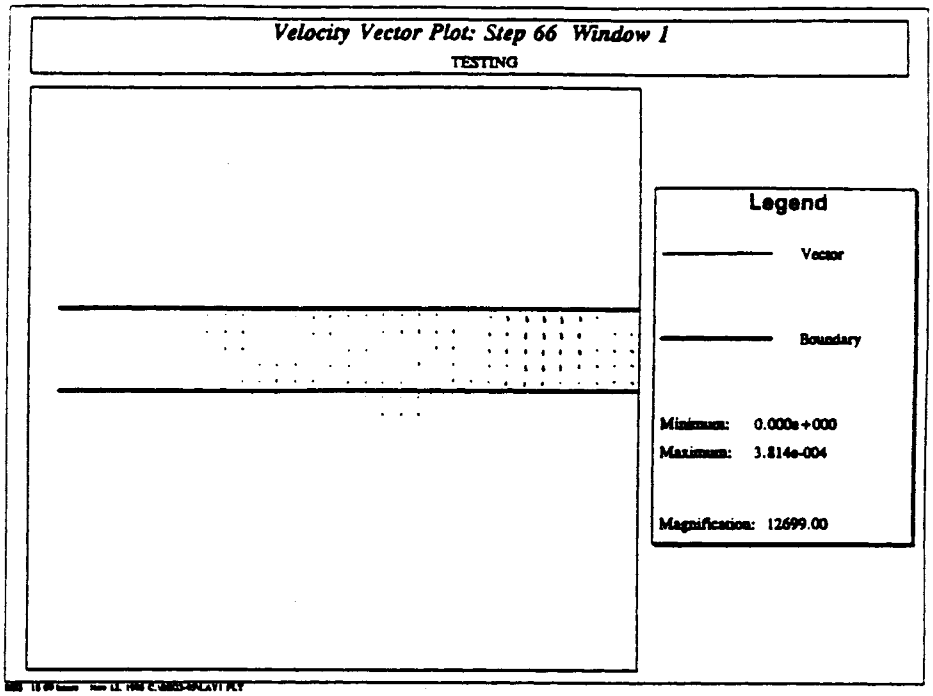

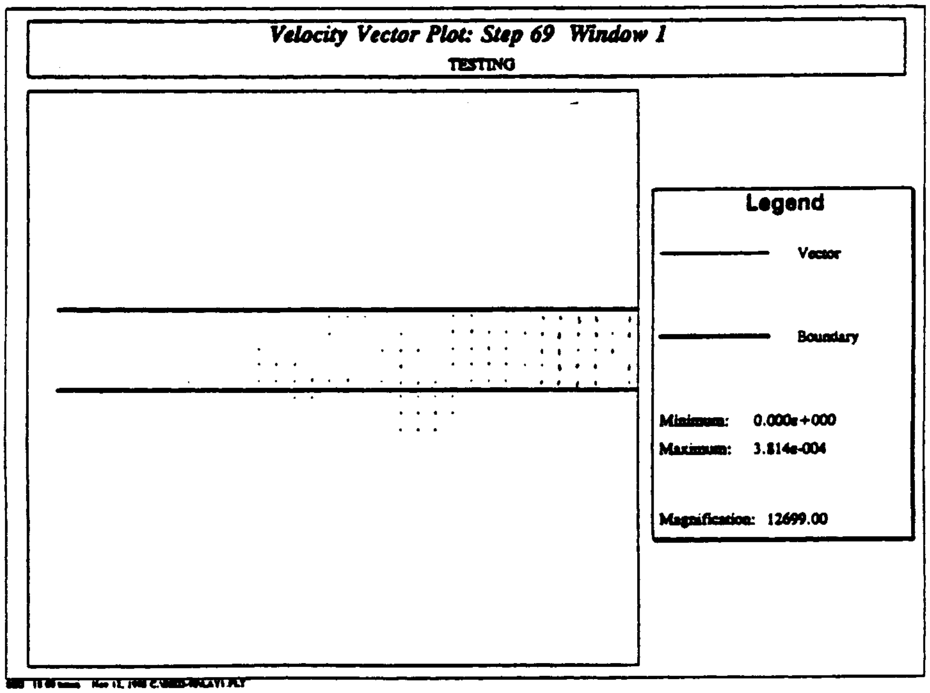

Figure D-36: Velocity vectors at times $66\Delta t$ and $69\Delta t$ for the wave propagation through layered material problem.

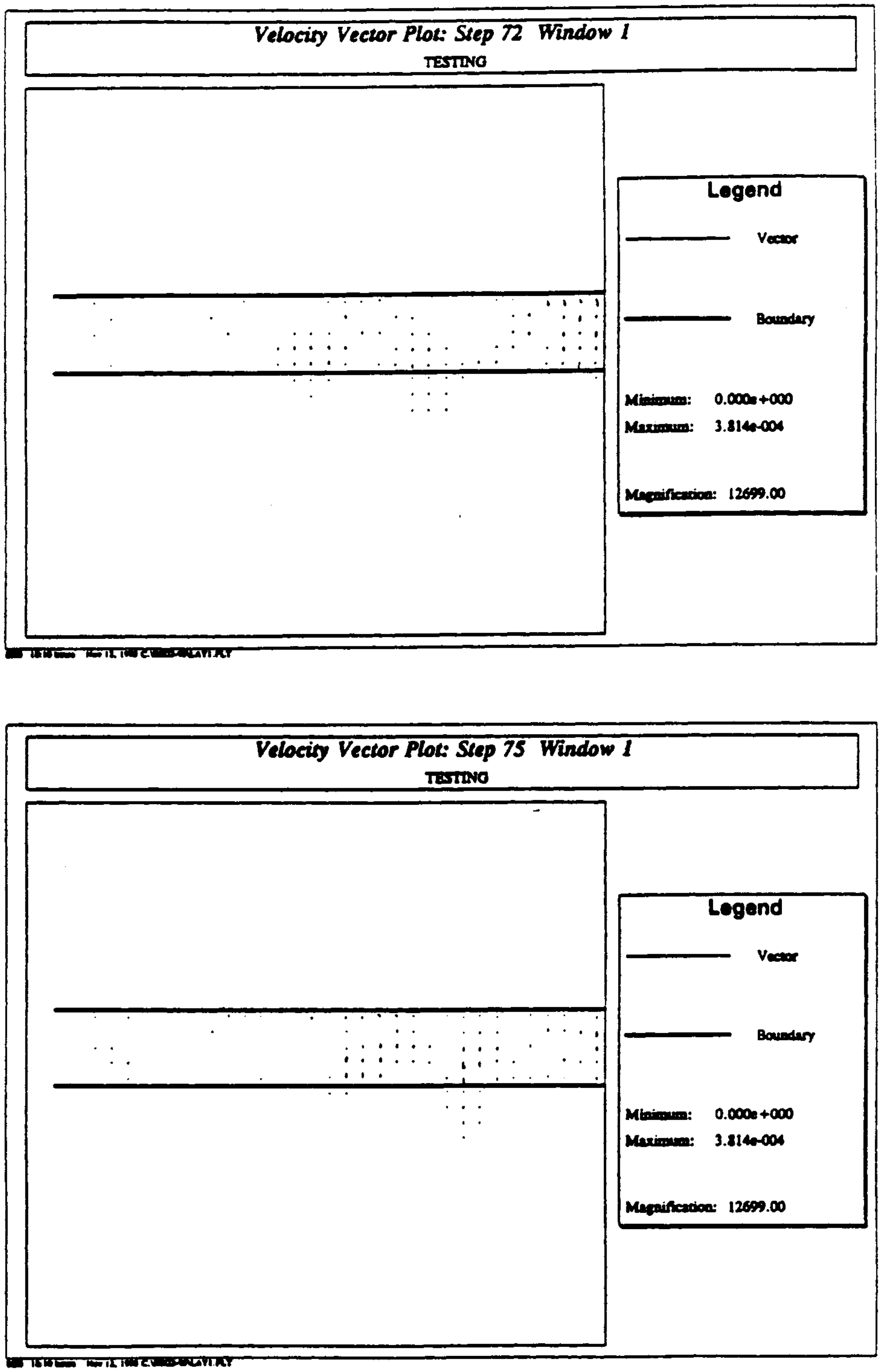

Figure D-37: Velocity vectors at times $72\Delta t$ and $75\Delta t$ for the wave propagation through layered material problem.

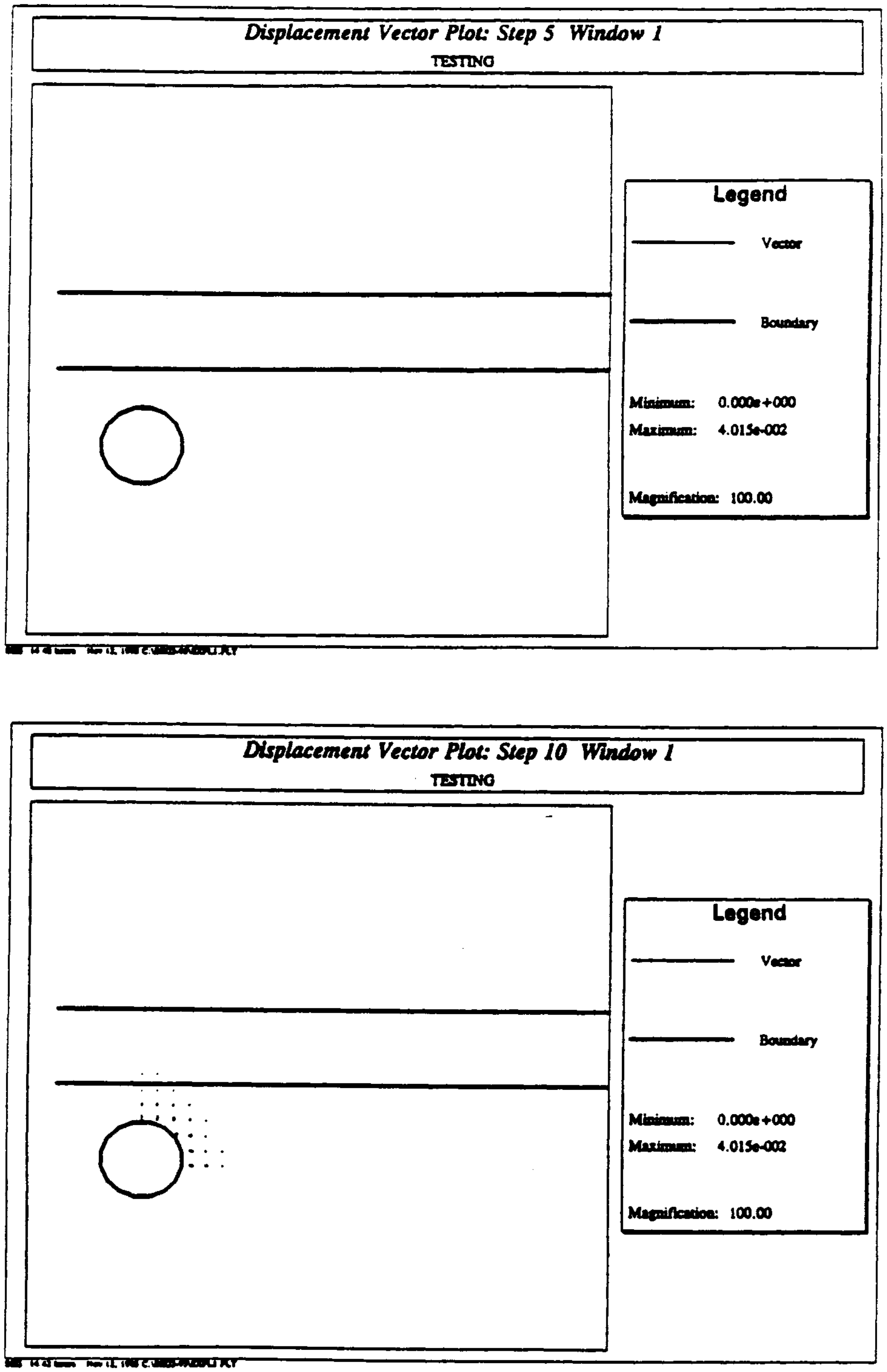

Figure D-38: Displacement vectors at times $5\Delta t$ and $10\Delta t$ for underground explosion in a two-layered rock.

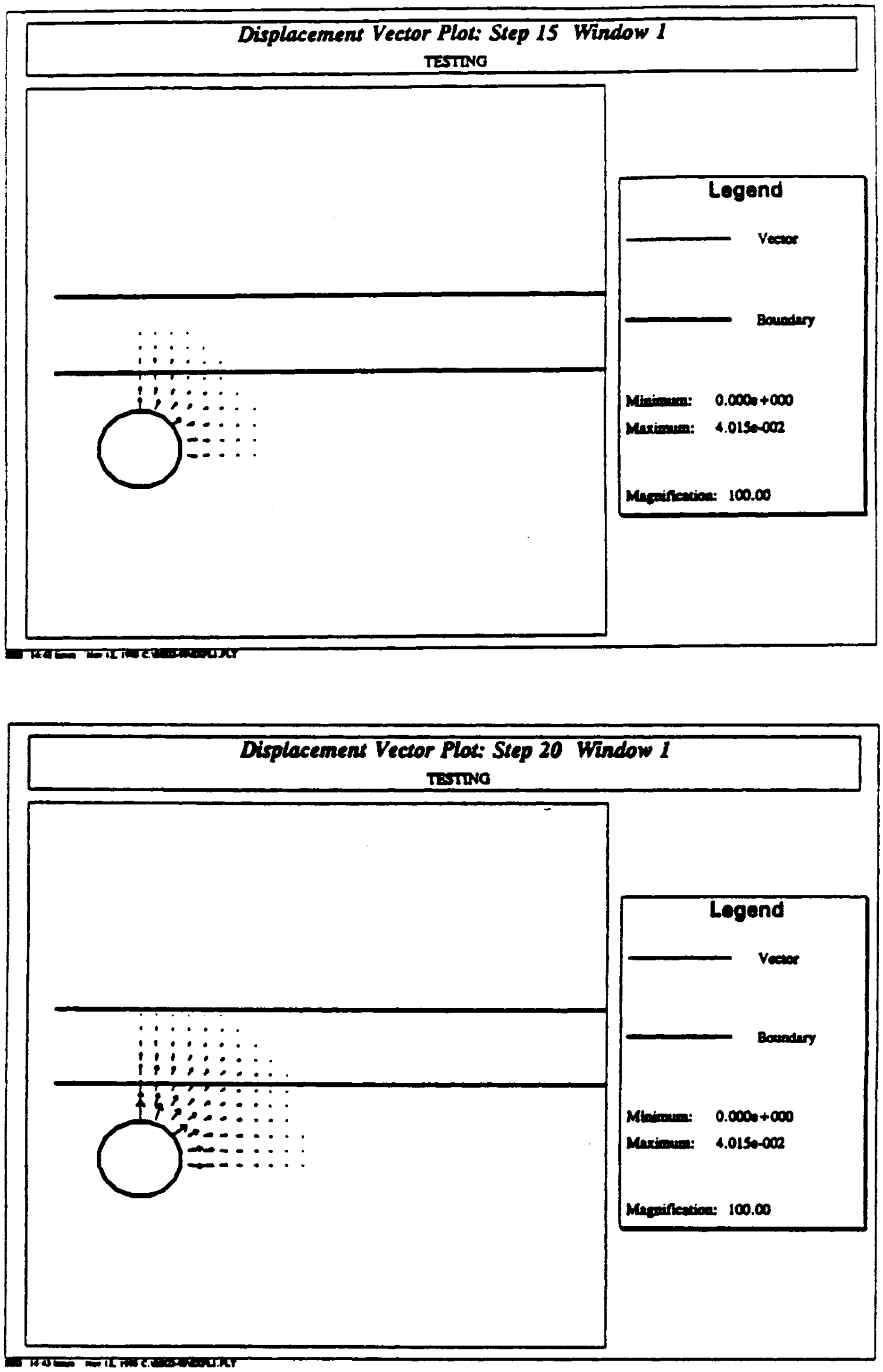

Figure D-39: Displacement vectors at times 15Δt and 20Δt for underground explosion in a two-layered rock.

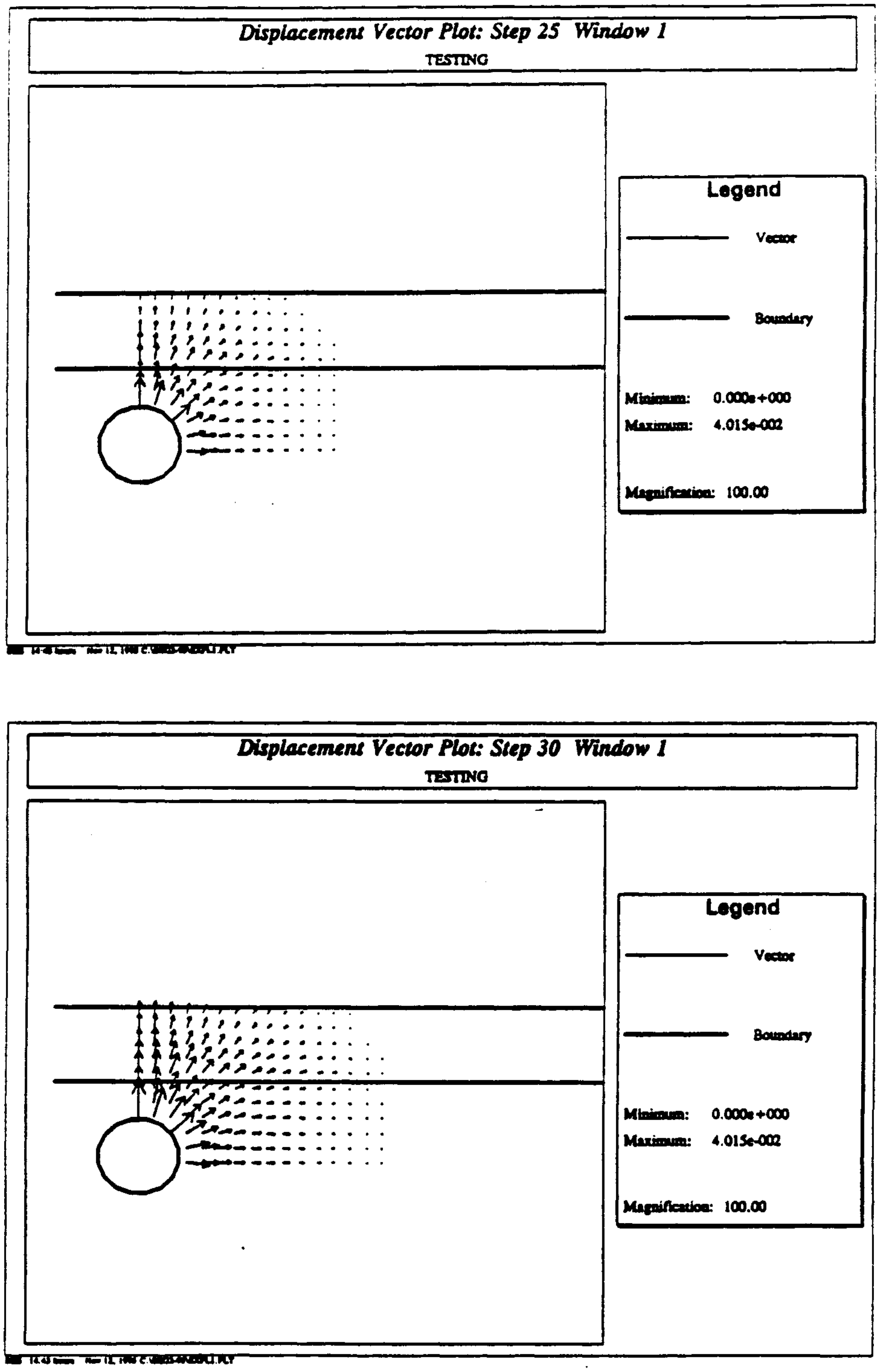

Figure D-40: Displacement vectors at times $25\Delta t$ and $30\Delta t$ for underground explosion in a two-layered rock.

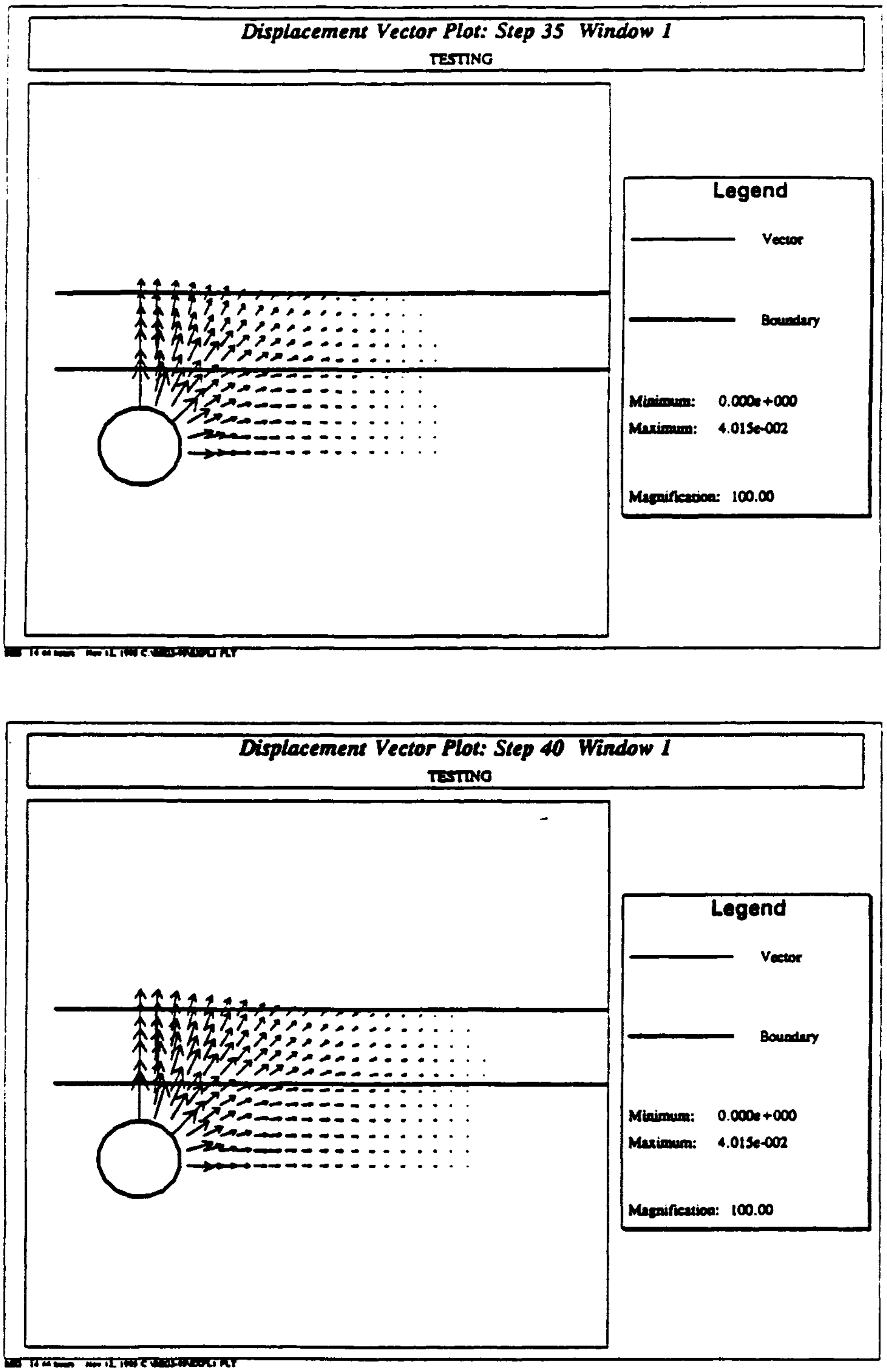

Figure D-41: Displacement vectors at times $35\Delta t$ and $40\Delta t$ for underground explosion in a two-layered rock.

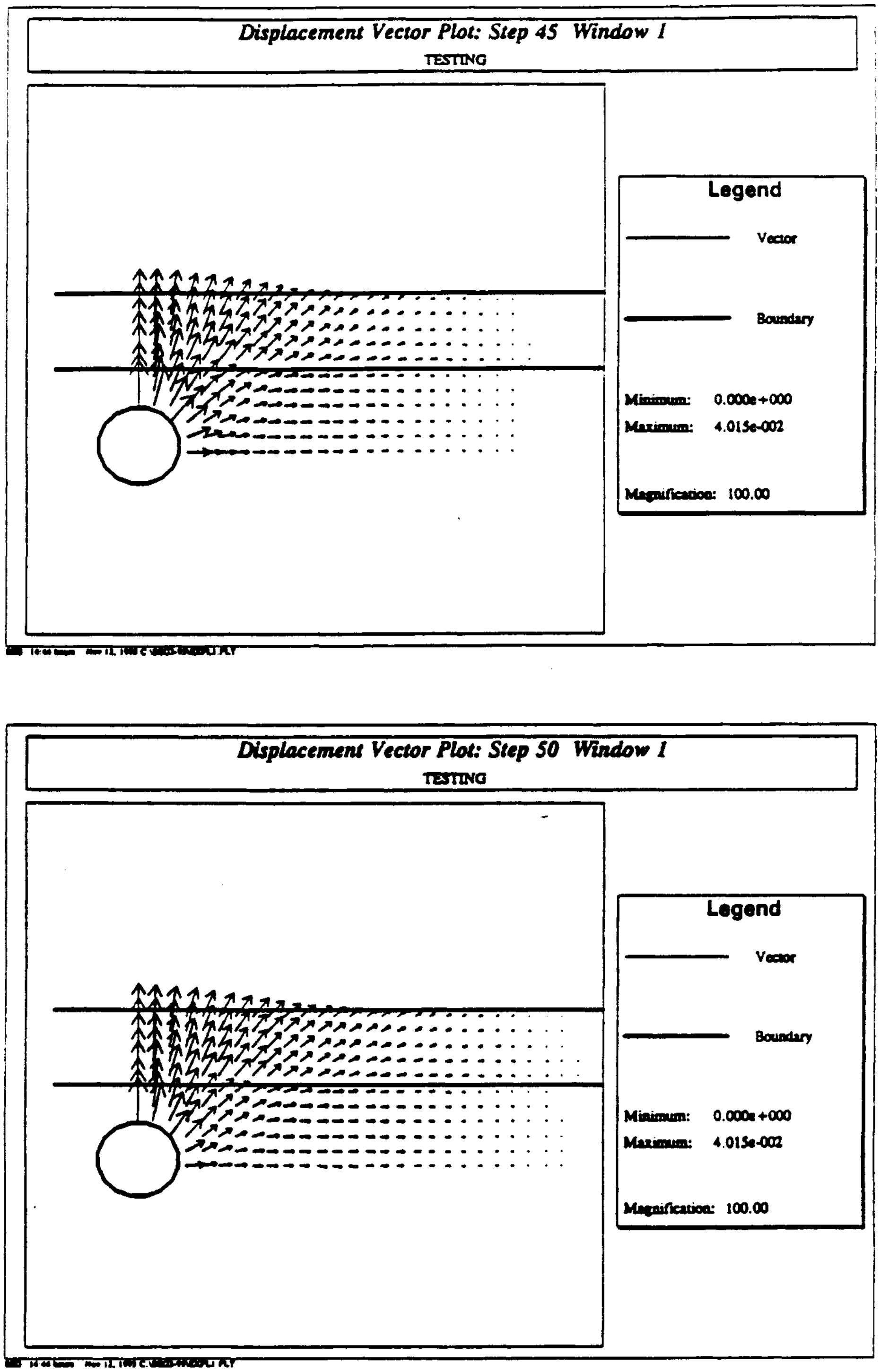

Figure D-42: Displacement vectors at times $45\Delta t$ and $50\Delta t$ for underground explosion in a two-layered rock.

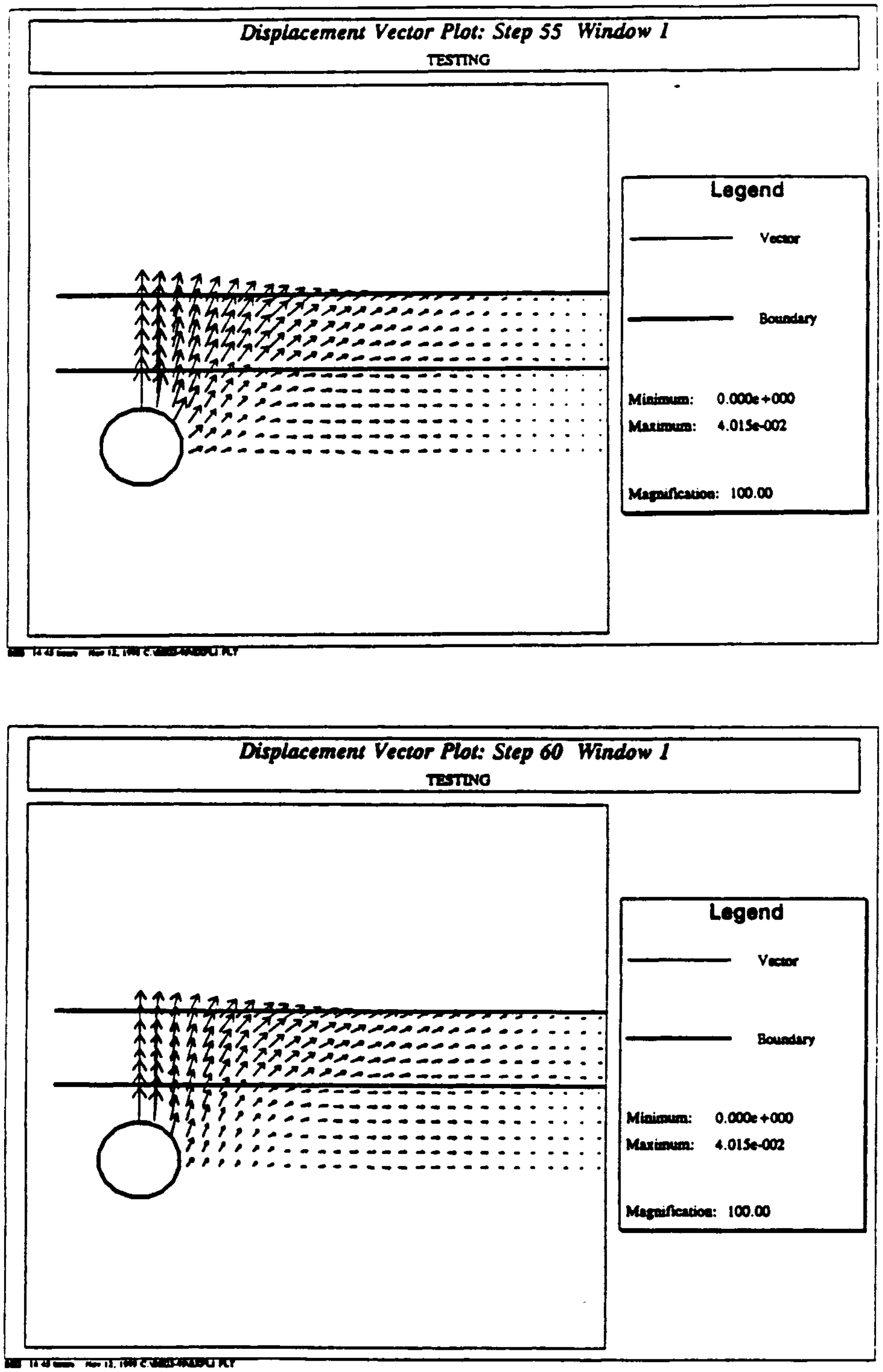
Displacement Vector Plot: Step 55 Window 1

TESTING

Displacement Vector Plot: Step 60 Window 1

TESTING

Figure D-43: Displacement vectors at times $55\Delta t$ and $60\Delta t$ for underground explosion in a two-layered rock.

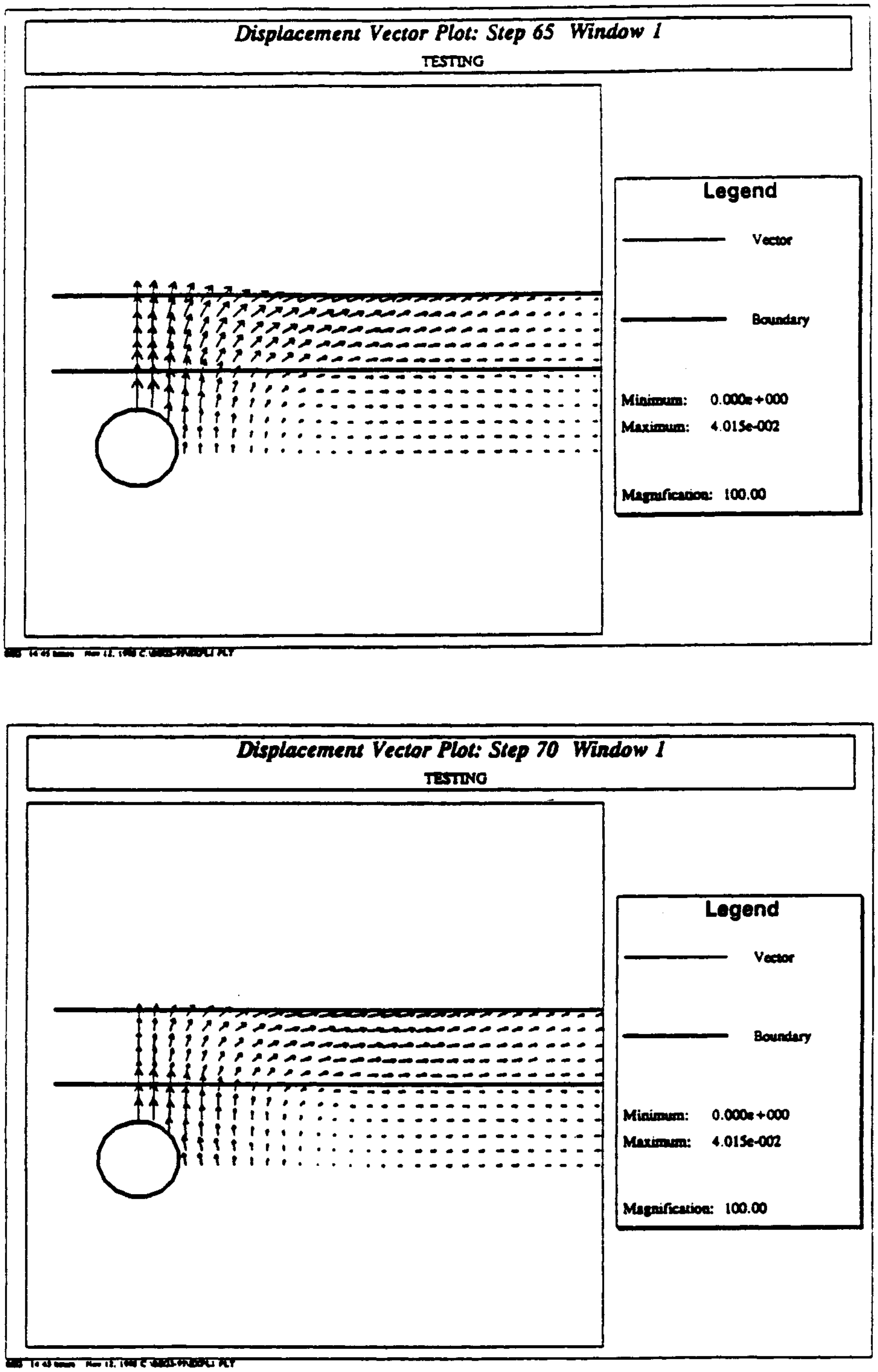

Figure D-44: Displacement vectors at times $65\Delta t$ and $70\Delta t$ for underground explosion in a two-layered rock.

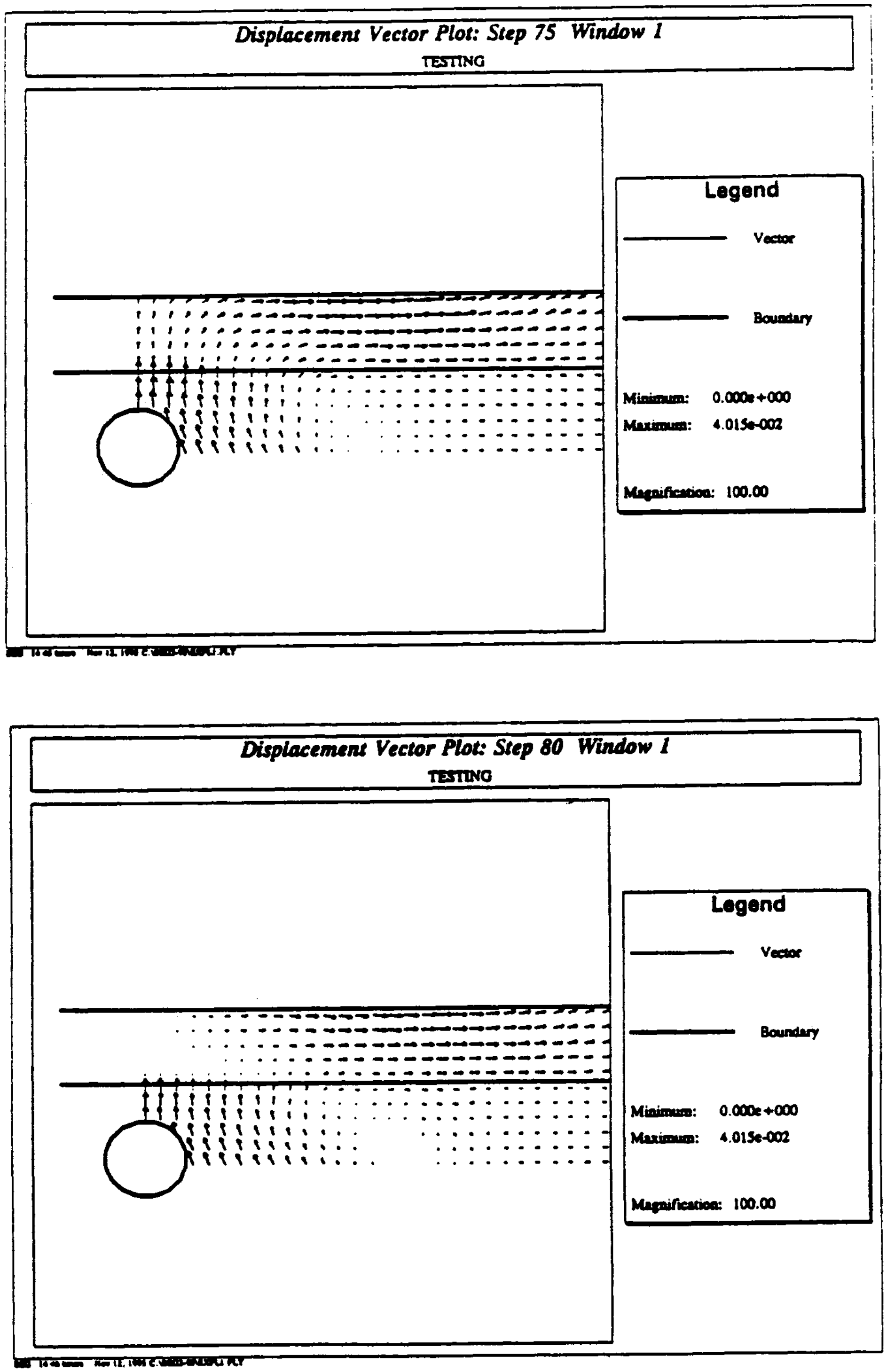

Figure D-45: Displacement vectors at times 75Δt and 80Δt for underground explosion in a two-layered rock.

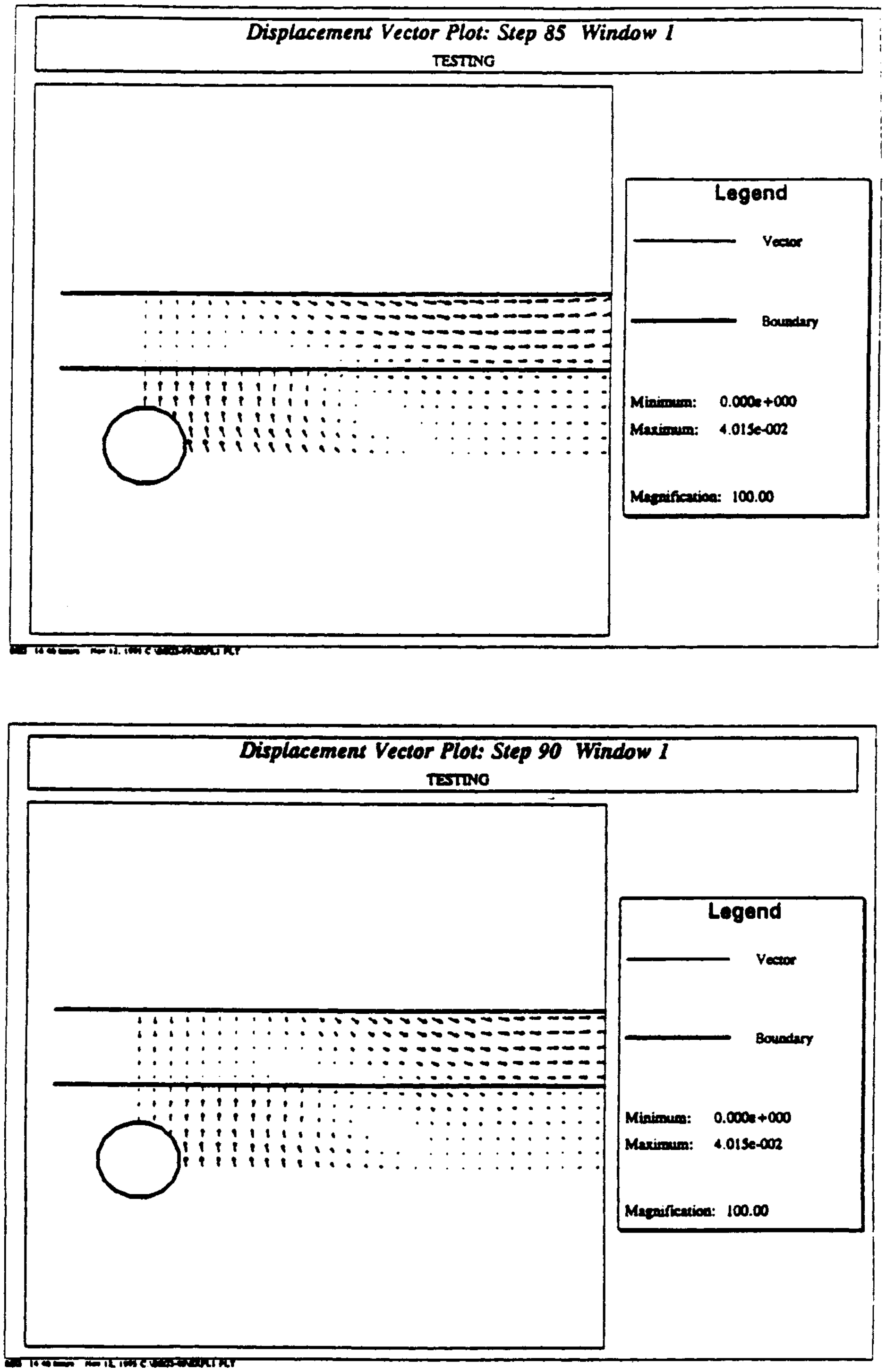

Figure D-46: Displacement vectors at times $85\Delta t$ and $90\Delta t$ for underground explosion in a two-layered rock.

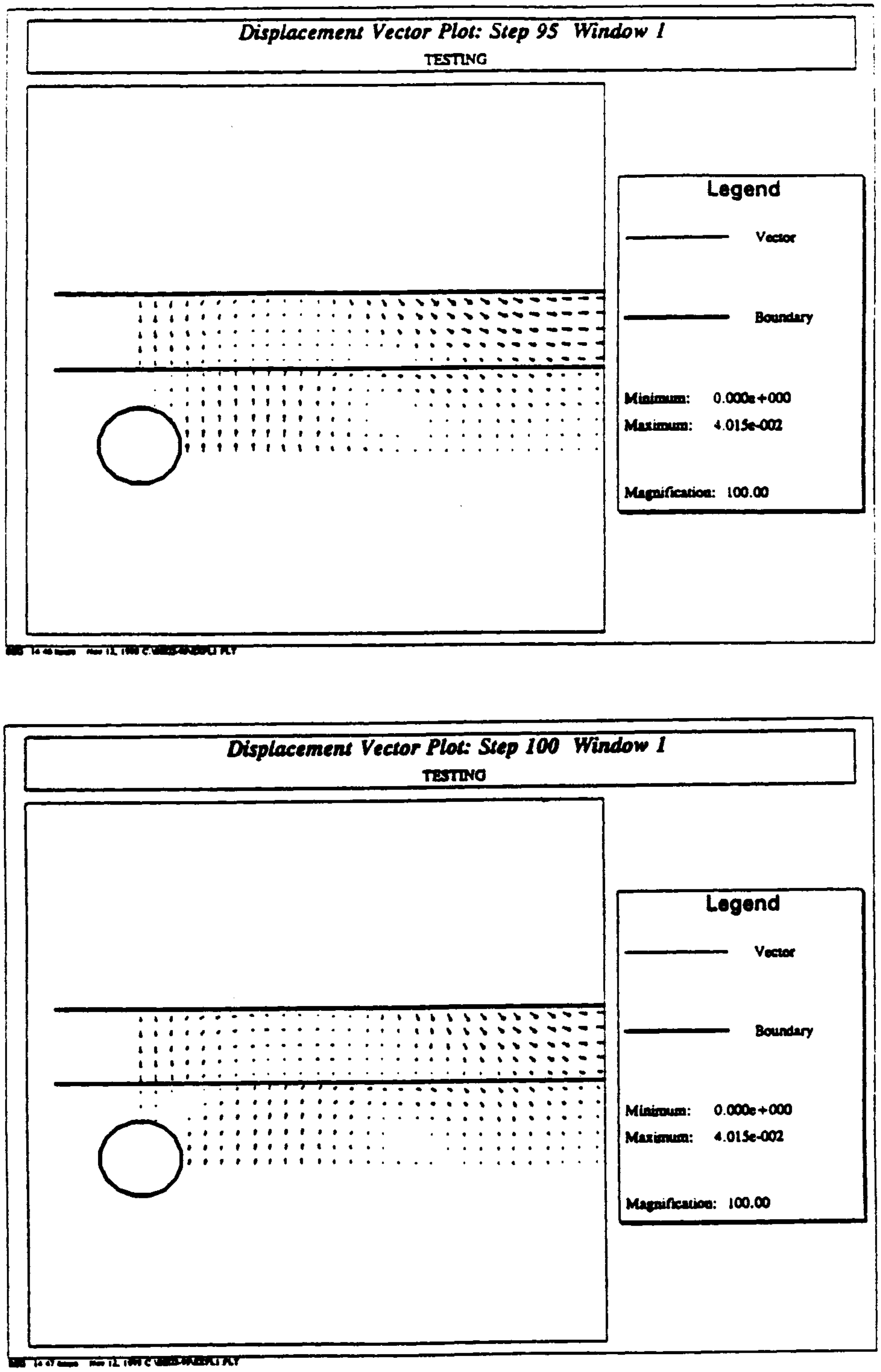

Figure D-47: Displacement vectors at times $95\Delta t$ and $100\Delta t$ for underground explosion in a two-layered rock.

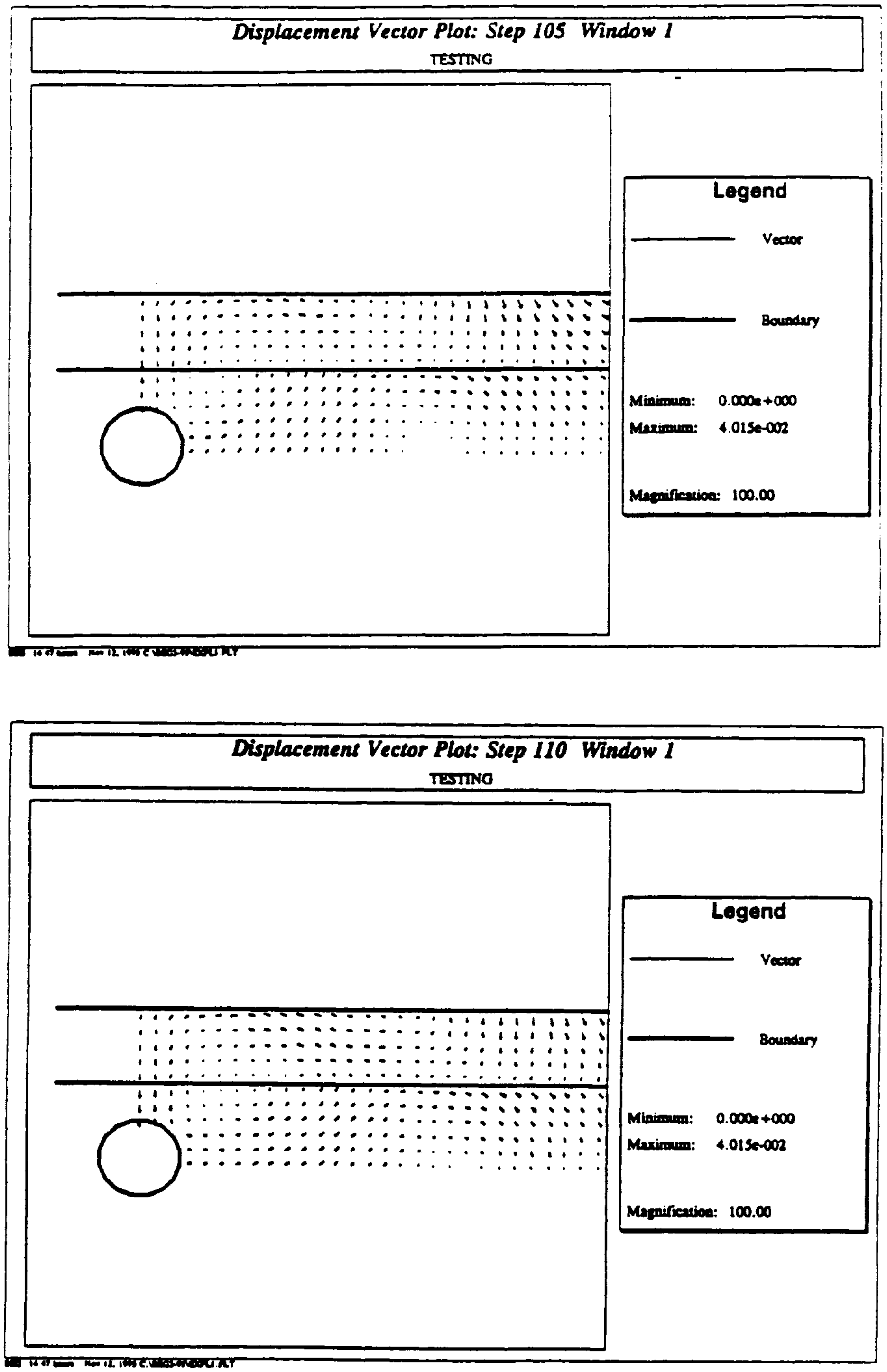

Figure D-48: Displacement vectors at times 105Δt and 110Δt for underground explosion in a two-layered rock.

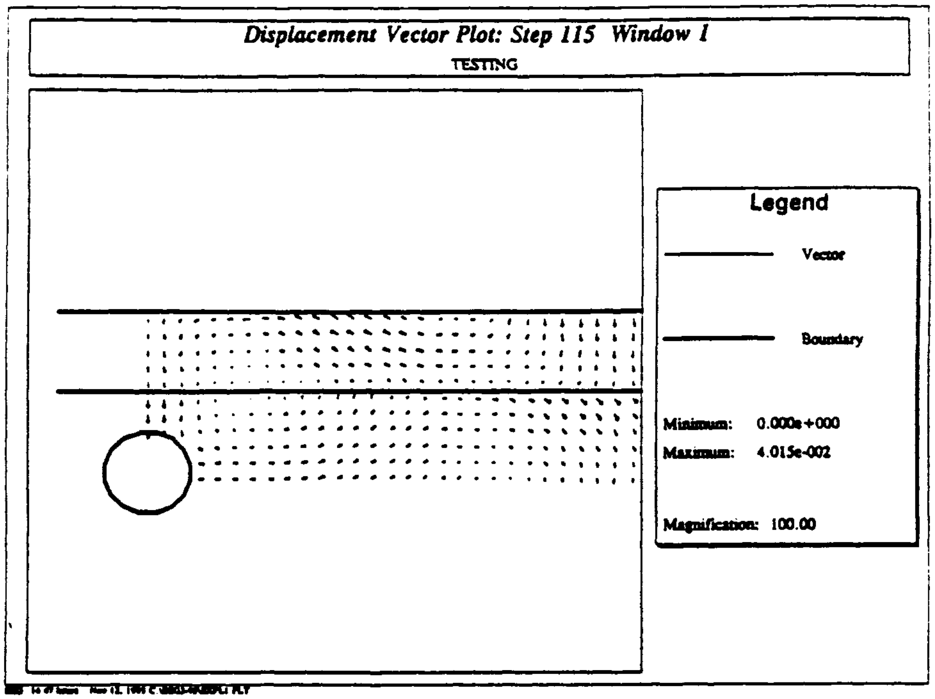

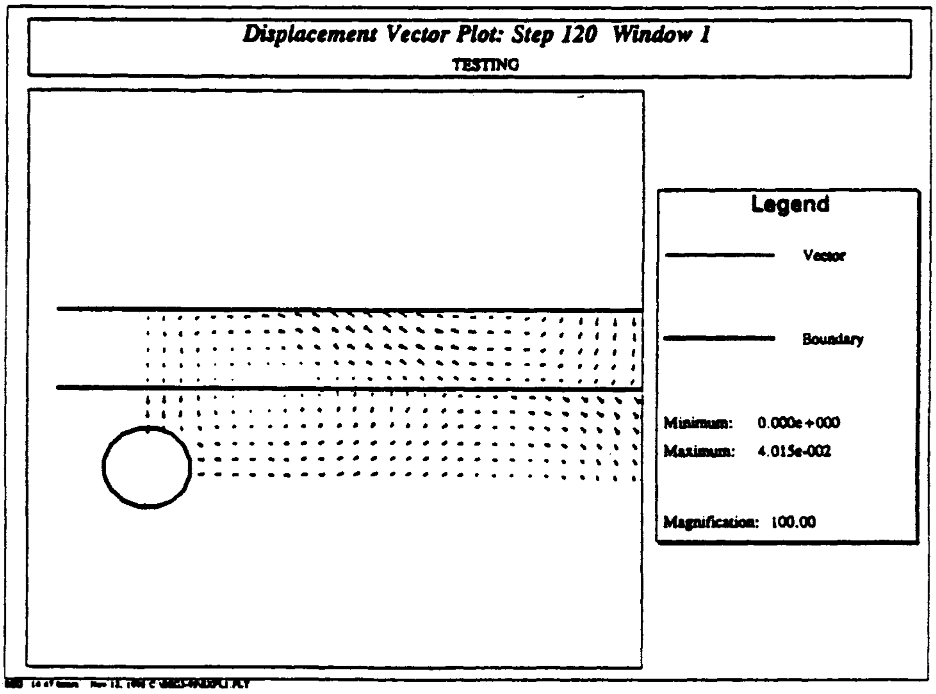

Figure D-49: Displacement vectors at times $115\Delta t$ and $120\Delta t$ for underground explosion in a two-layered rock.

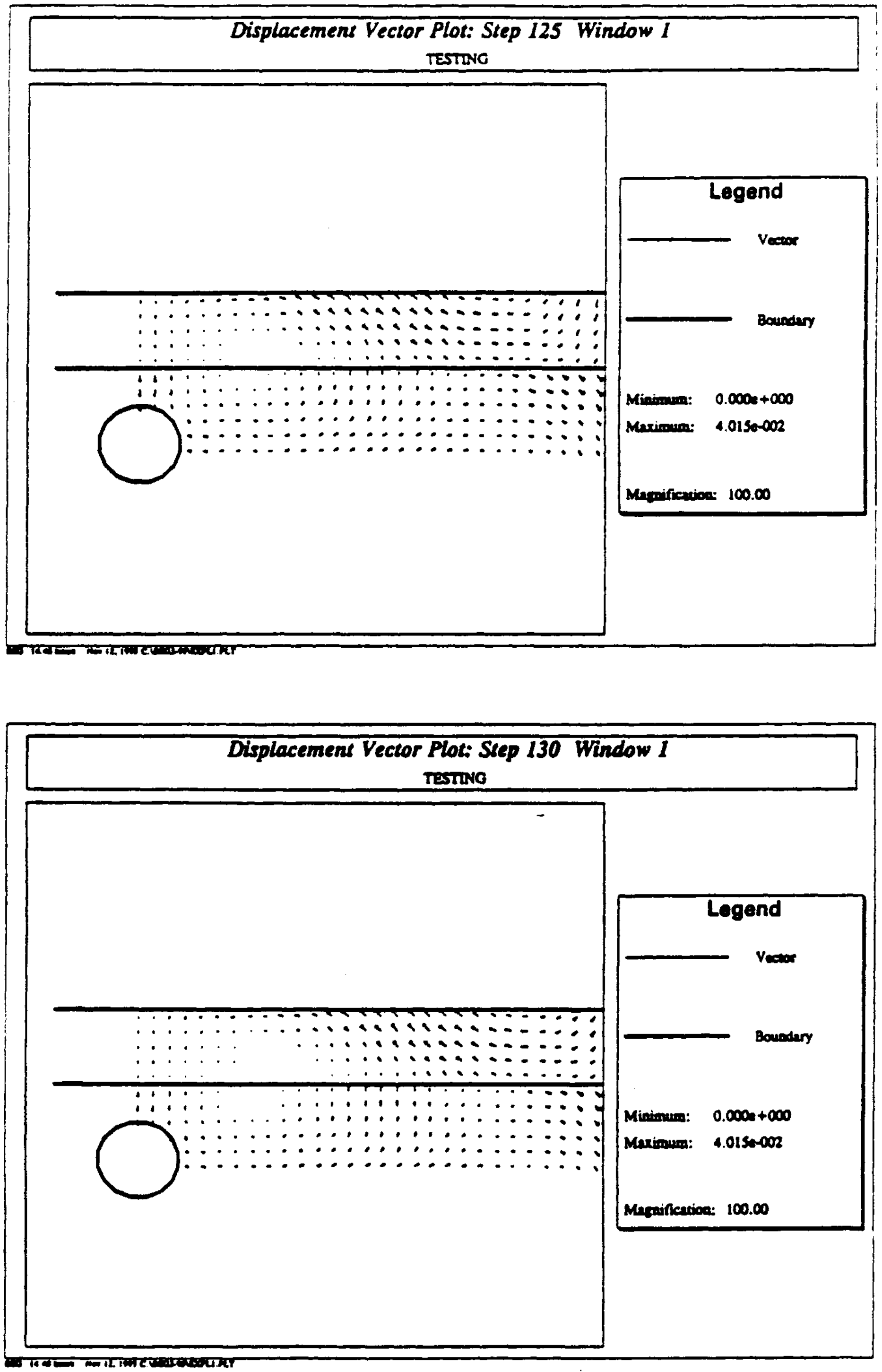

Figure D-50: Displacement vectors at times 125Δt and 130Δt for underground explosion in a two-layered rock.

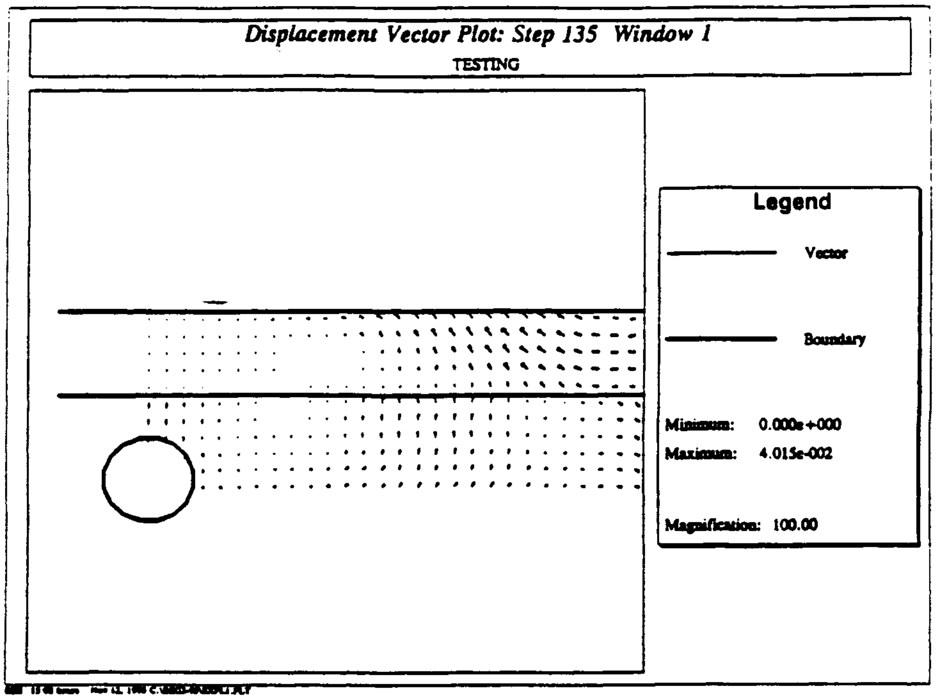

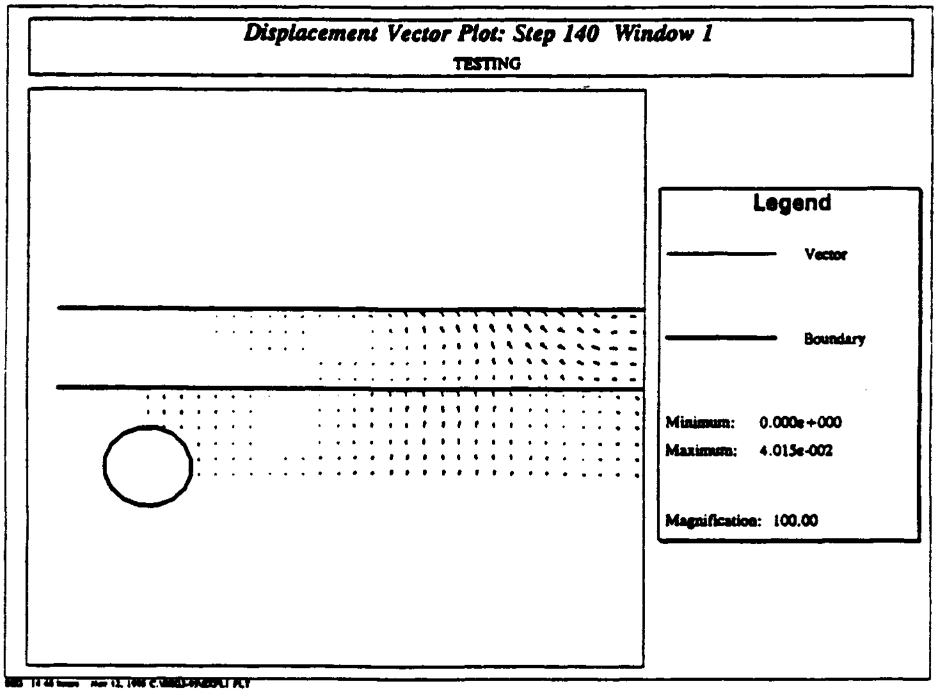

Figure D-51: Displacement vectors at times 135Δt and 140Δt for underground explosion in a two-layered rock.

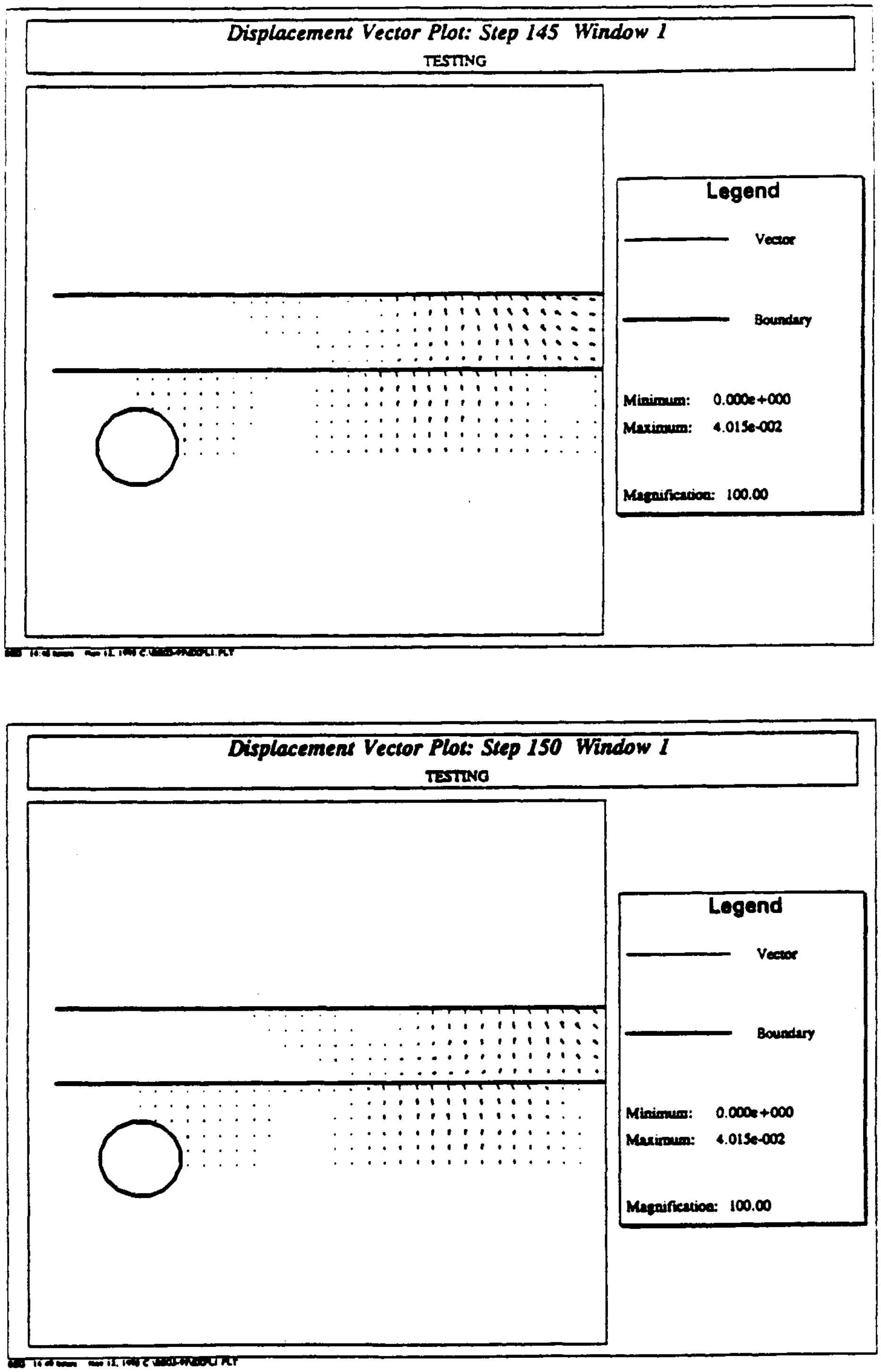

Figure D-52: Displacement vectors at times $145\Delta t$ and $150\Delta t$ for underground explosion in a two-layered rock.

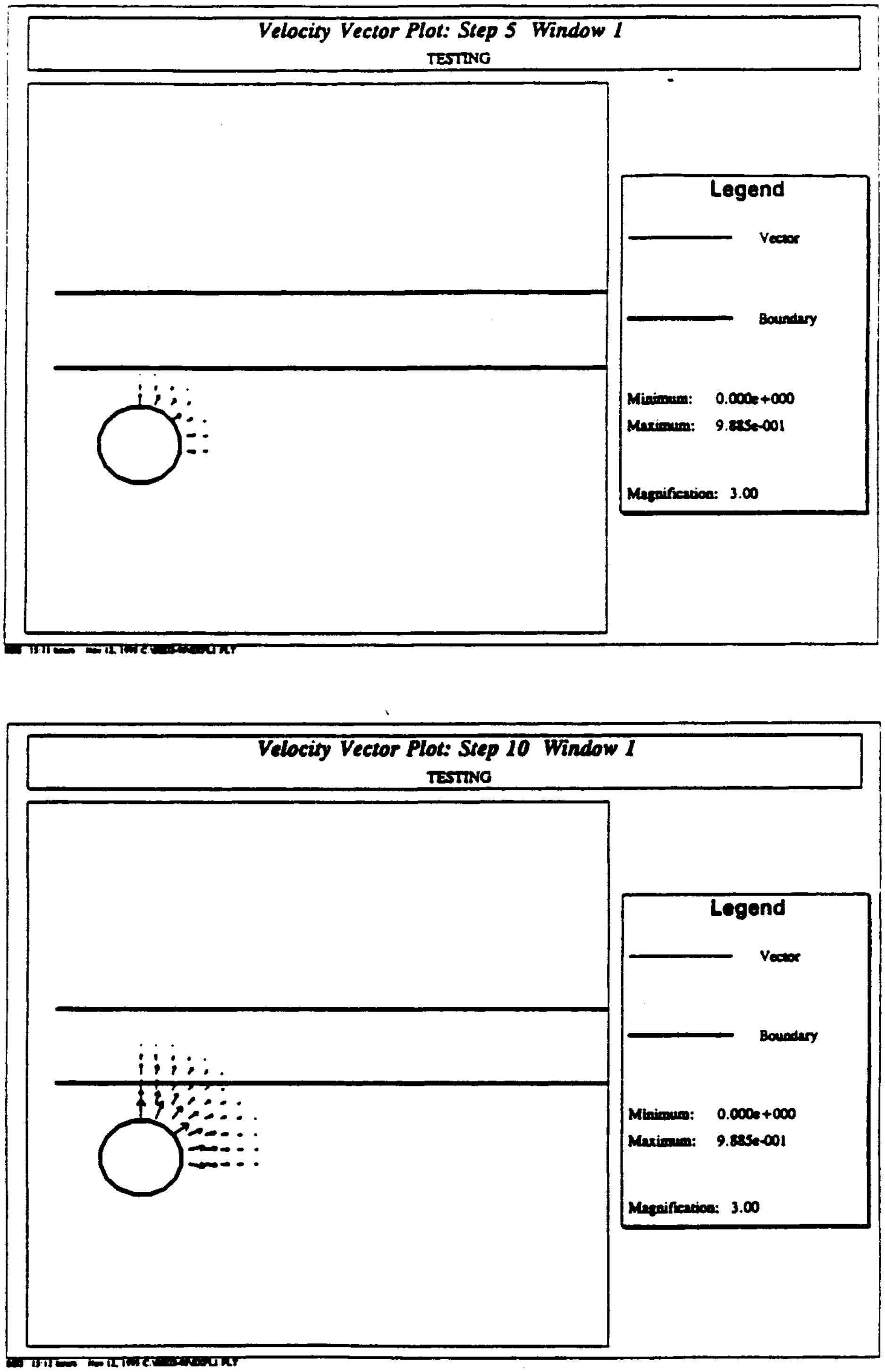

Figure D-53: Velocity vectors at times $5\Delta t$ and $10\Delta t$ for underground explosion in a two-layered rock.

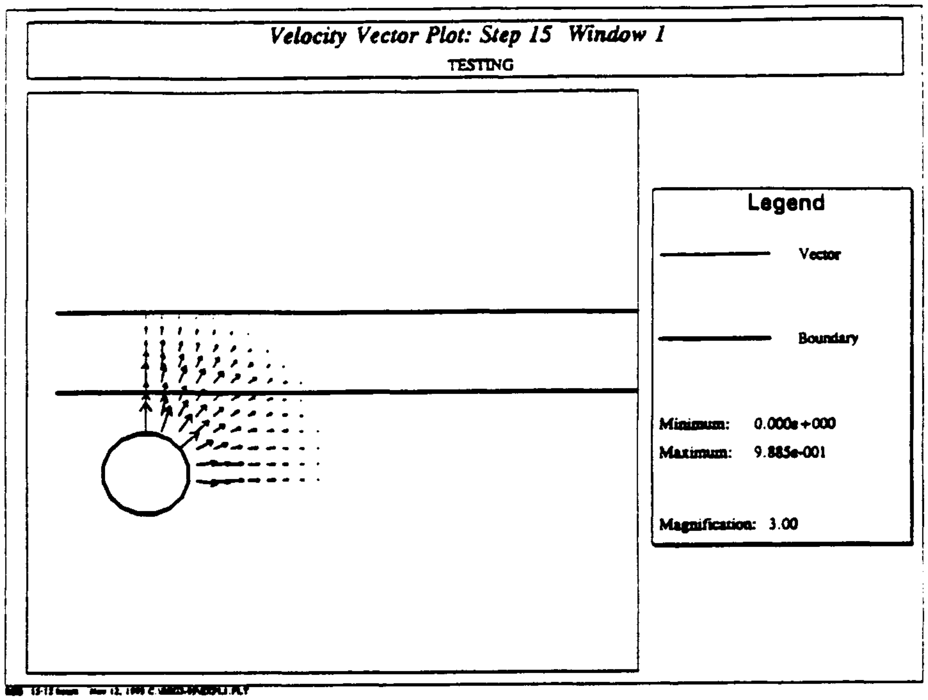

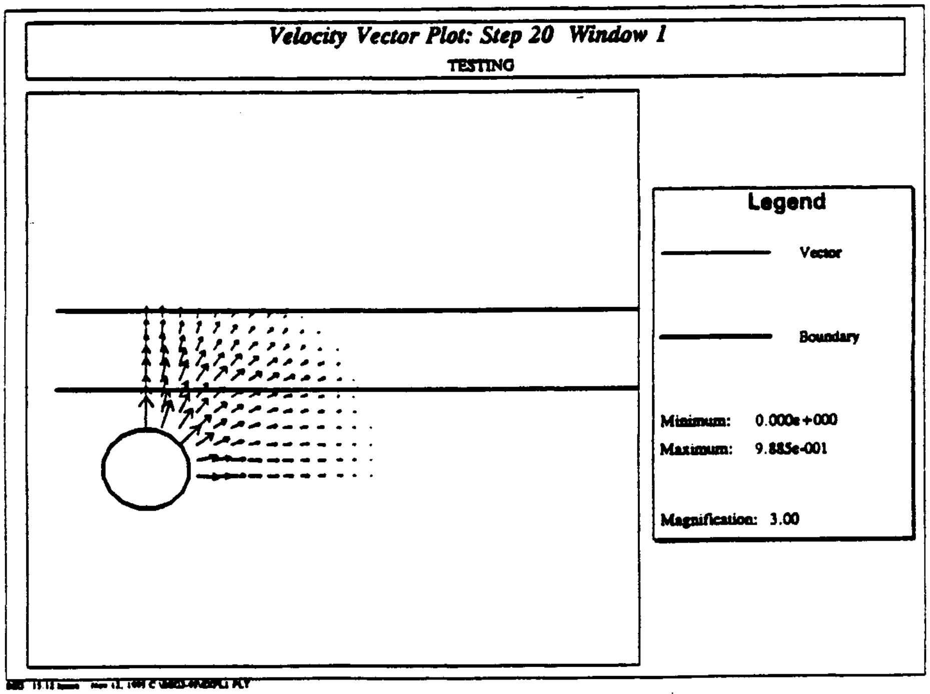

Figure D-54: Velocity vectors at times $15\Delta t$ and $20\Delta t$ for underground explosion in a two-layered rock.

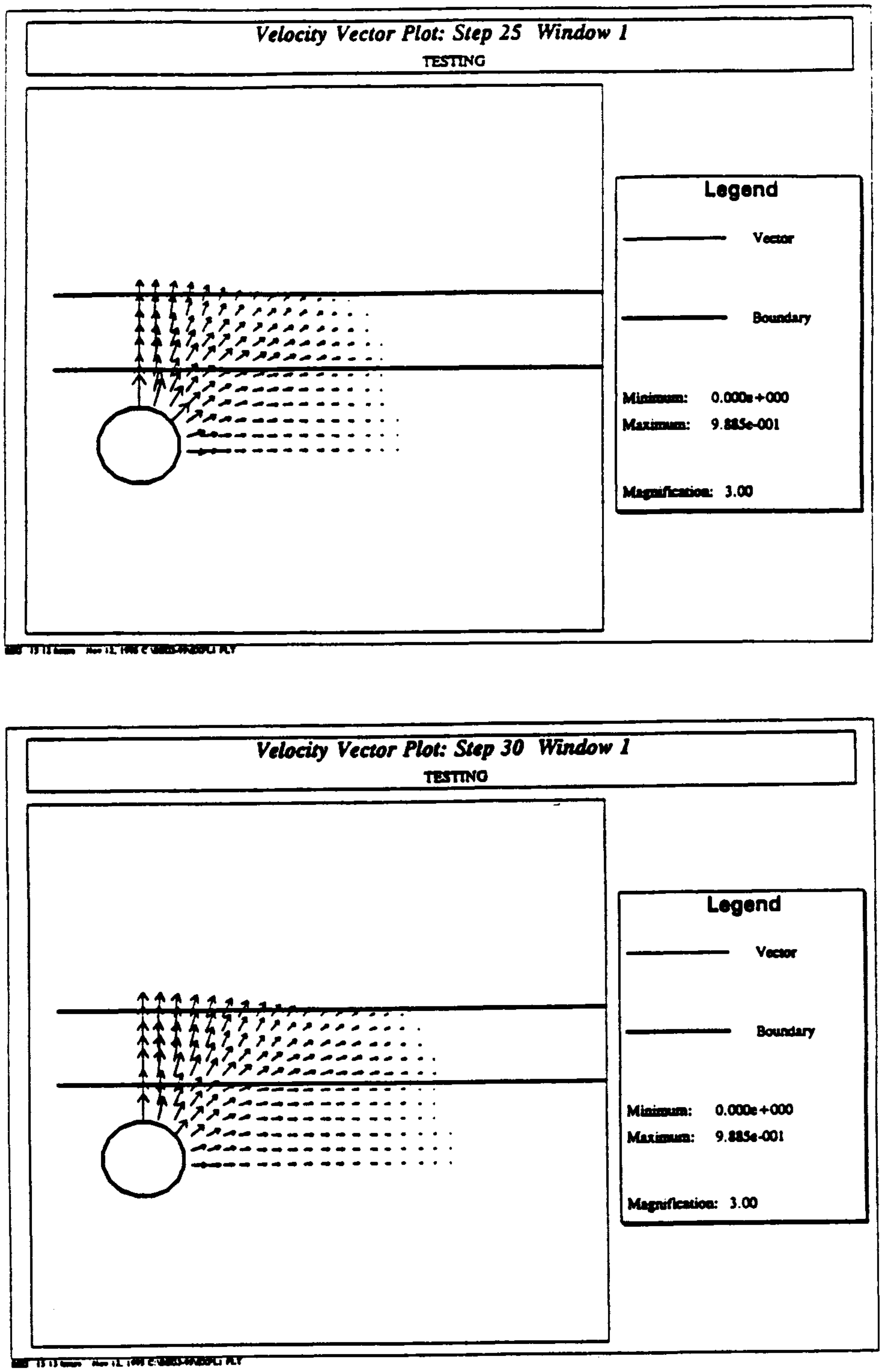

Figure D-55: Velocity vectors at times $25\Delta t$ and $30\Delta t$ for underground explosion in a two-layered rock.

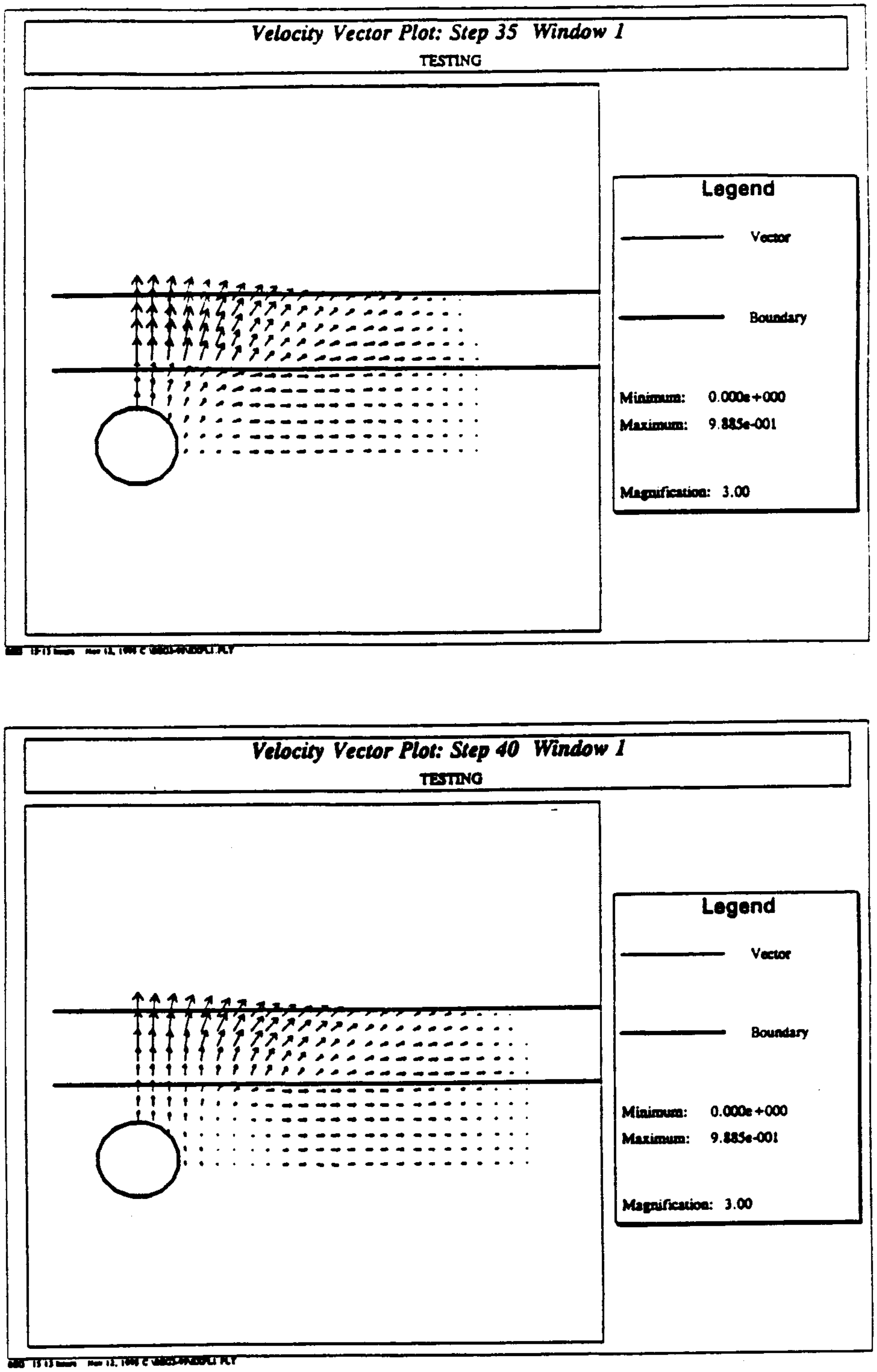

Figure D-56: Velocity vectors at times $35\Delta t$ and $40\Delta t$ for underground explosion in a two-layered rock.

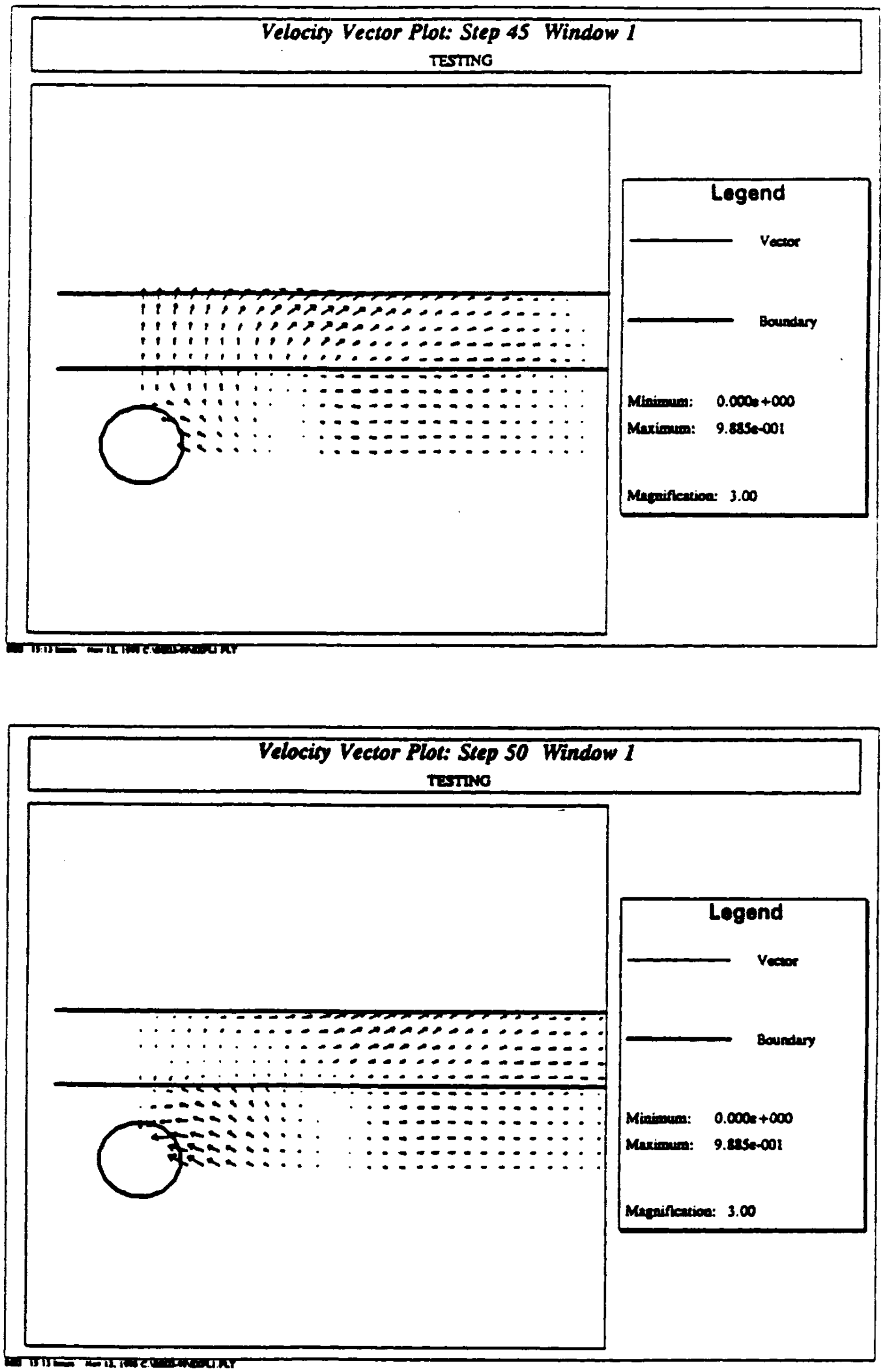

Figure D-57: Velocity vectors at times $45\Delta t$ and $50\Delta t$ for underground explosion in a two-layered rock.

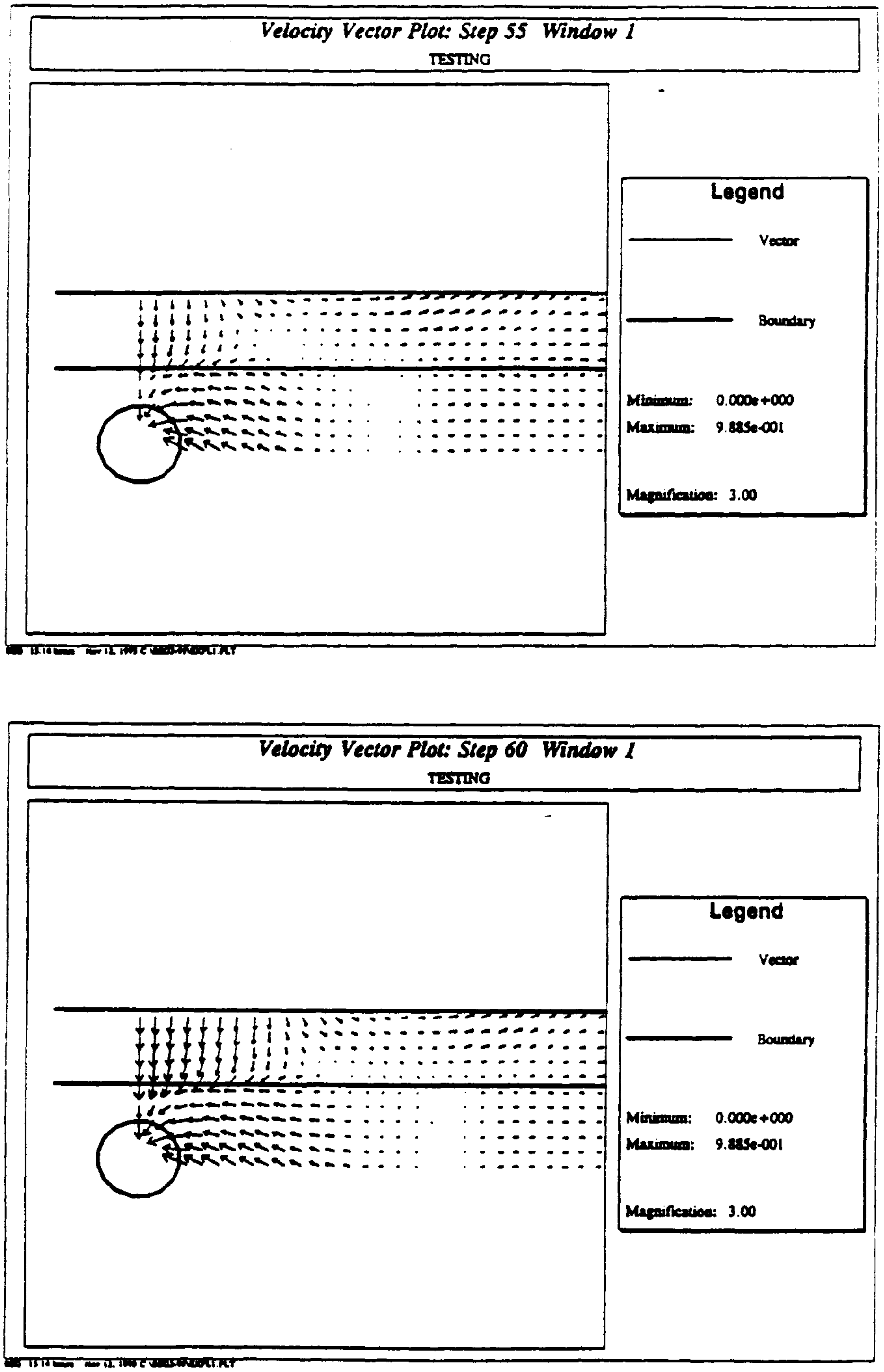

Figure D-58: Velocity vectors at times $55\Delta t$ and $60\Delta t$ for underground explosion in a two-layered rock.

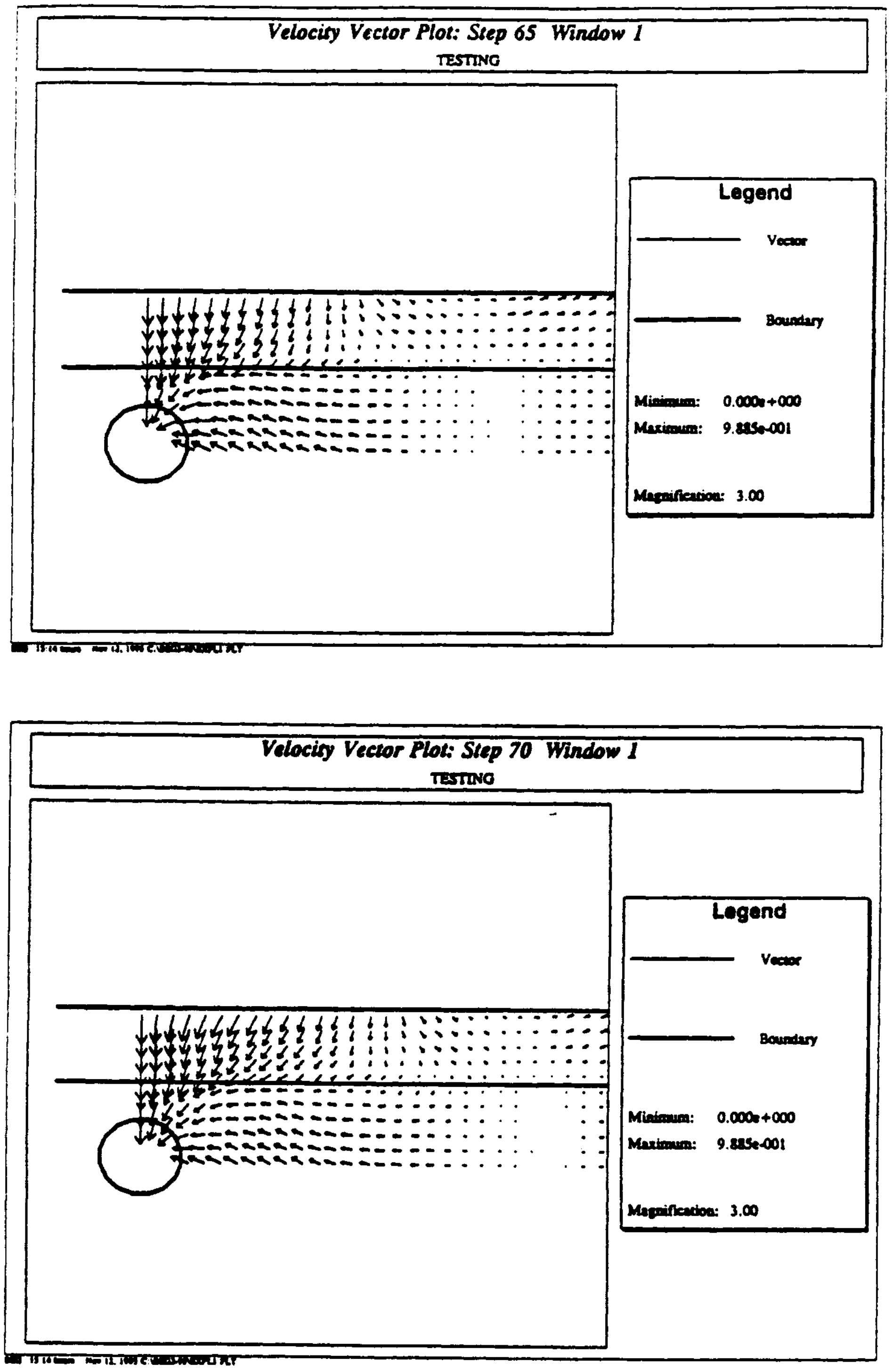

Figure D-59: Velocity vectors at times $65\Delta t$ and $70\Delta t$ for underground explosion in a two-layered rock.

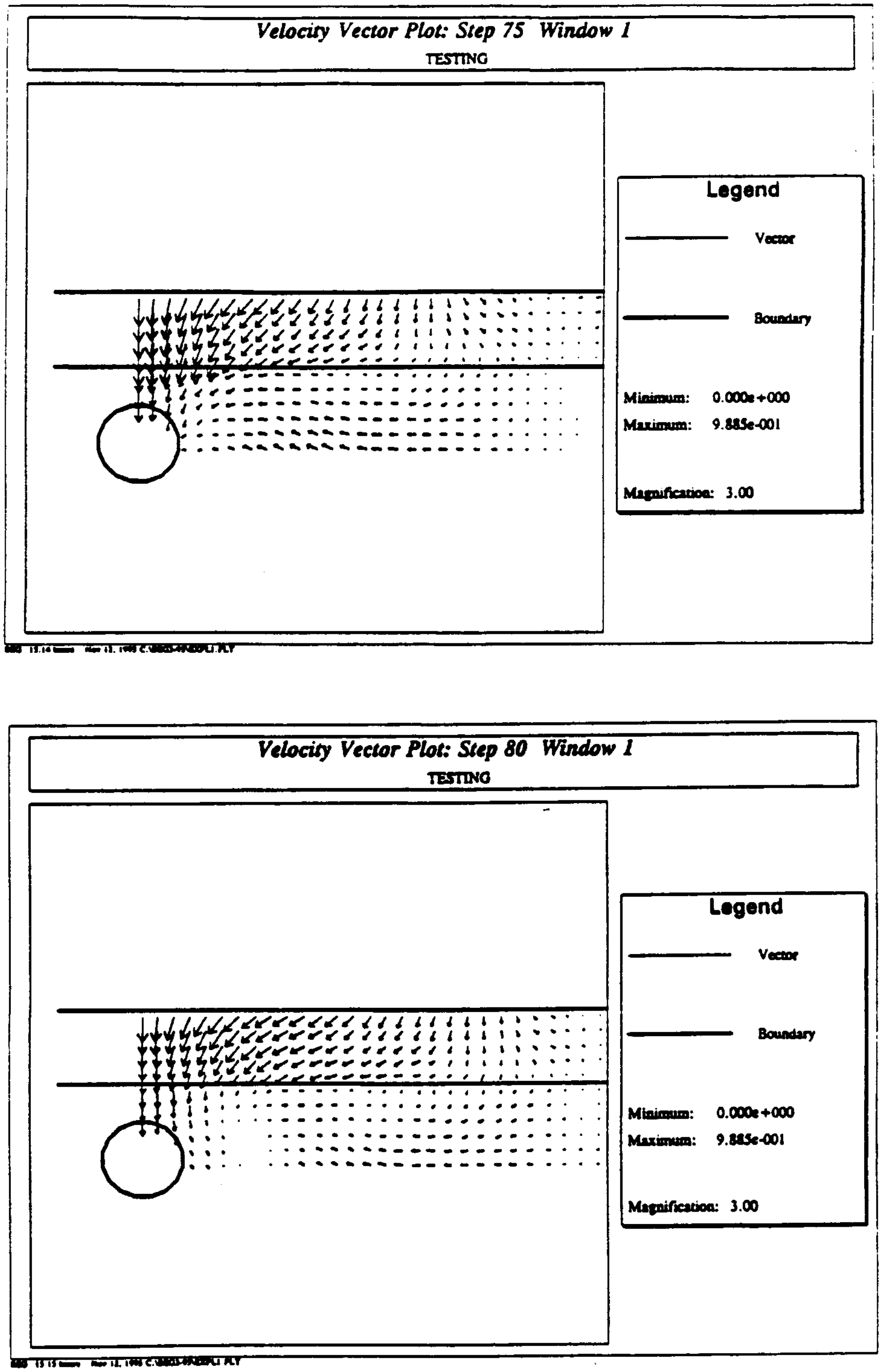

Figure D-60: Velocity vectors at times $75\Delta t$ and $80\Delta t$ for underground explosion in a two-layered rock.

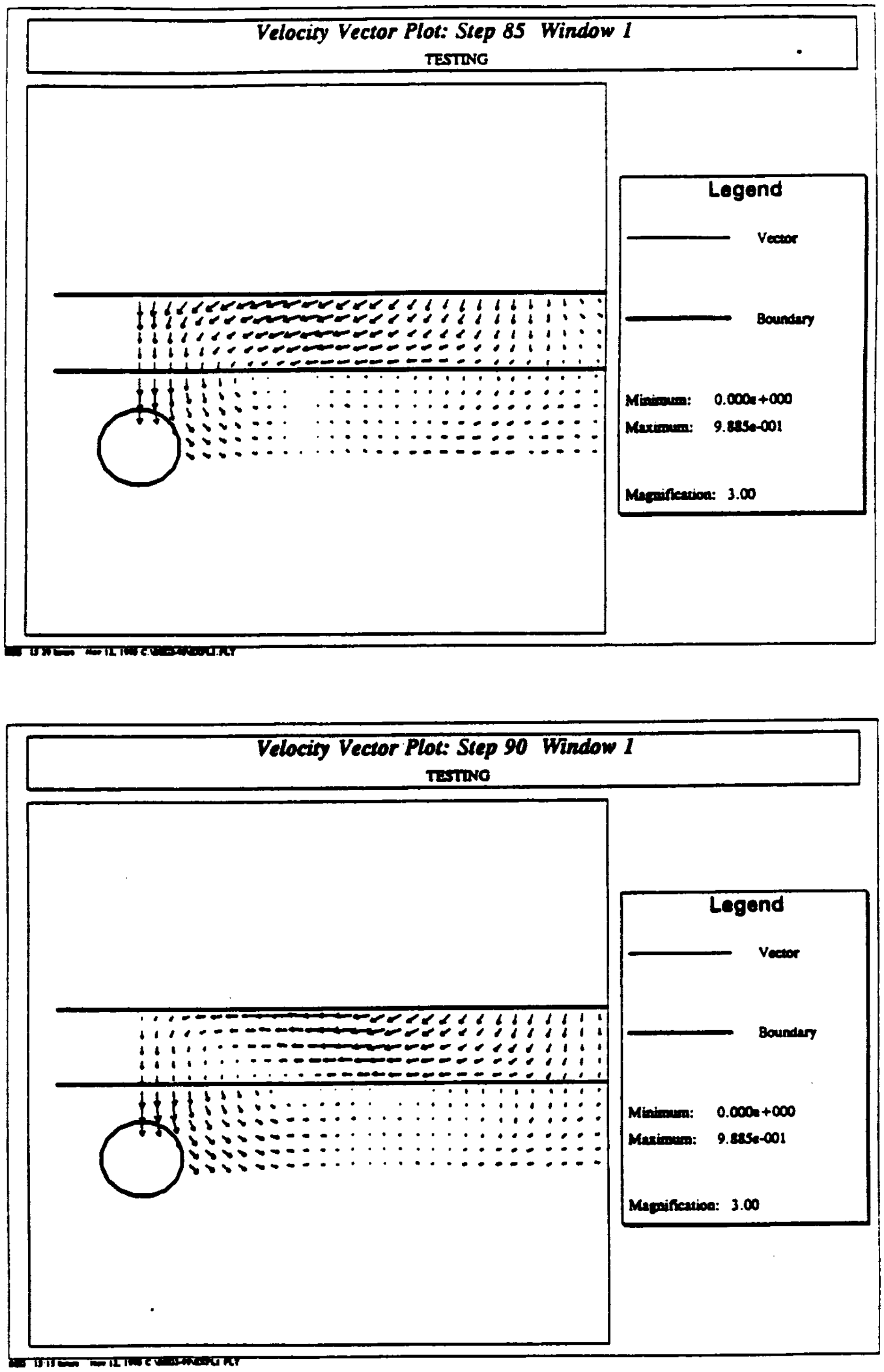

Figure D-61: Velocity vectors at times 85Δt and 90Δt for underground explosion in a two-layered rock.

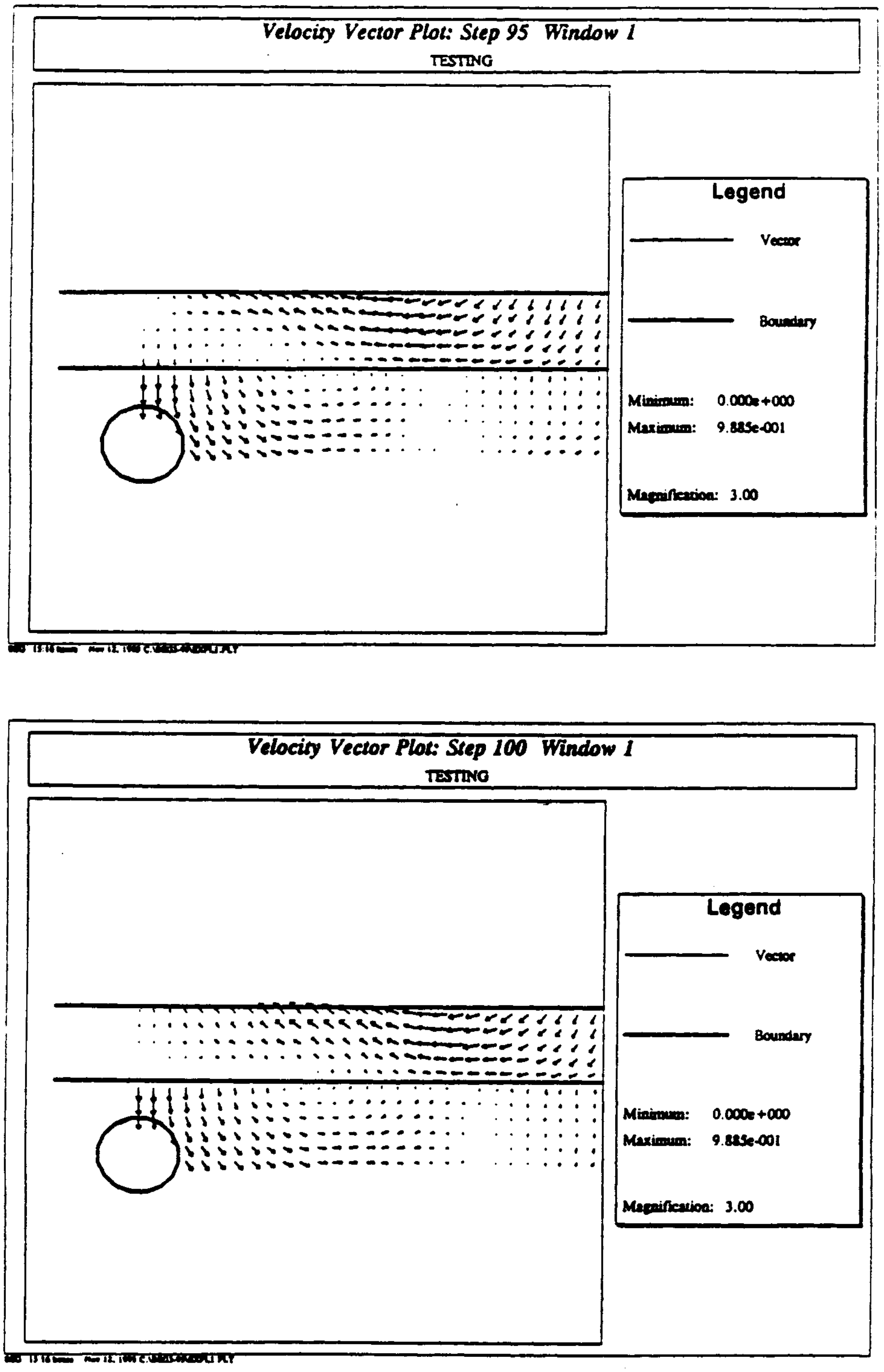

Figure D-62: Velocity vectors at times $95\Delta t$ and $100\Delta t$ for underground explosion in a two-layered rock.

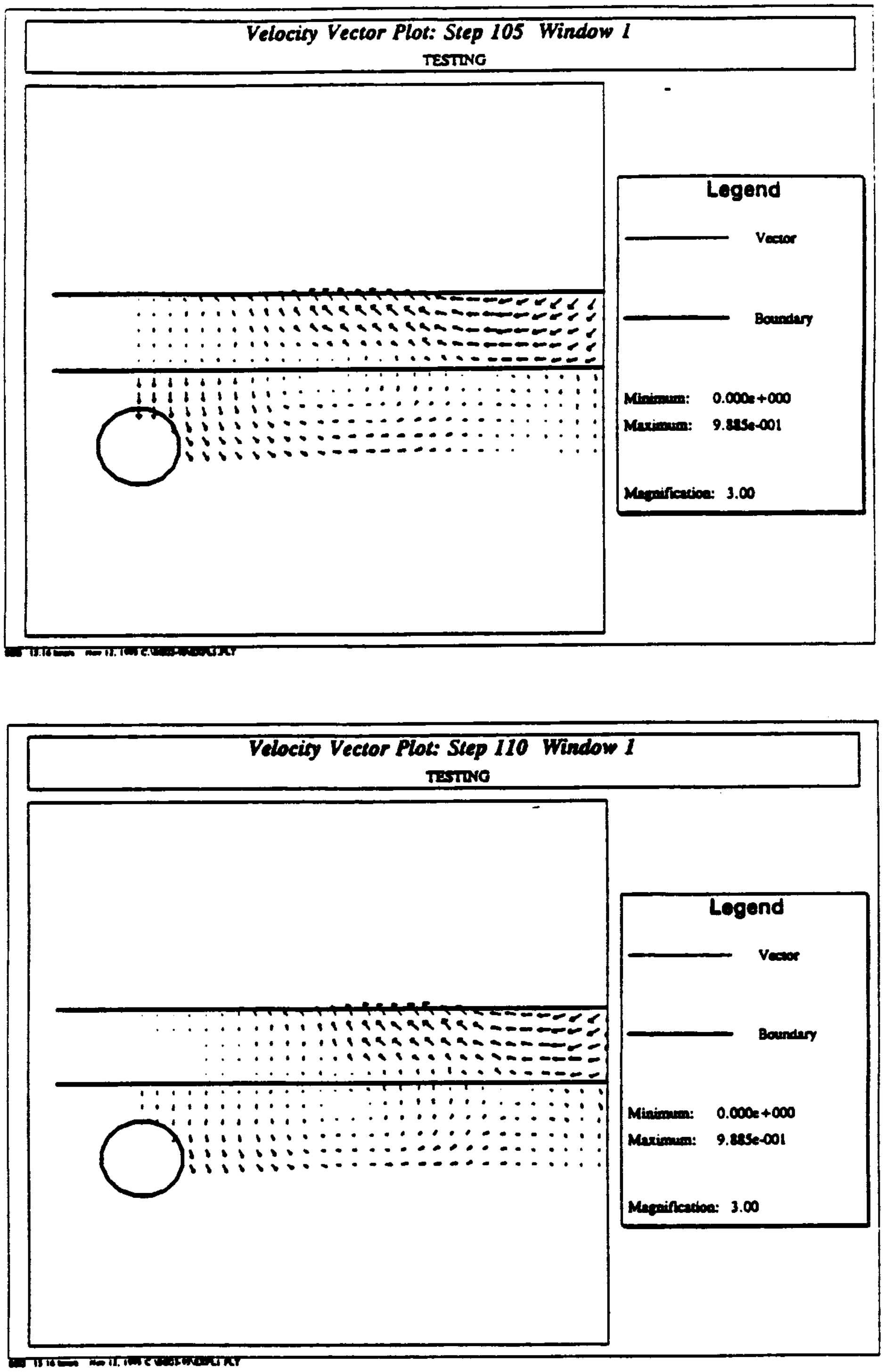

Figure D-63: Velocity vectors at times $105\Delta t$ and $110\Delta t$ for underground explosion in a two-layered rock.

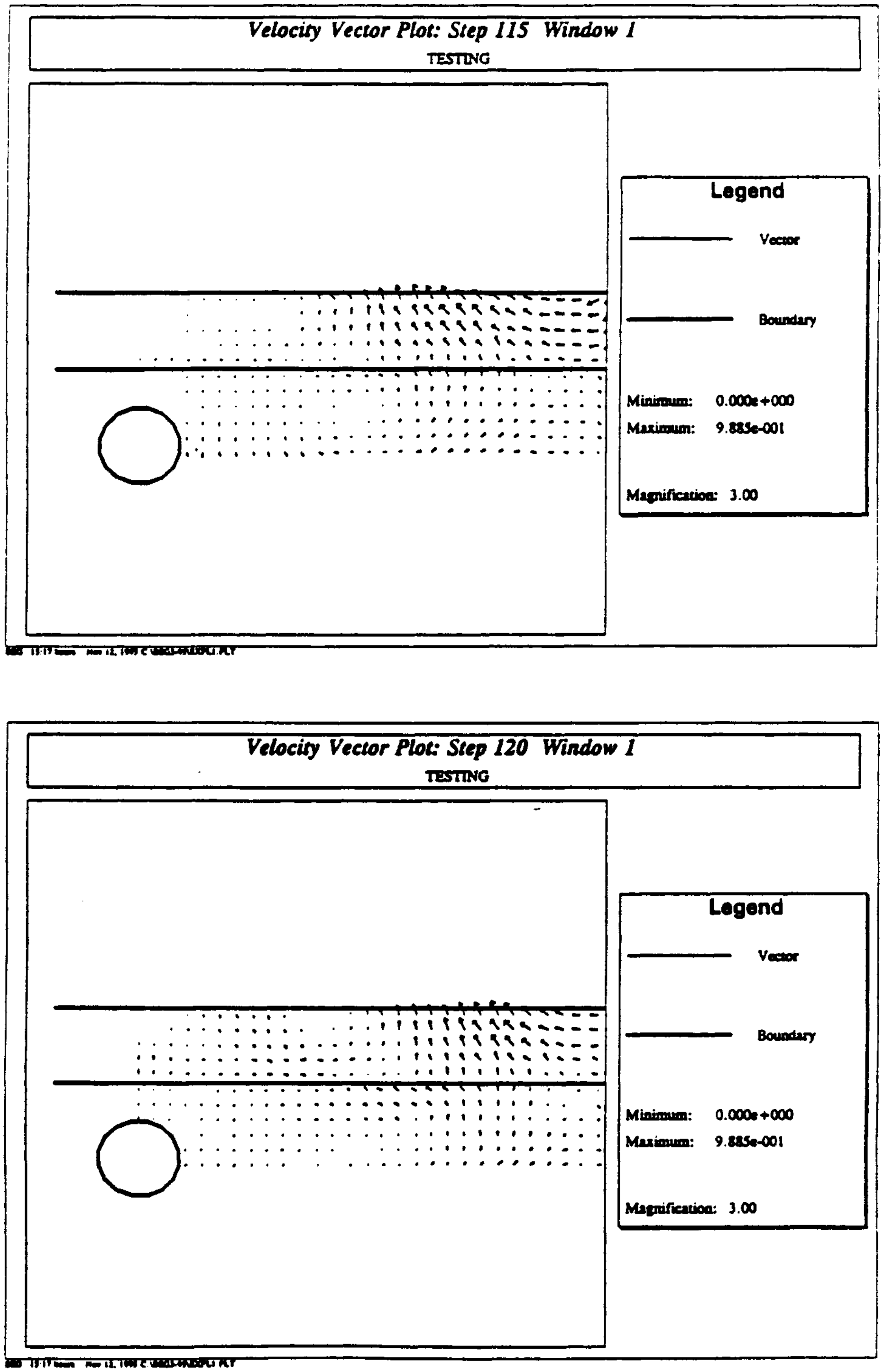

Figure D-64: Velocity vectors at times 115Δt and 120Δt for underground explosion in a two-layered rock.

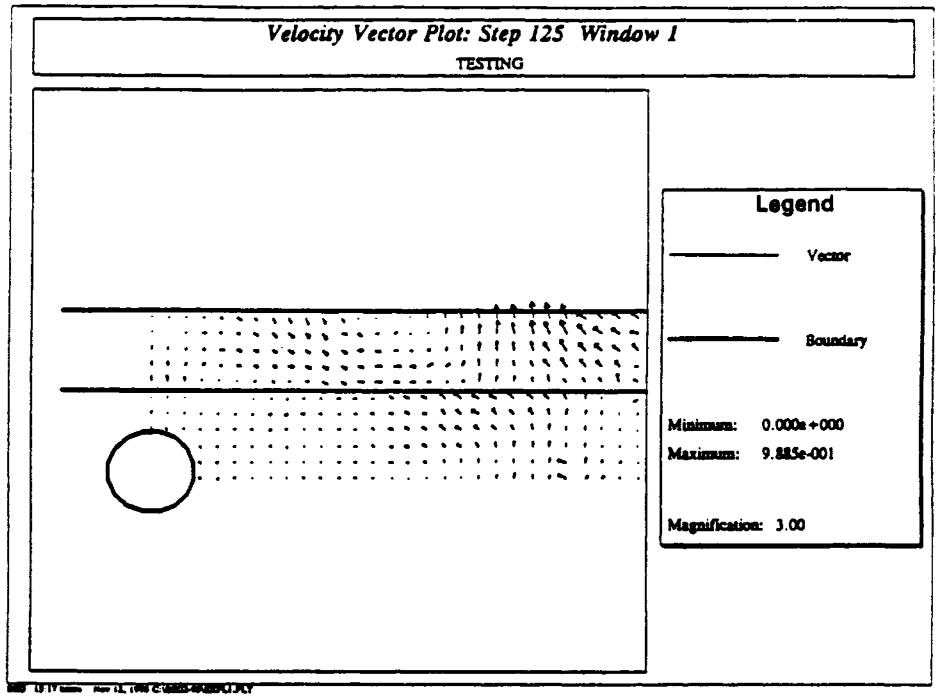

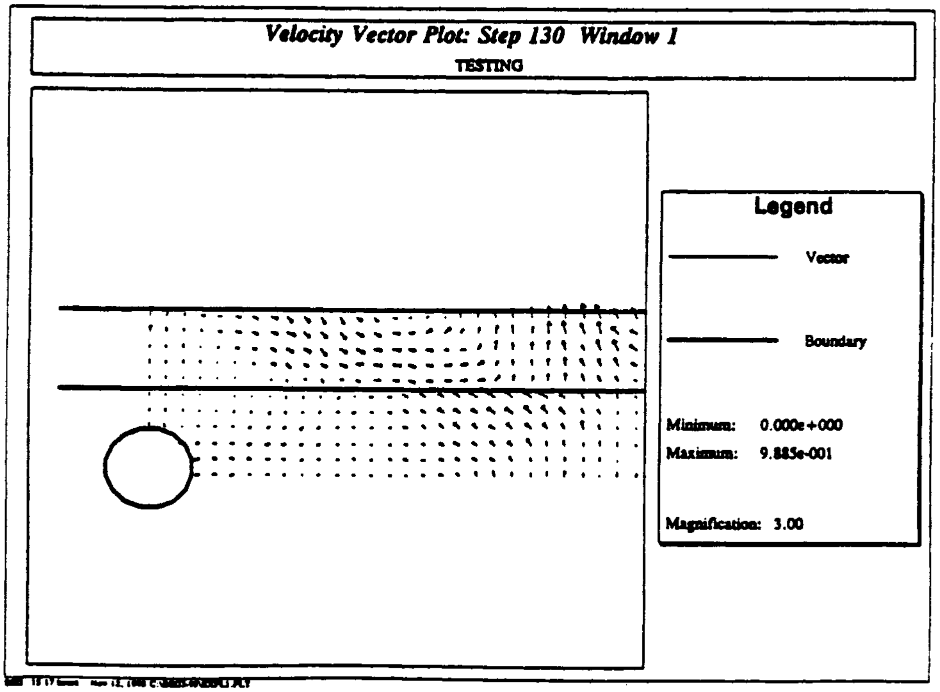

Figure D-65: Velocity vectors at times $125\Delta t$ and $130\Delta t$ for underground explosion in a two-layered rock.

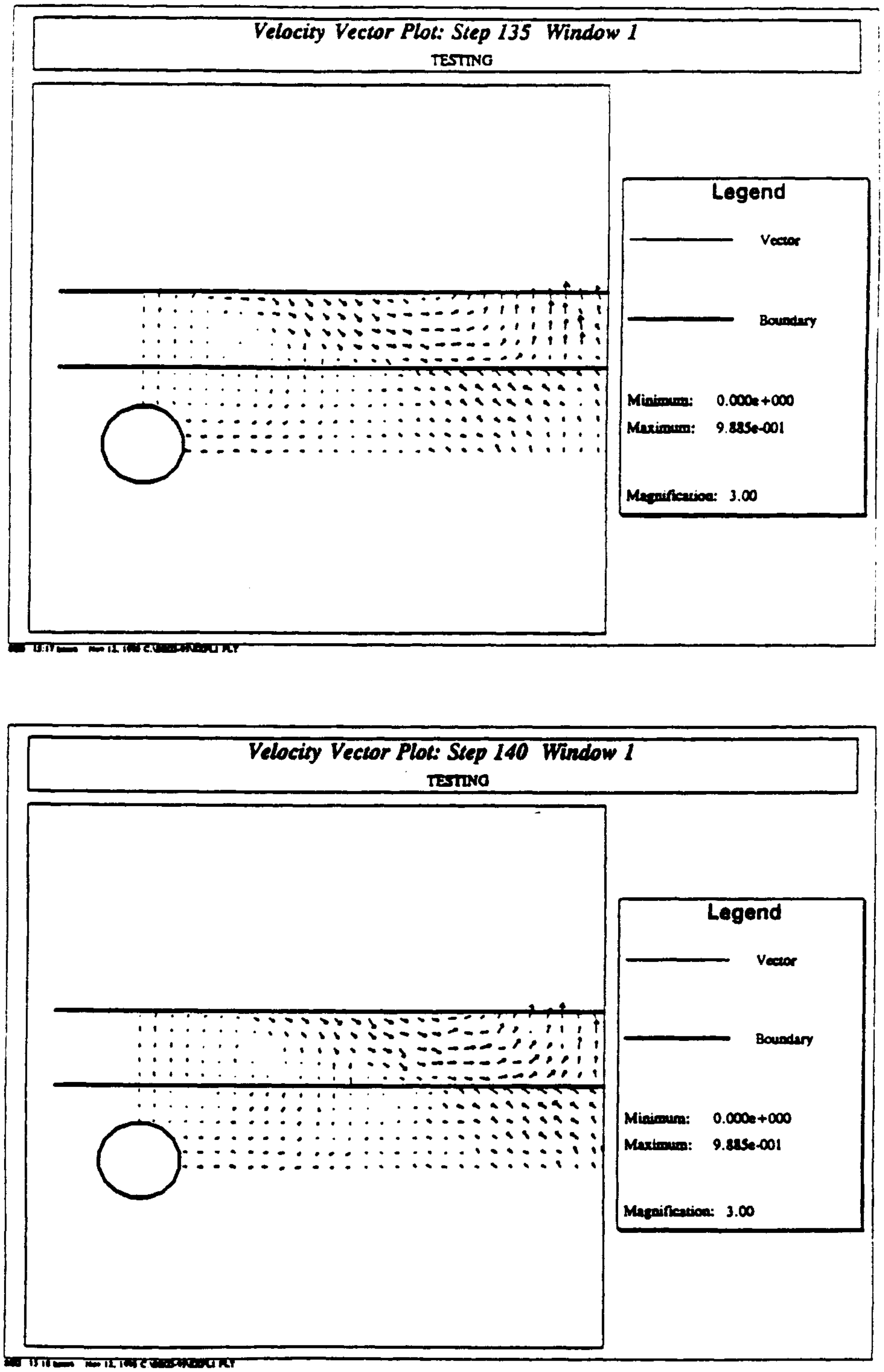

Figure D-66: Velocity vectors at times 135Δt and 140Δt for underground explosion in a two-layered rock.

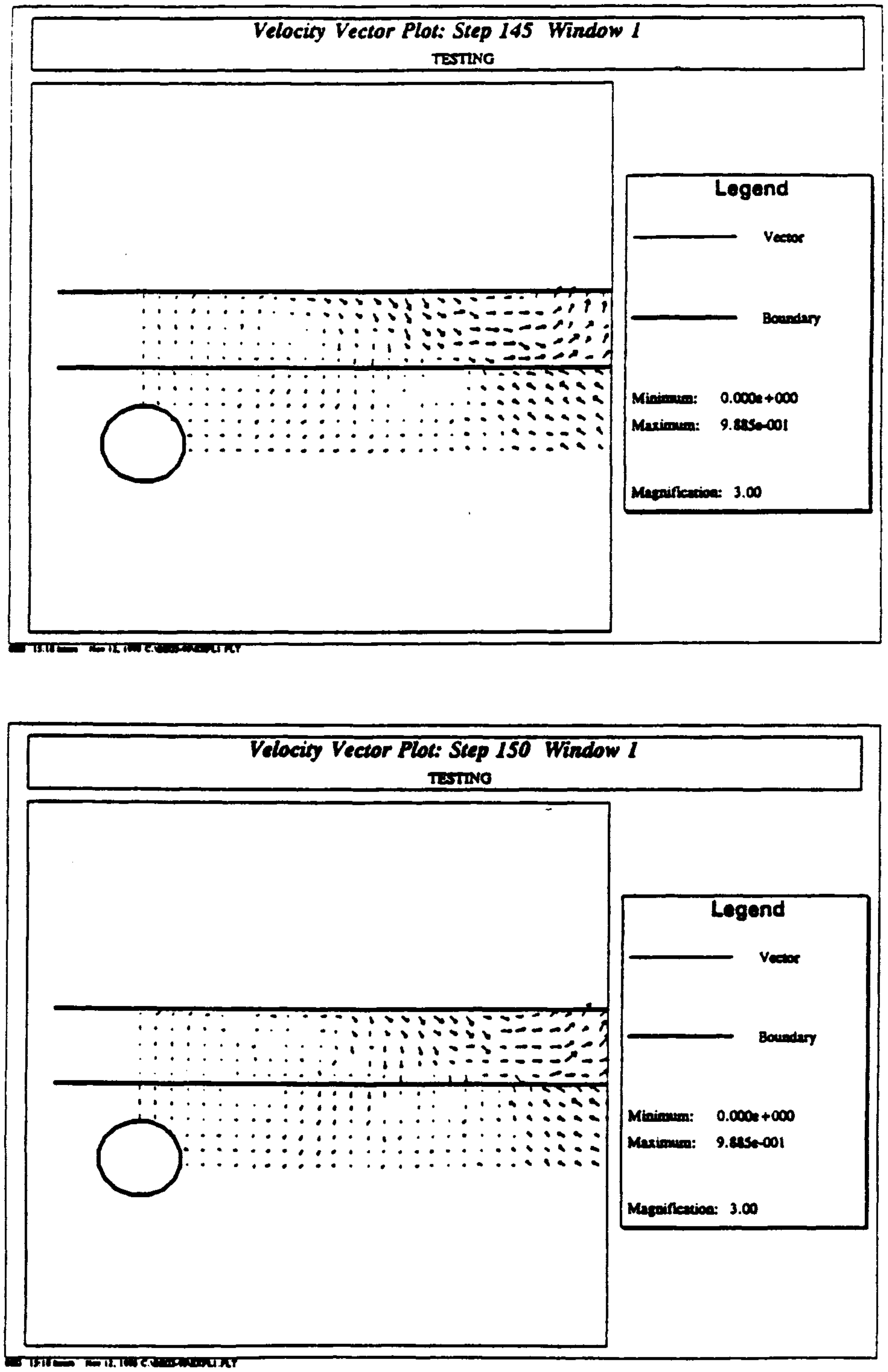

Figure D-67: Velocity vectors at times 145Δt and 150Δt for underground explosion in a two-layered rock.